

**Model-based scale-up of a continuously operated  
consolidated bioprocess based on a microbial  
consortium for the production of ethanol**

Présentée le 1<sup>er</sup> avril 2022

Faculté des sciences de base  
Groupe Kröcher  
Programme doctoral en chimie et génie chimique

pour l'obtention du grade de Docteur ès Sciences

par

**David Beat DEMPFLÉ**

Acceptée sur proposition du jury

Prof. B. Fierz, président du jury  
Prof. O. Kröcher, Prof. M. Studer, directeurs de thèse  
Prof. H. Trajano, rapporteuse  
Prof. Ph. Rudolf von Rohr, rapporteur  
Prof. F. Maréchal, rapporteur



---

## Acknowledgements

---

I thank both of my thesis directors, Oliver Kröcher from the Group of Catalysis for Biofuels at the École Polytechnique Fédérale de Lausanne and Michael Studer from the Laboratory of Biofuels and Biochemicals at the Bern University of Applied Sciences, who gave me the chance to work on a topic of great interest with various exciting challenges. The production of biochemicals is of great importance and being able to be part of this exciting research has been very fulfilling. I want to thank both of you for your great support and thoroughly interesting discussions.

For being part of the examination committee and attending my defense of my PhD work, I would like to thank Prof. Heather Trajano, Prof. Beat Fierz, Prof. em. Philipp Rudolf von Rohr and Prof. François Maréchal.

My special thanks to Simone Brethauer-Studer, Elisabeth Cazier, Simon Bowald, Patrice Bühler, Robert Shahab and Dominik Blaser for all the good times in the laboratory and the intellectual discussions, too . The work environment was very pleasant and I enjoyed the time very much.

Thank you Carsten Wagner, for your support regarding the Matlab® modeling. Your excellent understanding of modeling, from which I could benefit with an incredibly amount of understanding in modeling, helped to keep model consistent and rigorous. Thank you, Dilan Celebi, for your explanations regarding the techno-economic model.

I would like to thank Manfred Muhr and Roman Studer for their support in manufacturing experimental components and IT infrastructure, respectively. For your attentive, administrative support, thank you, Anne Lene.

The work of this PhD thesis was supported by the Swiss Confederation through Innosuisse - Swiss Innovation Agency in the framework of the SCCER BIOSWEET (contract number 1155002550). I am beyond thankful for this financial support.

For their unlimited support through my entire PhD, I want to cordially thank Christina and my family.

David Beat Dempfle, Lausanne 2021



---

## Abstract

---

The conversion of non-edible biomass such as lignocellulose to valuable chemicals has been proven to maximize the CO<sub>2</sub> reduction potential of biomass without letting arise ethical conflicts regarding food and feed supply. 2<sup>nd</sup> generation ethanol, being the predominant product of lignocellulosic biomass conversion, however, lacks in economic competitiveness compared to 1<sup>st</sup> generation ethanol from corn or sugar crops. This is due to the required pretreatment of the lignocellulose to break its recalcitrance against microbial activity and the costly enzyme production and enzymatic hydrolysis to depolymerize the cellulose to glucose, which is fermented to ethanol. Consolidated bioprocessing (CBP) based on the synergistic collaboration of a filamentous, cellulolytic fungus *Trichoderma reesei* and the yeast *Saccharomyces cerevisiae* was identified as potential solution for economic competitiveness of 2<sup>nd</sup> generation ethanol. CBP involves the highest degree in process intensification for bioprocessing: Enzyme production, enzymatic hydrolysis and fermentation of the released glucose to ethanol are carried out in one process step. This thesis aims to investigate the economics of ethanol production from cellulosic substrates by CBP, to design and conduct continuous CBP experiments and to develop a deep understanding of the process from a chemical engineering point of view in order to enable scale-up of CBP from 2.7 L laboratory scale to 130 L pilot scale.

A techno-economic assessment was conducted to investigate the cost savings by consortium-based CBP at industrial scale and to identify the critical process parameters in terms of costs. Compared to conventional ethanol production from lignocellulose in individual process steps, CBP operated at full-scale (2,000 t/d) saves up to 27.5 % of the total ethanol production costs. The cost savings are mainly achieved through lower CAPEX due to less apparatus requirements because of the integrated process, as well as through lower OPEX since no glucose is needed for enzyme production. As a result of a detailed sensitivity analysis, scale and yield were identified as the main cost-pushers from a process point of view, whereas the price level of the plant location has the highest impact on the investment conditions. In the EU, CBP yields enough margin for profitable production and the possibility to decentralize biomass valorization, whereas in the world's largest ethanol market, the US, profitable production of lignocellulosic ethanol can only be achieved by CBP combined with other cost saving techniques, such as

utilization of cost-free waste feedstocks, since ethanol has undergone a considerable price slump.

The conduction of continuous experiments is of central importance in this work for two reasons: First, the techno-economic assessment demonstrated the considerable cost savings when CBP is operated continuously. Second, continuous steady-state operation is time-invariant and thus, allows to fit and validate a rigorous process model without the need to account for growth dynamics. Steady-state operation was achieved multiple times with a maximum titer of  $3.258 \pm 0.007 \frac{g}{L}$  and a productivity of  $0.025 \frac{g}{L \cdot h}$ . It was proven, that *T. reesei* produces constantly enzymes over 750 h, which is in agreement with kinetic models considering enzyme production a growth-unrelated process carried out by the secondary mycelia of *T. reesei*. The continuous experiments showed that the oxygen flux per membrane area is a critical parameter for the process. Setups with identical volumetric oxygen transfer rate  $k_L a$ , but different oxygen fluxes per membrane area (large area & low concentration gradient vs. small area and high concentration gradient) showed titer differences of ca. 80 % ( $1.83 \frac{g}{L}$  vs  $3.26 \frac{g}{L}$ ) in favor of setups with the large membrane surface. The difference was attributed to long diffusion paths in thicker biofilms and thus, shortage in nutrient supply. A rigorous process model, which included all reaction kinetics and mass transfer limitations of the system confirmed this hypothesis. The fungal biofilm thickness  $\delta_f$  was found to be a critical parameter with an optimum for every membrane configuration. Smaller  $\delta_f$  reduced the fungal biofilm volume and thus, the enzyme production unnecessarily and larger  $\delta_f$  increased the diffusion path length and caused shortage in nutrient supply as well as lower enzyme concentrations in the bulk.

Scaling up bioprocesses is a complex tasks because of the heterogeneity of the biological system as well as chemical and mechanical sensitivity of the cells, which often cause performance decrease at higher scales. In this work, the systematic scale-up approach of non-dimensionalizing the problem and requesting non-dimensional similarity was combined with the simulation outcome of the rigorous process model in order to scale up a membrane aerated biofilm reactor to produce lignocellulosic ethanol by consolidated processing. The synergy of identifying trade-offs with a basic, systematic approach and resolve them with a highly differentiated model with the minimum selling price as optimization criterion was proven. Regarding the final results, it was distinguished between an industrial favorable solution and an academically feasible solution to experimentally prove the scale-up guidelines at 150 L pilot scale fermenter based on model data with 3 L lab scale fermenter.

Finally, popular rate-controlled separation techniques in biotechnology, were investigated regarding their potential together with CBP. It was focused on in-situ and slip stream ethanol separation setups in order to reduce yeast inhibition additional to the general advantages of

rate-controlled separations such as avoiding limitations by an azeotrope or the unfavorable vapor-liquid equilibrium of highly diluted ethanol-water mixtures.

However, except from CO<sub>2</sub> stripping and pervaporation, all mechanism fail to handle the solids of the fermentation broth. CO<sub>2</sub> stripping is limited by a poor ethanol recovery due to the trade-off between bubble residence time and stable bubble flow regime. Pervaporation, being the most promising concept for *in-situ* product removal, would be a cost-saving alternative to distillation for batch operation, but is limited by an unfavorable vapor-liquid equilibrium due to low bulk concentrations during continuous operations.

**Keywords:** Consolidated bioprocessing, lignocellulose, ethanol, techno-economic assessment, continuous bioprocess, rigorous model, scale-up, *in-situ* product removal, *Trichoderma reesei*, *Saccharomyces cerevisiae*



---

## Zusammenfassung

---

Die Umwandlung von nicht-essbarer Biomasse wie Lignozellulose in wertvolle Chemikalien maximiert nachweislich das CO<sub>2</sub>-Reduktionspotenzial von Biomasse, ohne ethische Konflikte in Bezug auf die Lebensmittel- und Futtermittelversorgung auszulösen. Ethanol der 2. Generation, das häufigste Produkt der Umwandlung von Lignozellulose-Biomasse, ist jedoch wirtschaftlich nicht gleichermassen wettbewerbsfähig wie Ethanol der 1. Generation. Dies liegt an der erforderlichen Vorbehandlung der Lignozellulose, um ihre Resistenz gegenüber mikrobieller Aktivität zu brechen, sowie an der kostspieligen Enzymproduktion und enzymatischen Hydrolyse zur Depolymerisierung der Zellulose zu Glukose, die zu Ethanol vergoren wird. Ein konsolidierter Bioprozess (CBP), welcher auf der synergetischen Zusammenarbeit eines filamentösen, zellulolytischen Pilzes *Trichoderma reesei* und der Hefe *Saccharomyces cerevisiae* basiert, stellt eine mögliche Lösung für die wirtschaftliche Wettbewerbsfähigkeit von Ethanol der 2. Generation dar. CBP erreicht den höchsten Grad der Prozessintensivierung in der Biotechnologie: Enzymproduktion, enzymatische Hydrolyse und Fermentation der freigesetzten Glukose zu Ethanol werden in einem Prozessschritt durchgeführt. Ziel dieser Arbeit ist es, die Wirtschaftlichkeit der Ethanolproduktion aus zellulosehaltigen Substraten mittels CBP zu untersuchen, kontinuierliche CBP-Experimente zu konzipieren und durchzuführen und ein verfahrenstechnisches Verständnis des Prozesses zu entwickeln, um einen Scale-up basierend auf CBP im 2.7-Liter-Laborvolumen hin zu einem Pilotfermenter mit 130-Liter-Volumen zu ermöglichen.

Es wurde eine technisch-ökonomische Bewertung durchgeführt, um die Kosteneinsparungen durch den Konsortium-basierten CBP im industriellen Massstab zu untersuchen und die kritischen Prozessparameter in Bezug auf die Kosten zu identifizieren. Im Vergleich zur konventionellen Ethanolproduktion aus Lignozellulose in einzelnen Prozessschritten spart CBP bei industriellem Massstab (2'000 t/d) bis zu 27.5 % der gesamten Ethanolproduktionskosten ein. Die Kosteneinsparungen werden vor allem durch geringere CAPEX erreicht, da aufgrund des integrierten Prozesses weniger Apparate benötigt werden, sowie durch geringere OPEX, da keine Glukose für die Enzymproduktion benötigt wird. Als Ergebnis einer detaillierten Sensitivitätsanalyse wurden die Grösse der Anlage und die Ausbeute als die wichtigsten Kostentreiber

aus verfahrenstechnischer Sicht identifiziert, während das Preisniveau des Anlagenstandorts den grössten Einfluss auf die Investitionsbedingungen hat. In der EU bietet CBP genügend Spielraum für eine rentable Produktion und die Möglichkeit, die Biomasseverwertung zu dezentralisieren, während im weltgrössten Ethanolmarkt, den USA, eine rentable Produktion von lignozellulosehaltigem Ethanol nur durch CBP in Kombination mit anderen kostensparenden Massnahmen, wie z.B. der Nutzung von kostenfreien Abfallrohstoffen, erreicht werden kann, da Ethanol einen erheblichen Preisverfall erlebt hat.

Die Durchführung von kontinuierlichen Versuchen ist in dieser Arbeit aus zwei Gründen von zentraler Bedeutung: Erstens hat die technisch-ökonomische Bewertung gezeigt, dass der kontinuierliche Betrieb von CBP zu erheblichen Kosteneinsparungen führt. Zweitens ist der kontinuierliche Betrieb im stationären Zustand zeitinvariant und ermöglicht somit die Anpassung und Validierung eines rigorosen Prozessmodells, ohne dass die Wachstumsdynamiken berücksichtigt werden müssen. Der stationäre Zustand wurde mehrfach erreicht und ein maximaler Titer von  $3.26 \pm 0.01 \frac{\text{g}}{\text{L}}$  sowie eine Produktivität von  $0.025 \frac{\text{g}}{\text{L} \cdot \text{h}}$  gemessen. Es wurde nachgewiesen, dass *T. reesei* über 750 h konstant Enzyme produziert, was mit kinetischen Modellen übereinstimmt, die die Enzymproduktion als einen nicht direkt wachstumsabhängigen Prozess betrachten, der von den sekundären Myzelien von *T. reesei* durchgeführt wird. Die kontinuierlichen Experimente zeigten, dass der Sauerstofffluss pro Membranfläche ein kritischer Parameter für den Prozess ist. Bei Versuchen mit identischer volumetrischer Sauerstofftransferate  $k_L a$ , aber unterschiedlichen Sauerstoffflüssen pro Membranfläche (grosse Fläche und niedriger Konzentrationsgradient vs. kleine Fläche und hoher Konzentrationsgradient) ergaben sich Titerunterschiede von ca. 80 % ( $1.83 \frac{\text{g}}{\text{L}}$  vs.  $3.26 \frac{\text{g}}{\text{L}}$ ) zugunsten der Versuchsanordnung mit der grossen Membranfläche. Der Unterschied wurde auf die langen Diffusionswege in dickeren Biofilmen und damit auf einen Mangel an Nährstoffzufuhr zurückgeführt. Ein rigoroses Prozessmodell, das alle reaktionskinetischen und stofftransportbedingten Einschränkungen des Systems berücksichtigte, bestätigte diese Hypothese. Die Pilz-Biofilmdicke  $\delta_f$  erwies sich als relevanter Parameter mit einem Optimum für jede Membrankonfiguration. Ein kleineres  $\delta_f$  verringerte das Volumen des Pilzbiofilms und damit die Enzymproduktion unnötig, während ein grösseres  $\delta_f$  die Diffusionsweglänge vergrösserte und zu einem Mangel der Nährstoffzufuhr sowie zu geringeren Enzymkonzentrationen in der flüssigen Phase führte.

Die Skalierung von Bioprozessen ist eine komplexe Aufgabe, da die Heterogenität des biologischen Systems sowie die chemische und mechanische Empfindlichkeit der Zellen oft zu einem Leistungsabfall bei höheren Skalen führen. In dieser Arbeit wurde der systematische Scale-up-Ansatz der Entdimensionalisierung des Problems und der Forderung nach dimensionsloser Ähnlichkeit mit den Simulationsergebnissen des rigorosen Prozessmodells kombiniert, um einen membranbelüfteten Biofilmreaktor zur Herstellung von Ethanol aus Lignozellulose mithilfe eines konsolidierten Bioprozesses zu vergrössern. Die Synergie zwischen

der Identifizierung von Zielkonflikten mit einem grundlegenden, systematischen Ansatz und deren Lösung mit einem hochdifferenzierten Modell und dem minimalen Verkaufspreis als Optimierungskriterium wurde nachgewiesen. In Bezug auf die Endergebnisse wurde zwischen einer industriell favorisierten Lösung und einer akademisch machbaren Lösung unterschieden, um die Scale-up-Richtlinien für einen 150 L-Fermenter auf der Grundlage von Modelldaten mit einem 3 L-Laborfermenter experimentell zu beweisen.

Zuletzt wurden gängige ratengesteuerte Trenntechniken in der Biotechnologie auf ihr Potenzial in Verbindung mit CBP untersucht. Zusätzlich zu den allgemeinen Vorteilen von ratengesteuerten Trennungen, wie z.B. die Vermeidung von Einschränkungen durch ein Azeotrop oder das ungünstige Dampf-Flüssigkeits-Gleichgewicht von stark verdünnten Ethanol-Wasser-Gemischen, lag der Schwerpunkt dabei auf *in-situ*- und Slip-Stream-Ethanolabtrennungen, um die Inhibierung der Hefe zu reduzieren.

Mit Ausnahme des CO<sub>2</sub>-stripping und der Pervaporation sind jedoch alle Verfahren nicht in der Lage, mit dem Feststoffgehalt der Fermentationsbrühe umzugehen. Das CO<sub>2</sub>-stripping ist durch eine schlechte Ethanolrückgewinnung aufgrund des Zielkonflikts zwischen Blasenverweilzeit und stabilem Blasenfluss begrenzt. Die Pervaporation, das vielversprechendste Konzept für die *in-situ*-Produktentfernung, wäre eine kostensparende Alternative zur Destillation für den Chargenbetrieb, wird aber durch ein ungünstiges Dampf-Flüssigkeits-Gleichgewicht aufgrund niedriger Endkonzentrationen im kontinuierlichen Betrieb eingeschränkt.

**Schlüsselwörter:** Konsolidierter Bioprozess, Lignozellulose, Ethanol, Techno-ökonomische Bewertung, kontinuierlicher Bioprozess, rigoroses Modell, scale-up, *in-situ* Produktentfernung, *Trichoderma reesei*, *Saccharomyces cerevisiae*





---

## Nomenclature

---

### List of abbreviations

<i>A. phoenicis</i>	<i>Aspergillus phoenicis</i>
BC	Boundary condition
CAPEX	Capital expenditure
CBH	Cellobiohydrolase
CBP	Consolidated bioprocessing
CCS	Carbon capture and storage
CDW	Cell dry weight
CEPCI	Chemical Engineering Plant Cost Index
CME	Chicago mercantile exchange
CNC	Computerized numerical control
CSTR	Continuously stirred tank reactor
<i>D. Bruxellensis</i>	<i>Dekkera bruxellensis</i>
DoF	Degree of freedom
EG	Endoglucanase
EPFL	École Polytechnique Fédérale de Lausanne
FoB	Free on board
FGD	Flue gas desulfurization
FPU	Filter paper unit
GHG	Greenhouse gas
GMO	Genetically modified microorganism
HPLC	High Performance Liquid Chromatography
IPCC	Intergovernmental panel on climate change
ISO	International organization for standardization
MESP	Minimum ethanol selling price

NREL	National Renewable Energy Laboratory
OPEX	Operational expenditure
PDMS	Polydimethylsiloxane
PFR	Plug flow reactor
PID	Proportional-integral-differential
PPP	Purchasing power parity
<i>rpm</i>	Rounds per minute
<i>S. cerevisiae</i>	<i>Saccharomyces cerevisiae</i>
SSF	Simultaneous saccharification and fermentation
<i>T. reesei</i>	<i>Trichoderma reesei</i>
UV	Ultraviolet

## List of symbols

### Orders of magnitude

<i>n</i>	Nano [ $10^{-9}$ ]
$\mu$	Mikro [ $10^{-6}$ ]
<i>m</i>	Milli [ $10^{-3}$ ]
<i>c</i>	Centi [ $10^{-2}$ ]
<i>k</i>	Kilo [ $10^3$ ]
<i>M</i>	Mega [ $10^6$ ]
<i>G</i>	Giga [ $10^9$ ]
<i>E</i>	Exa [ $10^{18}$ ]

### Latin & Greek letters

<i>A</i>	Surface area [ $m^2$ ]
$\beta$	Selectivity [–]
$\beta - G$	$\beta$ -glucosidase
<i>C</i>	Clearance [ $m$ ]
[C]	Concentration of active substrate sites $\frac{kg}{m^3}$
<i>c</i>	Concentration $\frac{kg}{m^3}$
$\delta_f$	Fungal biofilm thickness [ $m$ ]

$D$	Dilution rate [ $s^{-1}$ ] resp. diffusion coefficient [ $\frac{m^2}{s}$ ]
$d$	diameter [ $m$ ]
$\eta$	Dynamic viscosity [ $Pa \cdot s$ ] resp. yield $[-]$
$[E]$	Enzyme concentration $\frac{kg}{m^3}$
$E_A$	Activation energy $\frac{J}{mol}$
$[EC]$	Concentration of enzyme-substrate-complexes $\frac{kg}{m^3}$
$Eu$	Euler number
$\varphi$	Angular coordinate
$\gamma$	Arrhenius number $[-]$
$g$	Gravitational acceleration [ $\frac{m}{s^2}$ ]
$H$	Henry coefficient $\frac{kg}{m^3 Pa}$ resp. height [ $m$ ]
$h$	Height [ $m$ ]
$J$	Mass flux $\frac{kg}{m^2 s}$
$K$	Half-saturation constant $\frac{kg}{m^3}$
$k$	Rate constant [ $\frac{1}{s}$ ]
$k_{conv}$	Konvective mass transfer coefficient [ $\frac{m}{s}$ ]
$k_L a$	Volumetric oxygen transfer coefficient [ $s^{-1}$ ]
$\lambda$	Kolmogorov scale [ $m$ ]
$L$	Length [ $m$ ]
$\mu$	Microbial growth rate [ $s^{-1}$ ]
$M$	Maintenance coefficient [ $\frac{1}{s}$ ] resp. molar mass [ $\frac{kg}{mol}$ ]
$m$	Mass [ $kg$ ]
$\nu$	Reaction rate $\frac{kg}{m^3 s}$ resp. kinematic viscosity $\frac{m^2}{s}$
$n$	Mole fraction $[-]$
$Nu$	Nusselt number $[-]$
$P$	Performance $[-]$ resp. power [ $W$ ]
$p$	Pressure [ $Pa$ ]
$Pe$	Péclet number
$Pr$	Prandtl number
$Q$	Permeance $\frac{mol}{m^2 Pa}$
$\rho$	Density $\frac{kg}{m^3}$
$R$	Universal gas constant $\frac{J}{mol \cdot K}$
$r$	Radius [ $m$ ] resp. reaction rate $\frac{kg}{m^3 s}$
$Re$	Reynolds number
$\sigma$	Adsorption capacity $[-]$

$S$	Solubility $\frac{kg}{m^3 Pa}$ resp. pitch $[m]$
$Sc$	Schmidt number
$Sh$	Sherwood number
$\tau$	Residence time $[s]$
$t$	Time $[s]$
$u$	Velocity $\frac{m}{s}$
$V$	Volume $[m^3]$
$v$	Velocity $[\frac{m}{s}]$
$\dot{V}$	Volumetric flow rate $[\frac{m^3}{s}]$
$W$	Width
$wt.\%$	weight %
$[X]$	Concentration of microbial biomass $\frac{kg}{m^3}$
$x$	Liquid-phase mole fraction $[-]$
$Y$	Yield coefficient $[-]$
$y$	Gas-phase mole fraction $[-]$
$\zeta$	Pressure loss coefficient $[-]$
$z$	Axial coordinate $[m]$

## List of superscripts & subscripts

$abs$	Absolute
$b$	Bulk phase
$bf$	Biofilm
$\beta - G$	$\beta$ -glucosidase
$C$	Cellulose
$c$	conversion
$Cb$	Cellobiose
$CBH$	Cellobiohydrolase
$conv$	Convective
$CS$	Central screw
$CSTR$	Continuously stirred tank reactor
$d$	Delay resp. decay
$degr$	Degradation

<i>diff</i>	Diffusive
<i>E</i>	Enzyme
<i>eff</i>	Effective
<i>EG</i>	Endoglucanase
<i>endo</i>	Endoglucanase
<i>EtOH</i>	Ethanol
<i>exo</i>	Exoglucanase
<i>f</i>	Fungal biofilm layer resp. free
<i>G</i>	Glucose
<i>i</i>	Generic species i
<i>in</i>	Inlet
<i>L</i>	Length
<i>m</i>	Membrane
<i>max</i>	maximum
<i>min</i>	minimum
<i>o</i>	inner membrane phase
<i>O<sub>2</sub></i>	Oxygen
<i>out</i>	outlet
<i>ox</i>	Oxygen
<i>p</i>	Primary resp. pressure
<i>P</i>	Particle resp. permeate
<i>reac</i>	Reactor
<i>s</i>	secondary
<i>sec</i>	secondary
<i>synth</i>	Synthesis
<i>tot</i>	Total
<i>tr</i>	<i>Trichoderma reesei</i>
<i>w</i>	water
<i>Y</i>	yeast
<i>y</i>	yeast biofilm layer



---

## List of figures

---

- 1.1 Left: The light orange lines show all emission scenarios leading to global warming below 1.5 °C relative to pre-industrial level according to IPCC models. The blue dashed, dotted and dashed-dotted lines show representative scenarios with low, medium and high overshoot in GHG emissions. Right: The scenario with medium GHG emission overshoot is decomposed into the net emissions of the sectors agriculture (brown), transport (blue), industry (turquoise), electricity buildings (white) as well as carbon capture and storage (CCS, orange & yellow), which reduces the net emissions. [1] . . . . . 2
- 1.2 Process scheme of state-of-the-art ethanol production from lignocellulose. The lignocellulose is pretreated to break up its structure and make the cellulose fibers accessible for enzymes, which are produced by a fungus in a separate enzyme production unit. After enzymatic hydrolysis, where the polymeric cellulose is depolymerized to sugars, the slurry is sent to fermentation, where the fermenting microorganisms converts the released sugars to ethanol, which is purified afterwards. [2] . . . . . 3
- 1.3 Process scheme of CBP ethanol production from lignocellulose. The pretreatment does not differ from state-of-the-art ethanol production, but enzyme production, enzymatic hydrolysis and fermentation are merged into one process step to reduce the number of apparatus and save costs. [3] . . . . . 4

1.4	Schematic illustration of CBP based on a microbial consortium with well-established niches in a reactor system. An oxygen aerated membrane (grey tubular element) is winded in helical shape within a bioreactor (upper left corner). The oxygen (blue) diffuses across the membrane (grey) and creates an oxygen enriched layer around the membrane. The aerobic, enzyme producing fungus <i>T. reesei</i> (dark green) grows in this layer and consumes a large fraction of the oxygen. The remaining oxygen is consumed by a second layer on the biofilm (light green) consisting of yeast cells, which perform aerobic metabolism. In the anoxic bulk phase (turquoise), the cellulose is hydrolyzed by the enzymes, which diffused from the fungal biofilm layer into the bulk, and the suspended yeast cell ferment the released glucose to ethanol. A fraction of glucose diffuses back into the biofilm and feeds the aerobic fungus. [4] . . . . .	5
2.1	Simplified process flow diagrams for the production of lignocellulosic bioethanol employing separate hydrolysis and fermentation (a) and consolidated bioprocessing (CBP) (b). The recalcitrance of lignocellulose is overcome by a physico-chemical pretreatment. After the pretreatment, pH, temperature and pressure are conditioned for enzymatic hydrolysis and CBP, respectively. In the case of conventional production, the enzymes are produced by a fungus using glucose as carbon source in a separate reactor system. During enzymatic hydrolysis, the cellulose is converted to glucose. The hydrolyzed slurry is sent to the fermentation, where the sugars are fermented to ethanol. In the case of CBP, enzyme production, hydrolysis and fermentation are carried out in the same vessel. Finally, the ethanol is recovered from the product stream by distillation and adsorption. . . . .	12
2.2	Relative cost savings of consortium-based CBP compared to the base case for CAPEX, fixed and variable OPEX and the resulting MESP. CBP leads to savings in CAPEX, fixed and variable OPEX. The change in pretreatment increases the CAPEX but reduces the variable OPEX. The fixed OPEX are almost not affected by the pretreatment. The resulting MESP is reduced by 27.5 % compared to the base case due to the change in pretreatment and implementation of consortium-based CBP. . . . .	16
2.3	Share of CAPEX, fixed and variable OPEX of the MESP for the base case and the CBP scenario. . . . .	17



- 2.4 Development of the ethanol prices in the US and the EU compared to the costs for chemical plants represented by the CEPCI. From 2007 to 2019, the US ethanol price decreased by 30% [5], whereas the costs for chemical plants increased by 16%. For the EU ethanol price (domestic ethanol, FoB Rotterdam), data is available from 2011 to 2019 [6]. After a few years with lower price, the price level in 2019 stabilized around the same level as between 2011 and 2013. . . . . 18
- 2.5 Sensitivity analysis for (a) scale [% of base case feedstock consumption], (b) titer [wt.%], (c) yield [%], (d) residence time [days], (e) feedstock costs [\$/dry metric ton], (f) purchasing power parity [% rel. to US] and (g) capital charge rate [%]. The results for the base case, including the cost savings by employing CBP, are represented by open markers in each case, whereas the filled markers denote the variation of the specific parameter. Circular markers show the US MESP and rhombic markers show the EU MESP. The dashed-dotted lines represent the average ethanol stock exchange price in the US in 2019 of 36.75 ¢/L [5]. The dotted line represents the 2019 EU ethanol price (T2 FOB Rotterdam) [6]. Flat curves denote a high variation of the MESP with little variation of the specific parameter and thus, a high cost sensitivity. These parameters are targeted to shift the MESP (rhombic and circular markers) to the left of the dashed-dotted and dashed line, respectively, in order to meet the market price in the respective region. . . . . 21
- 3.1 Close-up photograph of the biofilm on a helically winded membrane on its support. The white layer on the top is the yeast biofilm layer and the yellowish layer is the biofilm formed by *T. reesei*. The membrane is visible, where the biofilm was scraped away manually after the experiments. . . . . 30
- 3.2 Photograph of the segmented flow from the feed bottle (background) to the 1<sup>st</sup> reactor. The green arrow exemplary shows a droplet with the solid-liquid suspension and the red arrow points out the settling limitation of Avicel at the phase boundary between droplet and nitrogen bubble . . . . . 31

- 3.3 The 3-phase flow feed design for continuous feeding of suspensions with insoluble substrates. The well mixed solid-liquid suspension is sucked into the feeding device, a T-junction, by a peristaltic pump. Additionally, nitrogen is injected via the perpendicular nozzle of the T-junction. Consequently, a 3-phase flow with solid-liquid suspension droplets and intermitting gas bubbles is formed. Sedimentation of the solid particles ends at the phase boundary to the gas bubbles since the gravitational force is outweighed by the surface tension between the droplet and the bubble. Figure taken from [7]. . . . . 33
- 3.4 Schematic representation of the oxygen recirculation system for membrane aeration (black lines) and the pneumatic transport of the fermentation slurry by nitrogen injection (blue lines). Oxygen is pumped through the membrane, where a certain amount of oxygen is lost due to diffusion across the membrane wall. The oxygen concentration in the make-up vessel is measured optically and an electromagnetic valve is opened to add pure oxygen to make up for the loss by diffusion. After each feeding interval, an electromagnetic valve is opened to inject nitrogen in the gas phase above the liquid level of the 1<sup>st</sup> reactor. The fermentation broth is pneumatically pushed through a dip tube and flows into the second reactor and from the second reactor into the collecting vessel, where the nitrogen is vented via a sterile filter. As soon as the filling level of each reactor reaches the desired state, the dip tubes do not reach into the liquid phase anymore. The remaining nitrogen is directly transported through the dip tubes to the vent. Figure adapted from [8]. . . . . 34
- 3.5 Qualitative comparison of estimated different control responses of the critical parameters after initializing nitrogen flushing for pneumatic fluid transport. . . 36
- 3.6 Ethanol degradation of *T. reesei* in an Erlenmeyer flask with ethanol as only substrate and ethanol together with cellulose as substrate at 28 °C. The dotted lines represent the linear fit with average degradation rates of  $0.0306 \frac{g}{L \cdot h}$  and  $0.01183 \frac{g}{L \cdot h}$  with ethanol as only substrate present and with ethanol and cellulose as substrate, respectively. The coefficients of determination are 0.9943 and 0.9922, respectively. The error bars are based on triplicate experiments. . . . . 39

- 3.7 Steady-state results for continuous consolidated bioprocessing based on a microbial consortium consisting of *T. reesei* with *S. cerevisiae* in a cascade of 2 reactors. Steady-state operation was reached after 564 h. Cellobiose was depleted in the 1<sup>st</sup> reactor and only present to a little extent in the 2<sup>nd</sup> reactor (ca. 0.2  $\frac{g}{L}$ ). The solid and dashed lines denote the average ethanol concentration and its standard deviation, respectively, in the 1<sup>st</sup> and second reactor. Steady-state operation was maintained over 111 h. The membrane (inner diameter  $d_i$ = 1.58 mm, outer diameter  $d_o$ = 3.18 mm, length L= 5.6 m) was aerated with 21 % oxygen fraction. The cellulose feed concentration was 17.5  $\frac{g}{L}$  and the residence time  $\tau$  was 130 h. . . . . 40
- 3.8 Steady-state ethanol production with consolidated bioprocessing based on a microbial consortium consisting of *T. reesei* and *S. cerevisiae* in a cascade of 2 reactors. The membrane (inner diameter  $d_i$ = 1.58 mm, outer diameter  $d_o$ = 3.18 mm, length L= 5.6 m (a) and L= 2.8 m (b), respectively, was aerated with 42 % oxygen fraction. The cellulose feed concentration was 17.5  $\frac{g}{L}$  and the residence time  $\tau$  was 130 h. . . . . 41
- 3.9 Batch ethanol and cellobiose production of *T. reesei* with *D. bruxellensis* [a] vs. *T. reesei* with *A. phoenicis* and *S. cerevisiae* [b]. . . . . 45
- 3.10 Schematic representation of the co-cultivation conditions for a microbial consortium consisting of *T. reesei*, *A. phoenicis* and *S. cerevisiae*. The blue, black and red square denote the range of temperature and pH, which allow growth for the respective species. The corresponding curves at the temperature and pH axis denote the growth rate as function of the axis variable, pH or T. The overlapping areas possibly allow co-cultivation. The green arrows denote the pH and Temperature condition, where *T. reesei* and *A. phoenicis* grow exactly at the same rate. Note that other parameters, which influence a co-cultivation such as secretion of antimicrobial substances are not considered in this plot. Figure adapted from [9]. . . . . 47
- 3.11 Growth rate comparison of *T. reesei* and *A. phoenicis* grown in separate Erlenmeyer flasks under identical conditions at different temperature and pH. The difference in growth rate is plotted against the time, meaning that values of zero correspond to identical growth rates. Positive values indicate faster growth of *A. phoenicis* and negative values faster growth of *T. reesei*, respectively. The growth rate does not have a unit since it was determined by means of spectrophotometry. . . . . 48

- 3.12 Continuous ethanol production with consolidated bioprocessing based on a microbial consortium of *T. reesei*, *A. phoenicis* & *S. cerevisiae*. The membrane (inner diameter  $d_i = 1.58 \text{ mm}$ , outer diameter  $d_o = 3.18 \text{ mm}$ , length  $L = 2.8 \text{ m}$  was aerated with 21 % oxygen fraction. The cellulose feed concentration was  $17.5 \frac{\text{g}}{\text{L}}$  and the residence time  $\tau$  was  $130 \text{ h}$ . . . . . 49
- 4.1 Kinetic network of consolidated bioprocessing of cellulose to ethanol by a microbial consortium of *T. reesei* & *S. cerevisiae*. *T. reesei* grows in the biofilm with oxygen and glucose as the two limiting substrates. The produced cellulases, consisting of cellobiohydrolase (CBH), endoglucanase (EG) and  $\beta$ -glucosidase ( $\beta$ -G), act synergistically to cleave cellulose to cellobiose and finally to glucose. Glucose is consumed by *T. reesei* and by *S. cerevisiae*, which ferments the sugar to ethanol. The target product ethanol may be depleted by aerobic metabolism of *S. cerevisiae* and by *T. reesei* if there is a shortage in a favored nutrient such as glucose. The solid lines represent desired reaction pathways. The dotted lines denote undesired side-reactions. . . . . 52
- 4.2 Schematic representation of consolidated bioprocessing of cellulose to ethanol by a microbial consortium of *T. reesei* & *S. cerevisiae*. Oxygen (blue) diffuses through a membrane (grey) and establishes an aerobic layer above the membrane in an otherwise anoxic reactor system. The aerobic, cellulolytic fungus *T. reesei* grows in this aerobic layer (dark green) and releases cellulases to the bulk (turquoise), where the cellulases hydrolyze cellulose to glucose. The glucose feeds both, *T. reesei* and *S. cerevisiae*, which grows anaerobically in the bulk, fermenting glucose to ethanol, as well as aerobically in the outer biofilm layer (light green), where oxygen residues are present. . . . . 53
- 4.3 Schematic representation of the layer formation with a tubular membrane (a) and the concept of the bulk phase as cylindrical shell around the membrane and biofilm layers (b). Note: The straight membrane tube is a simplification for illustration purposes. The actual setup contains a helically winded membrane (Fig. 1.4). . . . . 56
- 4.4 2D projection of the layer formation in the r-z-plane. Each layer is characterized by a reaction term  $v_i$  for species  $i$ . The mass fluxes between the layers are denoted by  $J_i$ . . . . . 57
- 4.5 Primary mycelia (a) and secondary mycelia (b) of *T. reesei*. Figure taken from [10] 62

- 4.6 Microbial growth rate as function of the oxygen concentration at different half-saturation constants, which were published for bacteria. [11–13] . . . . . 64
- 4.7 Grid system applied for finite difference method. A coordinate transformation of the form  $c_{ij} \rightarrow c_{(j-1)*M+i} = c_P$  is necessary to reduce the index to one variable. [14] Otherwise, it is impossible to address a certain element in the matrix/vector structure of the numerical solution procedure. The red nodes are subject to governing equations and boundary conditions whereas the inner nodes (grey) only are subject to the governing equations. Note that the coordinate system is still of cylindrical nature and the grid cell size is not constant. . . . . 72
- 4.8 Simulated oxygen profile for the standard membrane ( $d_i = 1.58$  mm,  $d_o = 3.18$  mm,  $L = 5.6$  m). Even at low Reynolds numbers in the membrane ( $Re = 306.5$ ),  $z$ -gradient of the system is almost negligible. The two discontinuities reflect the partition coefficients of oxygen for gas, PDMS and water. . . . . 75
- 4.9 Oxygen profile within the biofilm for the standard membrane ( $d_i = 1.58$  mm,  $d_o = 3.18$  mm,  $L = 5.6$  m). The detailed view demonstrates the curvature of the oxygen profile as a result of the tubular system. . . . . 76
- 4.10 Oxygen profile along  $z$ -axis for the standard membrane ( $d_i = 1.58$  mm,  $d_o = 3.18$  mm,  $L = 5.6$  m). The oxygen saturation within the membrane changes by 0.3 % over the length, which is lower than the maximum numerical error of the model. . . . 77
- 4.11 Ethanol profile along  $r$ -axis ( $z = 0$ ) over all layer elements for the standard membrane ( $d_i = 1.58$  mm,  $d_o = 3.18$  mm,  $L = 5.6$  m). The ethanol concentration at the right corresponds to the modeled bulk ethanol concentration of  $1.51 \frac{g}{L}$ , which has a 3.5 % deviation from the experimental value. . . . . 78
- 4.12 Projection of the oxygen and glucose gradient at  $z = 0$  as projection in the  $z$ -plane. Depending on the position in the fungal biofilm, either glucose or oxygen is the limiting nutrient. The maximum growth rate of ca. 45 %  $\mu_{max}$  is reached at a distance of ca. 0.25 mm from the membrane surface for the standard membrane ( $d_i = 1.58$  mm,  $d_o = 3.18$  mm,  $L = 2.8$  m) at an oxygen concentration of 21 %. 79

4.13	Projection of the oxygen and glucose gradient at $z = 0$ as projection in the $z$ -plane. Depending on the position in the fungal biofilm, either glucose or oxygen is the limiting nutrient. The maximum growth rate of ca. 40 % $\mu_{\max}$ is reached at a distance of ca. 0.32 mm from the membrane surface for the standard membrane ( $d_i = 1.58$ mm, $d_o = 3.18$ mm, $L = 2.8$ m) at an oxygen concentration of 42 %. The red circles denote glucose-depleted, but oxygen-enriched zones in the fungal biofilm, where <i>T. reesei</i> degrades high amounts of ethanol (Fig. 3.6) . . .	80
4.14	Evaluation of the optimum fungal biofilm thickness . . . . .	81
4.15	3D view of the experimental apparatus to measure the biofilm thickness by measuring the conductivity at the tip of a needle punctuating the biofilm. (CAD created by S. Bowald) . . . . .	82
4.16	Cross-section view of the experimental apparatus to measure the biofilm thickness by measuring the conductivity at the tip of a needle punctuating the biofilm. (CAD created by S. Bowald) . . . . .	83
4.17	Resistance at the needle tip over the distance of punctuation. The decrease in resistance from air to biofilm is discontinuous, whereas the increase in resistance from the biofilm to the membrane occurs slowly due to slight membrane deformation by the needle pressure. The red line marks the end of the $4\sigma$ confidence interval of the average biofilm resistance . . . . .	84
4.18	The measured biofilm thickness (triangle markers) of $\delta_f = 1.7 \pm 0.35$ mm on average (solid line) shows a deviation of ca. 12% to the model result (dashed line)	85
5.1	Schematic representation of the the biofilm growth (green) on one large membrane (right) and $n$ multiple small membranes (left). $n = 4$ was chosen solely for illustration purposes. . . . .	90

- 5.2 Model results of the productivity  $\frac{g_{EtOH}}{h}$  as function of the membrane length at standard conditions (membrane inner diameter  $d_i = 1.58 \text{ mm}$ , membrane outer diameter, 21 % oxygen fraction within the membrane,  $17.5 \frac{g}{L}$  cellulose feed concentration the residence time  $\tau$  was 130 h) in the pilot scale system. The linear increase at the beginning is caused by the higher enzyme loading in the bulk as consequence of more biofilm volume without affecting the biofilm thickness  $\delta_f$  (chapter 4). The flattening of the curve with the subsequent strong decline in productivity is a result of the reduced bulk volume since a large fraction of the reactor is occupied with the membrane and the biofilm. Consequently, two factors are responsible for the decreasing productivity: First, a large fraction of the fed cellulose is necessary to maintain the biofilm. Second, the Dilution rate  $D = \tau^{-1}$  is defined by the nominal reactor volume. Therefore, the effective dilution rate of the bulk is higher, if a large fraction of the reactor is occupied by the immobilized biofilm. The higher dilution rate reduces the effective residence time of substrate and enzymes and thus, the cellulose conversion. The productivity reaches zero, when the whole reactor system is completely filled with the membrane and the biofilm and no bulk phase is left. Note: The presented calculations assume infinite available cellulose without any substrate inhibition effects in order to evaluate only the effect of the membrane length. At low solid loadings, the optimum is reached with less membrane length as there is no more cellulose to hydrolyze in the bulk. However, this "optimum" arises from a solid loading limitation (a parameter, which could be changed easily) instead of from reactor geometry constraints (parameters, which are difficult to change) . . . . . 92
- 5.3 Experimental results (black circles; [15]) of the viscosity of a corn stover slurry at a shear rate of  $\dot{\gamma} = 9s^{-1}$  were fitted with an exponential function (green curve; coefficient of determination  $R^2=0.997$ ) to extrapolate the data for 1.75 % solid loading. . . . . 101
- 5.4 Design geometry of a helical ribbon impeller . . . . . 102
- 5.5 Configuration of helical ribbon impeller ([a], blue), membrane support ([b], turquoise) and central screw ([c], grey) for optimum mixing behavior over a large range of fluid viscosities [d]. . . . . 103

6.1	Illustration of the different separation setups: End-of-pipe separation (a), slip stream separation (b) and <i>in-situ</i> separation (c). With end-of-pipe separation, the whole reactor outlet is sent to the separation unit and there is no interaction with the bioreactor anymore. With slip stream separation, a circulating stream between the separation unit and the bioreactor is established. The reactor outlet is already ethanol-depleted and no further ethanol is recovered. <i>In-situ</i> separation works identically to slip-stream separation with the only difference, that the separation unit is installed within the bioreactor. Note: The inlet streams for the reactors are removed for illustration purposes . . . . .	109
6.2	Yeast inhibition by ethanol and CO <sub>2</sub> depending on their respective concentrations. [16,17] The modeled ethanol data is experimentally validated for ethanol concentrations up to 60 $\frac{g}{L}$ . [16] For concentrations above 60 $\frac{g}{L}$ , the data is extrapolated, but in agreement with the experimental findings of other published studies. [16,18] . . . . .	110
6.3	Determination of the maximum possible ethanol recovery of 30 % (red asterisks) by applying the reactor height requirements for bubble flow ( $h_{min}$ , blue line) and the bubble residence time ( $h_{max}$ , cyan line) . . . . .	114
6.4	Necessary CO <sub>2</sub> mass flow (magenta line) and ethanol concentrations as weight fraction in the gas stream (blue line) and the residual stream (blue dashed line) as function of the ethanol recovery. . . . .	115
A.1	Waterfall diagram depicting the normalized cost savings through GMO-based CBP published by Lynd et al. [3] The grey bar represents the published cost savings. The red and blue bars represent extra cost savings or reduced cost savings due to adapted titer, yield, residence time and capital charge rate, respectively. The green bar represents the resulting cost saving after applying the adaptations. . . . .	135



---

## List of tables

---

4.1	Specifications for each species $i$ considered in the model in every layer considered in the model. . . . .	58
4.2	Specifications for each species $i$ considered in the model in every layer considered in the model. (continued) . . . . .	59
4.3	Specifications for each species $i$ considered in the model in every layer considered in the model. (continued) . . . . .	59
4.4	Overview of the yield and maintenance coefficients of <i>T. reesei</i> for oxygen and glucose. [19] . . . . .	66
5.1	Overview of the laboratory scale reactor and the pilot scale reactor dimensions .	93
5.2	Overview of the 5 necessary dimensionless numbers (Reynolds number, modified Péclet number, Sherwood number, pressure loss coefficient, mole fraction of oxygen at the membrane wall) to obtain process similarity in the inside of the membrane. . . . .	95
5.3	Overview of the 10 necessary dimensionless parameters to ensure process similarity in the bulk phase. . . . .	97
5.4	Overview of the scaled dimensionless parameters . . . . .	100
5.5	Overview of the design parameter for the stirrer of the reactor . . . . .	103
A.1	Total Capital Investment (TCI) of the base case and consortium-based CBP derived from the total installed costs of all apparatuses. . . . .	125
A.2	Areas and their functions in the base case . . . . .	126

A.3	Comparison of the raw material costs between the base case and the case employing consortium-based CBP with steam explosion pretreatment. . . . .	130
A.4	Differences between the process assumptions of Lynd et al., the base case and this work. Values in brackets denote values of different scenarios published by Lynd et al. [3] . . . . .	134
A.5	Apparatus list of the base and CBP . . . . .	137
A.5	Apparatus list of the base and CBP (continued) . . . . .	138
A.5	Apparatus list of the base and CBP (continued) . . . . .	139
A.5	Apparatus list of the base and CBP (continued) . . . . .	140
B.1	Overview of the experimentally obtained validation parameters and the model results . . . . .	141

---

## Table of contents

---

<b>Acknowledgements</b>	<b>i</b>
<b>Abstract</b>	<b>iii</b>
<b>Zusammenfassung</b>	<b>vii</b>
<b>Nomenclature</b>	<b>x</b>
<b>List of figures</b>	<b>xvii</b>
<b>List of tables</b>	<b>xxvii</b>
<b>1 Introduction</b>	<b>1</b>
1.1 Thesis objectives . . . . .	6
<b>2 Techno-economic assessment of consolidated bioprocessing of lignocellulose to ethanol at industrial scale</b>	<b>9</b>
2.1 Abstract . . . . .	9
2.2 Introduction . . . . .	10
2.3 Materials & Methods . . . . .	13
2.4 Results and discussion . . . . .	15
2.5 Conclusion . . . . .	23

<b>3</b>	<b>Continuous operation of a membrane aerated biofilm reactor for consortium-based consolidated bioprocessing of cellulose to ethanol</b>	<b>25</b>
3.1	Abstract . . . . .	25
3.2	Introduction . . . . .	26
3.3	Materials & Methods . . . . .	27
3.4	Results and Discussion . . . . .	32
3.4.1	Continuous CBP with a consortium consisting of <i>T. reesei</i> and <i>S. cerevisiae</i>	32
3.4.2	Improvement of continuous CBP by enhanced utilization of cellobiose . .	43
3.5	Conclusion . . . . .	50
<b>4</b>	<b>Set-up and validation of a rigorous, spatially resolved model of the kinetics and mass transfer limitations of consortium-based consolidated bioprocessing for ethanol production</b>	<b>51</b>
4.1	Abstract . . . . .	51
4.2	Introduction . . . . .	52
4.3	Results and Discussion . . . . .	54
4.4	Conclusion . . . . .	85
<b>5</b>	<b>Scale-up of a 2.7 L laboratory scale consortium-based consolidated bioprocess to 130 L pilot scale</b>	<b>87</b>
5.1	Abstract . . . . .	87
5.2	Introduction . . . . .	87
5.3	Results and Discussion . . . . .	89
5.4	Conclusions . . . . .	106
<b>6</b>	<b>Evaluation of <i>in-situ</i> product removal strategies to improve the productivity and economics of consolidated bioprocessing</b>	<b>107</b>

6.1	Abstract . . . . .	107
6.2	Introduction . . . . .	107
6.3	Results and Discussion . . . . .	111
6.4	Conclusion . . . . .	117
7	<b>Summary and conclusions</b>	<b>119</b>
A	<b>Supplementary material for chapter 2: Techno-economic assessment of consolidated bioprocessing of lignocellulose to ethanol at industrial scale</b>	<b>123</b>
A.1	Calculations for redimensioning . . . . .	123
A.2	Calculations GMO-based CBP . . . . .	134
A.3	Apparatus list of the base and CBP . . . . .	136
B	<b>Supplementary material for chapter 4: Set-up and validation of a rigorous, spatially resolved model of the kinetics and mass transfer limitations of consortium-based consolidated bioprocessing for ethanol production</b>	<b>140</b>
B.1	Overview of the validation of the model . . . . .	141
B.2	Matlab programming files . . . . .	142
C	<b>Supplementary material for chapter 6: Evaluation of <i>in-situ</i> product removal strategies to improve the productivity and economics of consolidated bioprocessing</b>	<b>175</b>
C.1	Calculations for CO <sub>2</sub> stripping . . . . .	175
D	<b>References</b>	<b>189</b>
E	<b>List of publications</b>	<b>205</b>
F	<b>Curriculum vitae</b>	<b>207</b>



# CHAPTER 1

---

## Introduction

---

In the framework of the Paris Agreement, 195 nations agreed on reducing the greenhouse gas (GHG) emissions in order to keep global warming below 1.5 °C compared to pre-industrial level. [20] According to simulations of the intergovernmental panel on climate change (IPCC), the 1.5 °C goal may be achieved by either a reduction of CO<sub>2</sub> emissions by 50 % - 70 % within 10 years a net negative CO<sub>2</sub> emissions below 5 Gt p.a. from 2060 onwards or by less reductions in the near future and net negative CO<sub>2</sub> emissions of 10 Gt p.a. - 20 Gt p.a. towards the end of the 21<sup>st</sup> century to compensate for the "overshoot" (Fig. 1.1 left). [1]

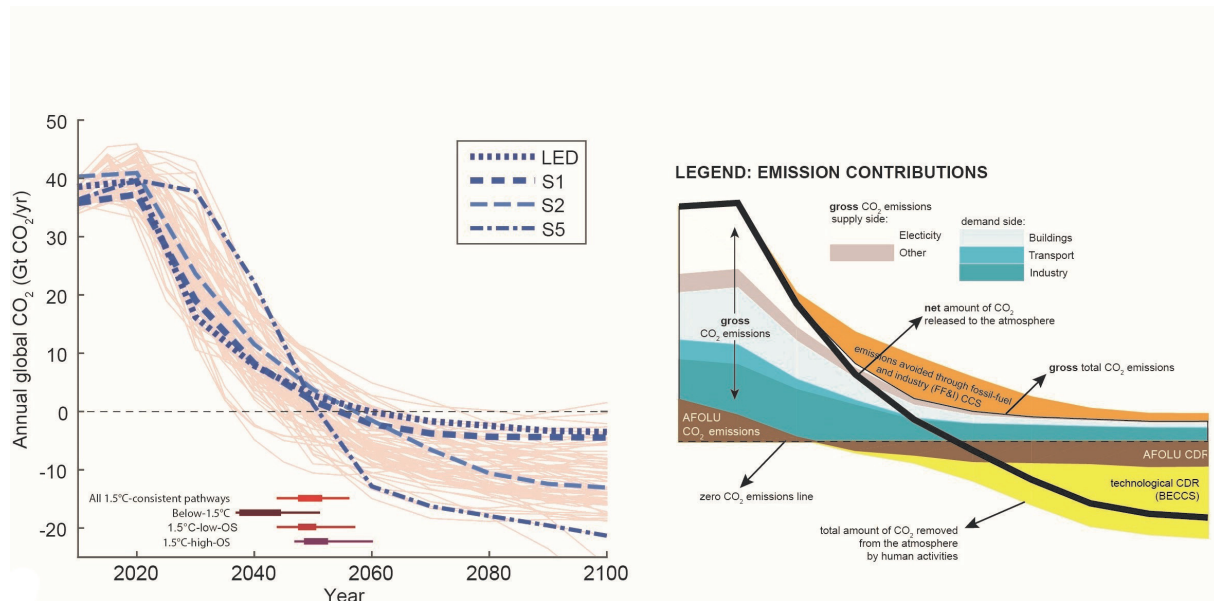


Figure 1.1: Left: The light orange lines show all emission scenarios leading to global warming below 1.5 °C relative to pre-industrial level according to IPCC models. The blue dashed, dotted and dashed-dotted lines show representative scenarios with low, medium and high overshoot in GHG emissions. Right: The scenario with medium GHG emission overshoot is decomposed into the net emissions of the sectors agriculture (brown), transport (blue), industry (turquoise), electricity buildings (white) as well as carbon capture and storage (CCS, orange & yellow), which reduces the net emissions. [1]

However, a GHG emission overshoot may kick off a cascade of self-reinforcing effects leading to a new equilibrium, the "hothouse earth", with serious disruptions to ecosystems society and economies. [20] In order to avoid these self-reinforcing effects, it is important to deploy any renewable resource in the short-term within the existing infrastructure. In the long term, the CO<sub>2</sub> saving potential of each renewable resource needs to be maximized to achieve CO<sub>2</sub> neutrality and more specifically net negative emissions.

Ethanol is a suitable example for distinguishing between short term and long term utilization: It has gained a lot of attention as a blend for biofuels despite the controversial discussion whether biofuels are a suitable way to decarbonize individual transport. [21,22] Given the fact, that in Switzerland, a 94 % fraction of the energy for the transport sector in 2019 was provided by fossil fuels, which contributes 34 % to the total fossil resource demand of Switzerland [23], ethanol as fuel blend or substitute could immediately contribute to emission reductions in the short term. However, in the long term, the concerns of using ethanol for individual transport are justified since the sustainable biomass potential in Switzerland is not even sufficient to supply aviation, cargo shipping with fuel and satisfy the Swiss chemical demand, which would lead to the largest CO<sub>2</sub> savings. [23–25] While being unsuitable as fuel for aviation or cargo shipping, ethanol is used as chemical in numerous industrial and consumer products as



intermediate of other chemicals (e.g. in the production of drugs, plastics, lacquers etc.) or as solvent (e.g. cosmetics). [26] Concluding, it can be said, that depending of its use, ethanol is an important chemical to effectively mitigate climate change by reducing GHG emissions in the short and long run. [27]

However, currently bioethanol is produced mainly from edible feedstocks (share >96 %). [28] These so-called first generation biofuels not only cause a conflict between fuel supply and food/feed issues, but they may have a non-compensable carbon footprint [29]. Lignocellulosic biomass, the most abundant resource of fixed renewable carbon in the world, serves as feedstock for second generation biofuels having a much lower or even no carbon debt compared to first generation biofuels and the conflict with the feed and food industry is avoided since it is non-edible [29,30]. The production of lignocellulosic ethanol gained attraction in the context of the “bio-based economy” strategy of several entities such as the US & the EU and has been in growth on an industrial scale since the early 2000s [31,32].

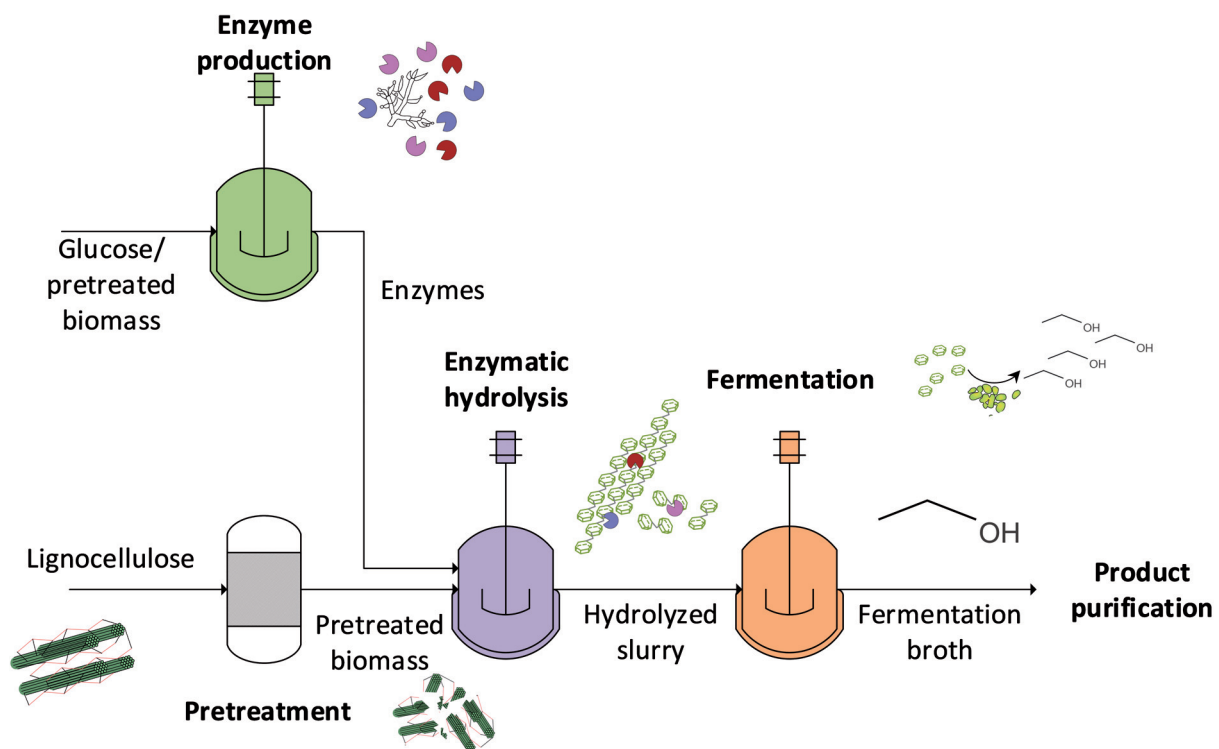


Figure 1.2: Process scheme of state-of-the-art ethanol production from lignocellulose. The lignocellulose is pretreated to break up its structure and make the cellulose fibers accessible for enzymes, which are produced by a fungus in a separate enzyme production unit. After enzymatic hydrolysis, where the polymeric cellulose is depolymerized to sugars, the slurry is sent to fermentation, where the fermenting microorganisms converts the released sugars to ethanol, which is purified afterwards. [2]

Lignocellulose is a non-edible, complex structure in the cell wall of plant biomass. [9] It consists of cellulose (40-50 %), hemicellulose (25-30 %) and lignin (15-20 %). [30] In contrast to edible carbon sources such as corn or sugar crops, lignocellulose needs to be pretreated to overcome the recalcitrance induced by the lignin and it needs to be hydrolyzed before fermentation, because the glucose molecules are covalently bonded in the  $\beta$ -(1-4) configuration (Fig. 1.2). [9] During hydrolysis, enzymes depolymerize the cellulose and release the glucose monomer (Fig. 1.2). [30] The necessary pretreatment and the hydrolysis lead to increased costs of so-called 2<sup>nd</sup> generation ethanol resulting in a competitive disadvantage compared to 1<sup>st</sup> generation ethanol from edible resources. [2,33]

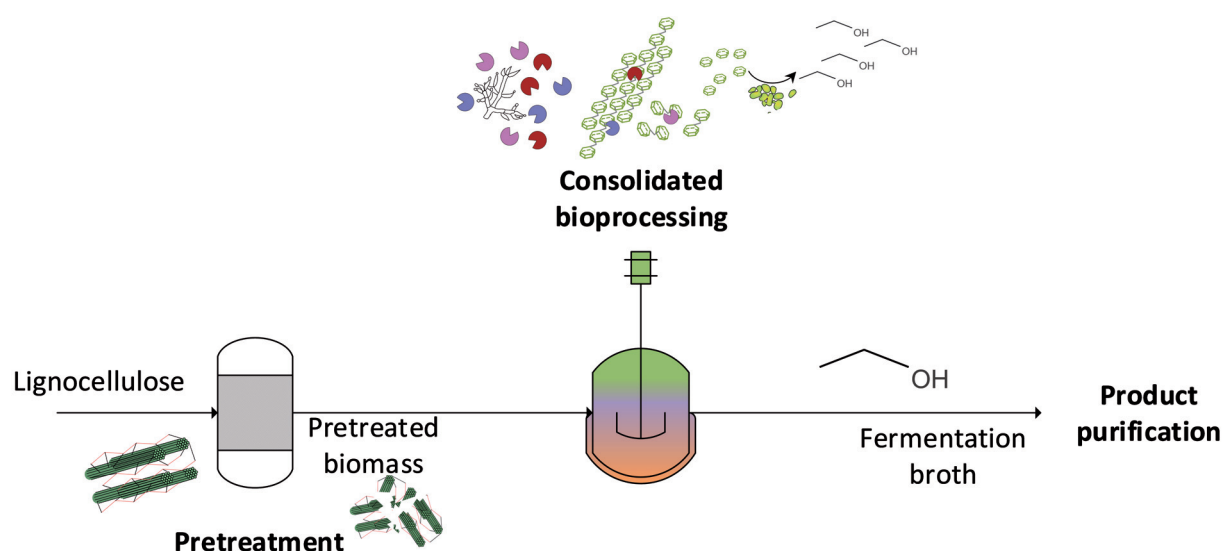


Figure 1.3: Process scheme of CBP ethanol production from lignocellulose. The pretreatment does not differ from state-of-the-art ethanol production, but enzyme production, enzymatic hydrolysis and fermentation are merged into one process step to reduce the number of apparatus and save costs. [3]

Continuously operated consolidated bioprocessing (CBP) was identified as strongest lever to reduce the processing costs of 2<sup>nd</sup> generation bioethanol in order to achieve profitable production. [33] CBP describes a highly integrated bioprocess, where enzyme production, enzymatic hydrolysis and fermentation of the released glucose to ethanol is carried out in one process step (Fig. 1.3). [4] CBP is either realized by deploying a genetically modified microorganism (GMO), which is able to do both, hydrolyzing cellulose and fermenting sugars to ethanol, in conventional bioreactors or by co-cultivating a microbial community, where the labor of hydrolysis and fermentation is divided between different species, in well-designed reactor systems with niches for each community member. [3,34]

In this work, CBP is realized based on a microbial consortium consisting of a filamentous,

cellulolytic fungus *Trichoderma reesei* and a yeast *Saccharomyces cerevisiae*, which ferments glucose. [4] The community is stabilized by biofilm formation on an aerated membrane, which results in two well-established niches (Fig. 1.4): An aerobic biofilm layer on top of the membrane, where the aerobic fungus *T. reesei* secretes enzymes for cellulose hydrolysis, and an anoxic bulk phase, where enzymatic hydrolysis happens and released glucose is fermented to ethanol by the facultative anaerobe *S. cerevisiae*. [4] This setup allows to take advantage of a stable community of robust industrial strains instead of using fragile genetically modified microorganisms [34] as well as to exploit the beneficial features of a biofilm such as higher enzyme expression of surface-attached cultures [35] or the immobilization of the microbial biomass allowing to omit the costly cell recycling processes, which are used in industry for bioprocesses with suspended cultures. [36,37]

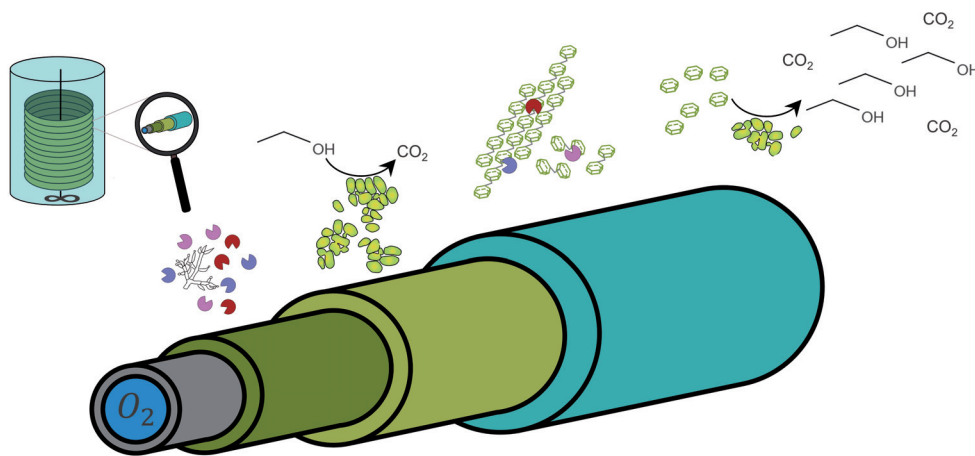


Figure 1.4: Schematic illustration of CBP based on a microbial consortium with well-established niches in a reactor system. An oxygen aerated membrane (grey tubular element) is wound in helical shape within a bioreactor (upper left corner). The oxygen (blue) diffuses across the membrane (grey) and creates an oxygen enriched layer around the membrane. The aerobic, enzyme producing fungus *T. reesei* (dark green) grows in this layer and consumes a large fraction of the oxygen. The remaining oxygen is consumed by a second layer on the biofilm (light green) consisting of yeast cells, which perform aerobic metabolism. In the anoxic bulk phase (turquoise), the cellulose is hydrolyzed by the enzymes, which diffused from the fungal biofilm layer into the bulk, and the suspended yeast cell ferment the released glucose to ethanol. A fraction of glucose diffuses back into the biofilm and feeds the aerobic fungus. [4]

This thesis is a project in the framework of the Swiss energy strategy 2050, which targets CO<sub>2</sub> neutrality and opting out of the nuclear energy program. [38] The Swiss competence center for energy research (SCCER) BIOSWEET was established to maximize the role of biomass in this energy transition. The clear objective was to bring innovative biomass conversion technologies, which can be implemented seamlessly, to the industry and with that to the market. [39] As

shown above, consortium-based consolidated bioprocessing of lignocellulose to ethanol is such an innovative conversion technology, for what reason this thesis is expected to deliver the engineering work for industrial implementation of CBP.

## 1.1 Thesis objectives

This thesis aims to pave the way for industrial implementation of consortium-based CBP in order to efficiently produce chemicals from lignocellulose and thus, maximize the CO<sub>2</sub> savings. [4] Prerequisites for industrial implementation of a process are profitability, a deep understanding of the process on an engineering level and a robust guideline for scale-up. These requirements laid the groundwork for the thesis goals, which are briefly described in the following.

1. **Techno-economic assessment of consolidated bioprocessing of lignocellulose to ethanol at industrial scale.** A techno-economic assessment of consortium-based CBP is essential as it depicts the economic potential of CBP when compared to conventional ethanol production as well as the critical process parameters in terms of costs. Furthermore, any design trade-offs during scale-up are likely to be resolved in favor of lower processing costs. A techno-economic model allows to set the ethanol selling price as optimization criterion and perform simulations with different process condition to identify the optimum conditions with the minimum selling price. The techno-economic model is presented in chapter 2.
2. **Continuous operation of a membrane aerated biofilm reactor for consortium-based consolidated bioprocessing of cellulose to ethanol.** Continuously operated CBP at steady-state conditions is beneficial in various aspects such as lower costs due to reduced downtimes or potentially higher productivity since product and substrate inhibition are avoided or at least effectively reduced. However, the continuous operation of consortium-based CBP was never proven at laboratory scale. Continuous CBP experiments were conducted within this project for two purposes: First, as proof-of-concept that the microbial consortium can be maintained at a productive state during continuous operation and second, the experimental results of the continuous steady-state were used to fit and validate the process model because they are time-invariant. Batch data is dominated by growth dynamics, which strongly depend on the given initial conditions and thus, useless for the process model. However, continuously operated consolidated bioprocessing is challenging: An insoluble substrate needs to be fed continuously and homogeneously, wash-out of enzymes has to be avoided and stable population equilibria of the microbial

community members must be obtained. Chapter 3 discusses the design adjustments of the experimental setup for continuous operation and the respective results.

3. **Development and validation of a rigorous, spatially resolved model of the kinetics and mass transfer limitations of consortium-based consolidated bioprocessing for ethanol production.** The development and validation of a rigorous process model provides the above-mentioned and needed understanding of CBP from an engineering level, which is the prerequisite for successful scale-up. Both, the kinetics and the mass transfer limitations of CBP differ considerably from suspended cultures for separate enzyme production, hydrolysis and fermentation. This is due to the interaction of the microbial community members, the heterogeneous reactor layout with the different niches and the different aeration technique (membrane diffusion vs. bubble aeration). The process model is presented in chapter 4.
4. **Scale-up of 2.7 L laboratory scale consortium-based consolidated bioprocessing to 130 L pilot scale.** Based on the findings above, the economics of the process, the knowledge, how to operate the system continuously, and the rigorous model, the scale-up from 2.7 L laboratory scale to 130 L pilot scale was designed. Critical scale-up parameters were identified by a classic approach of non-dimensionalizing the system. The optimization for the critical parameters was done with the help of the process model as calculation basis and the techno-economic model as optimization criterion for the lowest costs. A pending experiment at pilot scale should serve as proof of concept that the rigorous process model is scale-invariant and provides a robust scale-up guideline when combined with the classic similarity approach based on non-dimensionalizing the problem. The scale-up calculations are found in chapter 5.
5. **Evaluation of *in-situ* product removal strategies to improve the productivity and economics of consolidated bioprocessing.** *In-situ* product removal seems to be a promising upgrade for consolidated bioprocessing of ethanol since rate-controlled separation techniques bypass the unfavorable equilibrium of low ethanol titers in the bulk of the CBP unit. Furthermore, ethanol losses due to degradation in the biofilm could be minimized by *in-situ* product removal and one option to perform *in-situ* product removal, the membrane, is already installed in the reactor. A detailed overview of different product removal strategies is given and their applicability for CBP is discussed in chapter 6.



## CHAPTER 2

---

### **Techno-economic assessment of consolidated bioprocessing of lignocellulose to ethanol at industrial scale**

---

#### **2.1 Abstract**

Lignocellulose-based biofuels are of major importance to mitigate the impact of international traffic and transport on climate change while sustaining agricultural land for food supply. Highly integrated systems like consolidated bioprocessing (CBP), where enzyme production, enzymatic hydrolysis and fermentation of the released sugars are carried out in one reactor, offer the highest potential to save costs and to make lignocellulose-based biofuels economically competitive. The work described here showed that CBP based on a microbial consortium operated at full-scale (2,000 *t/d*) saves up to 27.5 % of the total ethanol production costs compared to conventional ethanol production from lignocellulose in individual process steps. The cost savings are mainly achieved through lower capital expenditures (CAPEX) due to less apparatus requirements because of the integrated process, as well as through lower operating expenditures (OPEX) since no glucose is needed for enzyme production. A comparison with literature estimations of cost savings of CBP based on genetically modified microorganisms results in approximately the same range. As a result of a detailed sensitivity analysis, scale and yield were identified as the main cost-pushers from a process point of view, whereas the price level of the plant location has the highest impact on the investment conditions. In the EU, CBP yields enough margin for profitable production and the possibility to decentralize biomass valorization, whereas in the world's largest ethanol market, the US, profitable production of lignocellulosic ethanol can only be achieved by CBP combined with other cost saving techniques, such as utilization of cost-free waste feedstocks, since ethanol has undergone a considerable price slump.

This chapter is based on published work (without any permission needed): D. Dempfle, O. Kröcher, M. H. Studer *Techno-economic assessment of bioethanol production from lignocellulose by consortium-based consolidated bioprocessing at industrial scale*. *New Biotechnology*, 65 (2021) 53–60, doi: 10.1016/j.nbt.2021.07.005

## 2.2 Introduction

According to the international energy outlook 2020 of the US Energy Information Administration the world's energy consumption for transportation will continue to increase at an average annual rate of  $1.3 \pm 0.2$  %, leading to a projected total consumption of roughly 290 *Exajoule* (EJ) in 2050, which is mainly driven by a doubled energy demand in non-OECD countries in 2050 compared to 2018 [40]. The expected share of electrical power supply in the light duty transportation sector will not exceed 30 % until 2050 and will remain negligible in the heavy duty transportation sector (<1 % in 2040) due to several drawbacks such as low energy density and limited storage possibilities [41–43]. If these 290 EJ were to be provided by fossil fuels, the average world temperature would increase by about 6 °C, or 4 °C above the limit of the Paris agreement reached by the UN Framework Convention on Climate Change in 2015 [44]. Models based on the 2 °C International Energy Agency Technology Perspective claim that 12, 25 and 38 % of the world's transportation energy must be provided by liquid biofuels in 2030, 2050 and 2075, respectively [42,45].

As the predominant liquid biofuel, bioethanol plays a major role as reactant for heavy duty transport fuel additives or as fuel for adapted light duty vehicles [21,46]. However, currently bioethanol is produced mainly from edible feedstocks (share >96 %) [28]. These so-called first generation biofuels not only cause a conflict between fuel supply and food/feed issues, but they may have a non-compensable carbon footprint [29]. Lignocellulosic biomass, the most abundant resource of fixed renewable carbon in the world, serves as feedstock for second generation biofuels having a much lower or even no carbon debt compared to first generation biofuels and the conflict with the feed and food industry is avoided since it is non-edible [29,30]. The production of lignocellulosic ethanol gained attraction in the context of the “bio-based economy” vision and has been in growth on an industrial scale since the early 2000s [31,32]. Policy makers aim to further incentivize the use of lignocellulose, as was done by the US government with the “Second generation biofuel producer tax credit”, which expired by the end of 2021. [47] The EU set a target of a 3.5 % share of second generation biofuels in the transport sector by 2030 with an intermediate milestone of a 1 % share in 2025 in the framework of the Renewable Energy Directive II [28].



State-of-the-art lignocellulosic bioethanol production is carried out in the following process steps (Fig. 2.1a). The raw feedstock is pretreated mechanically (e.g. chipping) to reduce the particle size and physiochemically (e.g. steam pretreatment or dilute acid pretreatment) to break up the entanglement between cellulose, hemicellulose and lignin and to make the poly-sugars accessible to enzymes [30,48]. The facilitated accessibility of the cellulose fibers increases the yield and rate of hydrolysis by a factor of 3-10 [49]. The pretreated biomass is conditioned to adjust pH and temperature for enzymatic hydrolysis. A washing step to reduce the concentration of inhibitors formed during the pretreatment is not mandatory since the abilities of white rot fungi to detoxify the fermentation broth are well-known [50]. The hydrolytic enzymes are either produced in a separate aerobic fed-batch culture or purchased from an external vendor. The sugars released by enzymatic hydrolysis are fermented in a subsequent step. Finally, the solids and the major part of the water is removed in a first distillation column (beer tower) and anhydrous ethanol is obtained from rectification in a second distillation column usually followed by dehydration using molecular sieves. Lignocellulosic bioethanol is currently more expensive than ethanol from sugar crops or corn despite the cheaper raw material price per unit mass of feedstock. This is due to: [3,30,31,51]

- Lower concentration of carbohydrates in the feedstock leading to lower final ethanol concentrations
- Lower conversion rates of lignocellulosic feedstocks leading to larger vessels and with that higher capital costs
- The necessity of an elaborate pretreatment

In 2008, the hypothesis was proposed that lignocellulosic ethanol will become cheaper than ethanol produced from corn or sugar crops as a result of improved technology due to maturing of the process [3]. Improvements by integration of several process steps were identified as the strongest levers to reduce processing costs, which is not only true for biotechnology but for chemical engineering in general [52]. The highest degree of process integration for bio-ethanol production is achieved by consolidated bioprocessing (CBP), where enzymatic hydrolysis, enzyme production and fermentation are performed in a single process step (Fig. 2.1b).

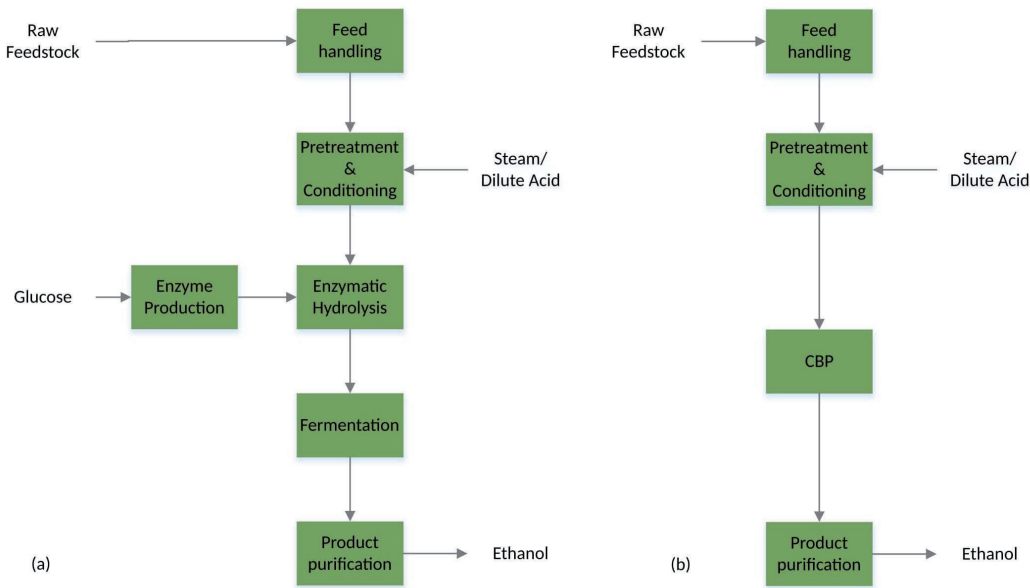


Figure 2.1: Simplified process flow diagrams for the production of lignocellulosic bioethanol employing separate hydrolysis and fermentation (a) and consolidated bioprocessing (CBP) (b). The recalcitrance of lignocellulose is overcome by a physicochemical pretreatment. After the pretreatment, pH, temperature and pressure are conditioned for enzymatic hydrolysis and CBP, respectively. In the case of conventional production, the enzymes are produced by a fungus using glucose as carbon source in a separate reactor system. During enzymatic hydrolysis, the cellulose is converted to glucose. The hydrolyzed slurry is sent to the fermentation, where the sugars are fermented to ethanol. In the case of CBP, enzyme production, hydrolysis and fermentation are carried out in the same vessel. Finally, the ethanol is recovered from the product stream by distillation and adsorption.

The enzyme production and the fermentation can be carried out simultaneously either with a single culture of a genetically modified microorganism or with a community of industrial, microbial strains [34]. A single culture strategy (hereafter termed GMO-based CBP) must employ a genetically modified microorganism, since no known natural strain is able to hydrolyze cellulosic substrates and to ferment the released sugars exclusively to the desired target product ethanol. In contrast, in a microbial community the task of hydrolysis and fermentation is divided and assigned to single strains, which are co-cultivated to act synergistically as consortium, with each community member having its own stable niche in the reactor [53,54]. Such a system, hereafter named consortium-based CBP, has been deployed by developing a suitable reactor design and co-cultivating a stable microbial community of a cellulolytic fungus and ethanolytic yeast [4]. Oxygen is fed through a membrane to the otherwise anaerobic reactor to introduce a stable oxygen gradient into the system, which provides an aerobic niche for the cellulolytic strain *T. reesei*. The fungus forms a biofilm on top of the membrane in the oxygen-enriched layer, while the fermenting strain, *S. cerevisiae*, grows suspended in the

anaerobic fermentation broth [4].

Considering a GMO-based CBP approach, cost savings of up to 41 % of the processing costs of lignocellulosic ethanol have been reported [3]. However, imposed metabolic burden, cytosolic or periplasmic space limitations, competing biochemical reactions and toxic intermediates limit the implementation possibilities of GMOs and yield poor fermentation performance. Therefore, complex tasks are distributed in nature either within subcellular compartments or between different microorganisms [53]. In a microbial community designed for synergistic division of labor, where each species has its own well-designed niche and a very specific task, complex biotransformations can be carried out in a stable and robust manner [34,55,56].

This work aims to investigate the cost savings of the consortium-based CBP approach compared to conventional bioethanol production from lignocellulose (separate hydrolysis and fermentation) and to GMO-based CBP. Furthermore, a sensitivity analysis of the profitability as a function of scale, feedstock price, yield, residence time, cost of capital and price level of the country is carried out to investigate the commercial potential of bioethanol production from lignocellulosic feedstocks via consortium-based CBP in the light of the current ethanol market situation.

## 2.3 Materials & Methods

### *Base case conventional bioethanol production from lignocellulose*

The most recent process design and economics of lignocellulose-to-ethanol conversion at a scale of 2,000 dry tons per year throughput published by the NREL was used as base case for the techno-economic analysis (hereinafter referred to as “base case”) [2]. A MESP of 57 ¢/annual L ethanol results from the total processing costs and the cost of capital per year apportioned to the annual production of ethanol. All cost data of the base case refers to 2007 and the US.

### *Process parameters of the consortium-based CBP*

Feedstock properties, ethanol titer and yield were assumed to be the same as in the base case in order to calculate the net savings by using CBP. The pretreatment was changed to a pure steam pretreatment instead of a dilute acid-catalyzed steam pretreatment used in the base case, because previous studies have successfully shown that steam-pretreated lignocellulose can be converted by consortium-based CBP and the CBP parameters are based on the available experimentally derived data with steam gun pretreatment [50,57,58]. The necessary, specific membrane surface was set to 10 m<sup>2</sup>/m<sup>3</sup>. The temperature of the CBP unit was set to 28 °C in favor of enzyme production to maximize the enzyme concentration, since the temperature

dependence of the activity per enzyme unit following the Arrhenius law is negligible in the temperature band where the cultivated microorganisms grow ( 27-32 °C) [4,59].

#### *Cost estimations*

Apparatus costs were either taken from the base case, from the previous NREL report of 2002 or by using well-accepted cost functions from the literature [60–63]. Any calculations, mass and energy balances as well as adapting cost values, were performed with Microsoft Excel®. Cost data for the same equipment at different scales were converted according to equation 2.1 with the help of a size exponent  $n$  taken either from the NREL base case or literature (Supplementary material A.2) [2,60–63]:

$$\left( \frac{\text{size equipment}_i}{\text{size equipment}_j} \right)^n = \frac{\text{cost equipment}_i}{\text{cost equipment}_j} \quad (2.1)$$

Unless otherwise stated, all equipment sizes are directly proportional to the volumetric flow. Installation factors were used to derive the installed costs, which include piping, armatures and sensors, from the equipment costs [2,60–63]. The calculation of the CAPEX proceeding from the apparatus costs was done according to the base case. The OPEX were subdivided into variable and fixed OPEX. The variable OPEX denote the costs for the consumables (mainly chemicals) and the feedstock. The costs per unit of consumable or feedstock were assumed to be the same as in the base case. The fixed OPEX consist of labor cost, maintenance, property insurance and tax. The same labor costs per worker are assumed as in the base case. All other fixed OPEX scale linearly with CAPEX and were calculated with the new CAPEX data according to the base case.

All costs are expressed either in absolute terms (US\$) or in annual costs divided by the annual ethanol production (¢/annual L ethanol). The chemical engineering plant cost index (CEPCI) was used to convert cost data from different years. Comparisons with the NREL base case were performed with a CEPCI from 2007, the reference year of the NREL base case. The sensitivity analysis is based on a CEPCI from 2019 in order to discuss the results with respect to the current situation in the ethanol market. Apart from re-dimensioning the apparatus (eq. 2.1), all cost calculations as well as the CEPCI are linear. Thus, the cost savings of each apparatus could also have been evaluated with the CEPCI of 2019. However, since single apparatus may differ strongly from the general cost trends, it was decided to retain the cost calculations for single apparatus as close as possible to the base case and convert the overall results, where single outliers are likely to be cancelled out, with the help of the CEPCI.

## 2.4 Results and discussion

### *Cost savings through consortium-based CBP with steam pretreatment*

The process economics of ethanol production of lignocellulose reported by NREL serve as the base case to determine the saved costs by CBP (process scheme in Fig. 2.1a). [2] This section presents the cost savings of the different process steps, re-dimensioning of individual apparatus may be found in the Supplementary material A.1. The throughput of 2,000 dry *tons* of corn stover per day as feedstock, which are converted to 231 *million L* of ethanol per year was kept constant as the same yield range could be confirmed experimentally with CBP [4]. The costs for feedstock acquisition and handling were also kept constant. The pretreatment of the corn stover was changed from dilute acid-catalyzed steam pretreatment to pure steam pretreatment. This increased CAPEX, since the apparatus must withstand higher pressures necessary in a pure steam pretreatment. Variable OPEX are saved due to the substantially reduced need for chemicals (acid for the pretreatment and base for conditioning). Applying CBP through merging enzyme production, hydrolysis and fermentation in one process step saves CAPEX due to a reduced number of apparatus for hydrolysis and fermentation, as well as to the omission of the enzyme production unit. Variable OPEX are mainly saved by leaving off the use of glucose for enzyme production as the enzymes are produced in situ consuming carbon from the feedstock. The cellulose-to-ethanol yield in the CBP case was adjusted to 76 % in order to be the same as in the base [4]. Despite the fact that even small changes in yield might have considerable impact on the process economics, this adjustment was made to ensure comparability given the uncertainty of different operation modes (batch vs. continuous), substrates (corn stover vs. pure cellulose), resources for enzyme-production (in-situ vs. ex-situ) and maturity levels of the technologies. The ethanol rectification, dehydration and storage do not undergo appreciable changes. However, due to the considerably reduced salt concentration in the fermentation slurry as result of the changed pretreatment technique, a much larger fraction of the residues can be sent to combustion. This causes a net increase of CAPEX, since the increased CAPEX of an up-scaled combustor overcompensates the reduced CAPEX for a smaller wastewater treatment unit and the saved CAPEX because of flue gas desulfurization (FGD) may be omitted. The larger combustion unit produces a higher amount of excess electricity, which generates by-product revenues by selling it to the grid. These extra by-product revenues cause substantial OPEX savings compared to the base case.

To conclude, the CAPEX for a cellulosic ethanol production facility based on CBP increase by 4.77 % despite considerable savings by removing the enzyme production unit (A 400) completely (Fig. 2.2). The increase is mainly caused by the high apparatus costs for the larger combustor and boiler and the additional evaporators in the purification unit for the separation of process water and the solid residues after fermentation (A 500). Applying the base case

financing parameters (plant lifetime, equity share, interest rates on equity and debts, etc.), a capital recovery charge of 25.17 ¢/annual *L* ethanol over the lifetime of the plant instead of 24.02 ¢/annual *L* ethanol is obtained. The total variable OPEX per annual *L* ethanol for CBP amount to 13.86 ¢/annual *L* ethanol instead of 28.46 ¢/annual *L* ethanol in the base case, which corresponds to a reduction of 51.4 % (Fig. 2.2). 57.0 % of the OPEX savings result from the change in pretreatment (less use of chemicals and better valorization of the residuals due to lower salt concentrations) and 43 % come from applying CBP (omitting the need for glucose supply for enzyme production). The fixed OPEX are slightly reduced to 1.78 ¢/annual *L* ethanol, which corresponds to a reduction of 12.5 % (Fig. 2.2) The CAPEX-related fixed OPEX (e.g. insurance and maintenance) increase proportionally with the CAPEX, whereas labor costs are saved due the reduced number of process steps.

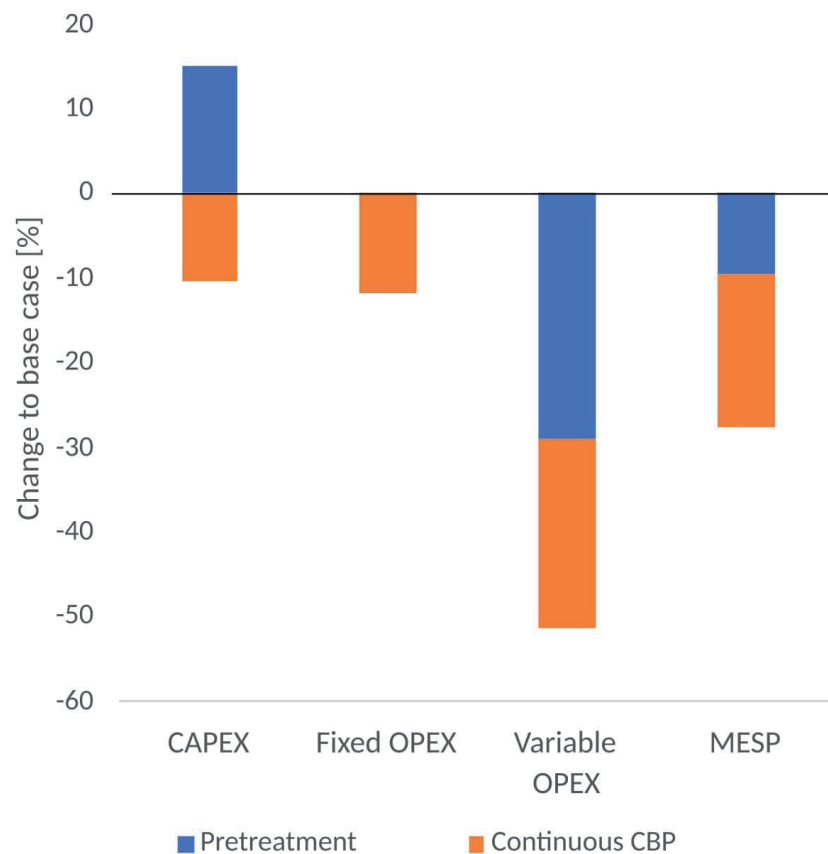


Figure 2.2: Relative cost savings of consortium-based CBP compared to the base case for CAPEX, fixed and variable OPEX and the resulting MESP. CBP leads to savings in CAPEX, fixed and variable OPEX. The change in pretreatment increases the CAPEX but reduces the variable OPEX. The fixed OPEX are almost not affected by the pretreatment. The resulting MESP is reduced by 27.5 % compared to the base case due to the change in pretreatment and implementation of consortium-based CBP.

The resulting minimum ethanol selling price (MESP) can be reduced from 56.80 ¢/annual *L* ethanol to 41.22 ¢/annual *L* ethanol (reduction of 27.5 %) (Fig. 2.3). According to CME Group (Chicago, US), one of the largest option exchange companies in the world, the average ethanol price in 2007 was 52.30 ¢/L ethanol showing an attractive producer surplus in the case of consortium-based CBP, whereas the base case is not profitable under the given conditions [5].

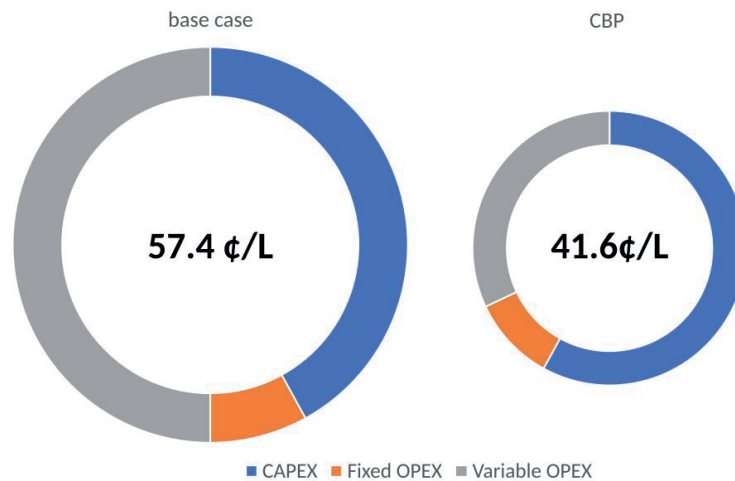


Figure 2.3: Share of CAPEX, fixed and variable OPEX of the MESP for the base case and the CBP scenario.

#### *Sensitivity analysis of the cost savings through consortium-based CBP*

In contrast to 2007, in 2019 the US MESP, including the cost savings achieved by CBP, was with 41.60 ¢/annual *L* ethanol higher than the average US price of ethanol, which amounted to only 36.75 ¢/L ethanol [5]. Despite fluctuations, the US ethanol price has decreased since 2007 on average by 3.9 % per year, while the costs for chemical plants, represented by the CEPCI, have increased by 16.0 % over the same period (Fig.2.4) [5].



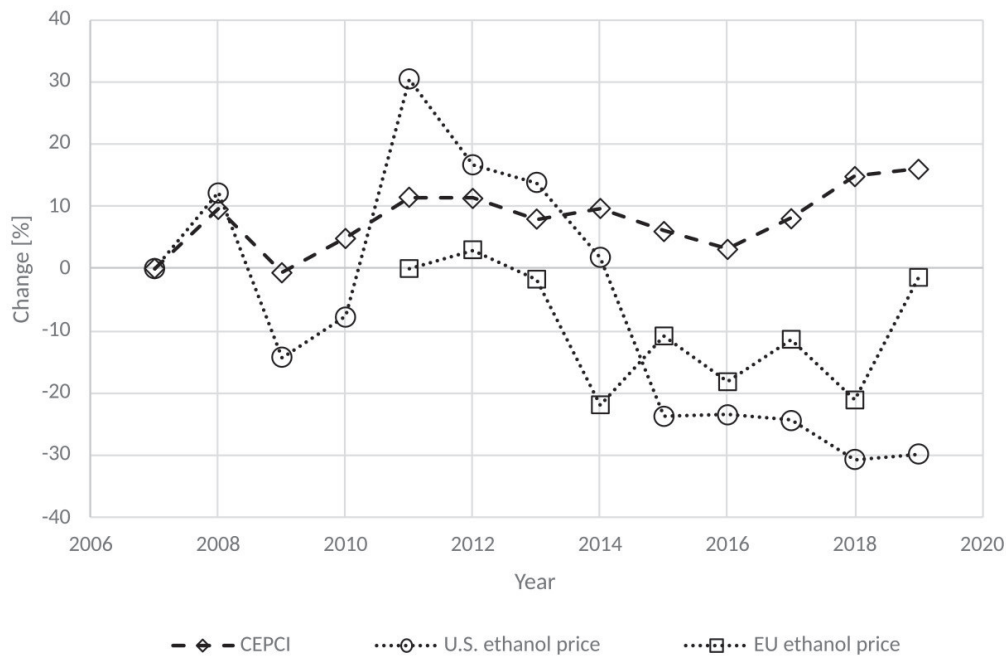


Figure 2.4: Development of the ethanol prices in the US and the EU compared to the costs for chemical plants represented by the CEPCI. From 2007 to 2019, the US ethanol price decreased by 30% [5], whereas the costs for chemical plants increased by 16%. For the EU ethanol price (domestic ethanol, FoB Rotterdam), data is available from 2011 to 2019 [6]. After a few years with lower price, the price level in 2019 stabilized around the same level as between 2011 and 2013.

CBP per se does not enable profitable bioethanol production from lignocellulose in the US nowadays. A sensitivity analysis of the MESP for several process parameters (scale, titer, yield, residence time) and investment parameters (feedstock price, price level in the country of the plant location, costs of capital) was conducted to investigate (a) necessary improvements of the process from an engineering point of view and (b) investment conditions, which allow profitable bioethanol production while still being interesting for shareholders (Fig. 2.5). In contrast to the base case, the total costs of the CBP scenario are dominated by the CAPEX (58 % vs. 42 % of MESP) as a result of the significant reduction of the variable OPEX (32 % vs. 50 % of MESP) (Fig. 2.3) by CBP. Thus, process/investment parameters affecting the CAPEX tend to be more relevant.

The MESP increases exponentially with a reduction in throughput (Fig. 2.5a), implying that the MESP is almost inelastic with varying scale above 50 and up to 120 % of the base case scale. For plants with a size below 10 % of the base case, the total costs tend to remain constant independent of the throughput. To calculate the MESP at different production scales, CAPEX and fixed OPEX were scaled with the weighted size exponent (Supplementary material A.1),



whereas the variable OPEX per  $L$  ethanol were kept constant. For scales below 10 % of the base case (i.e. <200 dry *tons* feedstock per day), a simple scaling with a size exponent was no longer applicable, since significant design adjustments to the process were economically favorable and/or technically necessary, such as omitting the combustion unit in order to operate the wastewater treatment at reasonable scales. A detailed listing of the design adjustments can be found in the Supplementary material A.1 and A.3. Given these calculations of the MESP at different scales, the exponential dependence is caused by the scaling of the CAPEX with the weighted size exponent. Since its overall value for the whole plant (between 10 % and 120 % of the base case scale) is 0.63 (Supplementary material A.1 and A.3), which is considerably lower than 1, strong economies of scale effects yield a high MESP sensitivity at lower scales. The economies of scale, and thus the MESP sensitivity, are further increased by synergies, such as production of process steam and electricity revenues due to lignin valorization as well as utilities, common facilities etc. working to capacity, which minimizes the specific costs at large scales. Above 50 % of the base case scale, i.e. 1,000 dry  $t/day$ , the economies of scale including all synergies seem to be fully exploited causing the low sensitivity. Below 10 % of the base case scale, economies of scale cannot be exploited further, resulting in almost constant equipment costs resulting in the tremendous increase of the MESP. The discontinuities in the curve below 10 % result from the necessary adaptation of the process layout mentioned above. Additionally, but less important, scale positively affects the variable OPEX, since the relative transport costs for the feedstock increase (Supplementary material A.1). It is not possible to match the ethanol US market price by only varying the scale of the plant.

The MESP also decreases exponentially with the obtained titer (calculations in Supplementary material A.1). The curvature is less remarkable than with throughput, but leading to high MESP sensitivities below 3 wt.% titer and almost inelastic MESP behavior above 4 wt.% (Fig. 2.5b). Thus, the calculations confirm literature stating that a minimum titer of 3-4 wt.% marks a threshold for any biofuel production process using distillation as part of the product purification [64]. The strong curvature results from the fact that distillation processes are rather inefficient from an exergetic point of view. The number of stages remains almost constant over varying titer (between 0.5 and 10  $\frac{g}{L}$ ) (cf. McCabe-Thiele diagram for ethanol water mixtures), but the reflux ratio and thus the energy demand of the rectification column strongly increases at low concentrations [65,66]. The final concentration offers no possibility of approaching the US ethanol market price.

The parameters of residence time, feedstock price, purchasing power parity (PPP) and the capital charge rate are all positively and linearly related to the MESP, while yield is negatively correlated. However, the different parameter sensitivity curves show vast differences in the constant of proportionality (Fig. 2.5c-g). The residence time has by far the lowest proportionality factor (calculations in Supplementary material A.1), causing +4/-2 % MESP by doubling/halving the residence time (Fig. 2.5d). The residence time affects only the CAPEX share of the hydrolysis and fermentation unit A 300, which is rather irrelevant due to the CBP savings.

The yield influences the MESP considerably more strongly (Fig. 2.5c): a 10 % difference in yield changes the MESP by around 5 ¢/L ethanol (calculations in Supplementary material A.1). Higher yields cause a lower MESP due to lower feedstock costs since an increased yield would save a certain amount of feedstock per unit product. From a mathematical point of view, this leads to the same result as if the original feed stock amount was purchased at a lower price per feedstock unit (neglecting very minor changes to the apparatus). Since the feedstock price has a significant influence on the MESP (ca. 30 %), the yield is also relevant. However, despite its significant impact, yield improvements do not lead to profitable production in the US since the yield is already at a high level (76 %).

Feedstock price, PPP and capital charge rate have a comparable, positively correlated, linear influence on the MESP, since they cause a MESP variation width of ca. 55 ¢/L ethanol in the observed range (Fig. 2.5e-g). Since neither the feedstock price, nor the PPP or the capital charge rate affect the sizing of specific apparatus, no size exponent is used and the MESP sensitivity towards these parameters appears linear. The feedstock price has a direct impact on the raw materials' share of the variable OPEX. The PPP is used as an indicator to compare price levels in different countries by denoting the costs of a defined basket of representative goods in a specific country. The PPP of the US is chosen as reference and set to 100 % [66]. It only affects all costs associated with work and with variable OPEX, since a large fraction of the variable OPEX consists of locally traded raw materials such as the feedstock amongst others. The capital charge rate is the return required on invested capital. It is defined by the interest rate on debt capital and the return on equity, as well as the fraction of debt capital and equity, and thus affects the total CAPEX instead of single apparatus/units. Only variations of the PPP and the capital charge rate allow the US market price of ethanol to be met, whereas scale, yield and feedstock price only approach close to the market price. Varying titer and residence time does not allow the market price to be approached substantially.

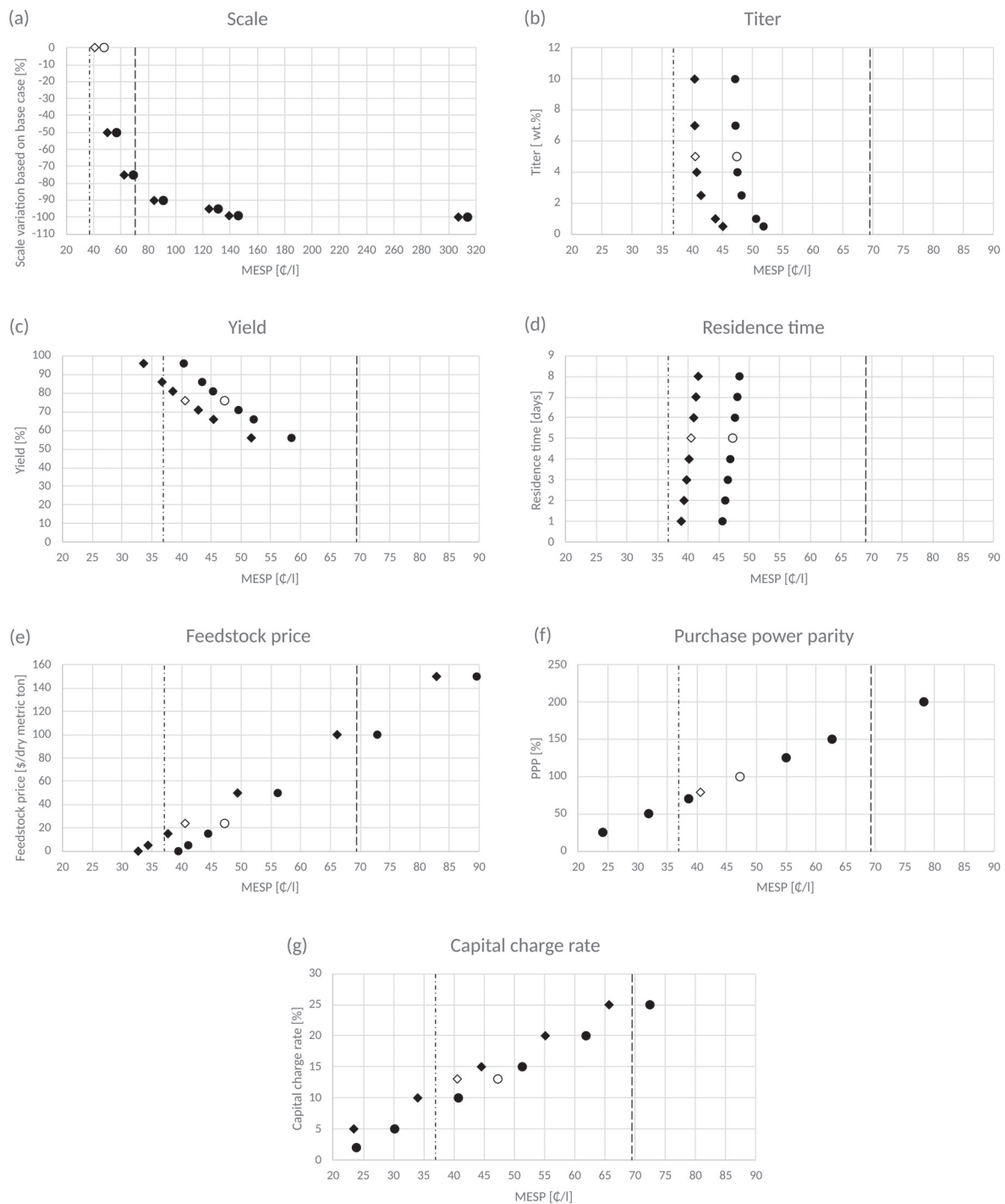


Figure 2.5: Sensitivity analysis for (a) scale [% of base case feedstock consumption], (b) titer [wt.%], (c) yield [%], (d) residence time [days], (e) feedstock costs [\$/dry metric ton], (f) purchasing power parity [% rel. to US] and (g) capital charge rate [%]. The results for the base case, including the cost savings by employing CBP, are represented by open markers in each case, whereas the filled markers denote the variation of the specific parameter. Circular markers show the US MESP and rhombic markers show the EU MESP. The dashed-dotted lines represent the average ethanol stock exchange price in the US in 2019 of 36.75 ¢/L [5]. The dotted line represents the 2019 EU ethanol price (T2 FOB Rotterdam) [6]. Flat curves denote a high variation of the MESP with little variation of the specific parameter and thus, a high cost sensitivity. These parameters are targeted to shift the MESP (rhombic and circular markers) to the left of the dashed-dotted and dashed line, respectively, in order to meet the market price in the respective region.

In contrast to the US, the situation in the EU appears to be much less restricted. The lower PPP in the EU (78 % of the US currency-adjusted [67]) yields an MESP reduction of 6.75 ¢/L ethanol (open rhombic marker in Fig. 2.5f). Furthermore, ethanol T2 (i.e. of domestic European origin) FOB Rotterdam, NL, has a market price of 69.40 ¢/L ethanol (dashed lines in Figure 2.5) [6]. Thus, the CBP base case is profitable in the EU (see open rhombic markers in Fig. 2.5). This allows either to decrease the size of the plant to 15 % of the base case size offering the possibility to valorize local biomass decentrally, which is important since plants with a throughput of 2000 dry *tons* feedstock per day are not feasible in Europe given the less centralized agricultural industry. Furthermore, beneficial economics give margin to imperfect process conditions or fluctuations of the feedstock price (filled rhombic markers and dashed lines in Fig. 2.5). With CBP at base case conditions, up to 30 % total return to shareholders (TRS) may be expected (Fig. 2.5f) meaning that applying CBP offers the potential to outperform the average TRS (24.0 %) of the chemical industry [68].

However, recalling that the US ethanol demand is ten times higher than that in the EU [28], it is worth showing profitable scenarios for the US with its much more competitive market environment. Under the given conditions, the only possible approaches to reduce the MESP to the US market price are (i) receiving the feedstock at negative costs (e.g. by utilizing waste feedstocks), (ii) to develop a business plan with much lower return on equity (assuming, that interest rates on debt stay constant), or (iii) production in a country with a lower price level. Considering a shift to waste feedstocks (e.g. solid manure), which could be obtained for free or at negative prices, it might be challenging to maintain the total costs and the amount of annually produced ethanol (e.g. due to abrasive wear as consequence of the high sand loading, which is not yet investigated). In case the use of corn stover as feedstock is required, price levels, which are low enough for the MESP to meet the stock exchange price, may be found in China, Ukraine, India, Indonesia and Russia among the largest corn producing countries [67,69]. However, outsourcing second generation bioethanol production to countries with low price levels appears to be a missed opportunity both for exploiting valuable biomass potential in the US and stimulating the economy in their rural areas.

Other options for a profitable process include increasing the local ethanol price at the production site to levels above the world stock exchange price (e.g. due to tariff barriers or if regional production has a market value) or benefiting from an added-value through sustainable production. Alternatively, lower costs of capital or fiscal incentives such as CO<sub>2</sub> taxes/compensations or fuel tax exemptions for bioethanol may also enable profitable production.

#### *Comparison of cost savings with GMO-based CBP*

Another economic study using GMO-based CBP for bioethanol production [3] reports 41 % cost savings, which are considerably higher than those of 19 % coming from the use of consortium-based CBP presented in this work. Slightly different input parameters were used

in [50] compared to the NREL base case and this scenario, i.e. costs of capital, scale, titer, yield and residence time and the pretreatment method.

In order to compare savings between GMO-based CBP and consortium-based CBP, the process conditions were levelled to base case conditions (Supplementary material A.2). By these adjustments, cost savings of around 20 % result for both variants of CBP, which can be considered identical given the uncertainty (+/- 30 %) of such early-stage cost estimations. [70] Thus, this work supports the conclusion that CBP is the strongest lever to reduce the costs of ethanol production from lignocellulose from a process point of view. [3] Cost savings in the production of cellulosic ethanol are urgently needed given the fact that several full-scale plants are currently either shut down or do not operate at full capacity because of profitability issues amongst others. [71–74]

## 2.5 Conclusion

The presented calculations have shown that hypothetically, consortium-based CBP with steam pretreatment can save up to 27.5 % of the total costs compared to conventional bioethanol production from lignocellulose, which is in the same range as published data on GMO-based CBP. However, even though CBP accounts for the strongest lever to reduce processing costs, per se it does not enable a competitive lignocellulosic ethanol production today. In the EU, the high ethanol market price combined with the low production costs when applying CBP offers a sufficient margin for profitable production or the possibility to decrease the plant size to 15 % and thus decentralize the biomass valorization. However, in the US where 56.2 % of the world's ethanol is currently consumed, the ethanol market is much more competitive. From 2007 to 2019, the ethanol price dropped by 31 % while the average CAPEX increased by 16 %, resulting in a strong competitive pressure for lignocellulosic bioethanol. A cost sensitivity analysis of several process parameters (scale, titer, yield and residence time) and investment parameters (feedstock price, price level in the country of the plant location and costs of capital) show that scale and yield are the main cost-pushers from a process point of view, whereas the price level of the plant location has the highest impact on the investment conditions. Since outsourcing second generation bioethanol production to third world countries with low price levels leaves valuable biomass potential unused and hinders economic growth in rural areas, it should be aimed at meeting the current ethanol market price by taking advantage of the cost levers of multiple process and/or investment parameters if necessary, such as utilizing cheaper waste feedstocks at comparable yields and reducing the costs of capital by accepting lower returns on equity. Alternatively, exploiting the added-value through sustainable production as well as local market disparities such as tariff barriers or tax exemptions may lead to profitable production of lignocellulosic bioethanol. In the short term, retrofitting of depreciated existing

corn ethanol plants to CBP operation, might be an interesting approach to reduce the CAPEX in order to meet the world market price of ethanol with lignocellulosic ethanol. Besides the recommendations for implementation of CBP at industrial scale, the presented model will serve as optimization criterion for under- and overspecified problems during scale-up (section 5) in order to resolve these constraints in favor of the lowest costs.

## CHAPTER 3

---

### Continuous operation of a membrane aerated biofilm reactor for consortium-based consolidated bioprocessing of cellulose to ethanol

---

#### 3.1 Abstract

A robust design for the conduction of continuous consolidated bioprocessing is of central importance: First, the techno-economic assessment demonstrated the considerable cost savings when CBP is operated continuously. Second, continuous steady-state operation is time-invariant and thus, allows to fit and validate a rigorous process model, the centerpiece of successful scale-up, without the need to account for growth dynamics. Steady-state operation was achieved multiple times with a maximum titer of  $3.26 \pm 0.01 \frac{\text{g}}{\text{L}}$  and a productivity of  $0.025 \frac{\text{g}}{\text{L} \cdot \text{h}}$ . It was proven, that *T. reesei* produces constantly enzymes over 750 h. The experiments showed that the oxygen flux per membrane area is a critical parameter for the process. Setups with identical volumetric oxygen transfer rate  $k_L a$ , but different oxygen fluxes per membrane area (large area & low concentration gradient vs. small area and high concentration gradient) showed titer differences of ca. 80 % ( $1.83 \frac{\text{g}}{\text{L}}$  vs  $3.26 \frac{\text{g}}{\text{L}}$ ) in favor of setups with the large membrane surface. The difference was attributed to long diffusion paths in thicker biofilms and thus, shortage in nutrient supply. Furthermore, it was proven that the continuous co-cultivation of two competitors, *T. reesei* & *Aspergillus phoenicis*, is possible, if the process conditions are adjusted to identical growth rate. The adding of *A. phoenicis* targeted the better utilization of the inhibiting intermediate cellobiose by balancing the fungal enzyme cocktail in terms of higher  $\beta$ -G concentrations. This goal was achieved, but however did not result in higher yields or productivities.



## 3.2 Introduction

Independent of the branch, continuous process operation offers various advantages such as omission of downtime for batch emptying and refilling, reduced CAPEX since the same productivity is maintained at lower reactor volume, the possibility to integrate continuous heating and cooling demands into an efficient heat management system and facilitated control due to time-invariance in steady-state operation. [75–77] In terms of bioprocesses, the reduced energy/chemicals demand for less frequent sterilization compared to batch processes as well as avoiding low productivities due to substrate and product inhibition at the beginning and the end of a batch process, respectively, are additional advantages. [78,79]

However, the interest in implementing of continuous bioprocesses compared to other process is rather new and successful industrial applications are rare. [80] The main obstacles of continuous operation are the handling of the solids for constant feeding, low productivities and maintaining long-term sterility. [75] Furthermore, in case of detecting a contamination, the contaminated batch can simply be disposed, whereas withdrawing the minimum, but sufficiently large amount of fermentation slurry in a continuous process is much more difficult. [81] Nevertheless, CBP and continuous processing were identified as most promising concepts to achieve economic competitiveness of bioproducts with fossil based products [3,82], which was confirmed for consortium-based consolidated bioprocess of lignocellulose to ethanol in the previous chapter. [33] Besides economics, consortium-based CBP predestined to overcome obstacles of continuous processing because the biofilm immobilizes cells and important extracellular products such as enzymes and surface-attached microbes are reported to show higher activity. [35] Two reactor concepts are available for continuous operation: The continuously stirred tank reactor (CSTR) and the plug flow reactor (PFR). [83] Bioprocesses are usually conducted in a CSTR since the viscous fermentation broth must be stirred. A CSTR is a well-mixed vessel with an inlet and an outlet. The concentration of the bulk is equal to the concentration of the outflow and the residence time (also referred to as hydraulic retention time) is defined as follows (eq. 3.1)

$$\tau = \frac{V_{CSTR}}{\dot{V}} \quad (3.1)$$

$$\tau^{-1} = D \quad (3.2)$$

The dilution rate  $D$ , the inverse of the residence time (eq. 3.2), is important for bioprocesses. If  $D$  is larger than the cell proliferation rate in the bulk, the reactor is washed-out. [84] The problem of wash-out is not relevant for immobilized biomass in the consortium-based CBP in contrast to industrial bioprocesses, where cell-recycling is mandatory to keep the cell concentrations at a sufficient level. During industrial ethanol production from 1<sup>st</sup> generation biofuels, the yeast cells are regained by centrifugation and afterwards washed with sulfuric acid



to reduce bacterial contamination. [36] Considering the production of 2<sup>nd</sup> generation biofuels, where the solid fraction of the reactor outflow consists of yeast cells and undigested lignin, a more sophisticated process is necessary to recycle only the yeast cells without the lignin particles. Besides the economic aspects of this process, the possible number of yeasts, which could be cultivated is reduced to the ones resistant to the chemical and mechanical stresses introduced by these kinds of recycling processes. [36] In contrast, the extracellular matrix of a biofilm protects the cells from inhibiting chemicals of the bulk allowing for a wider range of possible yeast cultivations. [37] However, the secreted enzymes diffuse from the biofilm into the bulk because they are only partly immobilized by attachment to the cell walls. Therefore, the yields will be poor, if the dilution rate is not adjusted accordingly to the microbial activity in the system with a special focus on the total enzyme activity. During steady-state, the fungal growth in the biofilm is equal to the decay rate, which is very low ( $\mu_{\max}/k_{\text{decay}} \approx 20$  for *T. reesei* [10]).

$$\mu \cdot [X]_p = k_{\text{decay}} \cdot [X]_s + [X]_p \cdot D \quad (3.3)$$

In a suspended culture, the mass balance additionally contains a wash-out term (eq. 3.3), which shifts the equilibrium towards higher concentrations of primary mycelia. In an immobilized biofilm, there is no wash-out ( $D = 0$ ) and the mass balance demands high concentrations of the enzyme producing secondary mycelia to "compensate" for the low decay rate. This explains the relatively high amount of enzymes within the system given the low concentration of microbial biomass compared to suspended cultures. In contrast, very low enzyme concentrations will be predicted by every model, which relates enzyme production to primary metabolism and thus, proportionally to the concentration of primary mycelia  $[X]_p$ . [85,86]

This work aims to prove that continuous consolidated bioprocessing based on a microbial consortium in a membrane aerated biomass immobilizing biofilm reactor is possible and results in good yields because enzyme production is not directly related to primary metabolism and the immobilization of the biomass and the cell-attached enzymes will lead to high enzyme activities per g biomass in the system. [10,87] Besides the proof-of-concept, which is important for the process economics (section 2), the time-invariant results of a parameter analysis with continuous experiments are intended to fit and validate a process model, which was developed to describe the process from an engineering point of view (chapter 4).

### 3.3 Materials & Methods

#### *Fungal strains & culturing models*

*T. reesei* RUT C30 (ATCC 56765) was purchased from VTT, Finland. Spore-populated agar pieces of 15 mm<sup>2</sup> size, obtained from a five-day-long cultivated agar plate (recipe adapted

from NREL protocol [88]: 20  $\frac{g}{L}$  agar and 22  $\frac{g}{L}$  D-glucose  $\cdot$  H<sub>2</sub>O in Mandel's medium) at 28 °C, were preserved in a 20 % (v/v) glycerol solution and stored at -80 °C as kryostocks. Mandel's medium consists of 2  $\frac{g}{L}$  KH<sub>2</sub>PO<sub>4</sub>, 1.4  $\frac{g}{L}$  (NH<sub>4</sub>)<sub>2</sub>SO<sub>4</sub>, 0.3  $\frac{g}{L}$  MgSO<sub>4</sub>  $\cdot$  7H<sub>2</sub>O, 0.4  $\frac{g}{L}$  CaCl<sub>2</sub>  $\cdot$  6H<sub>2</sub>O, 0.3  $\frac{g}{L}$  urea, 0.75  $\frac{g}{L}$  peptone, 0.25  $\frac{g}{L}$  yeast extract, 5  $\frac{mg}{L}$  FeSO<sub>4</sub>  $\cdot$  7H<sub>2</sub>O, 1.6  $\frac{mg}{L}$  MnSO<sub>4</sub>  $\cdot$  H<sub>2</sub>O, 1.4  $\frac{mg}{L}$  ZnSO<sub>4</sub>  $\cdot$  7H<sub>2</sub>O, 3.7  $\frac{g}{L}$  CoCl<sub>2</sub>  $\cdot$  6H<sub>2</sub>O, 10  $\frac{\mu L}{L}$  concentrated hydrochloric acid. The metallic salts and the hydrochloric acid were sterile filtered (pore size 0.2  $\mu$ m). MgSO<sub>4</sub>  $\cdot$  7H<sub>2</sub>O, CaCl<sub>2</sub>  $\cdot$  6H<sub>2</sub>O and the rest were autoclaved separately to avoid precipitation. Precultures of *T. reesei* consisting of Mandel's medium with 7.5  $\frac{g}{L}$  cellulose (Avicel PH-101, Merck KGaA, Darmstadt, Germany) were inoculated with 1.5 mL kryostock solution and incubated in a shaking incubator (Minitron, Infors-HT, Bottmingen, Switzerland) at 28 °C with 150 rpm. All chemicals were purchased either from Merck KGaA, Darmstadt, Germany, or from VWR International, Dietikon, Switzerland.

*Aspergillus phoenicis* (VTT D-76019) was purchased from VTT, Finland. The preparation of kryostocks and precultures was conducted analog to *T. reesei*.

*Saccharomyces cerevisiae* VTT C-79095 was purchased from VTT, Finland. Kryostocks were prepared by mixing cultures with an optical density of 0.5 at a wavelength of 600 nm (OD<sub>600</sub>) measured by spectrophotometry (Thermo Spectronic UV-1 (Thermo Fisher Scientific, Waltham, United States of America)) with glycerol to obtain a 20 % (v/v) glycerol solution. Precultures of *S. cerevisiae* consisting of YPD-medium were inoculated with a 1.5 mL kryostock and incubated in a shaking incubator (Minitron, Infors-HT, Bottmingen, Switzerland) at 28 °C with 150 rpm. YPD medium consists of 20  $\frac{g}{L}$  peptone, 10  $\frac{g}{L}$  yeast extract and 11  $\frac{g}{L}$  d-glucose  $\cdot$  H<sub>2</sub>O. All chemicals were purchased either from Merck KGaA, Darmstadt, Germany, or from VWR International, Dietikon, Switzerland.

#### *Experiments in Erlenmeyer flasks*

**Ethanol degradation:** 50 mL Erlenmeyer flasks were sterilized and prepared with 30 mL of 5  $\frac{g}{L}$  ethanol in Mandel's medium. A triplicate was prepared without cellulose and another triplicate was prepared with the same way with additional 4.5  $\frac{g}{L}$  cellulose. The flasks were inoculated with 1.5 mL *T. reesei* preculture. The experiment was carried out at 28 °C in a shaking incubator with 150 rpm. Ethanol was measured by means of HPLC. Ethanol loss by evaporation was determined by a blank triplicate (only ethanol in Mandel's medium) and the results were calibrated accordingly.

**Growth rate comparison:** 50 mL Erlenmeyer flasks were sterilized and prepared with 30 mL of 7.5  $\frac{g}{L}$  cellulose in Mandel's medium. The flasks were inoculated with 1.5 mL *T. reesei* or *A. phoenicis*, respectively. The experiment was carried out in a shaking incubator with 150 rpm. The temperature was set to 27 °C or 28 °C, respectively, and at a pH= 4 or pH= 5. The pH was

adjusted by adding citrate buffer. For each experimental condition, one Erlenmeyer flask was harvested after 1, 3 and 5 days to determine the amount of cell mass with the glucosamine assay.

#### *Experiments in the membrane aerated biofilm reactor*

The membrane aerated biofilm reactor is based on a Labfors 5 bioreactors (Infors HT, Bottmingen, Switzerland) with 3 L nominal volume and 2.7 L working volume. The reactor is stirred with a helical ribbon impeller and a tubular polydimethylsiloxane (PDMS) membrane with 3.18 mm outer diameter and 1.58 mm inner diameter (Dow Corning, Midland, United States of America) is winded within the reactor. The standard length of the membrane was defined to 2.8 m. 1/2 standard length corresponds to 1.4 m, accordingly. The pH of 5 was controlled by 4 N phosphoric acid and 4 M sodium hydroxide and measured by an EasyFerm Plus PHI Arc probe (Hamilton, Bonaduz, Switzerland). The temperature was set to 28 °C and 27 °C, respectively, for the co-cultivation of *A. phoenicis* and *T. reesei*. The membrane was flushed at a volumetric flow rate of  $0.368 \frac{L}{min}$  with a 21 % and 42 % oxygen-nitrogen mixture, respectively. After each pass, the oxygen concentration was measured optically (EOM-tO2-mini-180-T4D-v3 electro-optical module for oxygen measurements, Presens, Regensburg, Germany) in an expansion bag and the amount of diffused oxygen was injected into the expansion bag (PID-controlled electromagnetic valve (type 0255, Bürkert, Ingelfingen, Germany)). Trace oxygen in the bulk phase was detected by means of measuring the redox-potential with an EasyFerm Plus ORP Arc probe (Hamilton, Bonaduz, Switzerland). The sampling line for sampling the bulk phase was exposed to a UV barrier to prevent contaminations. [89] The membrane reactors, the feed bottle and the collecting vessel were sterilized by autoclaving for 20 minutes at 121 °C. Any connecting lines within the reactor cascade were closed during sterilization and connected afterwards in a laminar flow cabinet under aseptic conditions. Mandel's medium was added after autoclaving and the reactors were inoculated with 5 % (v/v) fungal inoculum (either 5 % (v/v) *T. reesei* or 2.5 % (v/v) *T. reesei* and *A. phoenicis* each. Additional 5 % (v/v) yeast inoculum was added after 48 h to reach OD<sub>600</sub> = 0.5 for the membrane reactor. For batch experiments, the yeast inoculate was centrifuged (3600 rpm at 4 °C for 30 min) and washed with Mandel's medium to exclude the impact of the preculture metabolites on the batch experiment. For continuous experiments, the feed solution was prepared analog to the reactor preparation. All technical gases were purchased from Pangas, Dagmarsellen, Switzerland.

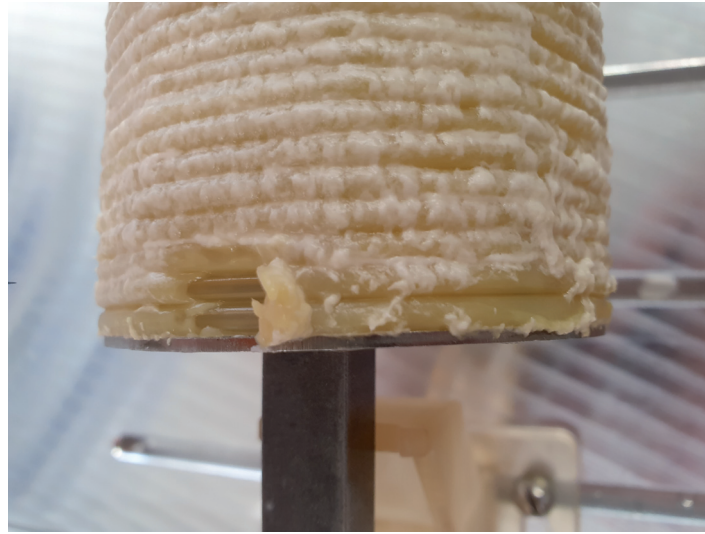


Figure 3.1: Close-up photograph of the biofilm on a helically wound membrane on its support. The white layer on the top is the yeast biofilm layer and the yellowish layer is the biofilm formed by *T. reesei*. The membrane is visible, where the biofilm was scraped away manually after the experiments.

#### *Feeding device and pneumatic transport for continuous experiments*

Avicel was sterilized and premixed with the sterile nutrients in a feed bottle (Volume 5 L, Schott Duran) with an impeller at 400 rpm. The nitrogen flow into the T-junction (Swagelok,  $\frac{1}{32}$ " inlet for nitrogen) to create the nitrogen bubbles was controlled by a mass flow controller (Vögtlin red-y series, 0-25  $\frac{NmL}{min}$ ) at 15  $\frac{NmL}{min}$ . The peristaltic pump (Watson Marlow 323d) was controlled at 15 % power to transfer the liquid-solid suspension from the feed bottle to the T-junction ( $\frac{1}{8}$ " inlet and outlet for the solid-liquid suspension) and subsequently the segmented flow through a  $\frac{1}{8}$ " pipe and peristaltic pump tubing (Tygon LMT-55, inner diameter 3.2 mm and outer diameter 6.4 mm) to the 1<sup>st</sup> reactor. The segmented flow was fed every 38 min for 60 s. Before and after each feeding, the T-junction was emptied by nitrogen flow for 30 s without pumping. Pneumatic transport from the 1<sup>st</sup> to the 2<sup>nd</sup> reactor to the collecting vessel through pipes and tubes with inner diameter of 5 mm was conducted every 38 min ca. 20 min after the feeding procedure for 90 s with nitrogen flushing (pressure of 1.6 bar).



Figure 3.2: Photograph of the segmented flow from the feed bottle (background) to the 1<sup>st</sup> reactor. The green arrow exemplary shows a droplet with the solid-liquid suspension and the red arrow points out the settling limitation of Avicel at the phase boundary between droplet and nitrogen bubble

#### *Glucosamine assay*

The glucosamine assay was conducted exactly according to [87]. By diluting the samples with distilled H<sub>2</sub>O and a total volume of 0.3 mL for the assay, the measurements were in the linear range of the glucosamine calibration curve. 0.3 mL HCl (4 M) was added to hydrolyze the fungal biomass and the samples were captured in Pyrex screw capped tubes. After adding the HCl, nitrogen was used to flush the samples. The hydrolization of the samples took 2 h at 121 °C. After cooling down, a neutralization step with 0.4 mL 2 M Na<sub>2</sub>CO<sub>3</sub> performed. In the meantime, % v/v acetyl acetone in 1.5 M Na<sub>2</sub>CO<sub>3</sub> were prepared and 0.5 mL were added to the samples. With a boiling water bath, the samples were heated for 20 min followed by the addition of 1 mL ethanol. Determining the glucosamine content with the color formation at 530 nm, 0.5 mL of the Ehrlich's reagent [2g *p*-dimethylaminobenzaldehyde in 30 mL EtOH and 30 mL concentrated HCl (3 % w/w)] were added. By using GlcN as a calibration curve, the linear range of the measurements were conducted. The cell dry weight (CDW) for each fungus, which were grown on glucose combined with their GlcN content correlated with the different calibration curves. [87]

#### *Analytical methods*

Cellobiose, glucose and ethanol concentrations were measured by HPLC (Waters 2695 Separation Module, Waters Corporation, Milford, United States of America). Separation was achieved in an Aminex HPX-87H column (Bio-Rad, Hercules, United States of America) at 65 °C with 5 mM H<sub>2</sub>SO<sub>4</sub> solution as mobile phase at a flow rate of 0.6  $\frac{mL}{min}$ . The substances were detected by a refractive index detector (Waters 410) at 40 °C and a photodiode array detector (Waters 2998).

## 3.4 Results and Discussion

### 3.4.1 Continuous CBP with a consortium consisting of *T. reesei* and *S. cerevisiae*

Li et al. proposed 7 key challenges when operating a system continuously [79]: Continuous feeding, continuous product removal, prevention of contamination, immobilization of cells, immobilization of extracellular products, long-term stability and high cell density, titer, yield & productivity. In the following, it is presented, how each of these 7 points was addressed in order to successfully conduct continuous experiments of consolidated bioprocessing of cellulose to ethanol at lab scale.

#### *Continuous feeding*

Continuous feeding is indeed a key challenge since cellulosic substrates are insoluble, but homogeneous feeding is unequivocal for reaching steady state operation given the sensitivity of the microbial community to fluctuations of external parameters like the substrate concentration. [7, 8] A published 3-phase-flow feeding design was adapted to feed the reactor cascade continuously from a feed bottle (Fig. 3.3). [8] The solid-liquid suspension is sucked into a T-junction by a peristaltic pump, where it is segmented into droplets by injecting nitrogen via the perpendicular nozzle of the T-junction. The surface tension between the gas bubbles and the suspension droplets prevents the cellulose from sedimentation. The feed flow rate is adjusted by the nitrogen gas flow rate and the rotational speed of the peristaltic pump.



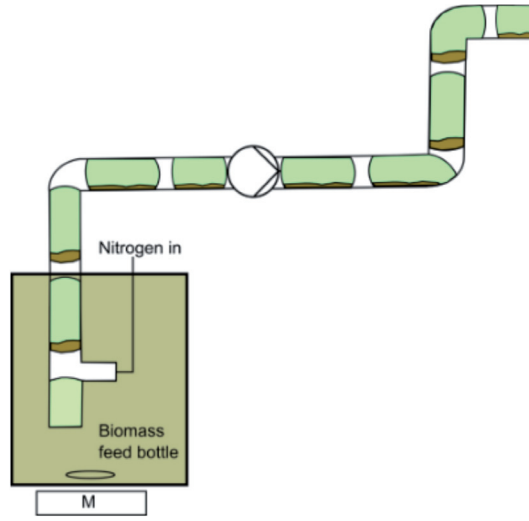


Figure 3.3: The 3-phase flow feed design for continuous feeding of suspensions with insoluble substrates. The well mixed solid-liquid suspension is sucked into the feeding device, a T-junction, by a peristaltic pump. Additionally, nitrogen is injected via the perpendicular nozzle of the T-junction. Consequently, a 3-phase flow with solid-liquid suspension droplets and intermitting gas bubbles is formed. Sedimentation of the solid particles ends at the phase boundary to the gas bubbles since the gravitational force is outweighed by the surface tension between the droplet and the bubble. Figure taken from [7].

Adjusting the residence time to 5 *days* like it was done for the industrial scale layout yields feeding rate of  $22.5 \frac{mL}{h}$  at lab scale. [33] The peristaltic pump works periodically since this flow rate is too low for steady feeding. Due to the periodically feeding & emptying, the reactor system may be regarded as a batch system between two feeding intervals. Eq. 3.4 compares the duration of such a batch period to the duration of the whole experiment (eq. 3.4).

$$\frac{t_{\text{batch}}}{t_{\text{Experiment}}} = \begin{cases} 1 & \text{for batch operation} \\ 0.25 - 0.056 & \text{for repeated fed batch operation} \\ 0.0056 & \text{for this work} \\ 0 & \text{for continuous operation} \end{cases} \quad (3.4)$$

The spectrum of  $\frac{t_{\text{batch}}}{t_{\text{Experiment}}}$  ranges from 0 (permanent feeding during continuous operation) to 1 (only initial feeding for batch operation). The value for repeated batch usually ranges between 0.25 and 0.1. [90] However, the minimum was found at 0.056. [91] This work still has a 10 times higher feeding frequency than the maximum frequency found for repeated batch operation. Thus, the feeding may be assumed to be continuous, which is confirmed by the experimental results presented later on.

#### Continuous product removal

Continuous product removal is either achieved by direct product removal (*in-situ* or slip stream) or by removal of the fermentation broth with subsequent separation. [64] The latter is done in this work. The fermentation broth was transported pneumatically from the 1<sup>st</sup> reactor in the cascade to the 2<sup>nd</sup> reactor and finally to the collecting vessel (blue line in Fig. 3.4). [8] After each feeding interval, a valve opened to inject nitrogen in the gas phase below the reactor lid. The exhaust port of the reactor was a dip tube, which height was precisely adjusted to the filling level of the desired reactor volume. Thus, the overpressure of the gas phase pushed the well-mixed solid-liquid suspension from the CSTR through the tube to the 2<sup>nd</sup> reactor in the cascade or the collecting vessel. The nitrogen is vented through a sterile filter at the top of the collecting vessel to release the overpressure. As soon as the desired filling level in both reactors is reached, the opening of the dip tube is above the liquid level and the nitrogen flows directly through the dip tubes to the collecting vessel and is vented.

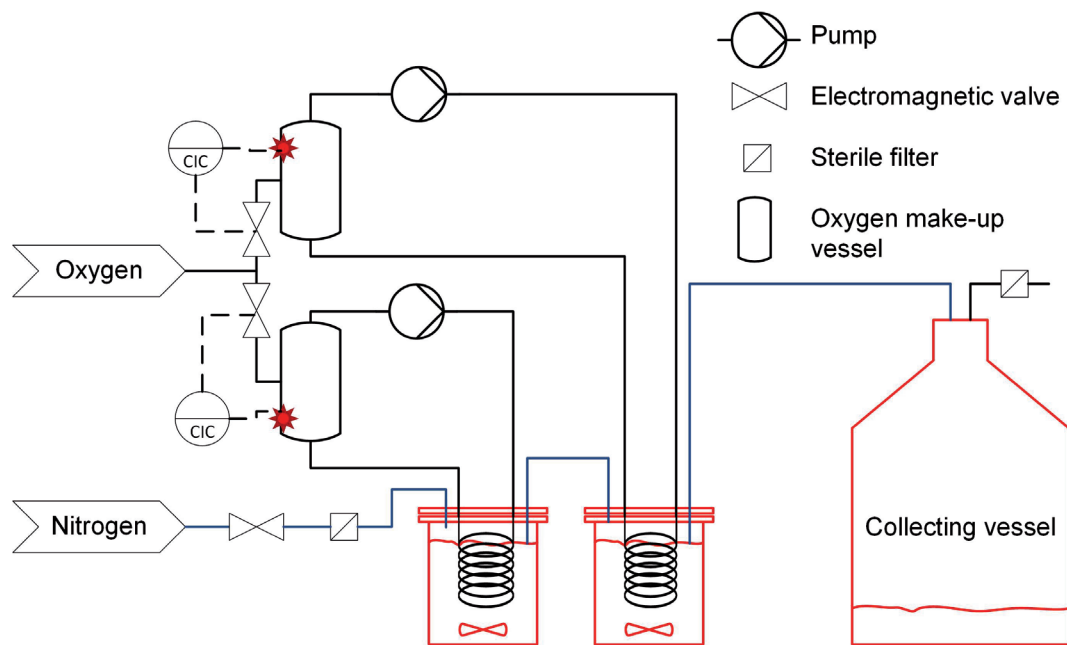


Figure 3.4: Schematic representation of the oxygen recirculation system for membrane aeration (black lines) and the pneumatic transport of the fermentation slurry by nitrogen injection (blue lines). Oxygen is pumped through the membrane, where a certain amount of oxygen is lost due to diffusion across the membrane wall. The oxygen concentration in the make-up vessel is measured optically and an electromagnetic valve is opened to add pure oxygen to make up for the loss by diffusion. After each feeding interval, an electromagnetic valve is opened to inject nitrogen in the gas phase above the liquid level of the 1<sup>st</sup> reactor. The fermentation broth is pneumatically pushed through a dip tube and flows into the second reactor and from the second reactor into the collecting vessel, where the nitrogen is vented via a sterile filter. As soon as the filling level of each reactor reaches the desired state, the dip tubes do not reach into the liquid phase anymore. The remaining nitrogen is directly transported through the dip tubes to the vent. Figure adapted from [8].



As there is no phase boundary to avoid settling during the pneumatic transport, the prevention of inhomogeneities has to be ensured otherwise: The maximum sedimentation velocity of cellulose particles is given by Stoke's law (assuming perfectly spherical cellulose particles settling in pure water) (eq. 3.5) [92]:

$$m_p g = 6\pi\eta_w r_p v_p \Leftrightarrow v_p = \frac{m_p g}{6\pi\eta_w r_p} \approx 8.2 \frac{mm}{s} \quad (3.5)$$

According to Stoke's law, the driving force for sedimentation, the gravitational force  $m_p g$ , is equal to the fluid resistance force, which is defined by its viscosity  $\eta_w$ , the particle's diameter  $r_p$  and velocity  $v_p$ . [92] The fluid velocity during pneumatic transport is ca. 0.25 m/s as experiments have shown. Thus, sedimentation is not an issue during steady pneumatic flow because the mean fluid velocity is larger than the sedimentation velocity at least by a factor of 30. It can be concluded that settling of the cellulose particles is not an issue during steady-pneumatic transport. However, there are ca. 900 start-ups of pneumatic transport during one experiment. Therefore, concentration distortions during start-up of the pneumatic transport could add up to considerable errors. The risk of concentration distortions during start-up is assessed by evaluating the control responses to pneumatic transport in a qualitative manner (Fig. 3.5). Pneumatic transport of the solid-liquid suspension is initialized by the control command to open the electromagnetic valve for nitrogen flushing at a certain point in time  $t_0$ . Since the opening of the valve is only damped by the inertia of the moving parts, which is negligible, its control response is a step function (step from *off* to *on* at  $t_0$  in Fig. 3.5). A step function describes a static control response. The response comes without any delay and the gradient between actual state and target state is equal to infinity. [93] Both, the overpressure and the superficial flow velocity are damped by a pressure loss due the sterile filter and the long dip tube. In both cases, the damping force is in the range of 5-10 % of the driving force. Thus, the control responses of the overpressure and the fluid velocity to reach their steady values are rather fast but show dynamic behavior. Dynamic behavior is characterized by the deviation to a step response: There is a delay time  $t_d$  until the response starts and the response gradient is smaller than infinity  $\frac{d\Delta P}{dt} < \infty$ . [93] As the settling of cellulose particles is damped by the fluid viscosity resulting in a damping force in the range of 100 % of the driving force, the dynamic response of the settling velocity is much slower than for the pneumatic transport (Fig. 3.5). Thus, there is no cellulose sedimentation during start-up as well as during steady pneumatic transport and continuous product removal is ensured.

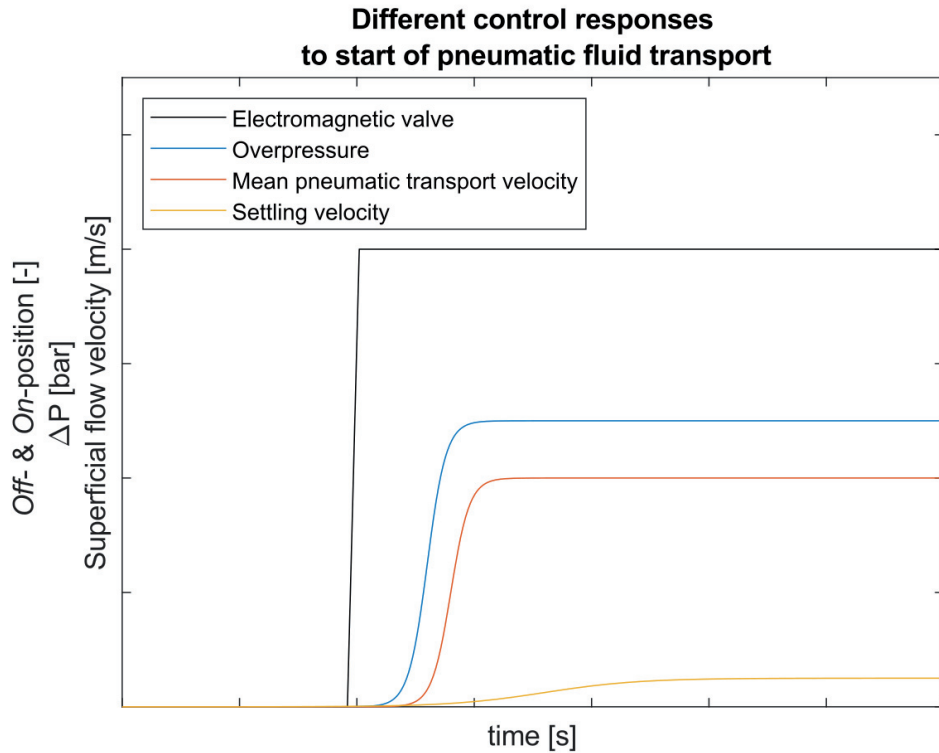


Figure 3.5: Qualitative comparison of estimated different control responses of the critical parameters after initializing nitrogen flushing for pneumatic fluid transport.

#### *Prevention of contamination*

Li et al. discussed the prevention of contaminations in the light of open and continuous processes. [78] Open means that no sterilization procedure is conducted. This is impossible for the setup in this work, although it is known that *T. reesei* and other filamentous fungi secrete antimicrobial substances to protect their niche against bacteria and other invaders. [94] However, it was shown that amongst others, the ubiquitously present *Lactobacillus pentosus* is able to grow at high rates in the presence of *T. reesei*. [50,95] Thus, any kind of contamination needs to be prevented by sterilizations procedures. During the preparation of the experiments, all reactors, the feed bottle and the collecting vessel were autoclaved. Every gas injection into the system passes a 0.2  $\mu\text{m}$  sterile filter and the sampling line has a UV barrier to allow sampling without any contamination. [89] All actions, which involved opening the closed system of the two reactors, the feed bottle and the collecting vessel, such as inoculation of the reactors, refilling the feed bottle and emptying the collecting vessel, were performed under aseptic conditions in a laminar flow cabinet.

### *Immobilization of cells and extracellular products*

The immobilization of cells is automatically given by the concept of deploying a biofilm. [4,35] The enzyme producer *T. reesei* is completely immobilized as biofilm on the membrane because there is no other oxygen source within the system. The enzymes produced by *T. reesei* are partly bound in the biofilm and partly released to the bulk. The ratio of immobilized enzymes to free enzymes is defined by the mass transfer equilibrium (Chapter 4) and the affinity of the enzyme to attach to the fungal cell wall. [87] *S. cerevisiae* also is present in both, the biofilm and the bulk phase. The yeast cells in the bulk phase convert the largest fraction of the released glucose to ethanol, whereas the yeast cells in the biofilm face higher oxygen concentrations and lower glucose concentrations, which allows them to overcome the Crabtree effect and perform aerobic metabolism, which is much more favorable in terms of cell proliferation rate. [96,97] Concluding it can be stated that all cells and extracellular products are either immobilized or the process is designed to prevent wash-out during continuous operation by keeping the dilution rate below the corresponding production/proliferation rates.

### *Long-term stability*

Long-term stability is crucial in continuous systems as the start-up procedure to reach steady-state operation already takes 3-5 residence times. [83] In this work, it is accounted for the long-term stability in terms of material choice and the biological system. All used materials (especially the non-metal parts such as the membrane and the tubes for the peristaltic pumps) were known to withstand the wear for a sufficiently long-time. The biological system consists of 2 industrial strains, *T. reesei* RUT C30 and *S. cerevisiae* VTT C-79095 known for their robustness. [34] In contrast to CBP with genetically modified microorganisms (GMOs), where each cell proliferation comprises the risk of a back mutation, which were implemented. [34] Additionally to the robustness of the chosen microorganisms themselves, the consortium formed by these two microorganisms is stable too. The membrane aeration gives a stable aerobic niche, and the yeast relies on the cellulolytic activity of *T. reesei*. [35] Thus, according to the cheater-cooperator model, there is an equilibrium to what extent *S. cerevisiae* will invade the niche of *T. reesei*. [34,35]

### *High cell density, titer, yield & productivity*

The setup of the presented work is reported to reach a titer of  $7 \frac{\text{g}}{\text{L}}$  ethanol, a yield of 70 % and a productivity of  $0.04 \frac{\text{g}}{\text{L} \cdot \text{h}}$ , which above-average numbers for CBP. [35,98] However, only the yield meets industrial requirements. The titer should be around  $40 \frac{\text{g}}{\text{L}}$  and the productivity around  $0.3 \frac{\text{g}}{\text{L} \cdot \text{h}}$ . [2,64,98] In order to increase the titer and the productivity, the following adjustments were proposed: Higher solid loading, elimination of ethanol losses through the membrane and better utilization of cellobiose.

As the yield meets industrial specifications, the necessary titer could be obtained by simply

increasing the input solid loading assuming constant productivity. For batch operation, an increased solid loading would cause problems such as increased substrate inhibition and poor mixing behavior of the highly viscous fermentation broth, during the initial batch phase. [15,99] However, in a CSTR, the bulk composition is equal to the outflow composition. [83] Thus, high solid loadings would be diluted in the partly hydrolyzed bulk phase and substrate inhibition as well as mixing problems can be avoided. Ethanol losses through the membrane were avoided by recirculating the gas in the membrane (Fig. 3.4). Since ethanol is a volatile component, a certain amount of ethanol diffuses through the biofilm and the membrane wall into the membrane. With an open end approach (the residual gas is released to the atmosphere after passing the membrane), any ethanol in the membrane would be lost to the atmosphere. [35] In this work, the gas in the membrane is recirculated. After each pass of the membrane, the gas enters a make-up vessel, where the oxygen concentration is measured and any lost oxygen by diffusion through the membrane is replaced (Fig. 3.4). During start-up, ethanol is concentrated within the recirculation loop until an equilibrium concentration is reached and the ethanol diffusion into the biofilm is reduced to the amount of ethanol, which is degraded within the biofilm (Fig. 3.6).

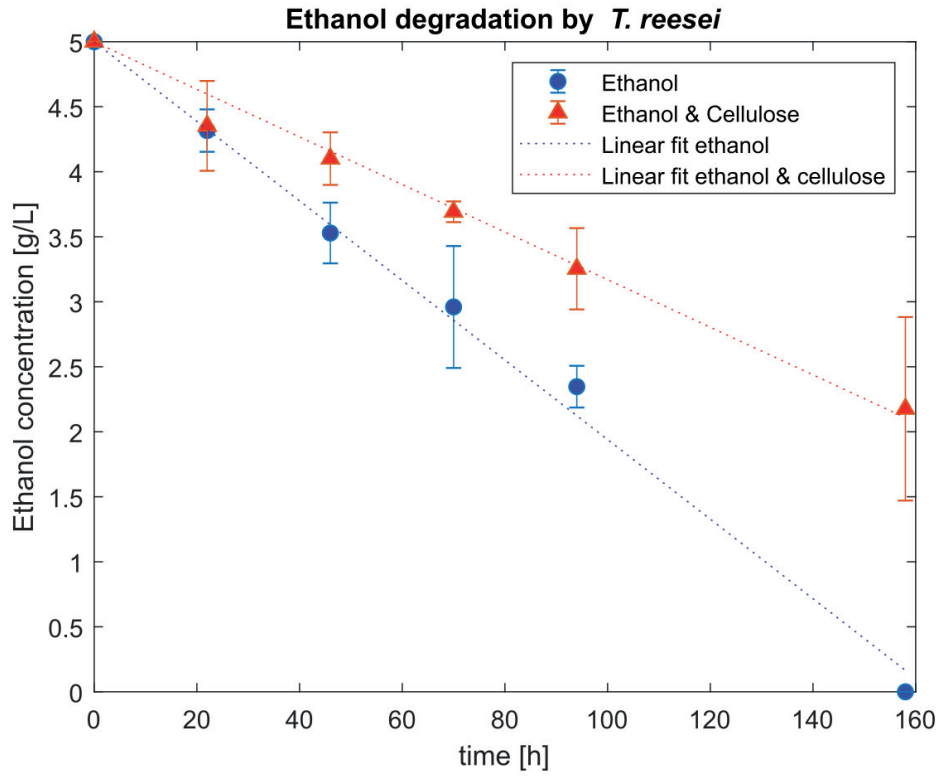


Figure 3.6: Ethanol degradation of *T. reesei* in an Erlenmeyer flask with ethanol as only substrate and ethanol together with cellulose as substrate at 28 °C. The dotted lines represent the linear fit with average degradation rates of  $0.0306 \frac{\text{g}}{\text{L}\cdot\text{h}}$  and  $0.01183 \frac{\text{g}}{\text{L}\cdot\text{h}}$  with ethanol as only substrate present and with ethanol and cellulose as substrate, respectively. The coefficients of determination are 0.9943 and 0.9922, respectively. The error bars are based on triplicate experiments.

Given the above-mentioned setup, steady-state could be achieved with the continuous co-cultivation of only *T. reesei* and *S. cerevisiae* showing a yield of 40.3 %, a titer of  $3.258 \pm 0.007 \frac{\text{g}}{\text{L}}$  and a productivity of  $0.025 \frac{\text{g}}{\text{L}\cdot\text{h}}$  (Fig. 3.7). The steady-state state was reached at around 560 h of operation, which corresponds to the rule of thumb, that a steady-state takes ca. 4-5  $\tau$  ( $\tau=130$  h).

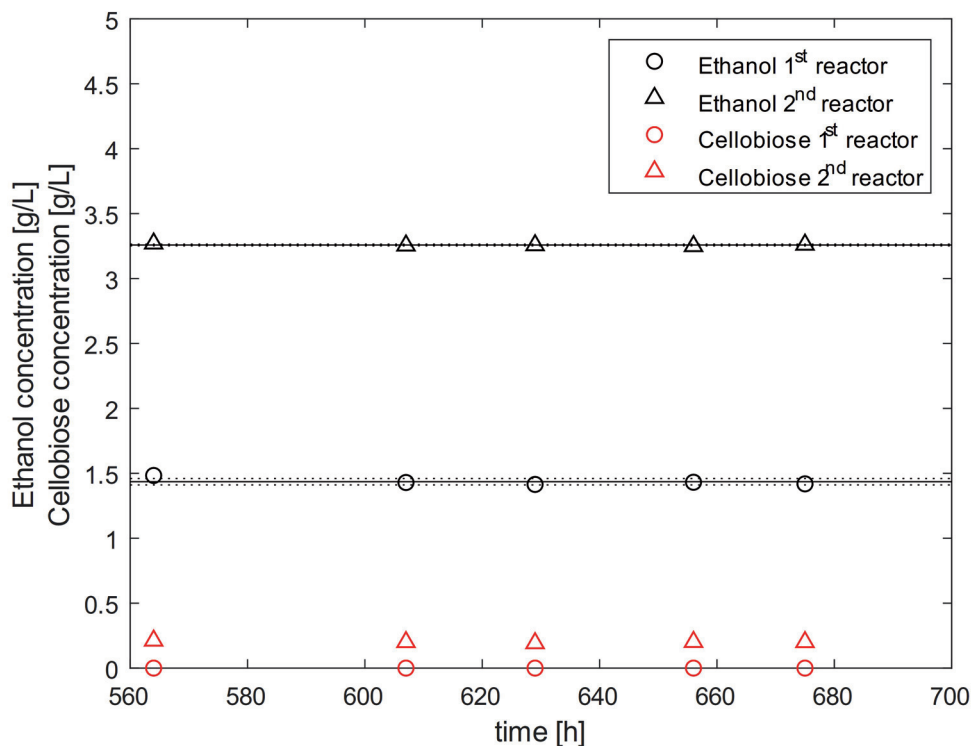


Figure 3.7: Steady-state results for continuous consolidated bioprocessing based on a microbial consortium consisting of *T. reesei* with *S. cerevisiae* in a cascade of 2 reactors. Steady-state operation was reached after 564 h. Cellobiose was depleted in the 1<sup>st</sup> reactor and only present to a little extent in the 2<sup>nd</sup> reactor (ca.  $0.2 \frac{g}{L}$ ). The solid and dashed lines denote the average ethanol concentration and its standard deviation, respectively, in the 1<sup>st</sup> and second reactor. Steady-state operation was maintained over 111 h. The membrane (inner diameter  $d_i = 1.58 \text{ mm}$ , outer diameter  $d_o = 3.18 \text{ mm}$ , length  $L = 5.6 \text{ m}$ ) was aerated with 21 % oxygen fraction. The cellulose feed concentration was  $17.5 \frac{g}{L}$  and the residence time  $\tau$  was 130 h.

In order to investigate the influence of the oxygen transfer rate to the system, the experiment was repeated at different membrane lengths and oxygen concentrations (Fig. 3.8).

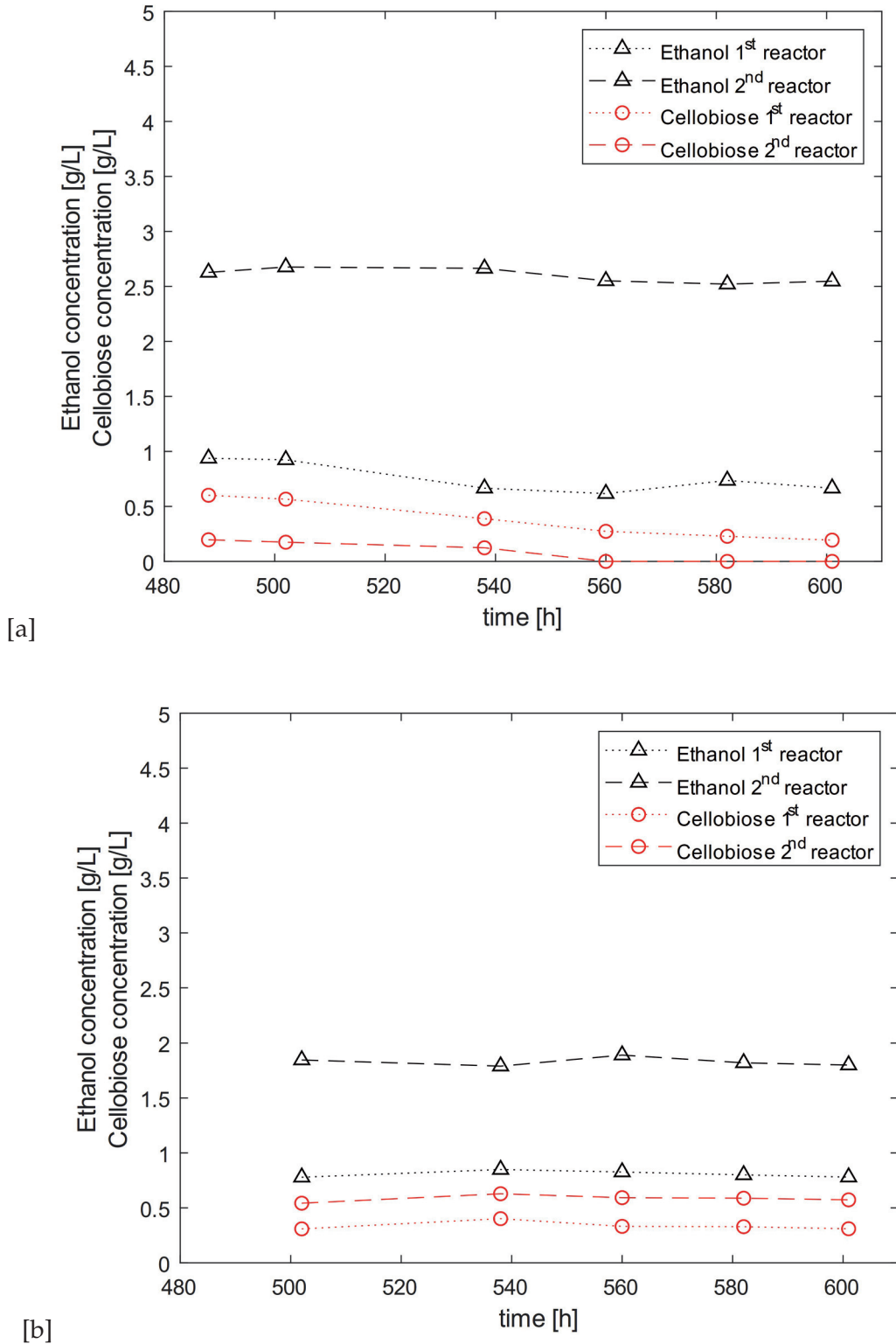


Figure 3.8: Steady-state ethanol production with consolidated bioprocessing based on a microbial consortium consisting of *T. reesei* and *S. cerevisiae* in a cascade of 2 reactors. The membrane (inner diameter  $d_i = 1.58 \text{ mm}$ , outer diameter  $d_o = 3.18 \text{ mm}$ , length  $L = 5.6 \text{ m}$  (a) and  $L = 2.8 \text{ m}$  (b), respectively, was aerated with 42 % oxygen fraction. The cellulose feed concentration was  $17.5 \frac{\text{g}}{\text{L}}$  and the residence time  $\tau$  was 130 h.

Doubling the oxygen concentration gradient across the membrane and halving the membrane length yields the same oxygen mass transfer into the system as the original setup (Fig. 3.7 & Fig. 3.8b). However, the ethanol titer is considerably lower ( $1.83 \frac{\text{g}}{\text{L}}$  vs  $3.26 \frac{\text{g}}{\text{L}}$ ). Hence, there is a difference whether the same amount of oxygen is transferred across small surfaces or large surfaces, which also means that the volumetric mass transfer coefficient  $k_L a$  is not a sufficient parameter to describe the system. A more rigorous model is necessary to account for the influence of oxygen transfer per area. Considering the higher cellobiose amounts in Fig. 3.8b compared to 3.7, one reason for the lower productivity of the system could be the following: The higher oxygen input per area allows more biofilm formation per area and thus, a thicker biofilm. This has two implications: The diffusion path for glucose from the bulk to the fungus is longer on average. Additionally, the average diffusion path of the enzymes, especially for  $\beta$ -G, which is known to likely adhere to the fungal cell surface [87], increases. Thus, the inner biofilm layers lack in glucose supply due to inhibited glucose formation in the bulk as consequence of less available  $\beta$ -G and longer diffusion paths of the formed glucose through the biofilm. *T. reesei* was found out to consume ethanol at considerable rates if no other substrate is present (Fig. 3.6). Thus, besides cellobiose inhibited hydrolysis, the lower ethanol concentrations may be caused by ethanol degradation of *T. reesei* in the biofilm.

Nevertheless, 3 different steady-states of CBP of cellulose to ethanol based on a microbial consortium consisting of *T. reesei* and *S. cerevisiae* were reached, which proves the constant enzyme production of *T. reesei* during steady-state although the fungal growth in the steady-state much smaller than in a batch process. This disagrees with theories attributing enzyme production to fungal growth, which were mostly inspired by the theory of Reinhardt, that a filamentous fungus only grows at the hyphal tip. [100] During steady-state, the growth rate of the fungus is equal to its decay rate resulting in the required time-invariance. The decay constant  $k_d = 0.16 \text{ day}^{-1}$  was found to be roughly 20 times smaller than the maximum growth rate  $\mu_{\max} = 3.0 \text{ day}^{-1}$ . [10] Thus, half of the productivity (Fig. 3.7), which was obtained in batch experiment, would be impossible to reach relating the enzyme production to a 20 times lower growth rate. [35] Gaden [101] expanded the kinetics of fermentation process to three types: Kinetics as result of primary metabolism (e.g. ethanol production by the yeast or oxygen consumption for fungal growth), kinetics related to primary metabolism (e.g. intermediate metabolites) and non-growth related kinetics. For *T. reesei*, it was found out that primary mycelia are formed during growth. Later on, these primary mycelia are converted to secondary mycelia, which are responsible for enzyme production. [10] Therefore, enzyme production of *T. reesei* is not directly related to primary metabolism, but can be described by the following kinetics (eq. 3.6-3.9) [10,101]:

$$\frac{d[X_s]}{dt} = 0 = k_c [X_p] - k_d [X_s] \quad (3.6)$$



$$\Leftrightarrow [X_s] = \frac{k_c}{k_d} [X_p] = \frac{k_c}{k_d} [X_{tot} - X_s] = \frac{2.4}{0.16} [X_{tot} - X_s] \quad (3.7)$$

$$\Leftrightarrow [X_s] = 93.75\% [X_{tot}] \quad (3.8)$$

$$\frac{d[E]}{dt} \propto [X_s] \quad (3.9)$$

The mass balance for the concentration of secondary mycelia  $[X_s]$  is given by a formation term (the conversion of primary to secondary mycelia  $k_c [X_p]$ ) and a depletion term (decay of secondary mycelia  $k_d [X_s]$ ) (eq. 3.6). These two terms are equal during steady-state. As the conversion of primary mycelia to secondary mycelia occurs much faster than the decay of secondary mycelia, a large fraction of the total fungal biomass  $[X_{tot}]$ , namely 93.75 %, consists of secondary mycelia (eq. 3.8). [10] Recalling that the enzyme formation rate is proportional to the amount of secondary mycelia (eq. 3.9), it becomes clear, that the biofilm immobilization, which eliminates a wash-out depletion term in the mass balance, strongly favors the accumulation of secondary mycelia, which ensures high, steady enzyme production. [10]

### 3.4.2 Improvement of continuous CBP by enhanced utilization of cellobiose

Considering the optimization measures presented in the introduction (section 3.2), increasing the solid loading for higher titers, avoiding ethanol losses across the membrane with a closed oxygen loop and making better use of cellobiose, only the closed membrane loop was addressed. Given the maximum observed productivity of  $0.025 \frac{g}{L \cdot h}$ , increasing the titer would demand residence times in the order of 240 h. Thus, increasing the productivity by better utilization of cellobiose was prioritized. Cellobiose is the intermediate product of cellulose hydrolysis to glucose. Hydrolysis of cellulose in general is a reactions process with 3 kind of enzymes involved: Cellobiohydrolases (CBHs) cleave cellobiose molecules from the end of cellulose chains. Endoglucanases (EGs) cleave cellulose chains unselectively and thus, create more chain ends for CBH activity. The resulting cellobiose molecules are cleaved by  $\beta$ -glucosidase ( $\beta$ -G) to glucose monomers. [102] As cellulose is insoluble in water, the enzymatic reactions of CBH and EG follow the same scheme of enzyme adsorption to the substrate surface, formation of an enzyme-substrate complex with subsequent enzymatic hydrolysis reaction. [103] Cellobiose is soluble in water, but cannot be digested, neither by *T. reesei* nor by *S. cerevisiae*. Furthermore, cellobiose can bind the active sites of CBH and EG, which results in deactivation of CBH and EG and a blockage for  $\beta$ -G to cleave the cellobiose. [104] Concluding, that cellobiose is not only an unused dimer of two glucose molecules, but also inhibits the activity of all 3

enzyme, its concentration needs to be kept as low as possible. Unfortunately, *T. reesei* lacks in  $\beta$ -G production to effectively reduce the cellobiose concentration. [87] Thus, two options to decrease cellobiose concentrations were evaluated: The co-cultivation of *T. reesei* and *Dekkera bruxellensis* and the co-cultivation of *T. reesei*, *A. phoenicis* and *S. cerevisiae*. *D. bruxellensis* is a yeast strain which is able to ferment both, glucose and cellobiose, to ethanol. [105] *A. phoenicis* is filamentous, aerobic fungus like *T. reesei* and is known as  $\beta$ -G hyperproducer. [87] Therefore, *A. phoenicis* is cultivated in the same niche as *T. reesei* to balance the enzyme cocktail. [87] The fermentation is carried out with *S. cerevisiae* as usual. An experimental comparison of the two configurations (Fig. 3.9) showed that both consortia lead to ethanol production and depletion of cellobiose after time. However, the co-cultivation of *T. reesei* and *A. phoenicis* with *S. cerevisiae* lead much faster to the desired results. Cellobiose was depleted completely already after 28 h and 50 % yield was reached after 120 h. With *T. reesei* and *D. bruxellensis*, the yield after 319 h was still below 5 % (42.7 %) and the cellobiose concentration was temporary at  $2.7 \frac{\text{g}}{\text{L}}$ , which reduces the hydrolysis speed by over 30 % based on literature data. [102] Such considerable hydrolysis inhibitions could cause a wash-out of enzymes during start-up of the continuous experiments. Therefore, the configuration with *T. reesei*, *A. phoenicis* and *S. cerevisiae* was chosen for the continuous experiment.

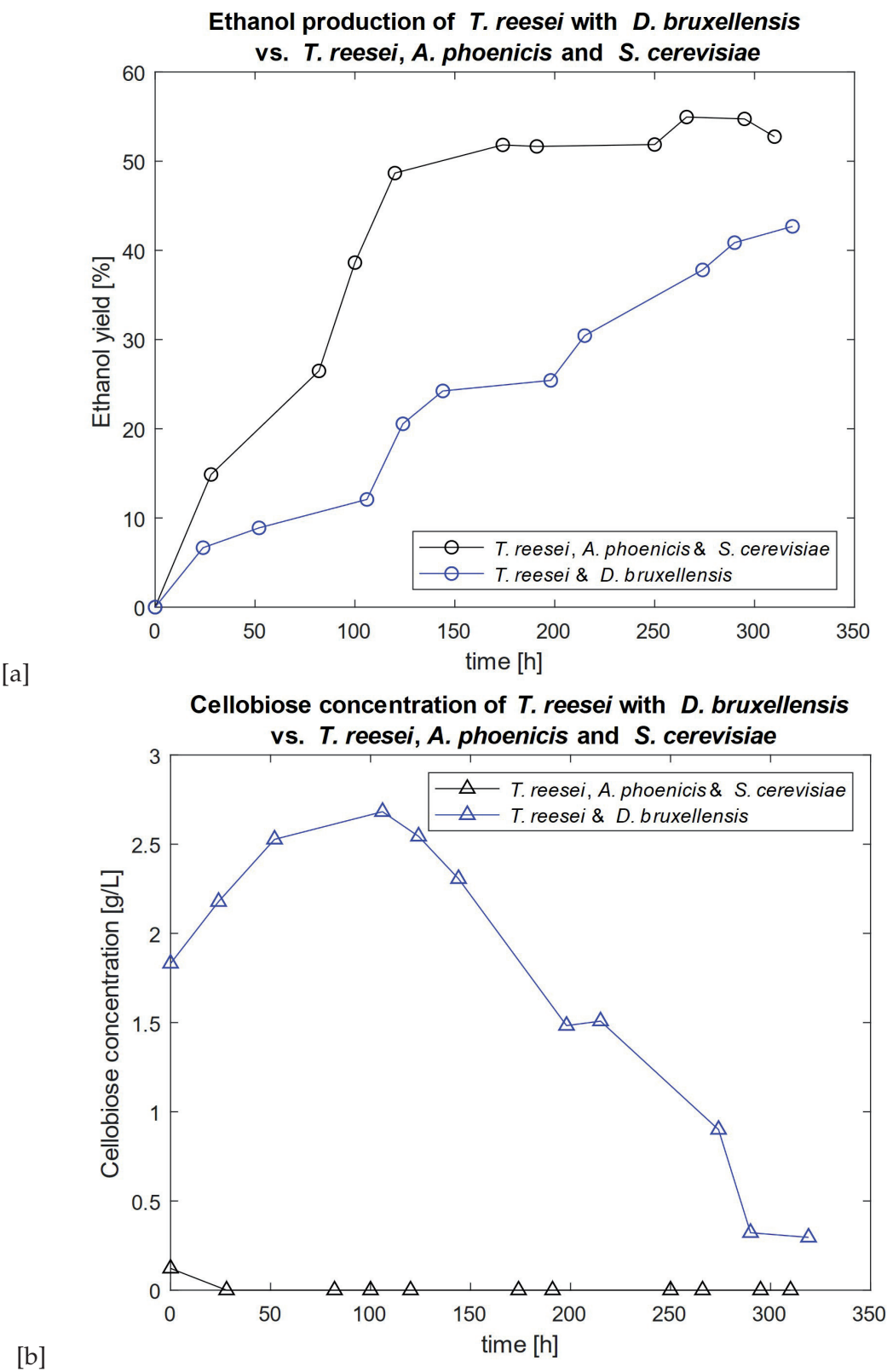


Figure 3.9: Batch ethanol and cellobiose production of *T. reesei* with *D. bruxellensis* [a] vs. *T. reesei* with *A. phoenicis* and *S. cerevisiae* [b].

The co-cultivation of *T. reesei*, *A. phoenicis* and *S. cerevisiae* imposes special requirements on the continuous setup since *A. phoenicis* and *T. reesei* share the same niche. Although their enzyme cocktails complement each other well [87], they are both aerobic, cellulolytic fungi, which will result in competition for the oxygen in the niche. [106] During batch experiments, the weaker competitor with the lower growth rate at the given conditions (temperature and pH) may be strengthened by an earlier inoculation to provide it with a longer growing time. [87] *T. reesei* was inoculated 24 h before *A. phoenicis* in batch experiments. [87] Fig. 3.10 depicts schematically the difference between co-cultivations in batch processes and continuous processes. The differently colored squares denote the temperature and pH range, where the respective species are able to grow. Consequently, overlapping squares represent possible conditions for co-cultivations. However, the growth rate of the involved species may differ vastly in the range of the given co-cultivation conditions (see accordingly colored lines at pH and T-axis in Fig. 3.10). In a batch experiment, a difference in growth rate may be compensated with an advantage in time as mentioned above. In a continuous steady-state process, which is time-invariant, the faster growing species would overgrow the slower growing species. Therefore, the range of possible co-cultivation conditions of *T. reesei* and *A. phoenicis* is reduced to one condition, where the growth rate of both fungi is identical. Note that this constraint does not apply for *S. cerevisiae* because the yeast will develop the earlier mentioned cheater-cooperator equilibrium with the fungus. [34] The growth rate constraint only applies to the two competing species, *T. reesei* and *A. phoenicis*. A temperature of 27 °C and a pH of 5 was identified to yield identical growth rates for *T. reesei* and *A. phoenicis* (Fig. 3.11).

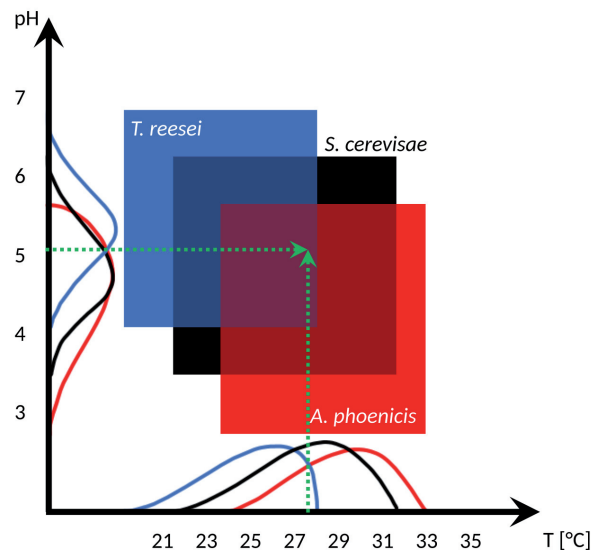


Figure 3.10: Schematic representation of the co-cultivation conditions for a microbial consortium consisting of *T. reesei*, *A. phoenicis* and *S. cerevisiae*. The blue, black and red square denote the range of temperature and pH, which allow growth for the respective species. The corresponding curves at the temperature and pH axis denote the growth rate as function of the axis variable, pH or T. The overlapping areas possibly allow co-cultivation. The green arrows denote the pH and Temperature condition, where *T. reesei* and *A. phoenicis* grow exactly at the same rate. Note that other parameters, which influence a co-cultivation such as secretion of antimicrobial substances are not considered in this plot. Figure adapted from [9].

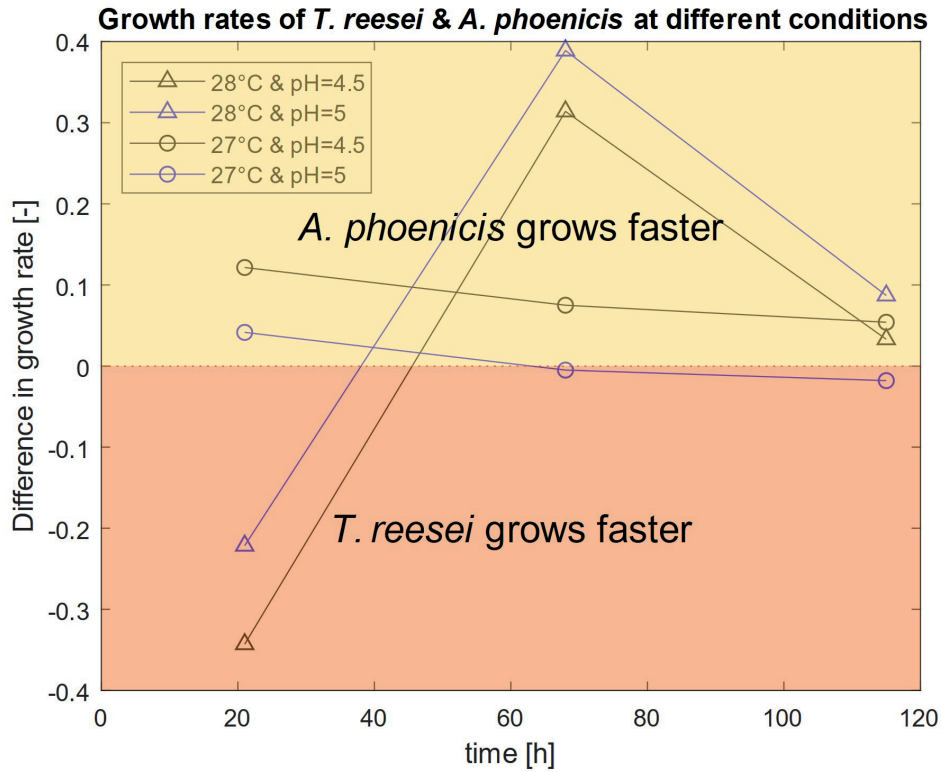


Figure 3.11: Growth rate comparison of *T. reesei* and *A. phoenicis* grown in separate Erlenmeyer flasks under identical conditions at different temperature and pH. The difference in growth rate is plotted against the time, meaning that values of zero correspond to identical growth rates. Positive values indicate faster growth of *A. phoenicis* and negative values faster growth of *T. reesei*, respectively. The growth rate does not have a unit since it was determined by means of spectrophotometry.

Fig. 3.12 shows the result of the continuous experiment with a co-cultivation of *T. reesei*, *A. phoenicis* and *S. cerevisiae* at 27 °C, pH= 5 and a residence time of 130 h. The time 0 denotes the switch from batch to continuous operation. The system was operated at batch conditions for 3 days to allow proper biofilm formation without any wash-out. At the moment of switching from batch to continuous operation, cellobiose was already depleted completely, which is in accordance with previous experiments, where the necessary time to deplete cellobiose was found to be around 28 h (Fig. 3.9). The first 27 h, the ethanol follows the wash-out trajectory, but afterwards the wash-out trajectory is left, and steady-state operation is reached with an ethanol concentration of  $0.784 \pm 0.042 \frac{\text{g}}{\text{L}}$  after the expected 3 to 5 residence times. [83] Steady-state operation was maintained over a period of 185 h. The steady-state ethanol production also confirms the hypothesis, that continuous co-cultivation of 2 competitors is possible if the growth rates are adjusted accordingly because an overgrowing of *A. phoenicis* by *T. reesei* would result in detectable cellobiose concentrations and an overgrowing of *T. reesei* by *A. phoenicis*

could not give an ethanol concentration of  $0.784 \frac{\text{g}}{\text{L}}$  because *A. phoenicis* does not provide enough CBH and EG activity. Given the enzyme production distribution of *T. reesei* and *A. phoenicis* [87], an ethanol concentration of  $0.91 \frac{\text{g}}{\text{L}}$  is the maximum for a co-cultivation of *A. phoenicis* and *S. cerevisiae*.

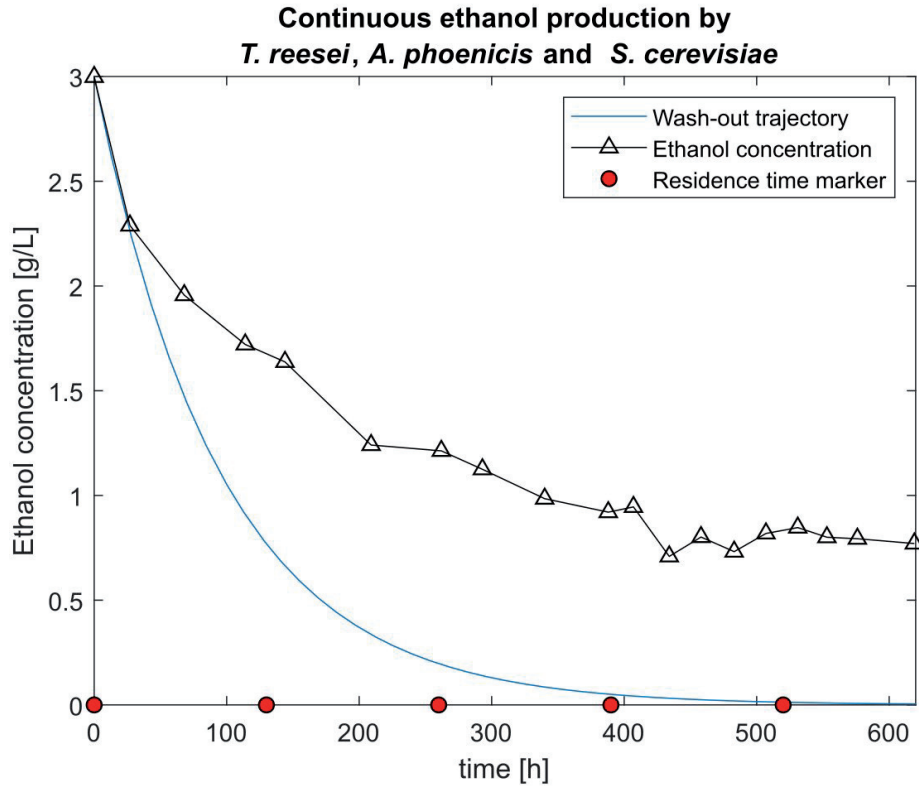


Figure 3.12: Continuous ethanol production with consolidated bioprocessing based on a microbial consortium of *T. reesei*, *A. phoenicis* & *S. cerevisiae*. The membrane (inner diameter  $d_i = 1.58 \text{ mm}$ , outer diameter  $d_o = 3.18 \text{ mm}$ , length  $L = 2.8 \text{ m}$ ) was aerated with 21 % oxygen fraction. The cellulose feed concentration was  $17.5 \frac{\text{g}}{\text{L}}$  and the residence time  $\tau$  was 130 h.

However, the titer ( $0.784 \frac{\text{g}}{\text{L}}$ ), the yield (9.7 %) and the productivity ( $0.006 \frac{\text{g}}{\text{L} \cdot \text{h}}$ ) are low regarding the fact that *A. phoenicis* was added to improve the performance of the system by utilizing the cellobiose better. The same experiment without *A. phoenicis* (only *T. reesei* and *S. cerevisiae*) appeared to be much more productive (by a factor of ca. 4) showing a yield of 40.3 %, a titer of  $3.26 \pm 0.01 \frac{\text{g}}{\text{L}}$  and a productivity of  $0.025 \frac{\text{g}}{\text{L} \cdot \text{h}}$  (Fig. 3.7). On the one hand, this seems to be due to the less inhibiting effect of cellobiose during continuous operation as it cannot accumulate unlike in batch operation. On the other hand, the ethanol degradation rate in the biofilm may be higher since there are two species present, which are able to utilize ethanol as carbon source. Furthermore, the metabolic activity of the two fungi may be affected by the competition. When facing competition, the microorganisms shift their metabolism towards optimized defense

against competitors and invaders resulting in maximized growth whereas it is optimized for efficient nutrient uptake in a cooperative scenario. [107–109] Thus, it may be hypothesized that the degradation rate of ethanol in the biofilm increases despite the presence of favored substrates because both fungi utilize any carbon source to maximize growth.

### 3.5 Conclusion

The key challenges for continuous CBP of cellulose to ethanol, namely continuous feeding and product removal, prevention of contamination, immobilization of cells and extracellular products, long-term stability were overcome and a steady-state operation was achieved multiple times with a maximum titer of  $3.26 \pm 0.01 \frac{\text{g}}{\text{L}}$  and a productivity of  $0.025 \frac{\text{g}}{\text{L} \cdot \text{h}}$ . It was proven that *T. reesei* produces constantly enzymes over 750 h, which is in agreement with kinetic models considering enzyme production a process, which is unrelated to primary metabolism and carried out by the secondary mycelia of *T. reesei*. Furthermore, it was proven that the continuous co-cultivation of two competitors, *T. reesei* & *A. phoenicis*, is possible, if the process conditions are adjusted to identical growth rate. The addition of *A. phoenicis* targeted the better utilization of the inhibiting intermediate cellobiose by balancing the fungal enzyme cocktail in terms of higher  $\beta$ -G concentrations. This goal was achieved, but however did not result in higher yields or productivities. Furthermore, the continuous experiments showed that the oxygen flux per membrane area is a critical parameter for the process. Setups with identical volumetric oxygen transfer rate  $k_L a$ , but different oxygen fluxes per membrane area (large area & low concentration gradient vs. small area and high concentration gradient) showed titer differences of ca. 80 % ( $1.83 \frac{\text{g}}{\text{L}}$  vs  $3.26 \frac{\text{g}}{\text{L}}$ ) in favor of setups with the large membrane surface. It is hypothesized that the difference is attributed to long diffusion paths in thicker biofilms and thus, shortage in nutrient supply. A rigorous process model is needed to examine this hypothesis in a quantitative manner.



## CHAPTER 4

---

### Set-up and validation of a rigorous, spatially resolved model of the kinetics and mass transfer limitations of consortium-based consolidated bioprocessing for ethanol production

---

#### 4.1 Abstract

The high degree of process intensification with CBP based on a microbial consortium in a membrane aerated biofilm reactor demands high standards for modeling. Various microbial interactions need to be considered and the heterogeneous reactor design causes considerable mass transfer limitations. A rigorous process model, which included all reaction kinetics and mass transfer limitations of the system was developed in this work. 9 species were considered (oxygen, glucose, *T. reesei*, secondary mycelia of *T. reesei*, enzymes, cellulose, cellobiose, yeast density and ethanol). 8 of these 9 species (all except cellulose) are present in the biofilm. In order to account properly for mass transfer limitations due to length of diffusion paths, these 8 species needed to be modeled spatially resolved. The fungal biofilm thickness  $\delta_f$  was found to be a critical parameter with an optimum for every membrane configuration. Smaller  $\delta_f$  reduced the fungal biofilm volume and thus, the enzyme production unnecessarily and larger  $\delta_f$  increased the diffusion path length and caused shortage in nutrient supply as well as lower enzyme concentrations in the bulk. The results of the model were able to explain the different productivities observed in the continuous experiments. The enzyme synthesis rate of the secondary mycelia was used as fitting parameter of the model. A reduction of ca. 40 % ( $0.67 \frac{FPU}{mL*d}$  vs  $1.152 \frac{FPU}{mL*d}$ ) compared to batch models yielded agreement with the continuous experiments.

## 4.2 Introduction

The efficient conversion of cellulosic substrates to various chemicals by CBP based on a microbial consortium in membrane aerated biofilm reactor has been proven numerous times. [4,9,50,110] Research was undertaken regarding the compatibility of different consortia and optimized biological pathways for maximized metabolic activity and minimized losses by CO<sub>2</sub> as byproduct of metabolism (e.g. by introducing the “lactate platform”). [9,50,110] A fundamental understanding of the process on a chemical engineering level is however still missing because modeling CBP rigorously is a complex task.

The complexity arises through the need to resolve a reaction network spatially (Fig. 4.1 & 4.2). Compared to other CBP experiments mentioned earlier, this is a rather simple layout, but still results in a complex reaction network (Fig. 4.1): *T. reesei* grows in the biofilm with oxygen and glucose as the two limiting substrates. The produced cellulases, consisting of cellobiohydrolase (CBH), endoglucanase (EG) and  $\beta$ -glucosidase ( $\beta$ -G), act synergistically to cleave cellulose to cellobiose and finally to glucose. Glucose is consumed by *T. reesei* and by *S. cerevisiae*, which ferments the sugar to ethanol. The target product ethanol may be depleted by aerobic metabolism of *S. cerevisiae* and by *T. reesei* if there is a shortage in a favored nutrient such as glucose.

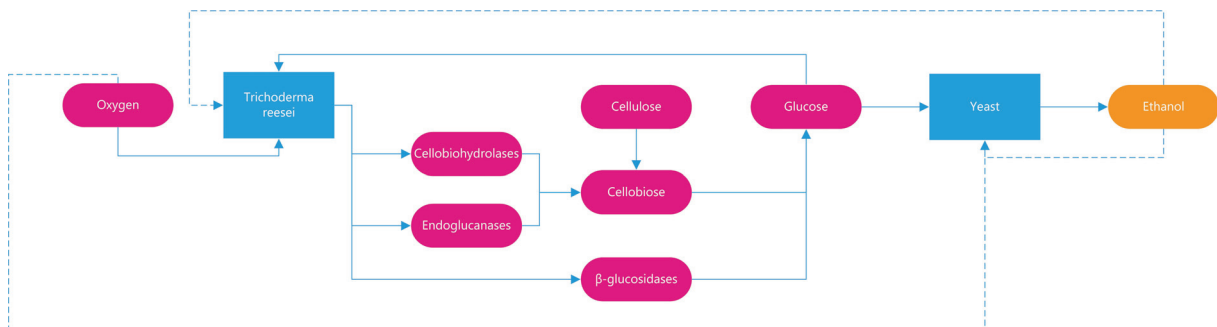


Figure 4.1: Kinetic network of consolidated bioprocessing of cellulose to ethanol by a microbial consortium of *T. reesei* & *S. cerevisiae*. *T. reesei* grows in the biofilm with oxygen and glucose as the two limiting substrates. The produced cellulases, consisting of cellobiohydrolase (CBH), endoglucanase (EG) and  $\beta$ -glucosidase ( $\beta$ -G), act synergistically to cleave cellulose to cellobiose and finally to glucose. Glucose is consumed by *T. reesei* and by *S. cerevisiae*, which ferments the sugar to ethanol. The target product ethanol may be depleted by aerobic metabolism of *S. cerevisiae* and by *T. reesei* if there is a shortage in a favored nutrient such as glucose. The solid lines represent desired reaction pathways. The dotted lines denote undesired side-reactions.

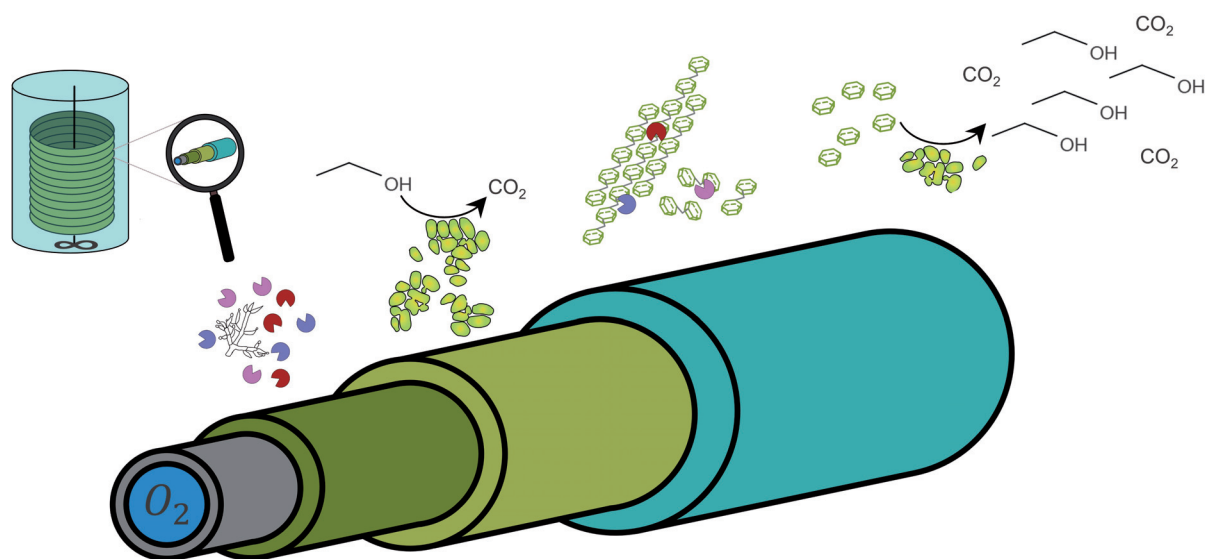


Figure 4.2: Schematic representation of consolidated bioprocessing of cellulose to ethanol by a microbial consortium of *T. reesei* & *S. cerevisiae*. Oxygen (blue) diffuses through a membrane (grey) and establishes an aerobic layer above the membrane in an otherwise anoxic reactor system. The aerobic, cellulolytic fungus *T. reesei* grows in this aerobic layer (dark green) and releases cellulases to the bulk (turquoise), where the cellulases hydrolyze cellulose to glucose. The glucose feeds both, *T. reesei* and *S. cerevisiae*, which grows anaerobically in the bulk, fermenting glucose to ethanol, as well as aerobically in the outer biofilm layer (light green), where oxygen residues are present.

Fig. 4.2 depicts the spatial arrangement of ethanol production by CBP. An aerobic, cellulolytic fungus, *T. reesei*, grows in an cylindrical aerobic layer provided by membrane aeration and releases cellulolytic enzymes, which diffuse to the bulk and synergistically hydrolyze the cellulose to glucose as mentioned above. The released soluble substances glucose and cellobiose are partly converted in the bulk and diffuse partly into the biofilm. Every component given in the reaction network except cellulose (Fig. 4.1) is present in the biofilm. Thus, a spatially resolved model accounting for mass transfer of every species except cellulose is necessary. Models are available describing each aspect of CBP: The mass transfer within a biofilm grown on a membrane [111,112], the growth kinetics of *T. reesei* and *S. cerevisiae* [10,19,102], microbial interaction in a community [34] and simultaneous enzymatic saccharification and fermentation (SSF) in a homogeneous bulk phase [102]. The key to rigorously modeling the present system is interlinking the different models, account for the interactions of the different sub-models according to the reaction network (Fig. 4.1) and include any mass transfer limitations. Specifically, this implies a spatially resolved model with defined mass transfer mechanisms in the different reactor compartments such as the biofilm or the bulk. Moreover, the growth kinetics taken from other models are linked with the mass transfer equations and the dilution

of each species in the bulk due to the continuous operation. Applying time-invariance because of the steady-state assumption gives the set of equations, which needs to be solved.

This work aims to provide such a rigorous model for steady-state consolidated bioprocessing of cellulose to ethanol in order to enable a 50-fold scale-up from laboratory scale to pilot scale. The model data is validated with the results of the continuous CBP experiments (chapter 3).

## 4.3 Results and Discussion

### *Degrees of freedom & validation of the model*

Before advancing to the set-up and solution of the model equation, it is worth overviewing the degrees of freedom (DOFs) of the model as well as its validation parameters since the ratio of validation parameters to the DoFs has a large impact on the quality of the model. A model, which satisfies a lot of validation points with only a few DoFs without too large errors, can be considered as highly precise. In contrast, any poor model with much more DoFs than validation points could be fitted to the same problem. Regarding the DoFs it is important to distinguish between DoFs of the experimental setups (e.g. the oxygen concentration within the membrane, the membrane area or the dilution rate) and DoFs of the model. Any design and set parameters are DoFs of the experimental setup. These DoFs need to be exploited to create a set of representative validation points for the model. In this work, the oxygen concentration within the membrane and the membrane area was varied (section 3) to create a set of 24 validation parameters (the bulk concentrations of ethanol, glucose, cellobiose and enzyme activity of three steady-states in reactor cascades with two reactors each). The number of DoFs of the model reduces to its fitting parameters. Since this work builds upon published model literature for the single bioprocesses occurring in the CBP reactor [10,19,34,102,111,112], the model parameters, where the greatest deviation between a biofilm culture and a suspended culture was expected, were chosen as fitting parameters. The set of fitting parameters and thus, DoFs, was kept as small as possible in order to guarantee a good model quality, which is necessary for the optimization work to scale-up the system (section 5.3). In this work, the enzyme synthesis rate constant  $k_{synth}$  and the effective diffusivity of  $\beta$ -glucosidase  $D_{BG,eff}$  due to its affinity to cell wall attachment were used as fitting parameters. Varying  $k_{synth}$  allows to adjust the quantity of enzymes within the system to fit the model to the overall conversion results.  $D_{BG,eff}$  determines the fraction of cellobiose conversion in the bulk to cellobiose conversion in the biofilm, which influences the glucose supply for the two community members and thus, the microbial equilibrium. The fitting of these two parameters allowed for less than 0.5 % numerical error of model iterations and less than 15 % deviation of experimental results (validation parameters) and model results.

### *Spatial structure of the model*

As mentioned above, a spatially resolved model is crucial to account for mass transfer limitations. The biofilm forms two layers on the membrane, which are defined by the oxygen gradient (Fig. 4.2). The inner layer provides enough oxygen for growth of *T. reesei* and the outer layer provides enough oxygen for aerobic yeast metabolism. A tubular membrane design leads to the same layer formation, with cylindrical instead of plane shape (Fig. 4.3a). Note: Technically, the yeast is also a fungus. However, the yeast does not produce cellulase enzymes, but is able to perform anaerobic metabolism. The label “fungal biofilm” refers to the filamentous enzyme producing fungus *T. reesei*.

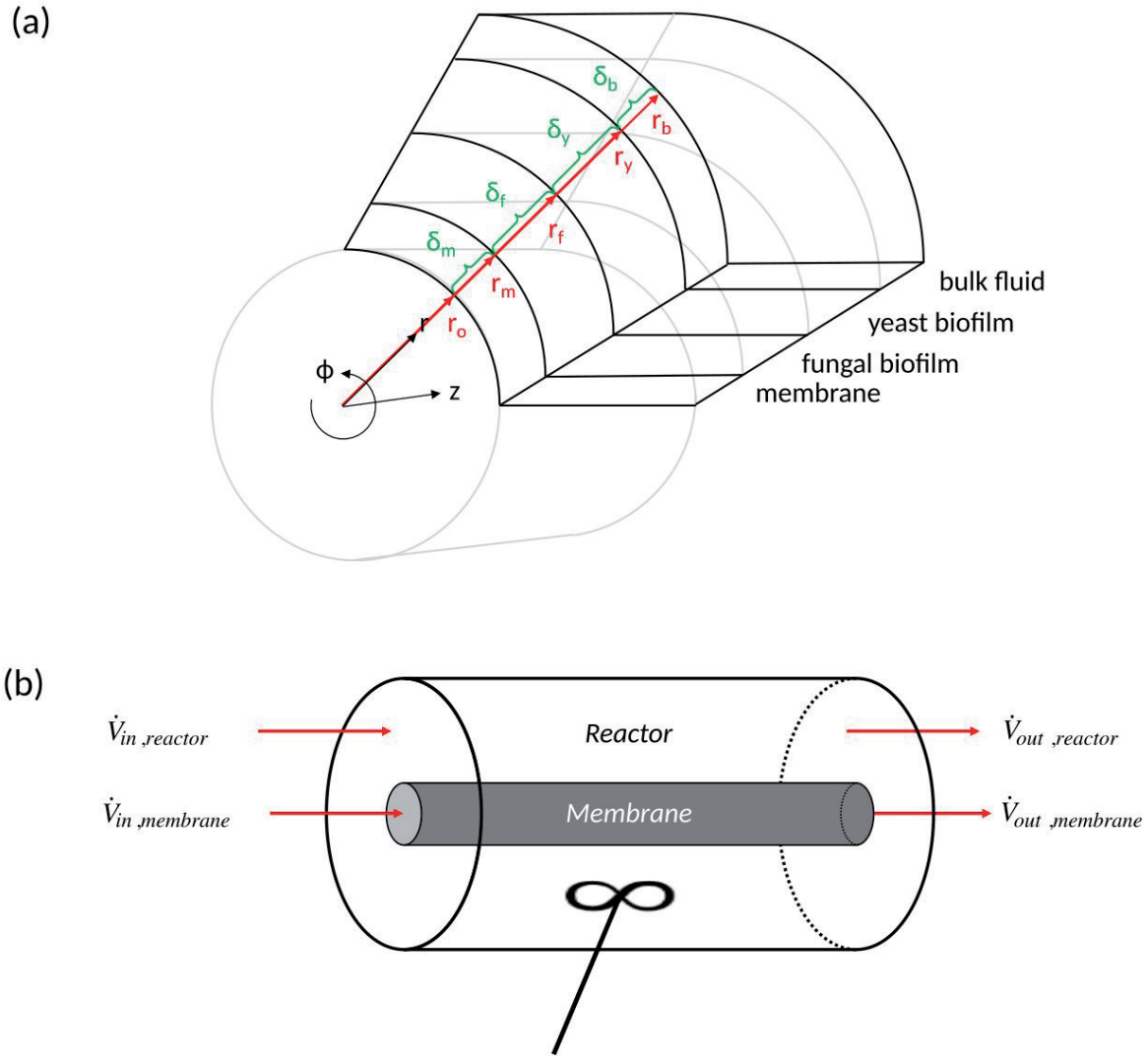


Figure 4.3: Schematic representation of the layer formation with a tubular membrane (a) and the concept of the bulk phase as cylindrical shell around the membrane and biofilm layers (b). Note: The straight membrane tube is a simplification for illustration purposes. The actual setup contains a helically winded membrane (Fig. 1.4).

From a mathematical point of view, the bulk phase is also considered to be a cylindrical layer element around the biofilm (Fig. 4.3b). Obviously, this does not hold for many reactor designs. However, since the bulk is defined to be perfectly mixed, the geometry of the bulk does not matter and assuming tubular shape serves to keep the model structure consistent. The radius of the bulk phase layer element is defined by the reactor volume subtracting the membrane and biofilm volume.

Although the membrane is winded densely within the reactor causing the upper and lower

side of the membrane touch each other, the system is considered to be of perfect tubular nature. Thus, there is no variance in the angular coordinate  $\varphi$ . A factor  $A_{eff} \in [0,1]$  is used to account for the effectively reduced membrane surface area. Hence, the 2D projection in the  $r$ - $z$ -plane is sufficient to characterize the system keeping in mind that the outer layers have larger area/volume due to the cylindrical geometry of the system (Fig. 4.4).

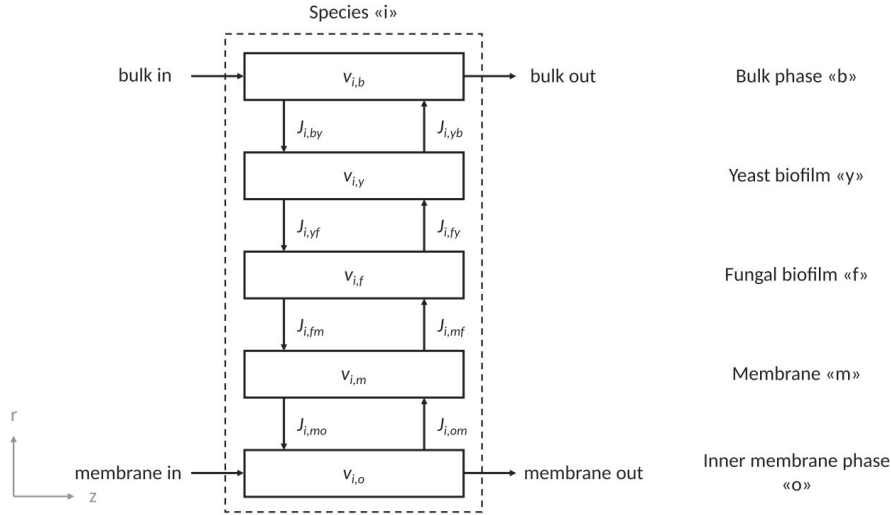


Figure 4.4: 2D projection of the layer formation in the  $r$ - $z$ -plane. Each layer is characterized by a reaction term  $v_i$  for species  $i$ . The mass fluxes between the layers are denoted by  $J_i$ .

Each layer element (inner membrane phase, membrane, fungal biofilm, yeast biofilm & bulk phase) is characterized by different properties, which allow different simplifications of the governing equations.

#### Set up of the model equations

The model is based on the mass conservation law at steady-state for each layer element (Fig. 4.4). Note that only the important parameters and coefficients are introduced in this chapter for the purpose of readability. A definition of each physical quantity used in this model including its units is given in the nomenclature and in the Matlab® code (section B.2). Given the spatial structure of the model, specification can be set up for each species  $i$ , which is considered in the model (Tab. 4.1). The number of species  $i$  includes all species of the reaction network (Fig. 4.1), whereby the enzymes are grouped together to one species and *T. reesei*'s total concentration as well as the concentration of secondary mycelia is considered. The enzymes are grouped

together since the composition of the enzymatic cocktail of *T. reesei* is known and assumed to be a material constant (eq. 4.1). [87]

$$c_E \begin{cases} \frac{0.7IU/ml}{81.93IU/ml} = 0.85\% c_{E,CBH} \\ \frac{81.1IU/ml}{81.93IU/ml} = 98.99\% c_{E,EG} \\ \frac{0.13IU/ml}{81.93IU/ml} = 0.16\% c_{E,\beta-G} \end{cases} \quad (4.1)$$

Distinguishing between the total cell density of *T. reesei* and the density of its secondary mycelia is necessary since enzyme synthesis of *T. reesei* is proportional to the concentration of secondary mycelia of *T. reesei*, whereas oxygen and glucose uptake are growth-related and thus depend on the primary mycelia density. The conversion of primary to secondary mycelia is modeled with 1<sup>st</sup> order reaction terms (Tab. 4.1). Note that the mass conservation law always requires a governing equation (e.g. Fick's law for diffusion) and a set of boundary conditions (BCs) depending on the order of the governing equations. Tab. 4.1 only refers to the specifications of the governing equations. The BCs for each species *i* are discussed later.

Table 4.1: Specifications for each species *i* considered in the model in every layer considered in the model.

Species/spatially resolved specifications	Inner membrane phase "o"				Membrane "m"			
	Present	Dominating mass transfer	Source term generated by	Depletion term generated by Outlet flow and convection to membrane wall	Present	Present	Dominating mass transfer	Depletion term generated by
Oxygen	✓	Convection	Inlet flow		✓	✓	Diffusion	X
Trichoderma reesei	X				X	X		
Trichoderma reesei secondary mycelia	X				X	X		
Enzymes	X				X	X		
Cellulose	X				X	X		
Cellobiose	X				X	X		
Glucose	X				X	X		
Yeast	X				X	X		
Ethanol	✓	Convection	Convection from membrane wall	Outlet flow	✓	✓	Diffusion	X



Table 4.2: Specifications for each species  $i$  considered in the model in every layer considered in the model. (continued)

					Yeast biofilm "Y"			
Species/spatially resolved specifications		Fungal biofilm "F"			Present	Dominating mass transfer	Source term generated by	Depletion term generated by Growth and maintenance of S. cerevisiae
	Present	Dominating mass transfer	Source term generated by	Depletion term generated by Growth and maintenance of T. reesei				
Oxygen	✓	Diffusion	X	Monod growth kinetics	✓	Diffusion	X	
Trichoderma reesei	✓	Stationary	1st conversion reaction of primary mycelia	1st order decay reaction	X			
Trichoderma reesei secondary mycelia	✓	Stationary	1st order enzyme synthesis reaction of T. reesei secondary mycelia	1st order decay reaction	✓	Diffusion	X	1st order decay reaction
Enzymes	✓	Diffusion			X			
Cellulose	X							
Cellobiose	✓	Diffusion	X	Enzymatic hydrolysis	✓	Diffusion	X	Enzymatic hydrolysis
Glucose	✓	Diffusion	Enzymatic hydrolysis	Growth and maintenance of T. reesei	✓	Diffusion	Enzymatic hydrolysis	Growth and maintenance of S. cerevisiae
Yeast	X				✓	Stationary	Monod growth kinetics	1st order decay reaction
Ethanol	✓	Diffusion	X	Degradation by T. reesei	✓	Diffusion	Fermentation kinetics of S. cerevisiae	Respiration kinetics of S. cerevisiae

Table 4.3: Specifications for each species  $i$  considered in the model in every layer considered in the model. (continued)

Species/spatially resolved specifications	Bulk phase "b"		
	Present	Dominating mass transfer	Depletion term generated by
Oxygen	✓		Source term generated by Convection from the biofilm
Trichoderma reesei	X		Outlet flow
Trichoderma reesei secondary mycelia	X		
Enzymes	✓		Convection from the biofilm
Cellulose	✓		1st order decay reaction & outlet flow
Cellobiose	✓		Enzymatic hydrolysis and outlet flow
			Enzymatic hydrolysis and outlet flow
			Enzymatic hydrolysis and outlet flow
Glucose	✓		Enzymatic hydrolysis
			Growth and maintenance of S. cerevisiae and outlet flow
Yeast	✓		Enzymatic hydrolysis
			1st order decay reaction and outlet flow
Ethanol	✓		Monod growth kinetics
			Fermentation kinetics of S. cerevisiae
			Respiration kinetics of S. cerevisiae and outlet flow

### Inner membrane phase "o":

Only oxygen and ethanol are present in the inner membrane phase. The steady-state assumption cancels out the time variance. The transport of gases from the inner membrane bulk to the membrane wall and vice versa is dominated by forced convection due to the gas flow within the membrane. In both cases, the mass balance shows that the difference in inlet and outlet flow of the membrane corresponds to the quantity of oxygen or ethanol, respectively, which is transported to or from the membrane wall by forced convection (eq. 4.2 & 4.3).

$$\frac{\partial (V_o c_{ox})}{\partial t} = 0 = \dot{V}_{o,feed} c_{ox,o,feed} - J_{conv,ox,om} - \dot{V}_{o,out} c_{ox,o,out} \quad (4.2)$$

$$\frac{\partial (V_o c_{EtOH})}{\partial t} = 0 = \dot{V}_{o,feed} c_{EtOH,o,feed} + J_{conv,EtOH,om} - \dot{V}_{o,out} c_{EtOH,o,out} \quad (4.3)$$

The convective mass transfer flux is defined as follows for both species:

$$J_{conv,i,om} = 2\pi r_o k_{conv,i,om} (c_{i,o} - c_i|_{r=r_o}) \quad (4.4)$$

The convective mass transfer coefficient is calculated by a Nusselt correlation and the Colburn analogy for either laminar or turbulent flow resp. the interpolation between both for transitional flow. [113,114] The model contains an if-loop to obtain the right Nusselt correlation for each flow regime. The correlation for laminar flow is shown here for illustration purpose (eq. 4.5).

$$Nu = \left\{ 3.66 + 0.08 \left[ 1 + 0.8 \left( \frac{d}{D_w \left[ \left( \frac{h}{\pi D_w} \right)^2 \right]} \right)^{0.9} Re^{0.5+0.2903} \left( \frac{d}{D_w \left[ \left( \frac{h}{\pi D_w} \right)^2 \right]} \right)^{0.194} Pr^{1/3} \right] \right\} \left( \frac{Pr}{Pr_W} \right)^{0.14} \quad (4.5)$$

The Nusselt correlation for a helically winded pipe is of empirical nature und depends only on the fluid properties and the geometry of the tube. The Colburn analogy allows to replace  $Nu$  with the Sherwood number  $Sh$  and the Prandtl number  $Pr$  with the Schmidt number  $Sc$ .  $Sh$  relates the convective mass transfer coefficient to the diffusivity, which is a known material constant (eq. 4.6).

$$Sh = \frac{k_{conv} d_i}{D_i} \quad (4.6)$$

Knowing  $k_{conv,i}$  allows to solve the mass balances for ethanol and oxygen in the inner membrane phase. However, at the membrane wall, both oxygen and ethanol will change from the gaseous/vapor phase to the dissolved phase as they can only diffuse through the membrane matrix as dissolved species. The absorption by the membrane is modeled with a Henry type law (eq. 4.7):

$$c_i|_{r=r_o} = S_{i,m} n_i p_m \quad (4.7)$$

The wall concentration of ethanol and oxygen is equal to their partial pressure times their solubility constant in PDMS. [14]

### Membrane “m”:

As no reactions occur in the membrane, the local concentrations of oxygen and ethanol are given by Fick’s law of diffusion:

$$\frac{\partial c_i}{\partial t} = \vec{\nabla} J_{i,f} + v_{i,f} \quad (4.8)$$

$$\Leftrightarrow \frac{\partial c_i}{\partial t} = 0 = \vec{\nabla} \left( \vec{\nabla} D_{i,f} c_i \right) + v_{i,f} \quad (4.9)$$

$$\Rightarrow 0 = D_{i,f} \Delta c_i + v_{i,f} \quad (4.10)$$

$$\Rightarrow 0 = D_{i,f} \left( \frac{2}{r} \frac{\partial c_i}{\partial r} + \frac{\partial^2 c_i}{\partial r^2} + \frac{\partial^2 c_i}{\partial z^2} \right) + v_{i,f} \quad (4.11)$$

Eq. 4.8 denotes the continuity equation. Applying Fick’s law of diffusion yields eq. 4.9. Assuming isotropic diffusivity (eq. 4.10) and neglecting the variance in the angular coordinate  $\varphi$  gives the final mass balance for the local concentrations (eq. 4.11). The first derivative term,  $\frac{2}{r} \frac{\partial c_i}{\partial r}$ , accounts for the cylindrical geometry of the system, whereas  $\frac{\partial^2 c_i}{\partial r^2} + \frac{\partial^2 c_i}{\partial z^2}$  simply describe a 2-D diffusion problem. [115] Note that the common approach to model diffusion is the solution-diffusion approach where the driving force is expressed as the gradient in the chemical potential. [116] However, since the pressure difference across the membrane is negligible, the difference in chemical potential is reduced to the difference in concentration. Furthermore, the Henry law is considered for the solution part of the solution diffusion model. The convective boundary layer and the gradient in z-direction were the reason, why the solution diffusion model could not be applied.

### Fungal biofilm “f”:

The fungal biofilm is a more complex layer since more species are present in the fungal biofilm layer and reactions take place. However, the mass transfer mechanism is diffusion for every species in the fungal biofilm except the stationary mycelia. Thus, Fick’s law will be applied again. The analysis of the fungal biofilm layer is started with the kinetic growth model of *T. reesei*.

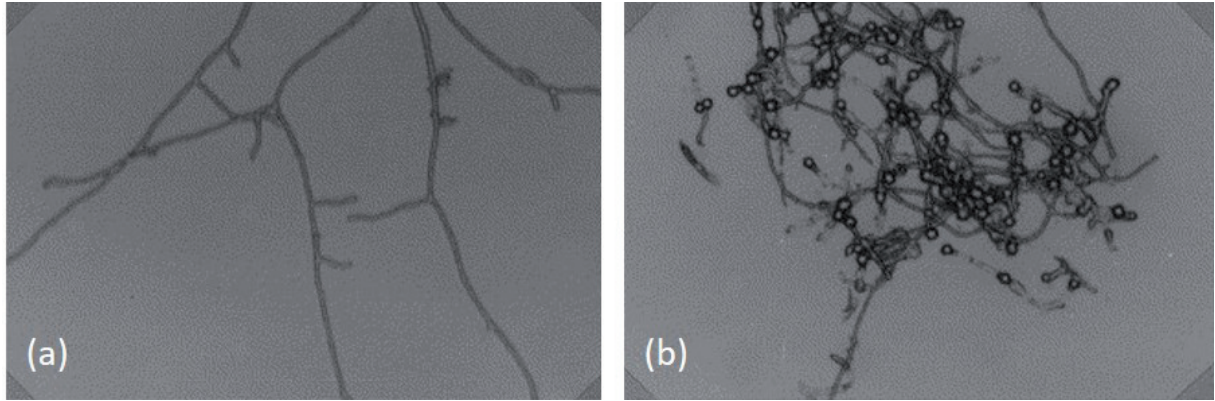


Figure 4.5: Primary mycelia (a) and secondary mycelia (b) of *T. reesei*. Figure taken from [10]

The growth kinetics of *T. reesei* were adapted from a published kinetic model for batch cultivation [10]:

The fungus consumes nutrients to grow primary mycelia (eq. 4.12 and Fig. 4.5a), which are converted to secondary mycelia (eq. 4.12 & 4.13 and Fig. 4.5b) responsible for the enzyme production, and finally, the secondary mycelia decay (eq. 4.13).

$$\frac{d[X]_{Tr,prim}}{dt} = \mu_{\max} \min \left[ \frac{c_g}{K_G + c_g}; \frac{c_{ox}}{K_{ox} + c_{ox}} \right] [X]_{Tr,prim} - k_{Tr,p-s} [X]_{Tr,prim} \quad (4.12)$$

$$\frac{d[X]_{Tr,sec}}{dt} = k_{Tr,p-s} [X]_{Tr,prim} - k_{decay} [X]_{Tr,sec} \quad (4.13)$$

Mycelia conversion and decay are modeled as 1<sup>st</sup> order reactions with reaction constants  $k_{Tr,p-s}$  and  $k_{decay}$ , respectively. The fungal growth is modeled with substrate-limited Monod-kinetics.  $\mu_{\max}$  is the maximum growth rate,  $K_G$  and  $K_{ox}$  are the half-saturation constants for glucose and oxygen, respectively. The limiting nutrient at each position in the biofilm is identified and considered by  $\min \left[ \frac{c_g}{K_G + c_g}; \frac{c_{ox}}{K_{ox} + c_{ox}} \right]$ . Given  $[X]_{Tr,sec} + [X]_{Tr,prim} = [X]_{Tr}$  (the fungus consists only of primary and secondary mycelia), allows to derive the local fraction of secondary mycelia and primary mycelia from eq. 4.13 with steady-state assumption:

$$0 = k_{Tr,p-s} ([X]_{Tr} - [X]_{Tr,sec}) - k_{decay} [X]_{Tr,sec} \quad (4.14)$$

$$\Leftrightarrow [X]_{Tr,sec} = \frac{k_{Tr,p-s}}{k_{Tr,p-s} + k_{decay}} [X]_{Tr} \quad (4.15)$$

$$\Rightarrow [X]_{Tr,prim} = \frac{k_{decay}}{k_{Tr,p-s} + k_{decay}} [X]_{Tr} \quad (4.16)$$

Applying steady-state for eq. 4.12 gives:

$$0 = \mu_{max} \min \left[ \frac{c_g}{K_G + c_g}; \frac{c_{ox}}{K_{ox} + c_{ox}} \right] [X]_{Tr,prim} - k_{Tr,p-s} [X]_{Tr,prim} \quad (4.17)$$

$$\Leftrightarrow \mu_{max} \min \left[ \frac{c_g}{K_G + c_g}; \frac{c_{ox}}{K_{ox} + c_{ox}} \right] = k_{Tr,p-s} \quad (4.18)$$

The conversion rate of primary to secondary mycelia is equal to the growth rate, which is limited either by glucose or by oxygen, because these two are the scarcest nutrients in the system. As the nutrient limitation will be time-invariant, but space-dependent, the conversion constant  $k_{Tr,p-s}$  cannot be a constant as proposed for batch operation. [10] It is a function of the concentration of the limiting nutrient and the material constants  $\mu_{max}$ ,  $K_G$  and  $K_{ox}$ .

Inserting eq. 4.18 into eq. 4.15 and applying steady-state yields:

$$[X]_{Tr,sec} = \frac{\mu_{max} \min \left[ \frac{c_g}{K_G + c_g}; \frac{c_{ox}}{K_{ox} + c_{ox}} \right]}{\mu_{max} \min \left[ \frac{c_g}{K_G + c_g}; \frac{c_{ox}}{K_{ox} + c_{ox}} \right] + k_{decay}} [X]_{Tr} \quad (4.19)$$

$\mu_{max}$  and  $K_G$  for *T. reesei* are taken from Velkovska et al. [10], whereas there is little information about the half-saturation constant of oxygen  $K_{ox}$ . *T. reesei* is usually cultivated in bubble aerated tanks with high oxygen concentrations of 5-13.5  $\frac{mg}{L}$ . [8,17] Oxygen half-saturation constants between 0.26  $\frac{mg}{L}$  and 1.1  $\frac{mg}{L}$  were published for different kinds of bacteria. [18–20] After evaluating the impact of  $K_{ox}$  values in the given range (Fig. 6), it was chosen to start the model with  $K_{ox} = 1 \frac{mg}{L}$  and fit  $K_{ox}$  to the experimental results if necessary.

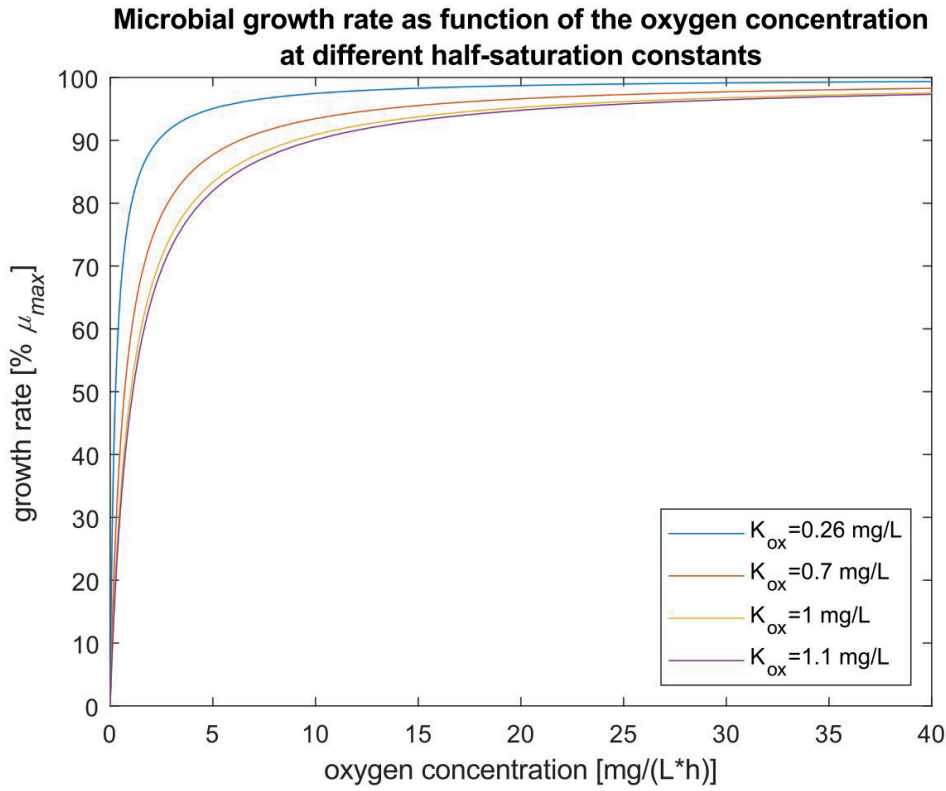


Figure 4.6: Microbial growth rate as function of the oxygen concentration at different half-saturation constants, which were published for bacteria. [11–13]

Hence, all parameters to determine  $[X]_{Tr,sec}$  from  $[X]_{Tr}$  are given, but  $[X]_{Tr}$  is still unknown. The given equations for  $[X]_{Tr}$ , the steady-state mass balance and the two boundary conditions (eq.4.20-4.22) form a homogeneous set of equations meaning that there is no constant part in any of the equations.

$$\frac{d[X]_{Tr}}{dt} = \frac{d[X]_{Tr,prim}}{dt} + \frac{d[X]_{Tr,sec}}{dt} = \mu_{max} \min \left[ \frac{c_g}{K_G + c_g}; \frac{c_{ox}}{K_{ox} + c_{ox}} \right] [X]_{Tr,prim} - k_{decay} [X]_{Tr,sec} = 0 \quad (4.20)$$

$$[X]_{Tr}|_{r=r_m} = 0 \quad (4.21)$$

$$[X]_{Tr}|_{r=r_f} = 0 \quad (4.22)$$

The mass balance is equal zero because of steady-state operation and the boundary conditions result from zero fungal growth in the membrane and the yeast biofilm. A homogeneous set of

equations has either only the zero-solution  $[X]_{Tr}$  or infinite solutions with the 0 solution among them. [117] Thus, the concentration profile of  $[X]_{Tr}$  has to be solved elsewhere: The fungal biofilm has a certain thickness  $\delta_f$ , which is yet unknown, but defined by the oxygen concentration. Below a certain oxygen concentration threshold, *T. reesei* will either be unable to perform aerobic metabolism, or the yeast will overgrow *T. reesei* at the given oxygen concentration. In any way, this oxygen concentration  $c_{O_2}^*$  will mark the end of the fungal biofilm:

$$\delta_f = r_f - r_m = r|_{c_{ox}=c_{ox}^*} - r_m \quad (4.23)$$

The density of fungal biomass of *T. reesei* is reported to be  $\bar{\rho}_{Tr} = 334 \frac{g}{L}$  and the mean cell fraction in biofilms is  $\bar{n}_{Tr,bf} = 0.15$ . [118,119] Thus, the mean cell concentration of *T. reesei* in the biofilm will be  $50.1 \frac{g}{L}$  (eq. 4.24):

$$\bar{\rho}_f = \bar{\rho}_{Tr} * \bar{n}_{Tr,bf} = 50.1 \frac{g}{L} = [X]_{Tr}|_{r_m < r < r_f} \quad (4.24)$$

Assuming a constant  $[X]_{Tr}$  over the biofilm is a improper simplification considering the vastly varying growth rate. Therefore, the cell concentration of *T. reesei* was adjusted to the local growth limitation while maintaining the given mean value (eq. 4.25):

$$[X]_{Tr} = \bar{\rho}_f * \frac{\mu}{\bar{\mu}} \quad (4.25)$$

Eq. 4.25 completes the set of equations for the *T. reesei* growth dynamics: Eq. 4.25 relates the fungal cell concentration to the oxygen and glucose concentration, eq. 4.19 gives the secondary mycelia concentration for the enzyme synthesis as function of the oxygen, glucose and total cell concentration.

Each other species diffuses across the biofilm and has source and/or depletion terms. The concentration profiles for oxygen and glucose can be derived from eq. 4.12, eq. 4.17 and Tab. 4.1: (eq. 4.26 & 4.27.

$$0 = D_{ox,f} \left( \frac{2}{r} \frac{\partial c_{ox}}{\partial r} + \frac{\partial^2 c_{ox}}{\partial r^2} + \frac{\partial^2 c_{ox}}{\partial z^2} \right) - \frac{\mu_{max}}{Y_{X,tr/o}} \min \left[ \frac{c_g}{K_G + c_g}; \frac{c_{ox}}{K_{ox} + c_{ox}} \right] \frac{k_{decay}}{k_{Tr,p-s} + k_{decay}} [X]_{Tr} - M_{X,tr/O} [X]_{Tr} \quad (4.26)$$

$$0 = D_{G,f} \left( \frac{2}{r} \frac{\partial c_G}{\partial r} + \frac{\partial^2 c_G}{\partial r^2} + \frac{\partial^2 c_G}{\partial z^2} \right) + \frac{K_{Cb} c_{Cb} 0.16\% c_E}{K_m \left( 1 + \frac{c_g}{K_{CbG}} \right) + c_{Cb}} - \frac{\mu_{max}}{Y_{X,tr/G}} \min \left[ \frac{c_g}{K_G + c_g}; \frac{c_{ox}}{K_{ox} + c_{ox}} \right] \frac{k_{decay}}{k_{Tr,p-s} + k_{decay}} [X]_{Tr} - M_{X,tr/G} [X]_{Tr} \quad (4.27)$$

*T. reesei* consumes oxygen and glucose for growth of new mycelia and maintenance of the existing mycelia. The corresponding consumption rate is determined by the product of a

yield coefficient respectively maintenance coefficient and the growth rate respectively the concentration of mycelia. These coefficients may be regarded as material constants and were taken from literature (Tab. 4.1). [19] The source term for glucose is hydrolysis of cellobiose in the fungal biofilm. [102]

Table 4.4: Overview of the yield and maintenance coefficients of *T. reesei* for oxygen and glucose. [19]

	Oxygen	Glucose
<b>Growth</b>	$Y_{X,tr/O} = 1.01 \frac{g_{X,tr}}{g_{O_2}}$	$Y_{X,tr/G} = 0.44 \frac{g_{X,tr}}{g_G}$
<b>Maintenance</b>	$M_{X,tr/O} = 0.0272 \frac{g_{O_2}}{g_{X,tr} * h}$	$M_{X,tr/G} = 0.0252 \frac{g_G}{g_{X,tr} * h}$

The mass balance for the enzymes in the fungal biofilm is given as follows (eq. 4.28)

$$0 = D_{E,f} \left( \frac{2}{r} \frac{\partial c_E}{\partial r} + \frac{\partial^2 c_E}{\partial r^2} + \frac{\partial^2 c_E}{\partial z^2} \right) + k_{synth} [X]_{Tr,sec} - k_{E,decay} c_E \quad (4.28)$$

Fick's law accounts for the diffusive mass transfer of enzymes within the biofilm,  $k_{synth} [X]_{Tr,sec}$  denotes the enzyme synthesis source term in the fungal biofilm and  $k_{E,decay} c_E$  is the enzyme decay depletion term.  $k_{synth}$  and  $k_{E,decay}$  again are material constants taken from literature. [10] Including cellobiose diffusion into the fungal biofilm in the model is important since it is an important nutrient support for *T. reesei*. Cellobiose cannot be digested by the yeast, but is hydrolyzed to glucose by  $\beta$ -G, which adheres mostly to the *T. reesei* cell surface (80 % adhesion, 20 % free enzymes). [87]

$$0 = D_{Cb,f} \left( \frac{2}{r} \frac{\partial c_{Cb}}{\partial r} + \frac{\partial^2 c_{Cb}}{\partial r^2} + \frac{\partial^2 c_{Cb}}{\partial z^2} \right) - \frac{K_{Cb} c_{Cb} 0.16\% c_E}{K_m \left( 1 + \frac{c_g}{K_{CbG}} \right) + c_{Cb}} \quad (4.29)$$

The mass balance for ethanol consists of the diffusion terms and a *T. reesei* degradation term for depletion.

$$0 = D_{EtOH,f} \left( \frac{2}{r} \frac{\partial c_{EtOH}}{\partial r} + \frac{\partial^2 c_{EtOH}}{\partial r^2} + \frac{\partial^2 c_{EtOH}}{\partial z^2} \right) - k_{degr} [X]_{Tr} \quad (4.30)$$

#### Yeast biofilm "y":

The mass balances in the yeast biofilm are formed analog to the fungal biofilm. Accordingly, the same problem of a homogeneous equation system arises for the immobilized yeast. The mean density for yeast cells is  $1100 \frac{g}{L}$ . [120, 121]

$$\bar{\rho}_y = \bar{\rho}_Y * \bar{n}_{Y,y} = 0.15 * 1100 \frac{g}{L} = 165 \frac{g}{L} = [X]_Y|_{r_f < r < r_y} \quad (4.31)$$



The thickness of the yeast biofilm layer is defined by the so-called Pasteur point. [122] The Pasteur point denotes the oxygen threshold, where *S. cerevisiae* switches to anaerobic metabolism. Since there is no point for the yeast to attach to the biofilm for anaerobic metabolism because the bulk is much richer in nutrients, it is assumed that the biofilm ends at the Pasteur point of the yeast. The mass balances for oxygen and glucose are formed by replacing the fungal depletion terms by yeast depletion terms: [102]

$$0 = D_{ox,f} \left( \frac{2}{r} \frac{\partial c_{ox}}{\partial r} + \frac{\partial^2 c_{ox}}{\partial r^2} + \frac{\partial^2 c_{ox}}{\partial z^2} \right) - \frac{\mu_{max}}{Y_{X,Y/O}} \left( \frac{c_g}{K_{GY} + c_g} \right) \left( 1 - \frac{c_{EtOH}}{K_{X-EtOH}} \right) \quad (4.32)$$

$$0 = D_{G,f} \left( \frac{2}{r} \frac{\partial c_G}{\partial r} + \frac{\partial^2 c_G}{\partial r^2} + \frac{\partial^2 c_G}{\partial z^2} \right) + \frac{K_{Cb} c_{Cb} 0.16\% c_E}{K_m \left( 1 + \frac{c_g}{K_{CbG}} \right) + c_{Cb}} - \frac{\mu_{max}}{Y_{X,Y/G}} \left( \frac{c_g}{K_{GY} + c_g} \right) \left( 1 - \frac{c_{EtOH}}{K_{X-EtOH}} \right) \quad (4.33)$$

Enzymes are not synthesized anymore in the yeast biofilm layer:

$$0 = D_{E,f} \left( \frac{2}{r} \frac{\partial c_E}{\partial r} + \frac{\partial^2 c_E}{\partial r^2} + \frac{\partial^2 c_E}{\partial z^2} \right) - k_{E, decay} c_E \quad (4.34)$$

The cellobiose mass balance does not change compared to the fungal biofilm:

$$0 = D_{Cb,f} \left( \frac{2}{r} \frac{\partial c_{Cb}}{\partial r} + \frac{\partial^2 c_{Cb}}{\partial r^2} + \frac{\partial^2 c_{Cb}}{\partial z^2} \right) - \frac{K_{Cb} c_{Cb} 0.16\% c_E}{K_m \left( 1 + \frac{c_g}{K_{CbG}} \right) + c_{Cb}} \quad (4.35)$$

The ethanol formation by the yeast needs to be considered in the ethanol mass balance:

$$0 = D_{EtOH,f} \left( \frac{2}{r} \frac{\partial c_{EtOH}}{\partial r} + \frac{\partial^2 c_{EtOH}}{\partial r^2} + \frac{\partial^2 c_{EtOH}}{\partial z^2} \right) + Y_{EtOH-G} \frac{\mu_{max}}{Y_{X,Y/G}} \left( \frac{c_g}{K_{GY} + c_g} \right) \left( 1 - \frac{c_{EtOH}}{K_{X-EtOH}} \right) - k_{degr}[X]_Y \quad (4.36)$$

### Bulk phase “b”:

The bulk phase is well-mixed and thus, there is no mass transfer limitation. The source term for all species from the immobilized phase is the convective mass flux into the bulk, which is calculated again with a Nusselt correlation and the Colburn analogy as explained above. The mass balances for the oxygen, glucose, enzymes and ethanol are:

$$0 = \frac{1}{V} J_{ox,conv,y} - \frac{1}{\tau} c_{ox} \quad (4.37)$$

$$0 = \frac{1}{V} J_{G,conv,y} + \frac{K_{Cb} c_{Cb} 0.16\% c_E}{K_m \left( 1 + \frac{c_g}{K_{CbG}} \right) + c_{Cb}} - \frac{\mu_{max}}{Y_{X,Y/G}} \left( \frac{c_g}{K_{GY} + c_g} \right) \left( 1 - \frac{c_{EtOH}}{K_{X-EtOH}} \right) - \frac{1}{\tau} c_G \quad (4.38)$$

$$0 = \frac{1}{V} J_{E,conv,y} - \left( \frac{1}{\tau} + k_{E,decay} \right) c_E \quad (4.39)$$

$$0 = \frac{-1}{V} J_{EtOH,conv,y} + Y_{EtOH-G} \frac{\mu_{max}}{Y_{X,Y/G}} \left( \frac{c_g}{K_{GY} + c_g} \right) \left( 1 - \frac{c_{EtOH}}{K_{X-EtOH}} \right) - \frac{1}{\tau} c_{EtOH} \quad (4.40)$$

The cellulose and cellobiose mass balance is governed by the kinetics of the enzymatic hydrolysis, which were taken from literature and adapted to continuous operation: [102]

$$[C]_{in,endo} + [C]_{in,exo} = [C]_{in} \quad (4.41)$$

$$[C]_{endo} + [C]_{exo} = [C] \quad (4.42)$$

$$[C] = [C]_{in} + \frac{r_C}{D} \quad (4.43)$$

$$0 = -k_{endo} \times \frac{[EC]_{endo}}{1 + \sigma_{endo}} \times \left( \frac{K_{C-Cb}}{[Cb] + K_{C-Cb}} \right) \times \left( \frac{K_{C-EtOH}}{[EtOH] + K_{C-EtOH}} \right) + D([C]_{in,endo} - [C]_{endo}) \quad (4.44)$$

$$0 = -k_{exo} \times \frac{[EC]_{exo}}{1 + \sigma_{exo}} \times \left( \frac{K_{C-Cb}}{[Cb] + K_{C-Cb}} \right) \times \left( \frac{K_{C-EtOH}}{[EtOH] + K_{C-EtOH}} \right) + D([C]_{in,exo} - [C]_{exo}) \quad (4.45)$$

$$0 = k_{fc} [E_{f,endo}] \times [C_{f,endo}] (1 + \sigma_{endo}) - \frac{k_{fc}}{K_{endo}} [EC]_{endo} - D[EC]_{endo} \quad (4.46)$$

$$0 = k_{fc} [E_{f,exo}] \times [C_{f,exo}] (1 + \sigma_{exo}) - \frac{k_{fc}}{K_{exo}} [EC]_{exo} - D([EC]_{exo}) \quad (4.47)$$

$$[E_{f,endo}] = [E_T] - \frac{[EC]_{endo} \times \sigma_{endo}}{(1 + \sigma_{endo})} \quad (4.48)$$

$$[E_{f,exo}] = [E_T] - \frac{[EC]_{exo} \times \sigma_{exo}}{(1 + \sigma_{exo})} \quad (4.49)$$

$$[C_{f,endo}] = [C] - \frac{[EC]_{endo}}{(1 + \sigma_{endo})} \quad (4.50)$$

$$[C_{f,exo}] = [C] - \frac{[EC]_{exo}}{(1 + \sigma_{exo})} \quad (4.51)$$

$$0 = - \left( \frac{342}{324} \right) r_C - \left( \frac{K_{Cb}[Cb][BG]}{K_m \times \left( 1 + \frac{[G]}{K_{Cb-G}} \right) + [Cb]} \right) - D[Cb] \quad (4.52)$$

$$0 = - \left( \frac{360}{342} \right) \times \left( \frac{K_{Cb}[Cb][BG]}{K_m \times \left( 1 + \frac{[G]}{K_{Cb-G}} \right) + [Cb]} \right) - \left( \frac{1}{Y_{X,Y,G}} r_{Y,b} + D[G] \right) \quad (4.53)$$

$$r_{Y,b} = \left( \frac{\mu_{max}[G]}{K_G + [G]} \right) \times [X]_Y \times \left( 1 - \frac{[EtOH]}{K_{X-EtOH}} \right) \quad (4.54)$$

$$0 = r_{Y,b} - D[X]_Y \quad (4.55)$$

$$0 = \left( \frac{Y_{EtOH,G}}{Y_{X,Y,G}} \right) \times r_{Y,b} - D[EtOH] \quad (4.56)$$

As mentioned above, the mass conservation law demands a set of boundary conditions besides the governing equations. At the boundaries of each layer element, a BC of one of the following type is present:

- Dirichlet BC:  $c_i|_{r_0} = \text{const.}$  (fixed values of certain species in the bulk or inner membrane phase)
- Neumann BC:  $\left. \frac{dc_i}{dr} \right|_{r_0} = \text{const.}$  (fixed gradients e.g. same diffusion flux between the fungal and yeast biofilm layer)
- Robin BC:  $c_i|_{r_0} + \left. \frac{dc_i}{dr} \right|_{r_0} = \text{const.}$  (fixed balance between gradient and absolute value, e.g. due to balance of diffusion and convection at the yeast biofilm boundary to the bulk)

In general, the BCs are straightforward except for the microbial biomass, which was discussed before and the oxygen BC at the inner membrane phase. Thus, this BC is derived below.

The Henry law needs to be applied at the inner membrane wall since oxygen is dissolved in the membrane for the diffusion process:

$$c_{ox}|_{r_o} = H_{cp}^{ox} p_{ox}|_{r_o} \quad (4.57)$$

If convective mass transfer in the boundary layer at the inner membrane wall is neglected, the BC at the inner membrane side simplifies to the above-mentioned Henry equation and depends only on the absolute pressure and the oxygen concentration of the flushing gas. However, the BC becomes more complex, if (a) pressure loss within the membrane is considered and (b) convective mass transfer at the inner membrane side is not neglected. Since the aim of this work is to model the system as rigorously as possible in order to achieve scale-independent results, the BC is calculated as follows: The factor  $p_{ox}|_{r_o}$  needs to be corrected for the pressure gradient within the membrane and the convective mass transfer at the inner membrane side. The pressure loss in a helical coil without any armatures is defined as [114]:

$$\Delta p = \zeta \frac{L}{d_i} \rho \frac{u^2}{2} \quad (4.58)$$

$\zeta$  denotes the friction factor for helical coils, which depends on the flow regime and the curvature of the helix.  $L$ ,  $d_i$  and  $u$  are fixed values and denote, the membrane length, inner diameter and the superficial velocity within the membrane, respectively. The fluid density  $\rho$  is either constant for incompressible fluids such as oxygen-saturated water or calculated with the ideal gas law for gases. Thus, the gas density is a function of the coordinate  $z$  due to the pressure loss.

$$\rho = M_{fluid} \frac{p(z)}{RT} \quad (4.59)$$

An iterative procedure with  $p = 1 \text{ atm} \forall z$  as starting value gives  $p(m * \Delta z)$  and  $\rho(m * \Delta z)$  for every grid nod along the membrane. The partial pressure of oxygen in the inner membrane bulk is obtained from the absolute pressure and the mole fraction of oxygen within the gas. The partial pressure of oxygen at the membrane wall  $p_{ox}|_{r_o}$  is expected to be lower due to oxygen losses as result of diffusion through the membrane. Empirical correlations for convective mass transfer are used to relate  $p_{ox}|_{r_o}(z)$  to  $p(z)$ :

$$Nu = f(Re, Pr) \rightarrow Sh = f(Re, Sc) \quad (4.60)$$

The convective heat transfer is calculated with a Nusselt correlation as explained above, which depends on the flow regime, the Reynolds number and the Prandtl number. The Colburn

analogy between heat and mass transfer is used to derive the Sherwood number, which relates convective mass transfer to diffusive mass transfer, from the Nusselt number and finally obtain the convective mass transfer coefficient.

$p_{ox}|_{r_o}(z)$  is calculated with the mass balance for the membrane:

$$-J_{diff,i,mf} = J_{conv,i,om} \quad (4.61)$$

$$\begin{aligned} -\frac{2\pi D_{ox,m}L}{\ln\left(\frac{r_o}{r_m}\right)M_{ox}}(c_{ox}|_{r_o} - c_{ox}|_{r_m}) &= -\frac{2\pi D_{ox,m}L}{\ln\left(\frac{r_o}{r_m}\right)M_{ox}}\left(H_{cp}^{ox}p_{ox}|_{r_o} - c_{ox}|_{r_m}\right) = \frac{k_{conv,ox,m}A}{RT}(p_{ox}|_{r=0} - p_{ox}|_{r_o}) \\ &= \frac{k_{conv,ox,m}2\pi r_o L}{RT}(p_{ox}|_{r=0} - p_{ox}|_{r_o}) \end{aligned} \quad (4.62)$$

$$\Leftrightarrow p_{ox}|_{r_o} = \left[ \frac{\frac{2\pi D_{ox,m}L}{\ln\left(\frac{r_o}{r_m}\right)M_{ox}}c_{ox}|_{r_m} - \left(\frac{k_{conv,ox,m}2\pi r_o L}{RT} * p_{ox}|_{r=0}\right)}{\frac{2\pi D_{ox,m}L}{\ln\left(\frac{r_o}{r_m}\right)H_{cp}^{ox}} - \frac{k_{conv,ox,m}2\pi r_o L}{RT}} \right] \quad (4.63)$$

$$\Leftrightarrow c_{ox}|_{r_o} = H_{cp}^{ox} \left[ \frac{\frac{D_{ox,m}}{\ln\left(\frac{r_o}{r_m}\right)M_{ox}}c_{ox}|_{r_m} - \left(\frac{k_{conv,ox,m}r_o}{RT} * p_{ox}|_{r=0}\right)}{\frac{D_{ox,m}}{\ln\left(\frac{r_o}{r_m}\right)H_{cp}^{ox}} - \frac{k_{conv,ox,m}r_o}{RT}} \right] \quad (4.64)$$

Since this expression depends on  $c_{ox}|_{r_m}$ , a part of the solution for internal nodes, which depends on the boundary conditions, again an iterative procedure is necessary to solve the equation.

#### *Solving model equations*

Matlab R2019a® was used to model the above-mentioned equations. Since a PDE with solution  $c_i=f(r,z)$  cannot be solved analytically, a numerical method needs to be applied. Finite difference method (FDM) in 2D and cylindrical coordinates was chosen as there is no need to include unequal grid cell sizes (finite element method), but reactions are important ( $\nabla c_i \neq 0$ , thus the finite volume method is not suitable). [14, 123] According to FDM, a grid pattern of suitable resolution is applied to each layer element (see Fig. 4.7).

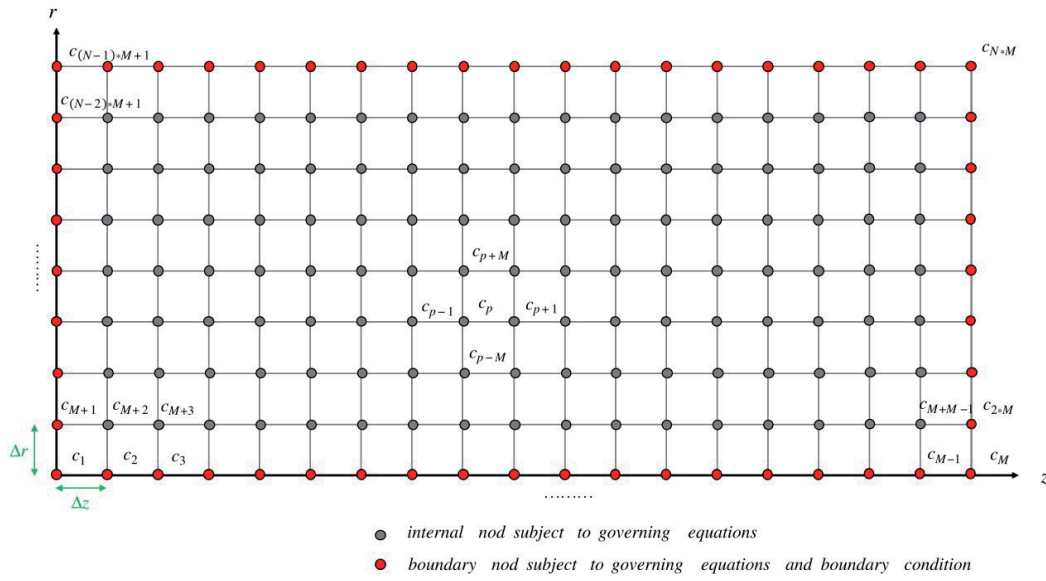


Figure 4.7: Grid system applied for finite difference method. A coordinate transformation of the form  $c_{ij} \rightarrow c_{(j-1)*M+i} = c_p$  is necessary to reduce the index to one variable. [14] Otherwise, it is impossible to address a certain element in the matrix/vector structure of the numerical solution procedure. The red nodes are subject to governing equations and boundary conditions whereas the inner nodes (grey) only are subject to the governing equations. Note that the coordinate system is still of cylindrical nature and the grid cell size is not constant.

The concept of FDM relies on the negligible impact of grid cells, which are far distant to the examined grid cell. Thus, the PDE can be discretized for each grid cell by means of the Taylor series expansion. The discretized forms of  $dr$  and  $dz$ ,  $\Delta r$  and  $\Delta z$ , respectively, correspond to the dimension of one grid cell. The degree of the Taylor series expansion defines the number of neighboring cells, which are not neglected. A 1<sup>st</sup> order Taylor series expansion only includes the directly neighbored elements in  $r$ - and  $z$ -direction. This leads to an error term, which is proportional to  $\Delta r^2$  and  $\Delta z^2$ , respectively. Higher order Taylor series expansion decrease the error further because the 2<sup>nd</sup> and further rows of neighboring elements are included. Thus, an infinite Taylor series expansion would result in the analytical solution considering the impact of each grid cell on every other grid cell. Applying 1<sup>st</sup> order Taylor series expansion to a defined number of grid cells leads to a set of algebraic equations, which include mass transfer and all kinetics of the system.

Eq. 4.71 shows exemplarily the result of a discretization (eqs. 4.67 - 4.70) of a concentration profile (eqs. 4.65 & 4.66) within the biofilm. Diffusion is the dominating mass transfer, and a 1<sup>st</sup> order reaction is added for illustrating purposes. [123]

$$\frac{\partial c_i}{\partial t} = \nabla (D \nabla c_i) + v_{i,j} \quad (4.65)$$

Assuming steady-state, isotropic diffusion coefficient and first order reactions:

$$0 = D\Delta c_i + k_{i,j}c_i \Leftrightarrow 0 = D \left[ \frac{1}{r} \frac{\partial}{\partial r} \left( r \frac{\partial c_i}{\partial r} \right) + \frac{1}{r^2} \frac{\partial^2 c_i}{\partial \varphi^2} + \frac{\partial^2 c_i}{\partial z^2} \right] + k_{i,j}c_i \quad (4.66)$$

Applying rotational symmetry:

$$0 = 2\pi D \left[ \frac{1}{r} \frac{\partial}{\partial r} \left( r \frac{\partial c_i}{\partial r} \right) + \frac{\partial^2 c_i}{\partial z^2} \right] + k_{i,j}c_i = 2\pi D \left[ \frac{1}{r} \left( \frac{\partial c_i}{\partial r} + r \frac{\partial^2 c_i}{\partial r^2} \right) + \frac{\partial^2 c_i}{\partial z^2} \right] + k_{i,j}c_i = 2\pi D \left[ \frac{1}{r} \frac{\partial c_i}{\partial r} + \frac{\partial^2 c_i}{\partial r^2} + \frac{\partial^2 c_i}{\partial z^2} \right] + k_{i,j}c_i \quad (4.67)$$

Discretization with a truncated Taylor series expansion ( $m,n$  define the node in  $z$ -/ $r$ -direction with  $M$  and  $N$  nodes in total per direction) yields:

$$0 = 2\pi D \left[ \frac{c_{i,m,n+1} - c_{i,m,n-1}}{2r_n \Delta r} + \frac{c_{i,m,n+1} - 2c_{i,m,n} + c_{i,m,n-1}}{(\Delta r)^2} + \frac{c_{i,m+1,n} - 2c_{i,m,n} + c_{i,m-1,n}}{(\Delta z)^2} \right] + k_{i,j}c_{i,m,n} \quad (4.68)$$

With  $r_n = r_i + (n-1)\Delta r$ :

$$0 = 2\pi D \left[ \frac{c_{i,m,n+1} - c_{i,m,n-1}}{2r_n \Delta r} + \frac{c_{i,m,n+1} - 2c_{i,m,n} + c_{i,m,n-1}}{(\Delta r)^2} + \frac{c_{i,m+1,n} - 2c_{i,m,n} + c_{i,m-1,n}}{(\Delta z)^2} \right] + k_{i,j}c_{i,m,n} \quad (4.69)$$

$$0 = \left[ \left( \frac{-2 * 2\pi D}{(\Delta r)^2} + \frac{-2 * 2\pi D}{(\Delta z)^2} \right) + k_{i,j} \right] c_{i,m,n} + \frac{2\pi D}{(\Delta z)^2} c_{i,m+1,n} + \frac{2\pi D}{(\Delta z)^2} c_{i,m-1,n} + \left( \frac{2\pi D}{(\Delta r)^2} + \frac{2\pi D}{2(r_i + (n-1)\Delta r)(\Delta r)} \right) c_{i,m,n+1} + \left( \frac{2\pi D}{(\Delta r)^2} - \frac{2\pi D}{2(r_i + (n-1)\Delta r)(\Delta r)} \right) c_{i,m,n-1} \quad (4.70)$$

Transforming the coordinate system (Fig. 4.7) to obtain single indices for numerical processing gives:

$$0 = \left[ \left( \frac{-2 * 2\pi D}{(\Delta r)^2} + \frac{-2 * 2\pi D}{(\Delta z)^2} \right) + k_{i,j} \right] c_{i,p} + \frac{2\pi D}{(\Delta z)^2} c_{i,p+1} + \frac{2\pi D}{(\Delta z)^2} c_{i,p-1} + \left( \frac{2\pi D}{(\Delta r)^2} + \frac{2\pi D}{2\Delta r \left[ r_i + f \text{loor} \left( \frac{p-1}{M} \right) \Delta r \right]} \right) c_{i,p+M} + \left( \frac{2\pi D}{(\Delta r)^2} - \frac{2\pi D}{2\Delta r \left[ r_i + f \text{loor} \left( \frac{p-1}{M} \right) \Delta r \right]} \right) c_{i,p-M} \quad (4.71)$$

$\text{floor}((p-1)/M)$  rounds  $p/M$  to the next smaller integer.

The central difference approach does not work for left/right boundary because there is no neighboring node in one direction. Thus, two time forward/backward Taylor series expansion

was applied for the left and right boundary since no boundary condition is given for the boundaries at  $z=0$  and  $z=L$  except for the inner membrane phase (eqs. 4.72 & 4.73).

$$\begin{aligned}
 0 &= 2\pi D \left[ \frac{c_{i,m,n+1} - c_{i,m,n-1}}{2r_n \Delta r} + \frac{c_{i,m,n+1} - 2c_{i,m,n} + c_{i,m,n-1}}{(\Delta r)^2} + \frac{c_{i,m+2,n} - 2c_{i,m+1,n} + c_{i,m,n}}{(\Delta z)^2} \right] + k_{i,j} c_{i,m,n} \\
 0 &= \left[ \left( \frac{-2 * 2\pi D}{(\Delta r)^2} + \frac{2\pi D}{(\Delta z)^2} \right) + k_{i,j} \right] c_{i,p} - \frac{2 * 2\pi D}{(\Delta z)^2} c_{i,p+1} + \frac{2\pi D}{(\Delta z)^2} c_{i,p+2} \\
 &\quad + \left( \frac{2\pi D}{(\Delta r)^2} + \frac{2\pi D}{2\Delta r \left[ r_i + f \text{loor} \left( \frac{p-1}{M} \right) \Delta r \right]} \right) c_{i,p+M} \\
 &\quad + \left( \frac{2\pi D}{(\Delta r)^2} - \frac{2\pi D}{2\Delta r \left[ r_i + f \text{loor} \left( \frac{p-1}{M} \right) \Delta r \right]} \right) c_{i,p-M}
 \end{aligned} \tag{4.72}$$

*Left boundary*

$$\begin{aligned}
 0 &= 2\pi D \left[ \frac{c_{i,m,n+1} - c_{i,m,n-1}}{2r_n \Delta r} + \frac{c_{i,m,n+1} - 2c_{i,m,n} + c_{i,m,n-1}}{(\Delta r)^2} + \frac{c_{i,m-2,n} - 2c_{i,m-1,n} + c_{i,m,n}}{(\Delta z)^2} \right] + k_{i,j} c_{i,m,n} \\
 0 &= \left[ \left( \frac{-2 * 2\pi D}{(\Delta r)^2} + \frac{2\pi D}{(\Delta z)^2} \right) + k_{i,j} \right] c_{i,p} - \frac{2 * 2\pi D}{(\Delta z)^2} c_{i,p-1} + \frac{2\pi D}{(\Delta z)^2} c_{i,p-2} \\
 &\quad + \left( \frac{2\pi D}{(\Delta r)^2} + \frac{2\pi D}{2\Delta r \left[ r_i + f \text{loor} \left( \frac{p-1}{M} \right) \Delta r \right]} \right) c_{i,p+M} \\
 &\quad + \left( \frac{2\pi D}{(\Delta r)^2} - \frac{2\pi D}{2\Delta r \left[ r_i + f \text{loor} \left( \frac{p-1}{M} \right) \Delta r \right]} \right) c_{i,p-M}
 \end{aligned} \tag{4.73}$$

*Right boundary*

All equations presented in the “set up of model equations” subsection were discretized accordingly. Also, the above-mentioned boundary conditions were discretized accordingly. However, the obtained set of discretized governing equations and discretized boundary conditions cannot be solved directly due to interdependences of the equations. For example, the oxygen uptake rate of *T. reesei* for maintenance metabolism influences the local oxygen concentration and depends on the concentration of fungal biomass, which itself depends on the local oxygen concentration. Thus, the system is solved by means of iteration. For each species, the arithmetic mean between initial bulk concentration and initial concentration in the inner membrane is chosen as initial value for the oxygen concentration of every volume element. Each run of the iteration gives a new solution for the local concentration of species  $i$  in each volume element. The solution vector is used as initial value set for the next iteration and then is overwritten by the new solution. The termination criterion for the iteration is a certain relative error threshold. To compute the relative error, the solutions of all included neighboring elements  $c_{k-1}$ ,  $c_{k+1}$ ,  $c_{k-M}$  and  $c_{k+M}$  of the examined cell  $c_k$  are plugged into the discretized equation of cell  $k$ . This gives a solution for  $c_k$ , which is different from the solution  $c_k$  in the solution vector. A relative error is calculated from these two values of  $c_k$ . As soon as the relative error comes under a certain threshold (0.1 % rel. error in this work), the termination criterion for the iteration is fulfilled. Since the convergence of the iteration is limited by the grid resolution, a suitable



grid resolution is needed for the corresponding iteration termination criterion (a 183x180 mesh converged to 0.1 % rel. error with 833 iterations).

#### Model simulations

Fig. 4.8 shows the 2D concentration profile for oxygen for the steady-state condition depicted in Fig. 3.7. The two discontinuities reflect the equilibrium at the phase boundaries gas-PDMS & PDMS-liquid defined by the partition coefficients of oxygen. The mass transfer limitation of the convective boundary layer at the inner membrane wall and the outer biofilm was found to be negligible, since large variations of the Reynolds number did not affect the convective mass transfer.

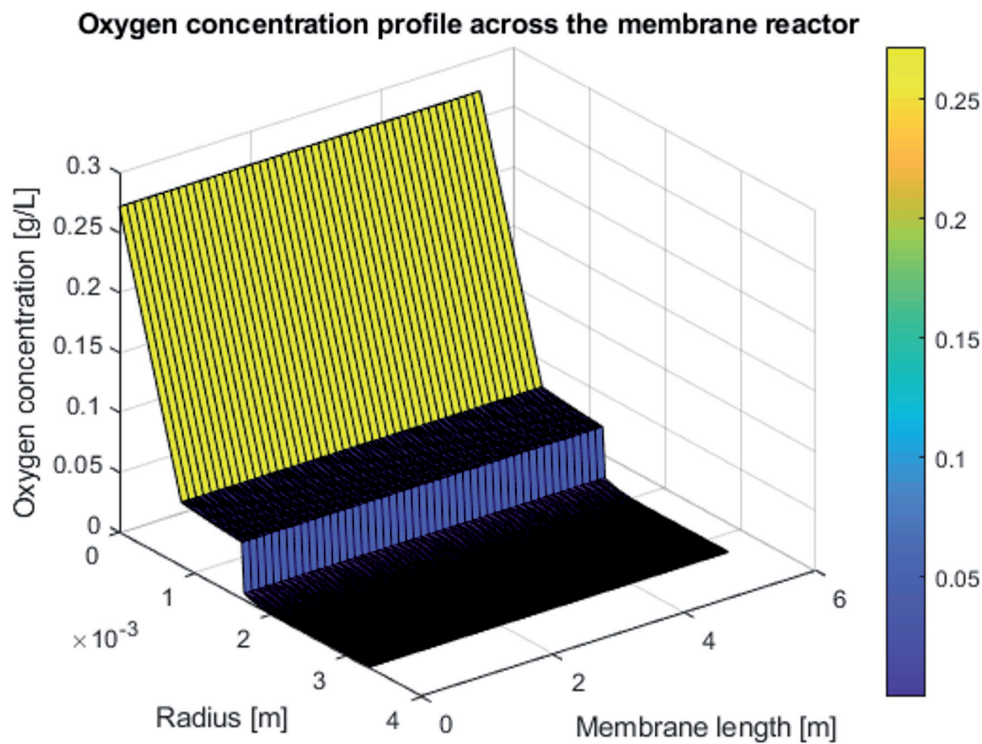


Figure 4.8: Simulated oxygen profile for the standard membrane ( $d_i = 1.58$  mm,  $d_o = 3.18$  mm,  $L = 5.6$  m). Even at low Reynolds numbers in the membrane ( $Re = 306.5$ ), z-gradient of the system is almost negligible. The two discontinuities reflect the partition coefficients of oxygen for gas, PDMS and water.

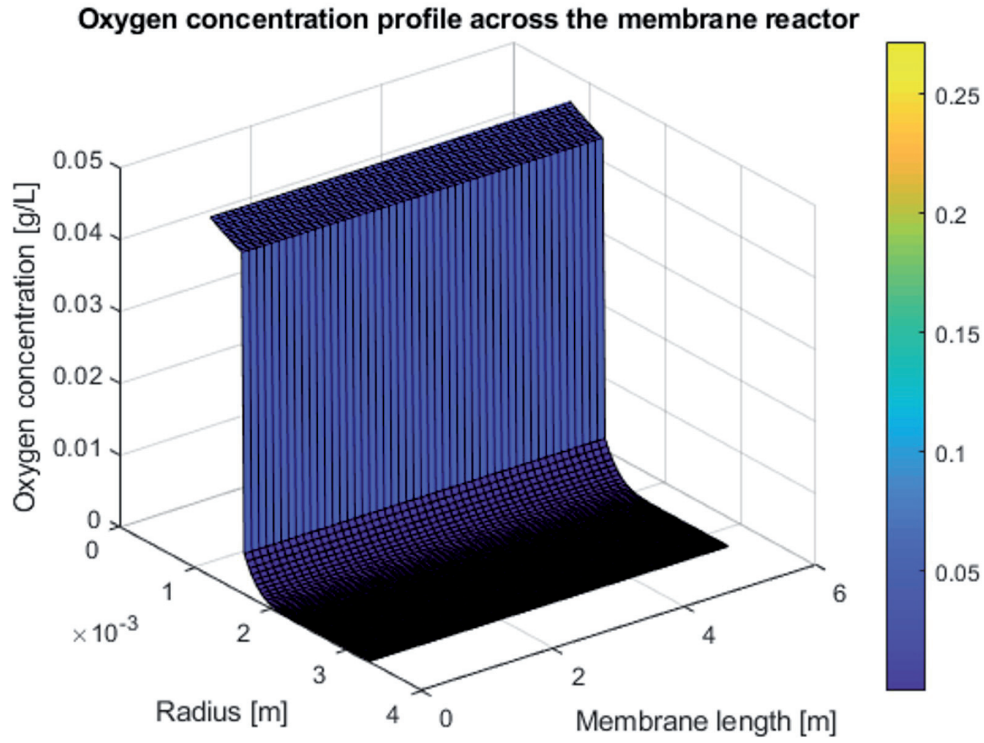


Figure 4.9: Oxygen profile within the biofilm for the standard membrane ( $d_i = 1.58$  mm,  $d_o = 3.18$  mm,  $L = 5.6$  m). The detailed view demonstrates the curvature of the oxygen profile as a result of the tubular system.

The logarithmic curvature due to the cylindrical membrane reflected by  $\frac{c_{i,m,n+1} - c_{i,m,n-1}}{2r_n \Delta r}$  in the discretization equation becomes clearly visible in the detailed view (Fig. 4.9). Furthermore, the  $z$ -gradient is almost negligible for the validation procedure. Oxygen shows the highest variance in  $z$  with a maximum of 0.3 % over the membrane length (Fig. 4.10), which is lower than the maximum numerical error of the model. Thus, the following graphs will be shown in 2D at  $z = 0$  for illustration purposes.

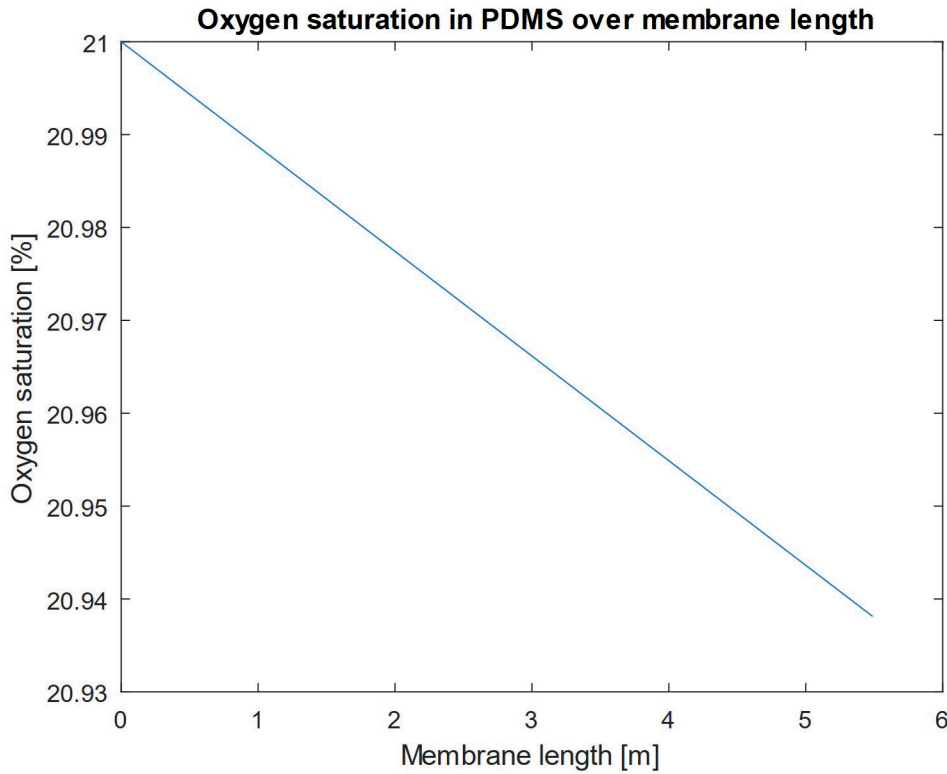


Figure 4.10: Oxygen profile along z-axis for the standard membrane ( $d_i = 1.58$  mm,  $d_o = 3.18$  mm,  $L = 5.6$  m). The oxygen saturation within the membrane changes by 0.3 % over the length, which is lower than the maximum numerical error of the model.

In order to fit the simulation outcome with the experiments of continuous CBP (chapter 3), the enzyme synthesis constant of *T. reesei* and the effective diffusivity of  $\beta$  – glucosidase were fitted within a range of 20 % - 100 % of the reported literature values (Fig. B.1). [10, 124, 125] It was assumed that these two parameters were affected the most by the change of bubble aerated batch suspension to immobilized membrane aerated biofilm formation during continuous operation. [10] Best agreement with the continuous results could be achieved by reduction of ca. 40 % ( $0.67 \frac{\text{FPU}}{\text{mL} \cdot \text{d}}$  vs  $1.152 \frac{\text{FPU}}{\text{mL} \cdot \text{d}}$ ) in enzyme production rate and a ca. 20 % reduced diffusivity of  $\beta$ -glucosidase compared to endoglucanase and cellobiohydrolase. The reduced diffusivity of  $\beta$ -glucosidase results in higher  $\beta$ -glucosidase concentrations in the biofilm and thus, accounts for the affinity of  $\beta$ -glucosidase to attach to the cell wall. The cell wall attachment of  $\beta$ -glucosidase could not be modeled with an adsorption equilibrium due to a lack of available data for the adsorption constants. The modeled ethanol concentration across all layers in the 1<sup>st</sup> reactor of the steady-state presented in 3.7 shows a deviation of 3.5 % compared to the validation parameter (Fig. 4.11).

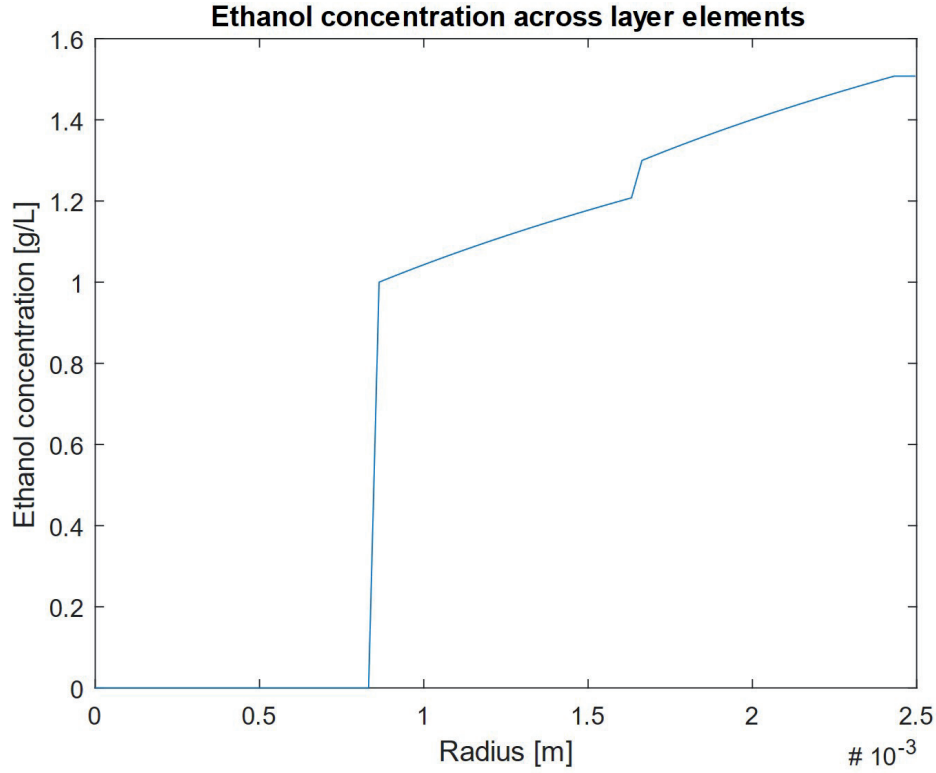


Figure 4.11: Ethanol profile along  $r$ -axis ( $z = 0$ ) over all layer elements for the standard membrane ( $d_i = 1.58$  mm,  $d_o = 3.18$  mm,  $L = 5.6$  m). The ethanol concentration at the right corresponds to the modeled bulk ethanol concentration of  $1.51 \frac{g}{L}$ , which has a 3.5 % deviation from the experimental value.

Having the model fitted to the continuous experiments at lab scale allows to examine low yields of the continuous experiments although  $k_L a$  was kept constant or even increased. Fig. 4.12 & 4.13 show the microbial growth rate as function of the radial coordinate in the fungal biofilm for 21 % and 42 % oxygen concentration. Since *T. reesei* growth is either limited by glucose or by oxygen, the optimum growth rate is achieved, where both limitations are equal. Given a higher mass transfer of oxygen per membrane area allows to grow a thicker biofilm (Fig. 4.12), which is not per se beneficial. On the one hand, there is more volume and thus, more production capacity. On the other hand, a thicker biofilm would extend the distance between glucose saturation and oxygen saturation (the dashed line from Fig. 4.12 moves to the right in Fig. 4.13). Thus, the activity decreases. Furthermore, thicker biofilms cause the problem of glucose-depleted, but oxygen-enriched zones (red circles in Fig. 4.13), where ethanol degradation by *T. reesei* increases by a factor of ca. 3, which was already discussed (section 3).

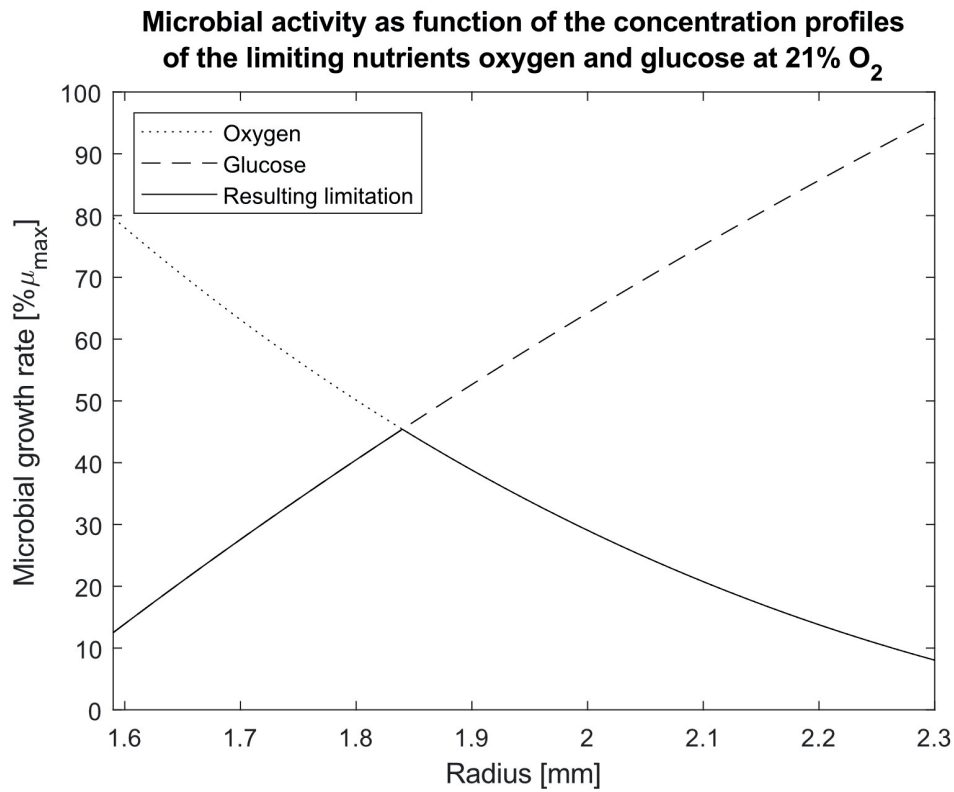


Figure 4.12: Projection of the oxygen and glucose gradient at  $z = 0$  as projection in the  $z$ -plane. Depending on the position in the fungal biofilm, either glucose or oxygen is the limiting nutrient. The maximum growth rate of ca. 45 %  $\mu_{\max}$  is reached at a distance of ca. 0.25 mm from the membrane surface for the standard membrane ( $d_i = 1.58$  mm,  $d_o = 3.18$  mm,  $L = 2.8$  m) at an oxygen concentration of 21 %.

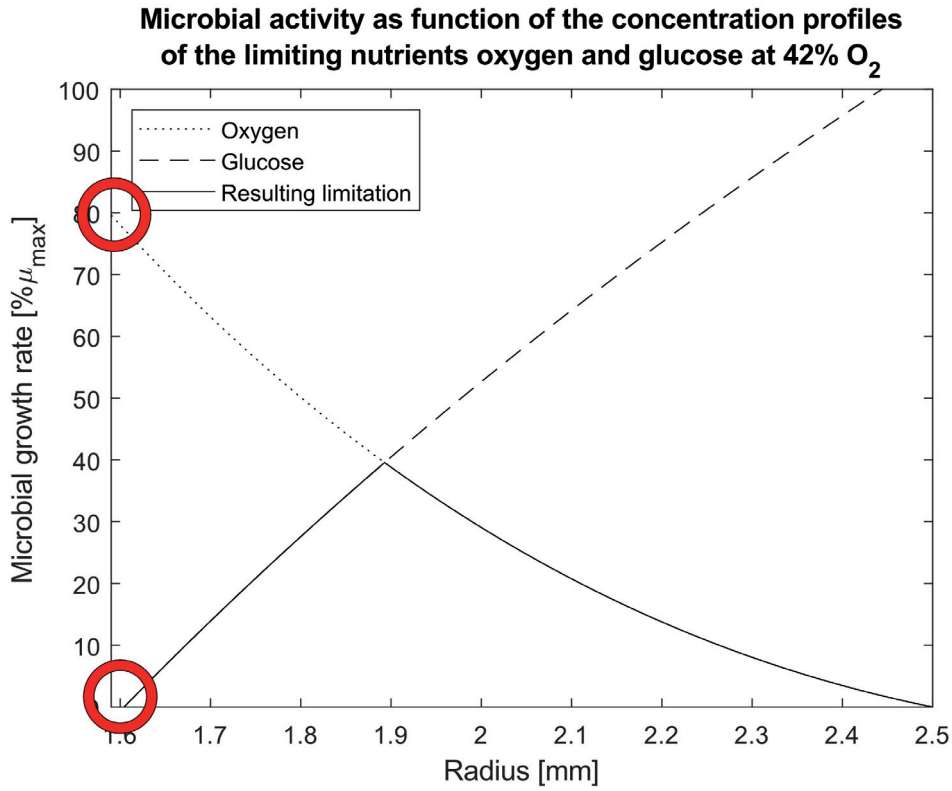


Figure 4.13: Projection of the oxygen and glucose gradient at  $z = 0$  as projection in the  $z$ -plane. Depending on the position in the fungal biofilm, either glucose or oxygen is the limiting nutrient. The maximum growth rate of ca. 40 %  $\mu_{\max}$  is reached at a distance of ca. 0.32 mm from the membrane surface for the standard membrane ( $d_i = 1.58$  mm,  $d_o = 3.18$  mm,  $L = 2.8$  m) at an oxygen concentration of 42 %. The red circles denote glucose-depleted, but oxygen-enriched zones in the fungal biofilm, where *T. reesei* degrades high amounts of ethanol (Fig. 3.6)

Fig. 4.14 summarizes the optimization problem. Increasing the fungal biofilm thickness (e.g. by a higher oxygen gradient or by a thinner membrane) causes a squared increase of the volume of the fungal biofilm (dashed line in Fig. 4.14). The microbial performance is proportional to the volume of the fungal biofilm (eq. 4.74).

$$P \propto V_f \propto \delta_f^2 \quad (4.74)$$

However, the shortage of the nutrient supply due to longer diffusion paths increases logarithmically due to the cylindrical geometry of the membrane (dotted line in Fig. 4.14) (eq. 4.75)

$$P \propto \frac{1}{\ln(\delta_f)} \quad (4.75)$$

As the logarithm outweighs the polynome for high  $\delta_f$ , but not for short  $\delta_f$ , an optimum fungal biofilm thickness of 1.5 mm is found for the standard membrane ( $d_i=1.58$  mm,  $d_o=3.18$  mm,  $L=2.8$  m) (solid line Fig. 4.14). Since  $\delta_f$  contains information about the benefits of high-volume biofilms as well as the disadvantages of long diffusion paths, it seems to be a promising scale-up parameter.

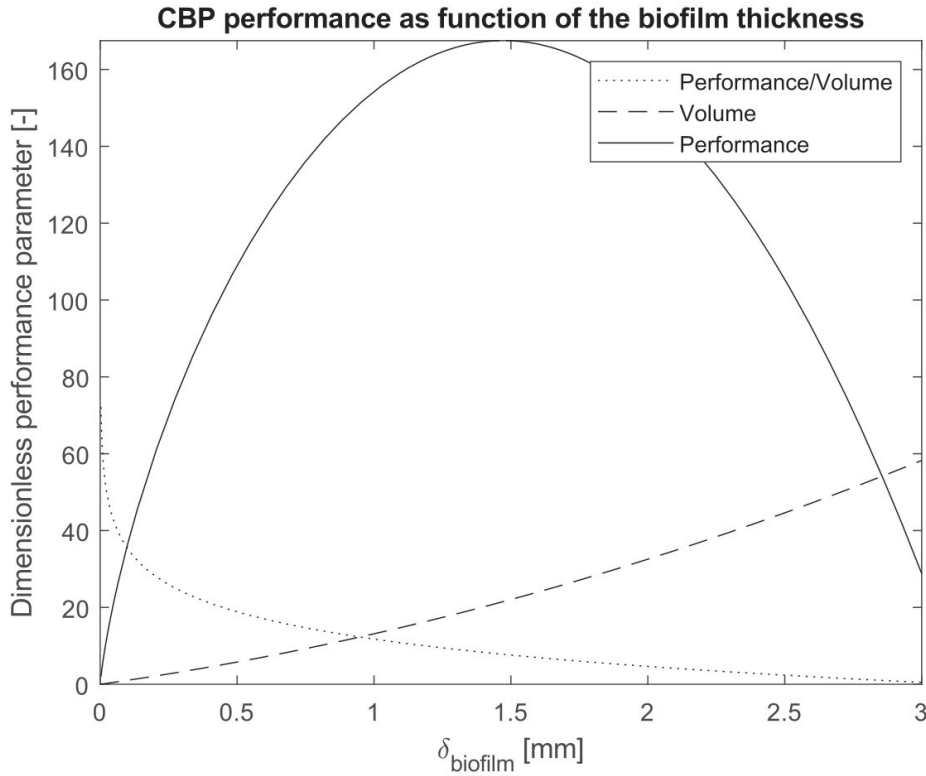


Figure 4.14: Evaluation of the optimum fungal biofilm thickness

### *Biofilm measurement*

As the fungal biofilm thickness was identified as critical parameter for the CBP performance, but did not belong the set of validation parameters, a batch experiment at the same conditions was conducted to grow a biofilm of comparable thickness. After 9 *d* of batch CBP operation, the reactor was harvested and the biofilm thickness was measured. The membrane support was mounted on a CNC apparatus (Fig. 4.15) and the biofilm was punctuated with a needle (Fig. 4.16), which was connected to a multimeter measuring the resistance at the needle tip. As the conductivity is the reciprocal of the resistance, the needle showed low conductivity & high resistance in the air and in the membrane, but high conductivity and low resistance within the biofilm, which consists of 85 % water with dissolved salts.

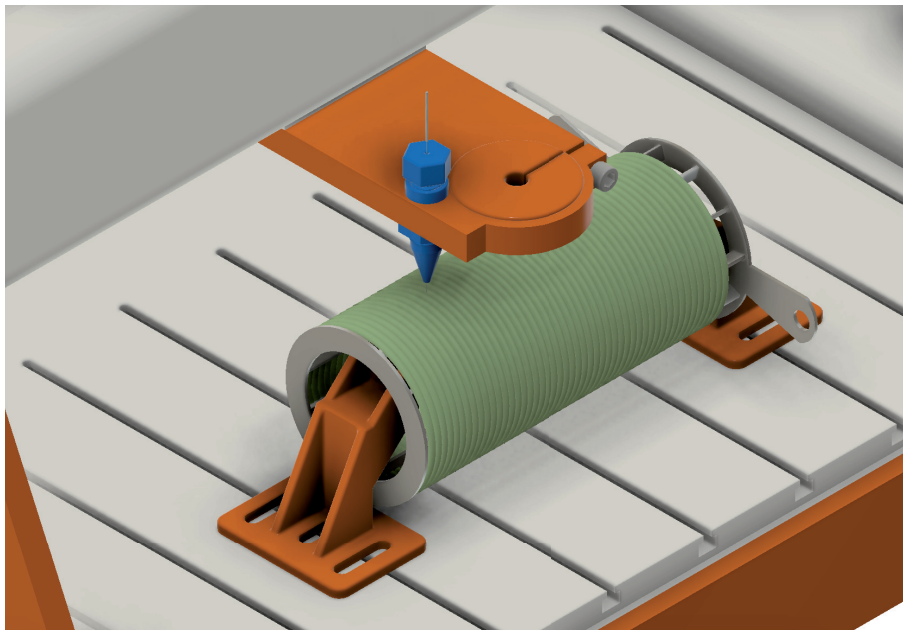


Figure 4.15: 3D view of the experimental apparatus to measure the biofilm thickness by measuring the conductivity at the tip of a needle punctuating the biofilm. (CAD created by S. Bowald)



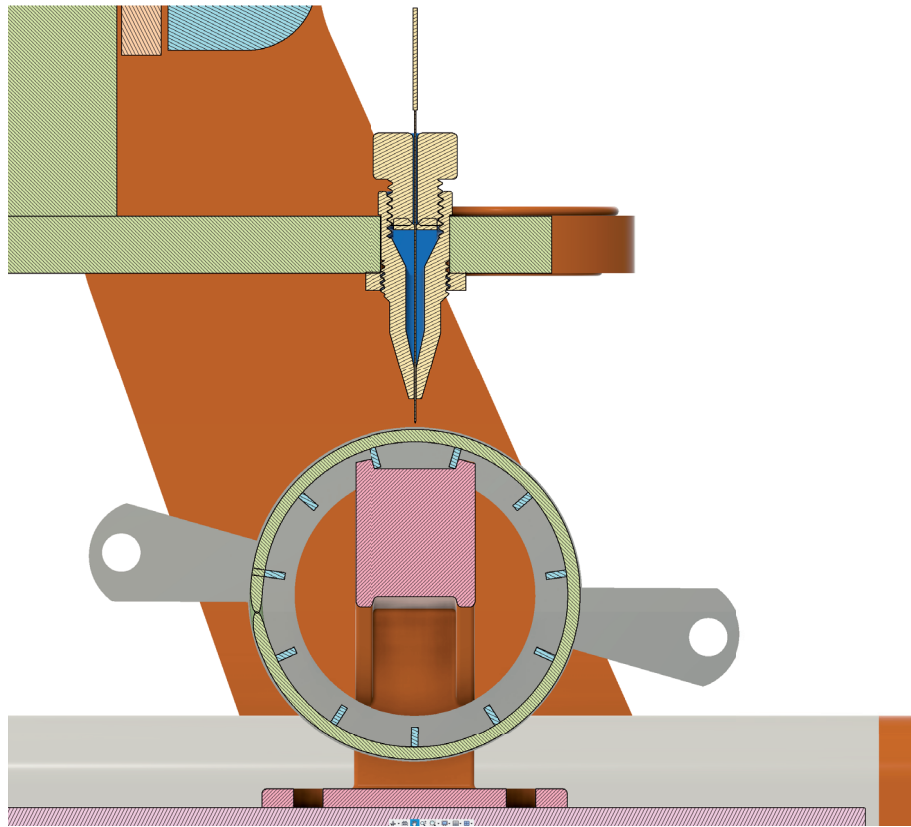


Figure 4.16: Cross-section view of the experimental apparatus to measure the biofilm thickness by measuring the conductivity at the tip of a needle punctuating the biofilm. (CAD created by S. Bowald)

The decrease in resistance from air to biofilm is discontinuous, whereas the increase in resistance from the biofilm to the membrane occurs slowly due to slight membrane deformation by the needle pressure (Fig. 4.17). In order to determine the boundary between the biofilm and the membrane properly, the biofilm was considered to end at that point, where the resistance is beyond a  $4\sigma$  confidence interval around the average resistance of the biofilm. Since a  $4\sigma$  confidence interval captures 99.4 % of the Gaussian normal distribution, the probability is sufficiently high, that a resistance outside of the confidence interval is rather due to membrane deformation than statistical uncertainty.

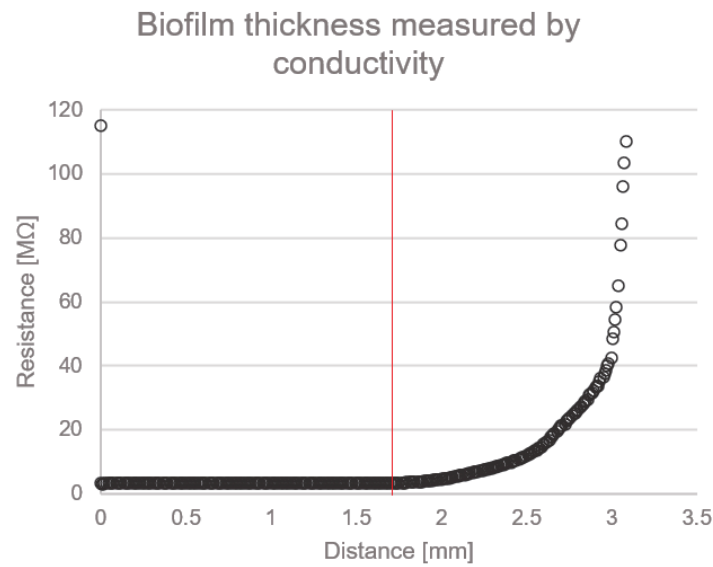


Figure 4.17: Resistance at the needle tip over the distance of punctuation. The decrease in resistance from air to biofilm is discontinuous, whereas the increase in resistance from the biofilm to the membrane occurs slowly due to slight membrane deformation by the needle pressure. The red line marks the end of the  $4\sigma$  confidence interval of the average biofilm resistance

The measured biofilm thickness (triangle markers in Fig. 4.18) of  $\delta_f = 1.7 \pm 0.35 \text{ mm}$  on average (solid line in Fig. 4.18) shows a deviation of ca. 12% to the model result (dashed line in Fig. 4.18). Given the difference in the setup (eg. batch vs. continuous), the model results regarding the biofilm thickness may be regarded as plausible.

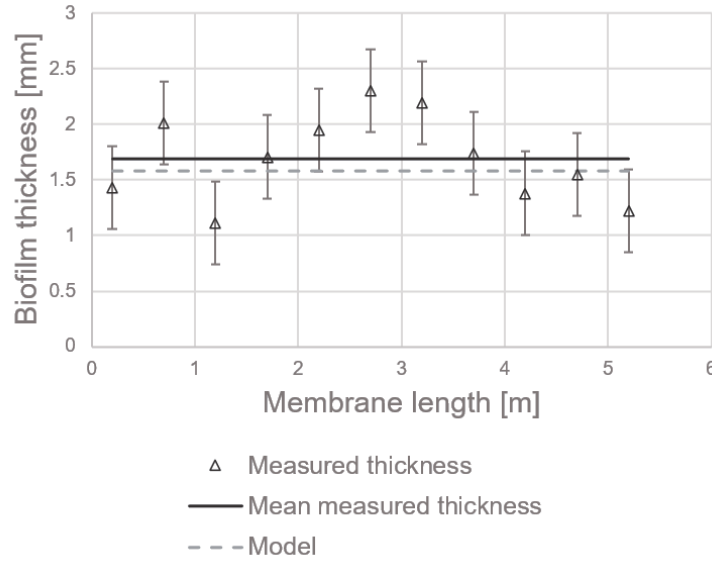


Figure 4.18: The measured biofilm thickness (triangle markers) of  $\delta_f = 1.7 \pm 0.35 \text{ mm}$  on average (solid line) shows a deviation of ca. 12% to the model result (dashed line)

## 4.4 Conclusion

A rigorous process model was developed for continuously operated consolidated bioprocessing of cellulose to ethanol. 9 species were considered (oxygen, glucose, *T. reesei*, secondary mycelia of *T. reesei*, enzymes, cellulose, cellobiose, yeast density and ethanol). 8 of these 9 species (each except cellulose) are present in the biofilm and thus, needed to be modelled spatially resolved in order to account properly for mass transfer limitations. The fungal biofilm thickness  $\delta_f$  was found to be a critical parameter with an optimum for every membrane configuration. Smaller  $\delta_f$  reduced the fungal biofilm volume and thus, the enzyme production unnecessarily and larger  $\delta_f$  increased the diffusion path length and caused shortage in nutrient supply as well as lower enzyme concentrations in the bulk. The results of the model were able to explain the different productivities observed in the continuous experiments. The enzyme synthesis rate of the secondary mycelia and the effective diffusivity of  $\beta$ -glucosidase  $D_{BG,eff}$  were used as fitting parameter of the model. A reduction of ca. 40 % ( $0.67 \frac{\text{FPU}}{\text{mL} \cdot \text{d}}$  vs  $1.152 \frac{\text{FPU}}{\text{mL} \cdot \text{d}}$ ) in enzyme activity and ca. 20 % ( $5 \cdot 10^{-11} \frac{\text{m}^2}{\text{s}}$  vs  $4 \cdot 10^{-11} \frac{\text{m}^2}{\text{s}}$ ) reduced effective diffusivity of  $\beta$ -glucosidase compared to batch models yielded agreement with the continuous experiments. The fitting of these two parameters allowed for less than 0.5 % numerical error of model iterations and less than 15 % deviation of experimental results (validation parameters) and model results. Furthermore, an experimental proof-of-concept for the plausibility of the model results regarding the fungal

biofilm thickness  $\delta_f$  was conducted. The fully validated rigorous process models allows to run optimization simulation for the best performing experimental setup at higher scales.

## CHAPTER 5

---

### Scale-up of a 2.7 L laboratory scale consortium-based consolidated bioprocess to 130 L pilot scale

---

#### 5.1 Abstract

The scale-up of innovative reactor concepts, which could enable bio-based bulk chemicals to replace their fossil-based counterparts, progresses slowly. The heterogeneity of the biological system often causes performance decrease at higher scales and thus, accentuate the lack of economic competitiveness against fossil-based pendants. It was aimed to combine the systematic scale-up approach of non-dimensionalizing the mathematical problem and requesting non-dimensional similarity with the simulation outcome of a rigorous process model in order to scale up a membrane aerated biofilm reactor to produce lignocellulosic ethanol employing consolidated processing. It became clear, that the simulation effort may be reduced significantly by identifying design trade-offs with a basic, systematic approach such as non-dimensionalizing the problem and resolving only the critical design constraints with a highly differentiated model. Whenever the the design constraints were overspecified, the minimum selling price was used as optimization criterion to minimize production costs. Regarding the final results, it was distinguished between an industrial favorable solution and an academically feasible solution to experimentally prove the scale-invariance of the model at 130 L pilot scale.

#### 5.2 Introduction

The scale-up of bioprocesses is gaining attention as governments around the globe realize the urgent need to promote industrial biotechnology as sustainable alternative to the fossil-based industry in the framework of a bio-based economy. [8,126] However, especially for low-margin

products such as bulk chemicals, the obstacles of scaling up a bioprocess (heterogeneity of microbial and plant biomass, mechanical and chemical sensitivity of cells etc.) paired with a lack of economic competitiveness of the bioprocess hinder wide-range implementation. [127–129] Ethanol, being produced from biomass to a large extent (share of bioethanol was 95 % in 2007 and increasing ever since [130, 131]), is an exception in this context. However, the production of bioethanol from direct fermentation of sugar crops or the cleavage of starch with amylases and subsequent fermentation is very “scale-up-friendly”. The fermentation of sugars to ethanol with *S. cerevisiae* is known for several thousands of years and conducted under reproducible conditions at large scale since the 1930s. [132] Besides the advantage through extensive experience, the fermentation occurs under anoxic conditions resp. the respiratory genes of a Crabtree-positive yeast such as *S. cerevisiae* are repressed by the high glucose concentrations, and thus, the most difficult challenge in most bioprocesses, the oxygen supply of the microbes, is not an issue. [133] However, the above-mentioned scale-up obstacles become relevant again, when replacing 1<sup>st</sup> generation bioethanol resources such as corn and sugar crops with non-edible 2<sup>nd</sup> generation bioethanol resources like lignocellulose, the most abundant organic carbon source in world, in order to avoid ethical conflicts as well as the hidden CO<sub>2</sub> footprint of 1<sup>st</sup> generation bioethanol resources due to land clearing measures or the use of fertilizers. [29, 134, 135] The economic competitiveness of 2<sup>nd</sup> generation bioethanol was addressed by many researches and CBP was identified as largest lever to reduce costs. [3, 33] CBP denotes the highest degree of process intensification, where enzyme production, enzymatic hydrolysis of the cellulose and fermentation of the sugars to ethanol is conducted in one process step. [4]

In chapter 2, it was shown, that the cost savings by continuously operated CBP allow for profitable 2<sup>nd</sup> generation biofuel production in the EU, but not in the US without applying an additional cost saving approach such as calculating with slightly lower returns on capital investment. [33] However, the cost savings of 27.5 % by applying continuously operated CBP are unmatched making it the most promising concept for large-scale production of 2<sup>nd</sup> generation bioethanol. [33] Since continuous operation demands long-term stability and robustness, a CBP approach with an industrial microbial consortium was preferred over a genetically modified “super-bug”. [34] In chapter 3 the proof-of-concept was delivered, that continuous CBP may be operated with a consortium of industrial microbes. The microbial community consisting of an aerobic enzyme producing filamentous fungus *T. reesei* and a facultative anaerobic single-celled fermenting organism *S. cerevisiae* is kept stable by assigning a niche for each species. The oxygen-enriched layer around a tubular, aerated membrane is the niche for *T. reesei*, whereas the oxygen-depleted zones in the reactor (outer biofilm layer and bulk suspension) are populated by *S. cerevisiae*. [4] Theoretically, *S. cerevisiae* could invade the niche of *T. reesei* and does likely to a minor extent (Chapter 4). However, the system stabilizes itself according to mechanisms of a “cheater-cooperator”-community. [34] *S. cerevisiae*, which cannot digest

cellulose, relies on the enzyme production of *T. reesei* to depolymerize cellulose and thus, an equilibrium is formed. It becomes clear, that mass transfer between the two niches is of central importance for the process. Therefore, a detailed rigorous process model was developed (Chapter 4) to enable model-based scale-up. However, the process model does not give direct insight about the relevance of certain design trade-offs, which have to be resolved at higher scales (e.g. maintaining the solid-liquid mixing behavior vs. maintaining the flow field and thus, the boundary layer thickness). Only extensive simulation efforts of all design trade-offs would reveal the critical constraints. Therefore, the starting point of scale-up consideration is the similarity-paradigm. [136] According to the Buckingham- $\Pi$  theorem, all relevant design parameters can be reduced to a set of dimensionless numbers, which needs to be kept constant for similar performance at model scale and technical scale. [136,137] As the similarity paradigm has known weaknesses (e.g. for surface-related processes [8,127]), the critical constraints are not solved by simply requesting similarity, but are addressed with simulations of the rigorous process model. Concluding, it can be stated, that the similarity paradigm is used as systematic approach to classify the severeness of the different design constraints, which reduces the computational effort. The critical parameters are scaled-up with the help of a rigorous process model.

With this procedure, the presented work aims to provide a reliable scale-up guideline for continuously operated, consortium-based CBP based on both, general scale-up laws and the simulation results of the rigorous process model, which was adjusted to any necessary design changes. A continuous experiment at 130 L pilot scale should confirm the results obtained from scale-up laws and the process model to validate both, the scale-up laws and the adjustments of the process model. Furthermore, implications with the techno-economic model have to be considered since the overall goal is to deliver a case for profitable 2<sup>nd</sup> generation ethanol production from lignocellulose at large scales.

### 5.3 Results and Discussion

The goal of a scale-up design in general is to maintain the process performance (yield, titer, residence time) while increasing the size of the apparatus. [138] However, this principle assumes a perfectly optimized small scale system, which does not hold for the laboratory scale setup presented in section 3.3. On the one hand this is due to limited resources in a lab environment and most important, on the other hand continuous CBP operation is a time-consuming and challenging task (Chapter 3). The design of the continuous CBP apparatus was designed to minimize the risk of failure instead of aiming at maximum productivities. Therefore, the state of optimization of laboratory scale CBP needs to be discussed before advancing to the scale-up considerations. pH and temperature were optimized regarding the enzyme production of *T.*

*reesei*. [4] The volume flow rate within the membrane was optimized with respect to a minimum convective mass transfer limitation. [89] However, the membrane dimensions with respect to the liquid reactor volume (inner diameter  $d_i$ , outer diameter  $d_o$  & length  $L$ ), the oxygen concentration within the membrane  $c_{ox}$ , the feed cellulose concentration  $c_{in}$  and the residence time  $\tau$  were not optimized towards maximum ethanol output. These six parameters form the degrees of freedom (DoF) for the scale up since there is no point in demanding similarity of non-optimized parameters from the laboratory setup. In section 4.3, it was found that there is an optimum biofilm thickness  $\delta_f$  for each pair of oxygen concentration at the outer membrane surface and glucose concentration within the bulk. Designing the scaled-up system for an optimum biofilm thickness reduces the number of DoFs by two: The oxygen concentration at the outer membrane surface depends on the oxygen concentration within the membrane and the membrane thickness. Thus, only two parameters of  $d_i$ ,  $d_o$  &  $c_{ox}$  can be chosen freely. The third is given by  $\delta_f$ .

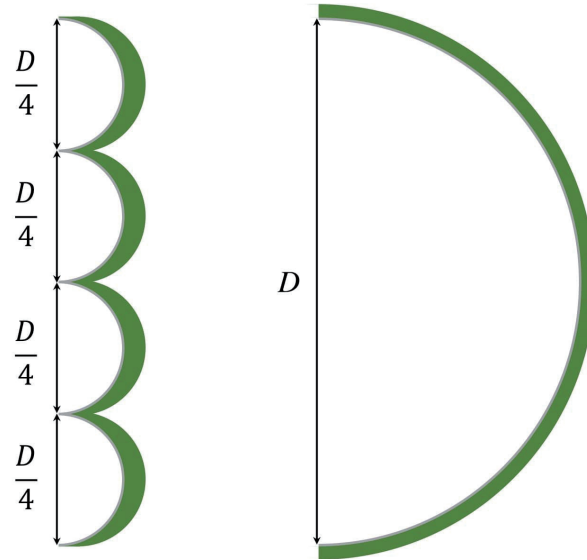


Figure 5.1: Schematic representation of the the biofilm growth (green) on one large membrane (right) and  $n$  multiple small membranes (left).  $n = 4$  was chosen solely for illustration purposes.

Fig. 5.1 depicts the different setup of a membrane with small diameter versus a membrane with a large diameter. Given a certain space available for the membrane winding, the membrane surface per winding height  $h_w = D$  is independent of the membrane (eq. 5.1) or rather in favor of the large membrane, where less membrane area is lost due to contact of the upper and lower membrane in the winding. However, the biofilm volume growing on the small membrane with a certain thickness  $\delta$  is always larger than the biofilm volume growing on a large membrane (eq. 5.2). Theoretically  $\lim n \rightarrow \infty$  would be the optimum solution. However, other factors



such as pressure loss and the oxygen gradient along the membrane shift the optimum towards lower  $n$ .

$$A_m = L \frac{\pi}{2} D = nL \frac{\pi D}{2n} \quad (5.1)$$

$$\begin{aligned} V_{bf,D} &= L\pi \left[ \left( \frac{D}{2} + \delta \right)^2 - \frac{D^2}{2} \right] = L\pi (\delta^2 + D\delta) < \\ V_{bf,D/n} &= nL\pi \left[ \left( \frac{D}{2n} + \delta \right)^2 - \frac{D^2}{2n} \right] = L\pi (n \times \delta^2 + D\delta) \end{aligned} \quad (5.2)$$

The same reduction of DoFs holds for the glucose bulk concentration, which depends on the cellulose conversion. The membrane length  $L$  influences the enzyme loading in the bulk and thus, the speed of cellulose conversion to glucose as well as the titer, by determining the total biofilm volume.  $\tau$  defines the time for cellulose conversion and  $c_{in}$  determines the maximum available substrate for conversion. Again, only two of the parameters may be chosen freely, whereas the third is given by the optimization for  $\delta_f$ . With respect to the glucose concentration, it makes sense to define  $L$  and  $c_{in}$  instead of  $\tau$  as it was shown in chapter 2, that  $\tau$  has a very low impact on the production costs.

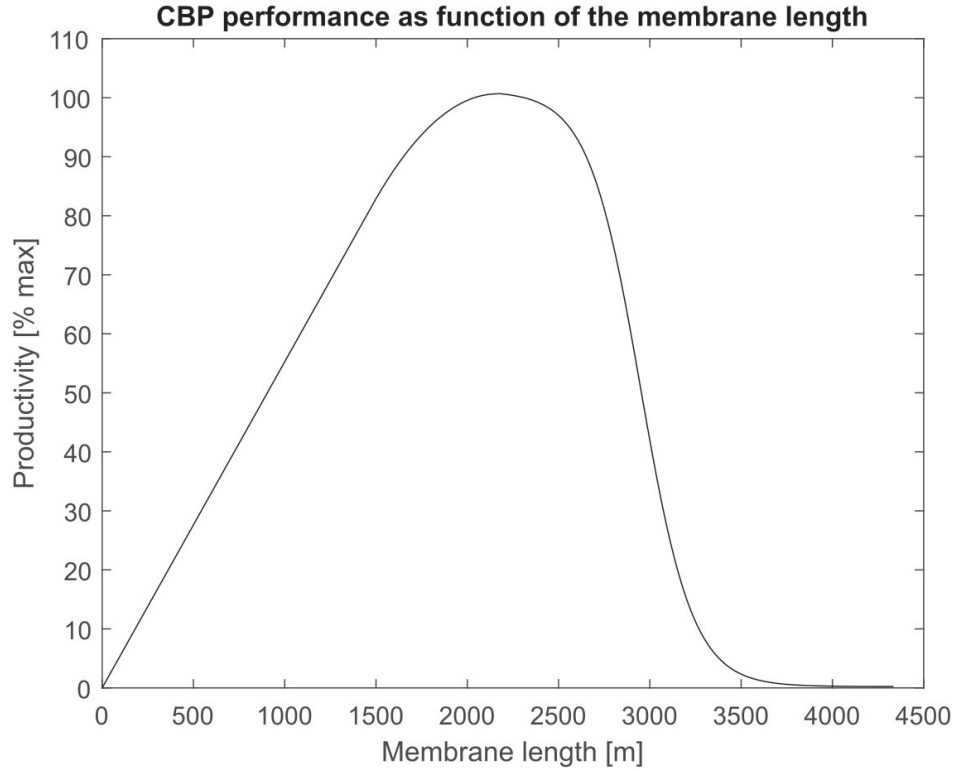


Figure 5.2: Model results of the productivity  $\frac{g_{EtOH}}{h}$  as function of the membrane length at standard conditions (membrane inner diameter  $d_i = 1.58 \text{ mm}$ , membrane outer diameter, 21 % oxygen fraction within the membrane, 17.5  $\frac{g}{L}$  cellulose feed concentration the residence time  $\tau$  was 130 h) in the pilot scale system. The linear increase at the beginning is caused by the higher enzyme loading in the bulk as consequence of more biofilm volume without affecting the biofilm thickness  $\delta_f$  (chapter 4). The flattening of the curve with the subsequent strong decline in productivity is a result of the reduced bulk volume since a large fraction of the reactor is occupied with the membrane and the biofilm. Consequently, two factors are responsible for the decreasing productivity: First, a large fraction of the fed cellulose is necessary to maintain the biofilm. Second, the Dilution rate  $D = \tau^{-1}$  is defined by the nominal reactor volume. Therefore, the effective dilution rate of the bulk is higher, if a large fraction of the reactor is occupied by the immobilized biofilm. The higher dilution rate reduces the effective residence time of substrate and enzymes and thus, the cellulose conversion. The productivity reaches zero, when the whole reactor system is completely filled with the membrane and the biofilm and no bulk phase is left. Note: The presented calculations assume infinite available cellulose without any substrate inhibition effects in order to evaluate only the effect of the membrane length. At low solid loadings, the optimum is reached with less membrane length as there is no more cellulose to hydrolyze in the bulk. However, this "optimum" arises from a solid loading limitation (a parameter, which could be changed easily) instead of from reactor geometry constraints (parameters, which are difficult to change)

Given a experimentally confirmed yield of 40.3 % (section 3.4),  $c_{in}$  is not a limiting factor of the current setup. Evaluating the simulated ethanol productivity as function of the membrane

length (Fig. 5.2) reveals an optimum membrane length at around 2.2 *km* for the pilot scale reactor. At membrane lengths larger than 2.2 *km*, the model predicts lower productivities as a result of the reduced bulk volume since a large fraction of the reactor is occupied with the biofilm. Two factors are responsible for the decreasing productivity: First, a large fraction of the fed cellulose is necessary to maintain the biofilm. Second, the Dilution rate  $D = \tau^{-1}$  is defined by the nominal reactor volume. Therefore, the effective dilution rate of the bulk is higher, if a large fraction of the reactor is occupied by the immobilized biofilm. The higher dilution rate reduces the effective residence time and thus, the cellulose conversion. The productivity reaches zero, when the whole reactor system is occupied with biofilm and no bulk phase is left. However, this optimum of 2.2 *km* membrane length within a 130 *L* reactor is not feasible. Within a technically feasible range (e.g. 0 – 50 *m*), the productivity increases quasi-linear with the membrane length. The linear increase results from the linear increase in biofilm volume and thus, enzyme loading of the system, without affecting the biofilm thickness  $\delta_f$ . Concluding, it can be stated that the available DoFs resulting from the not fully optimized laboratory scale cannot be resolved by optimizing the biofilm since the optima are found at the boundaries. As the optimization of whole system is too complex for an assessment with 4 DoFs, a classic approach of scale-up-theory is chosen to identify the critical design parameters for adjusting the DoFs: The scale-up is conducted by requiring similarity of all optimized parameters by aiming at geometric similarity, process similarity and physical similarity between small scale and large scale, respectively model scale and pilot scale in this work (see Tab. 5.1 for size comparison). [136] In order to properly account for the biology within the system, additionally the physical similarity is introduced. [136] Given this adjustment, the similarity concept promises good results because a lack of reproducibility at larger scale is mostly a consequence of cell sensitivity to poorly adjusted external parameters (e.g. mixing behavior) instead of the internal stochastic nature of gene expression. [8,139]

Table 5.1: Overview of the laboratory scale reactor and the pilot scale reactor dimensions

	Laboratory scale	Pilot scale
<b>Reactor</b>	Infors Labfors 5	Bioengineering P130
<b>Volume</b>	2.7 <i>L</i>	130 <i>L</i>
<b>Height</b>	0.18 <i>m</i>	0.975 <i>m</i>
<b>Diameter</b>	0.14 <i>m</i>	0.412 <i>m</i>

Since both reactors, the Labfors 5 (model scale;  $V = 2.7$  *L*) and the Bioengineering P130 (pilot scale;  $V = 130$  *L*), are cylindrical shaped, CSTRs, geometric similarity was achieved by installing the same type of stirrer and membrane support at pilot scale. Thus, the installed propeller mixer was replaced with a helical ribbon impeller at pilot scale and a membrane support

structure was installed allowing to wind a tubular membrane in helical shape. The exact design of the stirrer and the membrane support was defined by process similarity, which is discussed in the following. Process similarity is not as straightforward as geometric similarity because the reactor has three different zones (inside of the membrane, membrane & biofilm and the bulk phase), which underly different process conditions. The high degree of process integration with CBP yields exceptional cost savings but comes at the cost of much more difficulties when scaling the process. Universal optimization (e.g. saving the costs with an equally simplistic process design for scale-up) is not possible according to the “no free lunch”-theorem. [140] Process similarity in each of the reactor zones is achieved by keeping a certain set of dimensionless parameters, which reflect the process conditions, constant. This set of dimensionless parameters is obtained by applying the Buckingham- $\Pi$ -theorem. [137] By doing so, all relevant process parameters are grouped. The number of needed dimensionless parameters is equal to the number of relevant parameters subtracted by the number basic SI-units of the relevant parameter. For the inside of the membrane, the following group of dimensionless parameters is obtained (eq. 5.3):

$$\left\{ p_{abs} \left[ Pa = \frac{kg}{m * s^2} \right]; p_{O_2, wall} \left[ \frac{kg}{m * s^2} \right]; \dot{V} \left[ \frac{m^3}{s} \right]; L[m]; d_i[m]; D_{O_2, m} \left[ \frac{m^2}{s} \right]; \rho \left[ \frac{kg}{m^3} \right]; \nu \left[ \frac{m^2}{s} \right] \right\} - \{kg; m; s\} \\ = \begin{cases} Re \\ Pe' = Re * Sc \\ Sh \\ \zeta \\ n_{O_2, wall} \end{cases} \quad (5.3)$$

8 relevant parameters (absolute pressure, partial pressure of oxygen at the membrane wall, volumetric flow, length and inner diameter of the membrane, oxygen diffusivity in the membrane, density and kinematic viscosity of the fluid) minus 3 basic SI units (mass, length and time) yields 5 dimensionless parameters. Since the problems of pressure loss in a pipe, heat transfer from the inside of a hollow cylinder to its outside and the analogy between heat and mass transfer are well known, the obtained 5 dimensionless parameters are well-known and have given definitions (Tab. 5.2). Process similarity in the inside of the membrane is given, if all these 5 dimensionless parameters are kept constant. Note, that the temperature within the whole reactor system (incl. the membrane) is kept constant, which allows to omit the temperature as basic SI unit. Of course, the temperature could be used to vary parameters like  $D_{O_2, m}$  or  $\nu$  in order to achieve process similarity. However, the resulting heat transfer would directly affect the physical similarity, which is discussed later.

Table 5.2: Overview of the 5 necessary dimensionless numbers (Reynolds number, modified Péclet number, Sherwood number, pressure loss coefficient, mole fraction of oxygen at the membrane wall) to obtain process similarity in the inside of the membrane.

Dimensionless number	Definition	Comment
Reynolds number $Re$	$\frac{4\dot{V}}{\pi d_i \nu}$	The ratio of inertial forces caused by the flow to viscous forces represents the flow behavior and thus, defines the boundary layer thickness at the membrane wall.
Modified Péclet number $Pe'$ [21]	$\frac{4\dot{V}}{\pi d_i D_{O_2,m}}$	$Pe' = Re * Sc$ is the product of $Re$ and the Schmidt number $Sc$ . It is the mass transfer equivalent to the original Péclet number $Pe = Re * Pr$ . Since $Re$ is already part of the solution, $Pe'$ could be replaced by $Sc$ without any effect. However, as $Pe'$ directly relates the fraction of oxygen diffusing through the membrane to the whole amount of fluid flowing by, it represents the problem in this work better.
Sherwood number $Sh$	$\frac{k_{conv,O_2,m} d_i}{D_{O_2,m}} = f(Re, Sc)$	$Sh$ relates convective mass transfer to diffusive mass transfer at the membrane wall
Pressure loss coefficient $\zeta$	$\frac{\Delta p}{\frac{\rho}{2} \left( \frac{4\dot{V}}{\pi d_i^2} \right)^2 \frac{L}{d_i}}$ $= \frac{p_{abs} _{z=L} - p_{abs} _{z=0}}{\frac{8\rho L \dot{V}^2}{\pi^2 d_i^5}}$	Note: In other non-dimensional analyses, the Euler number $Eu = 2 * \zeta$ is used. However, the calculations are not affected by choosing $\zeta$ over $Eu$ or vice versa.
Oxygen mole fraction at membrane wall $n_{O_2,wall}$	$n_{O_2,wall} = \frac{p_{O_2,wall}}{p_{abs}}$	$n_{O_2,wall}$ is of great relevance as it denotes the driving force for oxygen diffusion through the membrane to feed the microbes in the biofilm

One might consider the  $k_L a$  value to be missing, since many researchers pronounce its crucial significance for any biotechnological scale-up design. [139] The  $k_L a$  value relates the oxygen transfer rate to the reactor volume. In this work, the bulk reactor volume is meant to be anoxic in order to avoid respiration of ethanol to  $CO_2$  by *S. cerevisiae*. Therefore, the  $k_L a$  value is not a relevant parameter in this context, because the oxygen transfer to the biofilm, which is reflected by the above-mentioned set of dimensionless parameters, and not to the bulk defines the process performance. Nevertheless, the enzymes, which are produced by *T. reesei* in the biofilm and released to the bulk, become more and more diluted, if the reactor volume is simply increased. Therefore, the volume ratio of the biofilm and the reactor volume  $V_{bf}/V_{react}$  is a critical parameter (eq. 5.4 & Tab. 5.3). It becomes clear that the  $k_L a$  value -although being a valuable parameter in other experimental setups- is an improper simplification by merging oxygen transfer characteristics with reaction kinetics in the biofilm (as already described in

chapter 3).

Besides the relevant process parameters for the inner membrane compartment of the reactor, it is necessary to define the critical parameters in the biofilm compartment and bulk compartment as well. As the biofilm layer and the bulk volume strongly interact with each other, the process similarity concept is developed for both phases simultaneously. In total, the system is governed by 13 relevant parameters, the inlet concentration, reactor volume, biofilm volume, reaction rate, residence time, rotational speed of the stirrer, stirrer power, stirrer diameter, bulk fluid density, viscosity, the yeast cell diameter, viscosity of the fluid fraction in the biofilm and diffusivity (eq. 5.4):

$$c_{in} \left[ \frac{kg}{m^3} \right]; V_{reac} \left[ m^3 \right]; V_{bf} \left[ m^3 \right]; r \left[ \frac{kg}{m^3 s} \right]; \tau [s]; N \left[ s^{-1} \right]; P \left[ \frac{kg * m^2}{s^3} \right]; d_{stirrer} [m]; \rho \left[ \frac{kg}{m^3} \right]; \nu \left[ \frac{m^2}{s} \right]; d_{yeast} [m]; \\ \nu_{bf} \left[ \frac{m^2}{s} \right]; D \left[ \frac{m^2}{s} \right] \quad (5.4)$$

Subtracting the 3 basic unit results in 10 dimensionless parameters (Tab. 5.3):

Table 5.3: Overview of the 10 necessary dimensionless parameters to ensure process similarity in the bulk phase.

Dimensionless number	Definition	Comment
Sherwood number $Sh$	$\frac{k_{conv,b}\sqrt[3]{V_{bf}}}{D} = f(Re_b, Sc_b)$	To ensure the same mass transfer rate for every species $i$ across the biofilm-bulk boundary layer, $Sh$ needs to be kept constant
Schmidt number $Sc$	$\frac{v_{bf}}{D}$	$Sc$ relates diffusive momentum transfer to diffusive mass transfer
Reynolds number $Re$	$\frac{Nd_{stirrer}^2}{\nu}$	In a stirred vessel, the inertial forces of $Re$ are defined by the rotational speed and the stirrer diameter. [117]
Newton number $Ne$	$\frac{P}{\rho N^3 d_{stirrer}^5}$	$Ne$ relates the stirrer power to the available hydrodynamic power in the vessel
Yield $\eta$	$\frac{r * \tau}{c_{in}} \left( = \frac{c_{out}}{c_{in}} \right)$	The yield denotes the process efficiency by relating the output to the input.
Dimensionless number $C_1$	$\frac{r * \tau}{\rho} \left( = \frac{r * V_{reac}}{\rho \dot{V}} \right)$	$C_1$ relates the productivity $r * V_{reac}$ to the solid content $\rho \dot{V}$ , which becomes clear, if the fraction is not reduced by $V_{reac}$ .
Dimensionless number $C_2$	$\frac{V_{bf}}{V_{reac}}$	$C_2$ relates the biofilm volume to the total reactor volume and thus, accounts for the dilution of biofilm products such as enzymes in the bulk.
Dimensionless number $C_3$	<p>Turbulent flow:</p> $\frac{\theta}{\tau} = \frac{\lambda^2}{D\tau} = \frac{\left(\frac{\nu^3}{\varepsilon}\right)^{1/2}}{\frac{D\tau}{\left(\frac{\rho V_{reac}\nu^3}{P}\right)^{1/2}}}$ <p>Laminar flow:</p> $\frac{t_c}{\tau} = \frac{V_{reac}}{K_Q N d_{stirrer}^3 \tau}$	<p>For turbulent flow, <math>C_3</math> relates the mixing time <math>\theta</math> of a solid-liquid suspension to the residence time in order to ensure proper mixing in the bulk. As mixing is rate-limited by the diffusion within the smallest-scale vortices, the mixing time is a function of <math>D</math> and the Kolmogorov scale <math>\lambda</math>.</p> <p>For laminar flow, <math>C_3</math> relates the circulation time of a fluid particle to its residence time. The circulation time depends on the reactor volume, the stirrer design and a constant, the circulation number <math>K_Q</math>. [128]</p>
Dimensionless number $C_4$	$\frac{D^3 \sqrt[3]{V_{bf}} \tau}{V_{reac}} \left( = \frac{D^3 \sqrt[3]{V_{bf}}}{\dot{V}} \right)$	$C_4$ relates the rate-limiting diffusive mass transfer through the biofilm with the wash-out by the reactor outflow. $C_4$ may be viewed as product of the productivity $C_1$ and the 2 <sup>nd</sup> order Damköhler number $Da_{II}$ , which relates reaction speed to diffusive speed.
Dimensionless number $C_5$	<p>Turbulent flow :</p> $\frac{\lambda}{d_{yeast}} = \frac{\left(\frac{\nu^3}{\varepsilon}\right)^{1/4}}{\frac{d_{yeast}}{\left(\frac{\rho V_{reac}\nu^3}{P}\right)^{1/4}}}$ <p>Laminar flow :</p> $\frac{\tau \sqrt{\dot{\gamma} \nu}}{d_{yeast}} = \frac{\tau \sqrt{k N \nu}}{d_{yeast}}$	<p><math>C_5</math> reflects the mechanical sensitivity of the cells by relating the Kolmogorov length scale to the yeast cell diameter in the case of turbulent flow. The yeast cell diameter needs to be smaller (<math>C_5 &gt; 1</math>) in order to neglect any negative shear stress influence on the cells. [120]</p> <p>For laminar flow, the shear tension defined by the viscosity and the shear rate <math>\dot{\gamma} = kN</math> is related to the exposed surface of the yeast cells. According to Metzner &amp; Otto, <math>k</math> is a constant depending on the stirrer type and geometry. [117]</p>

To achieve process similarity, it is crucial, that, besides the above mentioned parameters (Tab. 5.3), the reaction kinetics in the biofilm and the bulk phase should be the same in order to maintain productivity and yield. The similarity of substrate and inhibitor concentrations in the biofilm is considered by the above-mentioned dimensionless numbers (Tab. 5.3). Thus, the last missing criterion is the reaction temperature, which is reflected by the Arrhenius number  $\gamma$ , which is basically the exponential argument of the Arrhenius law (eq. 5.5):

$$\gamma = \frac{E_A}{RT} = \text{const} \quad (5.5)$$

Since  $E_A$  and  $R$  are constant, one could just set the temperature constant, which is the reason, why it does not appear in Tab. 5.3. However,  $\gamma$  is used here to keep the dimensionless approach consistent. It is important to note, that the fluid properties in the biofilm are not affected by the rheology of the bulk fluid, because the particles, which define the bulk rheology cannot diffuse into the biofilm. Thus, the biofilm always consists of a Newtonian fluid making the diffusivity within the biofilm only a function of the fluid composition and temperature (given the moderate pressures of any bioprocess). As both, composition and temperature similarity, are reflected by the two above-mentioned dimensionless parameters  $\gamma$  and  $C_2$ , the mass transfer similarity within the biofilm is automatically given. Furthermore, the hydrostatic pressure is not included in the similarity analysis for 2 reasons: First, the hydrostatic pressure at pilot scale is negligible. The reactor filling height of 0.975 m yields a maximum hydrostatic pressure of less than 0.1 bar. Second, it was shown, that *S. cerevisiae* reacts to higher pressures according to the Le Chatelier principle of least resistance and reduces any volume increasing biochemical activity such as fermentation, where one mole of soluble glucose is digested to two moles of soluble ethanol and two mol of dissolved CO<sub>2</sub>. [141] However, it is still at 60 % productivity when the pressure is increased by factor of 70 to 7 MPa. [142] Thus, it may be assumed, that any fungal cell can withstand higher pressures and operate closely to the optimum at reasonable hydrostatic pressure increases (especially given the fact, that *S. cerevisiae* is not always exposed to the full hydrostatic pressure due to mixing of the vessel).

In this work, the physical similarity is not reflected by equations as the other similarities, but by the choice of materials. To ensure the same biological activity at large scales, the biological system should face the same environment at large scale as at small scale. Therefore, all materials should be the same or at least biocompatible according to ISO 10993-1. The choice of the membrane is particularly important: On the one hand, changing the membrane material is a powerful lever to adjust the diffusion coefficient and thus, all related dimensionless numbers. On the other hand, a change of the membrane material introduces many uncertainties because little quantitative information is available on phenomena like the degradation rate of different materials by the biofilms or adhesion affinity of biofilms to different surface structures although



their existence is proven. [143,144] Thus, all materials were the same at small scale & large scale with two exceptions: First, the reactor wall at lab scale is made of glass, whereas it is EN 1.4401 stainless steel at pilot scale. Since both materials are biocompatible, no impact is expected from this change. Second the substrate was changed. The experiments at small scale were conducted with pure microcrystalline cellulose (Avicel®PH-101) to omit the influence of any inhibiting substances and thus, guarantee reproducibility, whereas the pilot plant will be fed with steam pretreated beech wood. Pretreated beech wood introduces new chemicals to the system such as lignin and small residues of inhibitors (acetic acid, furfural etc.) from the pretreatment. Therefore, it is only possible to keep either the solid loading or the cellulose concentration of the inlet stream constant. In terms of dimensionless parameters, ratio of the cellulose feed stream to the total feed stream is not kept constant (eq. 5.6).

$$C_6 = \frac{\dot{m}_{C,feed}}{\dot{m}_{tot,feed}} \neq \text{const} \quad (5.6)$$

Obviously, this is a harsh violation of the similarity paradigm for scale-up, but it is unequivocal since microcrystalline cellulose is valuable for facilitated reproducibility at lab scale, but the process needs to work with plant biomass at pilot and industrial scale.

The usual procedure of scale-up would be to derive all relevant parameters at large scale from an optimized small-scale model sticking to the similarity paradigm. [136] However, besides having already violated the similarity paradigm, the small-scale model cannot be regarded as fully optimized as shown in the beginning of this section. The impossibility to maintain similarity for all dimensionless parameters results in the importance of the rigorous process model, which can be used to simulate the change in CBP performance when violating the similarity paradigm. Besides  $C_6$ , the following dimensionless parameter cannot be maintained for different reasons (Tab. 5.4): The pressure loss coefficient  $\zeta$  may increase marginally due to longer membranes. However, as long as the membrane's stability is not affected and the pressure gradient along the membrane is still negligible, the process similarity may be considered as fulfilled. The oxygen concentration at the membrane wall is one of the DoFs mentioned earlier and thus, subject to optimization. The same holds for the dimensionless parameters reflecting the productivity ( $C_1$ , Tab. 5.3) and the biofilm volume ( $C_2$ , Tab. 5.3).  $Re_v$ ,  $Ne$ ,  $C_3$  &  $C_5$  all refer to the stirring of the tank and thus, only one can be kept constant. The stirring has to be similar with respect to either the flow field ( $Re_v$ ), the necessary stirring power ( $Ne$ ), the mixing time ( $C_3$ ) or the mechanical stresses on the cells ( $C_5$ ). Since the stirring affect the most dimensionless parameter and is affected itself by the change in feed cellulose concentration ( $C_6$ ), it is worth discussing the stirrer design in the following:

Table 5.4: Overview of the scaled dimensionless parameters

Parameter	Similarity paradigm fulfilled
$Re_m$	✓
$Pe'$	✓
$Sh_m$	✓
$\zeta$	(✓)
$n_{O_2,wall}$	×
$Sh_v$	✓
$Sc_v$	✓
$Re_v$	?
$Ne$	?
$\eta$	✓
$\gamma$	✓
$C_1$	×
$C_2$	×
$C_3$	?
$C_4$	✓
$C_5$	?
$C_6$	×

Besides the influence of lignin on the reaction kinetics, the change of substrate mainly implies one of the following consequences: Either, the rheology of the bulk will be considerably influenced by the higher solid loading at equal cellulose concentration or the titer, which already is critically low, would be reduced further by 50-60 % as a result of lower cellulose concentrations in the reactor at an identical solid loading and thus, identical rheological properties. [30] Second, the lignin in the feed will cause enzyme deactivation by adsorption, which has to be included in the model. If inhibitors are present in relevant concentration, their inhibition terms have to be included in the model as well. The influence of Lignin on the reaction kinetics is rather irrelevant for stirring, but the change in rheology is of crucial importance. There is little information about the rheology of pretreated beech wood slurries. However, the rheology of beech wood and corn stover with the same solid content should be comparable given the fact, that even different substrates with different pretreatment methods show viscosities in the same order of magnitude, if the solid content is equal. [145] Corn stover with 5 % solid content behaves like a Newtonian fluid over a wide range of shear rates with a viscosity higher by a factor of ca. 120 compared to water, whereas 10 % solid content and more

result in non-Newtonian fluid behavior (Fig. 5.3). [15] Since the pilot scale should be able to handle both, the 1.75 % cellulose content from lab scale (equivalent to 3.5 % solid content [30]) and the needed 15-20 % solid content to obtain ca. 4 wt% ethanol titer for feasible distillation afterwards, the stirrer needs to be able to handle a vast range of fluid properties. Extrapolating the viscosity of a 1.75 % solid content solution from data of Pimenova. et al. (2004) gives 0.059 *Pas* (Fig. 5.3). 2 % solid content result in a viscosity of ca. 20 *Pas* in a reasonable range of shear rates, which will be discussed later (Fig. 5.3).

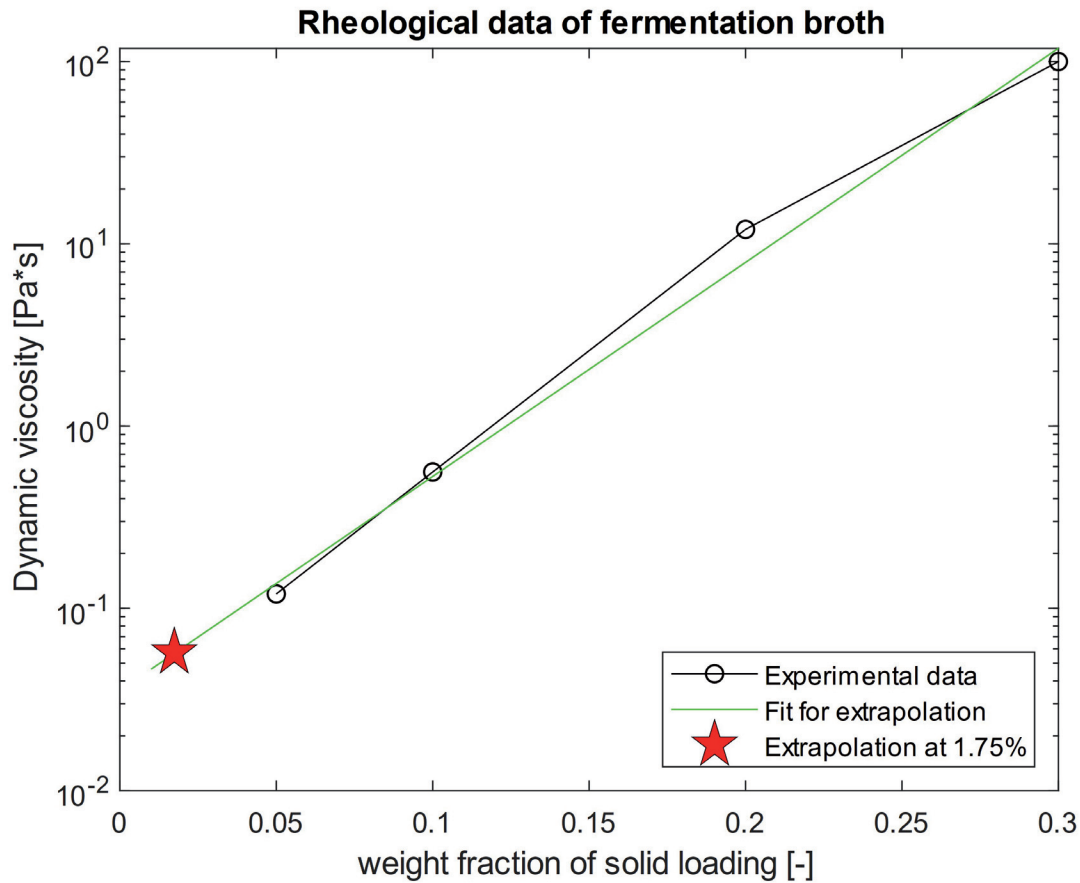


Figure 5.3: Experimental results (black circles; [15]) of the viscosity of a corn stover slurry at a shear rate of  $\dot{\gamma} = 9s^{-1}$  were fitted with an exponential function (green curve; coefficient of determination  $R^2=0.997$ ) to extrapolate the data for 1.75 % solid loading.

The upper viscosity limit demands a helical ribbon impeller as stirrer, because at such high viscosities, the mass and heat transfer from the reactor wall becomes crucial in order to ensure proper mixing quality. [146] Based on computational fluid dynamics, it is proposed to aim at minimal “clearance” (gap between helical blade and reactor wall, Fig. 5.4) when designing a helical ribbon impeller with optimum mixing properties. [146] In order to account

for manufacturing tolerance, a Clearance  $C = 0.03 d_{\text{vessel}}$  was chosen, which is higher than the ideal value of  $0.01 d_{\text{vessel}}$ , but below the critical value of  $0.1 d_{\text{vessel}}$ . [146] The clearance defines the stirrer diameter:  $d_{\text{stirrer}} = d_{\text{vessel}} - 2 * C = 0.94 d_{\text{vessel}}$ . Based on the stirrer diameter, the remaining design parameters, which are the pitch  $S = d_{\text{stirrer}}$  and the blade width  $W = 0.2 d_{\text{stirrer}}$ , are derived according to Tsui et al. [146]

The membrane is wound helically around a membrane support structure at the outer boundary of the stationary frame (Fig. 5.4) because it maximizes the possible membrane area at the given design and the region is characterized by good mixing. [146]

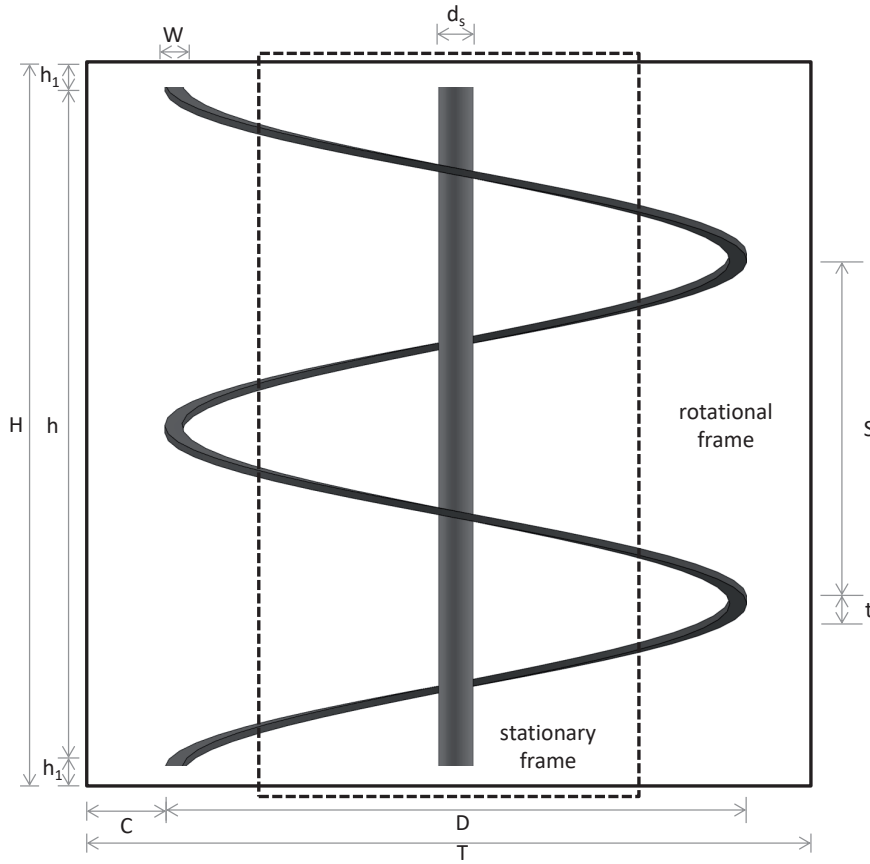


Figure 5.4: Design geometry of a helical ribbon impeller

However, the membrane support with the membrane occupies the full stirrer height  $h_{\text{stirrer}}$  likely leading to poor mixing in the inside at high viscosities. Thus, the inside of the membrane support was regarded as an own vessel and a central screw was designed for proper mixing within this virtual inner vessel. [147,148] The central screw clearance was again set to  $C_{cs} = 0.03 d_{\text{pseudo-vessel}}$ . The pitch of the central screw is slightly higher as for the helical ribbon impeller  $S_{cs} = \frac{2}{3} d_{cs}$  for improved mixing in the virtual vessel at reasonable power

consumption. [148] The blade width is defined by the clearance  $W_{cs} = \frac{d_{pseudo-vessel} - 2C_{cs} - d_{shaft}}{2}$ . The blade of the central screw is winded opposite to the helical ribbon impeller to support the axial flow regime within the reactor. [146,147] The complete configuration of helical ribbon impeller, membrane support and central screw is shown in Fig. 5.5. An overview of the design parameters and their calculation is given in Tab. 5.5.

Table 5.5: Overview of the design parameter for the stirrer of the reactor

Parameter	Helical ribbon impeller	Central screw	Reference
Vessel diameter	$d_{vessel} = 412 \text{ mm}$	$d_{pseudo-vessel} = d_i$ , membrane support $= 120 \text{ mm}$	-
Vessel filling height	$h_{filling} = 975 \text{ mm}$	$h_{filling} = 975 \text{ mm}$	-
Shaft diameter	$d_{shaft} = 56.6 \text{ mm}$	$d_{shaft} = 56.6 \text{ mm}$	-
Shaft height	$h_{shaft} = 740 \text{ mm}$	$h_{shaft} = 740 \text{ mm}$	-
Stirrer height	$h_{stirrer} = 1.1 * h_{filling}$ $= 1072.5 \text{ mm}$	$h_{cs} = h_{shaft} = 740 \text{ mm}$	-
Clearance	$C = 0.03d_{mrol} = 11.67 \text{ mm}$	$C_{cs} = 0.03d_{pseudo-vessel} = 3.6 \text{ mm}$	[107]
Impeller diameter	$d_{stirrer} = \frac{d_{vessel}}{1.06} = 389 \text{ mm}$	$d_{cs} = \frac{d_{pseudo-vessel}}{106} = 113.2 \text{ mm}$	-
Pitch	$S = d_{stirrer} = 389 \text{ mm}$	$S_{cs} = \frac{2}{3}d_{vessel} = 274.6 \text{ mm}$	[107,108]
Blade width	$W = 0.2d_{stirrer} = 77.8 \text{ mm}$	$W_{cs} = \frac{d_{cs} - d_{shaft}}{2} = 28.6 \text{ mm}$	[107]

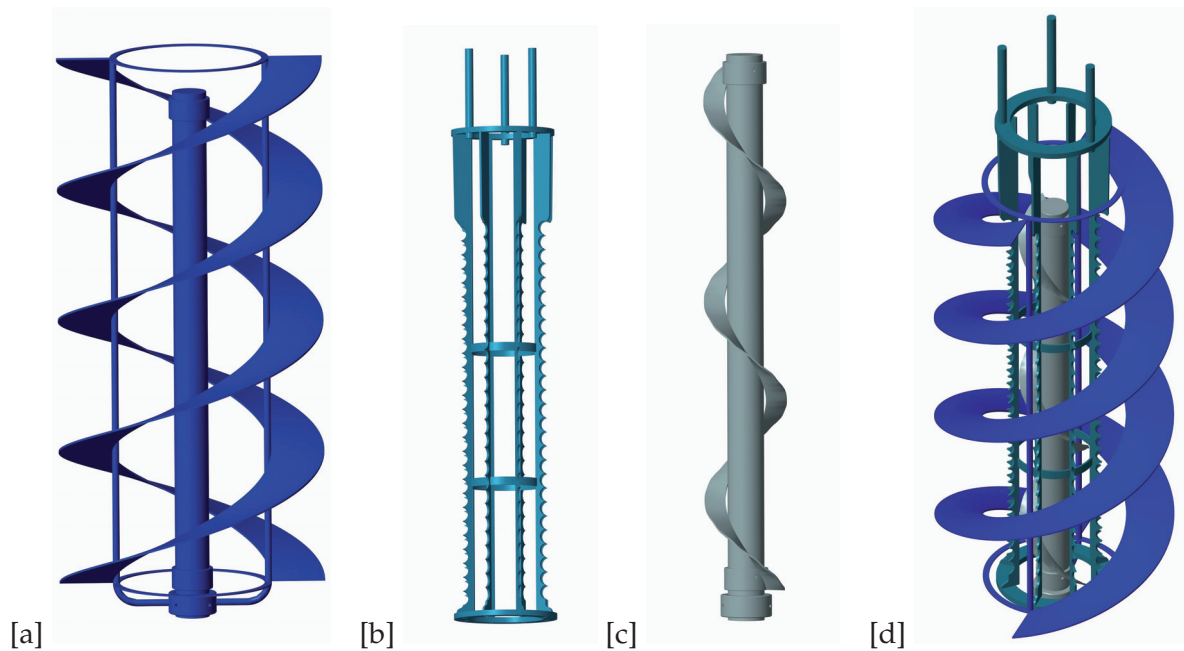


Figure 5.5: Configuration of helical ribbon impeller ([a], blue), membrane support ([b], turquoise) and central screw ([c], grey) for optimum mixing behavior over a large range of fluid viscosities [d].

Despite putting an unsolvable design constraint on the scale-up The stirrer design is consistent with the dimensionless analysis. The design parameter  $d_{stirrer}$  needed to be chosen in favor of proper mixing over a large range of viscosities and the dimensionless number for mixing quality  $C_3$  contains  $d_{stirrer}$  in case of laminar flow (laminar flow is expected as consequence of the high viscosities and the absence of any baffles [136]). The process similarity in terms of minimized mixing time is achieved by the stirrer design and reflected by  $C_3$ . Since the mixing time  $C_3$  was kept constant, the stirrer will need more power (higher  $Ne$ ), which is in agreement with the no-free-lunch theorem. The higher stirring power will slightly increase the mechanical stresses ( $C_5$ ), whereas ( $Re$ ) decreases by the power of  $2/3$  (cf. exponents of  $d_{stirrer}$  in Tab.5.3) leading to a larger boundary layer at the biofilm. However, as long as the changes  $Ne$ ,  $C_5$  and  $Re$  are still below certain thresholds (no considerable convective mass transfer limitation at the biofilm-bulk boundary and no harming of the cells), these dimensionless parameters may be considered similar. These thresholds are defined by model simulations, where the possible parameter variation without altering the model outcome significantly is evaluated. Due to the increased importance of the clearance at higher viscosity, the similarity paradigm needed to be violated in that sense, that  $d_{stirrer}$  cannot be adjusted anymore for other dimensionless parameters such as  $C_2$  to optimize the available space for the membrane. These additional design constraints make the set of equations overspecified. An overspecified set of equations does not allow for an exact solution. By applying an optimization criterion, the given equations may be solved by maximizing/minimizing the optimization criterion. [149] The minimum selling price, which can be related to every possible calculation outcome by the techno-economic model presented in chapter 2, is a predestined optimization criterion. [150] The calculations of the corresponding MESP are conducted with the sensitivity data of the process parameters presented in chapter 2.1. However, the pilot scale reactor is still in an academic environment with utilities different from industry. Thus, regarding some design specifications it will be distinguished between an industrial favorable solution and a feasible solution for pilot scale since the overall goal of this work is to demonstrate the proper functioning of the given scale-up design framework. For example, the stirrer was scaled-up with respect to the pilot scale setup available at site since the process model strongly relies on the assumption of a perfectly mixed bulk. The economic impact of poor mixing is hard to quantify without extensive CFD simulations. Therefore, it was decided to prioritize the mixing performance of the reactor over process economics in order to achieve the above-mentioned proof that the given scale-up framework is reliable.

Given the stirrer design, the membrane area is determined by the space on the cylindrical shell of the membrane support. In other words, the 2 DoFs of the membrane dimensions were sacrificed to ensure proper mixing. In terms of industrial scale-up, it is not favorable to put such a hard constraint on the membrane design by designing the stirrer, but from an academic point of view, proper mixing is unequivocal for the model validation at higher scales.

The membrane is scaled up by means of the fungal biofilm thickness  $\delta_f$ , which is a function of

the bulk glucose concentration and the oxygen concentration at the outer membrane surface. Regarding the oxygen concentration in the membrane, it would be economically favorable to do the oxygen make-up with air instead of expensive pure oxygen. Replacing the lost oxygen with air leads to an equilibrium within the membrane, which is reached as soon as 0.79/0.21 times as much nitrogen diffuses through the membrane meaning, that the gas diffusing through the membrane has exactly the composition of air. Since nitrogen is inert, it leaves the system only through the reactor outlet (eq. 5.7).

$$J_{N_2} = H_{cp}^{N_2} p_v \dot{V}_{out} = \frac{0.79}{0.21} J_{O_2} \approx \frac{0.79}{0.21} \frac{2\pi D_{O_2,m} L (H_{cp}^{O_2} p_{O_2,m} - 0)}{\ln(r_{i,m}/r_{o,m} + \delta_{bf})} \quad (5.7)$$

$$\Leftrightarrow p_{O_2,m} \approx \frac{0.21 M_{N_2} H_{cp}^{N_2} p_v \dot{V}_{out} \ln(r_{i,m}/r_{o,m} + \delta_{bf})}{1.58\pi D_{O_2,m} L H_{cp}^{O_2} M_{O_2}} = 0.01 \text{ bar at small scale}$$

Due to the low nitrogen removal from the system, a high amount of  $N_2$  accumulates in the membrane. The optimum fungal biofilm thickness for a partial oxygen pressure of 10 mbar would require a membrane thickness in the nanometer range, which is not feasible, of course. Thus, industrial oxygen needs to be purchased at 8.35 \$/Nm<sup>3</sup> (price adjusted to 2020 with the US producer price index, published by the US Bureau of Labor Statistics). [148,151] Using pure oxygen to feed *T. reesei* would yield a US MESP increase of 6.12 \$/L Ethanol (+15 %). [33] However, feeding *T. reesei* with pure oxygen allows any oxygen concentration within the membrane and thus, the degree of freedom regarding the membrane dimension is maintained (cf. beginning of this chapter), which is important since the membrane dimensions underlie other constraints as shown above. Since the performance of the bioreactor increases linearly with the membrane length at a given membrane diameter and a sufficiently high Reynolds number, the best membrane configuration will be the smallest available membrane, which could be winded the maximum number of times. The membrane should be segmented and connected to gas distributors in order to keep the pressure loss below 0.3 bar.

The highest ethanol titers, which were 40 % lower compared to the laboratory scale titers, were simulated with the standard membrane (membrane inner diameter  $d_i = 1.58 \text{ mm}$ , membrane outer diameter) at the maximum possible length of  $L = 116 \text{ m}$  with 26 % oxygen concentration in the membrane, 17.5  $\frac{g}{L}$  cellulose feed concentration and a residence time of  $\tau = 120 \text{ h}$ .

Concluding, it can be stated that the majority of the given non-dimensional parameters can be kept constant (all membrane parameters except  $n_{O_2,wall}$  and all bulk parameters except  $Ne$ ,  $C_1$  and  $C_2$ ) thanks to an elongated residence time  $\tau$ , which compensates for the lower cellulose conversion rate (smaller  $C_1$ ) as result of less enzyme loading in the bulk (smaller  $C_2$ ). The higher energy demand for stirring (higher  $Ne$ ) is subtracted from the excess electricity, which is sold to the grid. The model simulations with the fungal biofilm thickness  $\delta_f$  should ensure proper outcome when the similarity paradigm was violated, and the techno-economic model



may be used to optimize different outcomes with respect to minimizing the costs at higher scales. However, extensive model simulation runs at pilot scale could not yet be conducted due to a diverging algorithm in Matlab. It is assumed that the solving algorithm cannot handle the fast converging reaction kinetics of the bulk with the slow converging mass transfer equations in the biofilm.

## 5.4 Conclusions

A scale-up framework consisting of a rigorous process model and a set of non-dimensional parameters was developed to scale up consortium-based consolidated bioprocessing of cellulosic substrates from 2.7 L laboratory scale to 130 L pilot scale. The majority of the non-dimensional parameters could be kept constant during scale-up as requested by the similarity paradigm. Necessary changes were aimed to simulate with the model. Again, the fungal biofilm thickness  $\delta_f$  served as a relevant parameter for scale-up considerations. In general, the relative loss of biofilm volume is compensated by longer residence times since the residence time has by far the least impact on the process economics. [33] However, an experimental confirmation of the presented calculations remains still to be done. The synergy of a classic trade-off identifying approach such as the similarity paradigm and the rigorous model, which delivers precise information on any set of process conditions is designed to overcome the reported typical performance decreases of 10 %- 30 % at industrial scale. [8,127,139] Applying the economics as optimization criterion allowed to minimize the effect of increasing costs at higher scales, as process involving a surface  $A \propto L^2$  and reactor volume  $V \propto L^3$ , where the similarity paradigm cannot be maintained by definition. The expected price increase of ca. 15 % at industrial scale due to the need of pure oxygen could be reduced by exploiting synergies with other bioprocesses in the framework of a biorefinery. [152] E.g., algae produce oxygen in purity, which is by far sufficient to feed the membrane with the optimum concentration of 26 %. [153]



## CHAPTER 6

---

### Evaluation of *in-situ* product removal strategies to improve the productivity and economics of consolidated bioprocessing

---

#### 6.1 Abstract

Popular rate-controlled separation techniques in biotechnology, such as adsorption, liquid-liquid extraction, steam stripping, CO<sub>2</sub> stripping, vapor permeation and pervaporation, were investigated regarding their potential to replace distillation as industrial standard for ethanol separation from a fermentation broth. It was focused on *in-situ* and slip stream separation setups in order to reduce yeast inhibition by ethanol additional to the general advantages of rate-controlled separations such as avoiding limitations by an azeotrope or the unfavorable vapor-liquid equilibrium of highly diluted ethanol-water mixtures.

However, except from CO<sub>2</sub> stripping and pervaporation, all mechanisms fail to handle the solids of the fermentation broth. CO<sub>2</sub> stripping is limited by a poor ethanol recovery due to the trade-off between bubble residence time and stable bubble flow regime. Pervaporation, being the most promising concept for *in-situ* product removal, would be a cost-saving alternative to distillation for batch operation, but is limited by an unfavorable vapor-liquid equilibrium due to low bulk concentrations during continuous operations.

#### 6.2 Introduction

The current industrial standard for ethanol separation from a fermentation broth is distillation followed by an adsorption dehydration step with a molecular sieve disregarding whether it is 1<sup>st</sup> generation ethanol from edible biomass or 2<sup>nd</sup> generation ethanol from lignocellulose. [2, 64] The advantages of distillation are high ethanol recovery, reasonable efficiency already at titers

of 4 wt.% ethanol as well as extensive scale-up experience. [64] The main disadvantages are the high costs for titers below 4 wt.% ethanol and the separation limit by the azeotrope of ethanol and water, which results in the need of a second dehydration step. [64] Both disadvantages could be overcome by a rate-controlled separation mechanism as it is shown in the following. Distillation is an equilibrium-controlled separation mechanism, because each distillation stage exploits the higher volatility of ethanol in the vapor-liquid equilibrium of an ethanol-water mixture. [154] Thus, given a certain scale, the only parameter, which influences the separation efficiency and the costs, is the initial ethanol concentration of the fermentation broth, i.e. the titer of the fermentation. [154] Rate-controlled separations also rely on a concentration gradient as driving force, but equilibrium is never reached (e.g., by withdrawing the ethanol vapor from the permeate in a pervaporation process). As the name suggests, they are rate-controlled and the rate is always a product of the driving force and a rate constant. [154]

$$J_{\text{diff}} = D \frac{\partial c}{\partial x} \quad (6.1)$$

Given the Fick law of diffusion as example (eq. 6.1), the diffusion rate, called the flux  $J_{\text{diff}}$ , is equal to the product of the rate constant, the diffusivity  $D$ , and the concentration gradient  $\frac{\partial c}{\partial x}$  as driving force. [155] A membrane, which is very permeable for a species  $i$  (leading to a high  $D$ ), theoretically could give better results at lower concentrations of the substance  $i$  than another membrane with poor permeability for  $i$ . Generally spoken, a setup with a high rate constant allows a margin for poor concentration gradients. Furthermore, any rate-controlled separation is not subject to equilibrium-related phenomena such as an azeotrope. [154] Adjusting the rate of separation to be much higher than the rate of ethanol loss by the reactor outflow would also allow to remove ethanol during the fermentation process (eq. 6.2).

$$r_{\text{separation}} \gg r_{\text{outlet}} = \dot{V}c_{\text{out}} \quad (6.2)$$

A so-called slip-stream or *in-situ* separation setup (Fig. 6.1) for a rate-controlled separation technique has the possibility to increase the productivity by avoiding yeast inhibition by toxicity of ethanol above a certain threshold (Fig. 6.2) and additionally, in the case of *in-situ* separations, the possibility to reduce the capital expenses by reducing the number of apparatus for separation. [156,157]

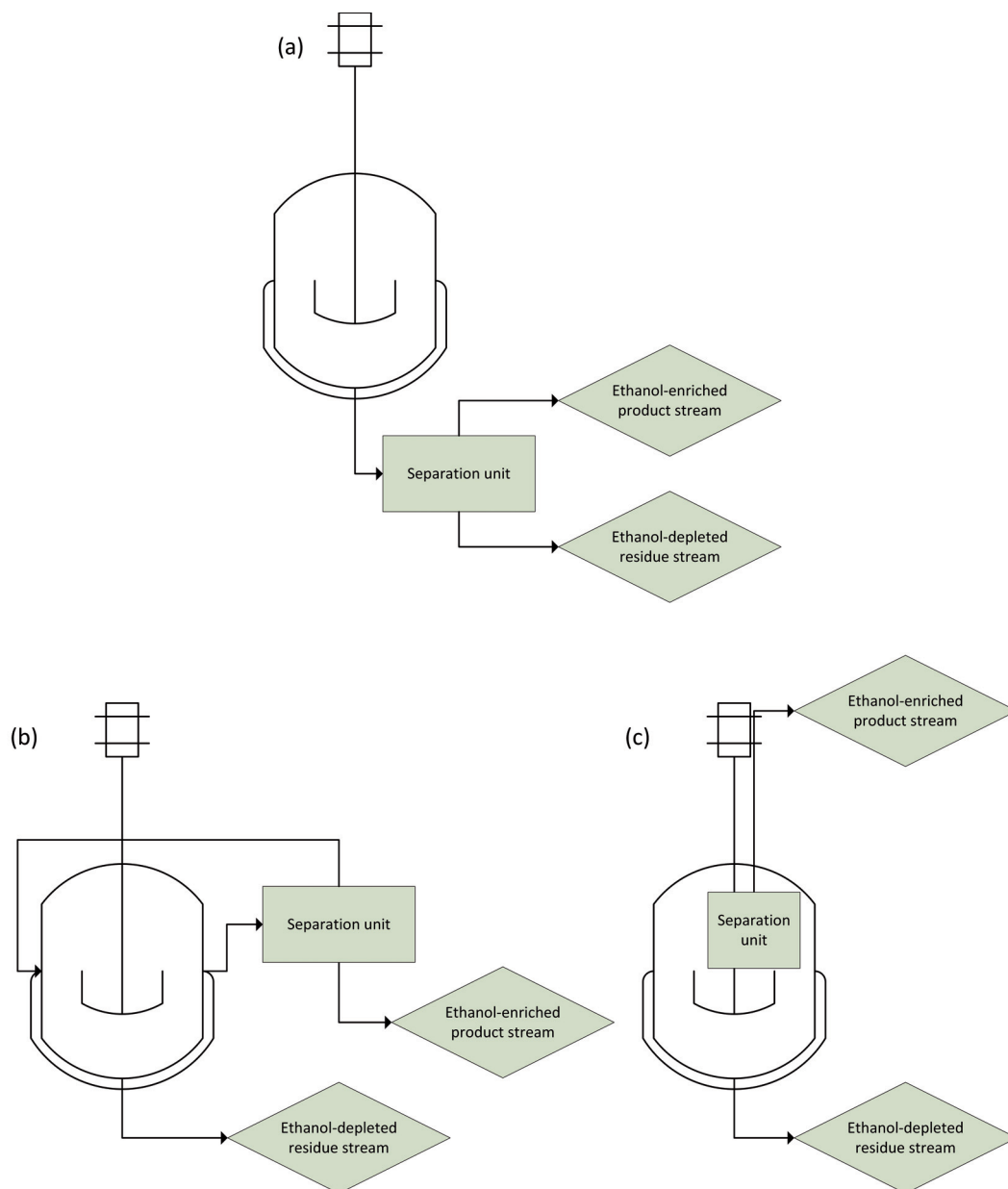


Figure 6.1: Illustration of the different separation setups: End-of-pipe separation (a), slip stream separation (b) and *in-situ* separation (c). With end-of-pipe separation, the whole reactor outlet is sent to the separation unit and there is no interaction with the bioreactor anymore. With slip stream separation, a circulating stream between the separation unit and the bioreactor is established. The reactor outlet is already ethanol-depleted and no further ethanol is recovered. *In-situ* separation works identically to slip-stream separation with the only difference, that the separation unit is installed within the bioreactor. Note: The inlet streams for the reactors are removed for illustration purposes

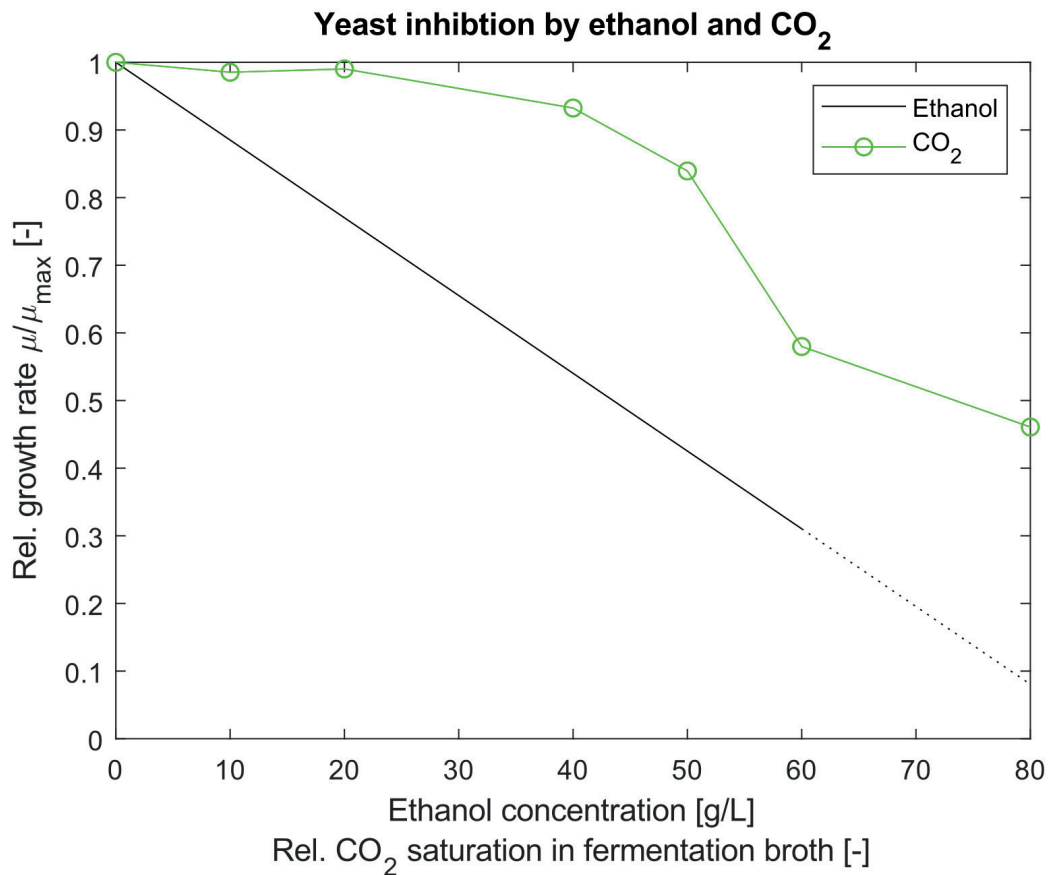


Figure 6.2: Yeast inhibition by ethanol and CO<sub>2</sub> depending on their respective concentrations. [16,17] The modeled ethanol data is experimentally validated for ethanol concentrations up to 60  $\frac{g}{L}$ . [16] For concentrations above 60  $\frac{g}{L}$ , the data is extrapolated, but in agreement with the experimental findings of other published studies. [16,18]

The possibility to cope with low titers, to decrease capital costs and to increase the productivity is a promising feature for continuously operated CBP. As previously shown (chapter 2), CBP costs are dominated by the CAPEX with a share of 58 %. [10] Thus, even small reductions of the CAPEX due to *in-situ* product removal (ISPR) would impact the MESP. Moreover, continuous ethanol production from lignocellulose by means of CBP lacks in productivity compared to 1<sup>st</sup> generation bioethanol (ca. 0.07  $\frac{g}{L \cdot h}$  vs. 4  $\frac{g}{L \cdot h}$ ). [4,33,98] Given a conservative approach by assuming, that the CBP productivity cannot be further increased, the necessary residence time to obtain a titer of 4 wt.% would be ca. 24 *days*. In terms of costs, this is doable as the residence time has a small impact on the total costs. However, the start-up phase to reach steady-state after the yearly maintenance would increase by a factor of 3 to 5 resulting in start-up durations of 72-120 *days*, which is not feasible. [33,83] Thus, ISPR could help to cope with both of the major drawbacks of CBP by increasing the productivity through decreasing inhibitory effects

and by obtaining dehydrated ethanol efficiently from lower titers.

This work aims to investigate different rate-controlled *in-situ* or slip stream ethanol separation techniques as alternative to the classic distillation-adsorption approach regarding their potential to address the weaknesses of continuous CBP (high capital costs, lack of productivity and titer) in order to make 2<sup>nd</sup> generation bioethanol economically competitive with 1<sup>st</sup> generation ethanol.

## 6.3 Results and Discussion

The state-of-the-art procedure of ethanol purification, distillation followed by adsorption, is an established industrial process yielding 99.5 % ethanol at arbitrary scale within the projected limits (chapter 2) and costs of 3.39 ¢/annual L ethanol at a throughput of 2000 dry tons per day.

The following rate-controlled separation techniques, which are subject to biotechnology research, are investigated regarding their potential to outperform the economics of the state-of-the-art at the given specifications [64]:

- Adsorption
- Liquid-liquid extraction
- Steam stripping
- CO<sub>2</sub> stripping
- Vapor permeation
- Pervaporation

Adsorption is conducted in a column packed with nano-porous material, which chemical composition allows for selective surface adsorption of the desired component. [158] It is well established to purify ethanol from 90-93 wt.% to 99.5 wt.% after distillation. [2,64] However, it is inappropriate as main separation technology disregarding whether it is and-of-pipe or slip stream separation setup. This is due to the following issues: First, the traditional adsorption approach (removing water from ethanol) would require huge capacities at titers of 4 wt.% or even lower causing an increase in CAPEX. Thus, an adsorption material, which is selective towards ethanol, would be necessary. Research is conducted to find suitable materials, but industrial maturity is not yet reached. [159,160] However, the main issue is the solid loading. The fermentation broth has a considerable solid loading, which would immediately clog the

adsorption column. Therefore, a solid-liquid separation step prior to adsorption would be necessary. One option for solid-liquid separation is evaporation in a column, but such a beer tower is operated at 103 °C to avoid ethanol losses through the liquid-solid outlet. [2] Thus, adsorption would require almost the same heat energy as distillation at much higher apparatus costs due to the adsorption packing [60], which is economically not favorable. Other options for solid-liquid separation such as a hydrocyclone or filtration are not feasible as well. A single hydrocyclone separates only ca. 60 % of the solids due to the low difference in density between water and yeast cells. [161] In order to achieve sufficiently high solids removal, a series of hydrocyclones is necessary, which again causes too large CAPEX. [62,161] Filtration faces the same problems as membrane separation, which are discussed later on.

Liquid-liquid extraction involves a second fluid, which most importantly has a high selectivity  $\beta$  towards ethanol and immiscible with the fermentation broth. [64] In a slip stream or end-of pipe application, the fermentation broth is mixed with the extractant, usually a long-chain alkane such as n-dodecane. [64,162] Ethanol is transferred to the extractant due to higher solubility.  $\beta$  defines the ethanol recovery, whereas the equilibrium distribution coefficient  $K_D$  defines the separation rate. High ethanol recoveries due to  $\beta > 100$  are possible, but unfortunately  $\beta$  is inversely proportional to  $K_D$  for most fluids. Therefore, the process is either selective and slow or fast and unselective. [64] Due to the immiscibility, the two fluids separate after the mixing unit by buoyancy and ethanol may be separated from the extractant by any separation technique. Apart from productivity-limiting interferences between the alkane and the fermentation product, which are discussed later, liquid-liquid extraction is suitable for a slip-stream separation approach. In a slip-stream separation, the reactor outlet is not further separated and thus, any ethanol in the reactor outlet is lost. In a CSTR, the reactor concentration is equal to its outlet concentration. [83] Given a required ethanol recovery of 99 % (distillation standard [2]) would result in an ethanol concentration of  $0.01 \cdot 4 \frac{\text{g}}{\text{L}} = 0.04 \frac{\text{g}}{\text{L}}$  in the bioreactor. Even with a high selectivity  $\beta$  [64], liquid-liquid extraction with an ethanol concentration of  $0.04 \frac{\text{g}}{\text{L}}$  would require roughly twice as much energy as distillation. At  $4 \frac{\text{g}}{\text{L}}$  ethanol concentration, liquid-liquid extraction may be performed with only ca. 4 % of the energy demand of distillation making it an interesting option for end-of-pipe separation. [64] However, again the solid content is a problem, because the extractant tends to emulsify with solids such as yeast cells, cellulose and lignin. [162–164] Apart from ecological issues, the costs to replace the loss of extractant (12 \$/kg resp. 70.45 \$/mol [165]) outweigh the savings in energy demand. A prior solid-liquid separation is not possible for the reasons mentioned above regarding adsorption.

Steam stripping and vapor permeation involve heating up the fermentation broth to vapor formation or the exposure of the fermentation broth to steam at low pressures or high temperatures. [64] Both is lethal to the microorganisms in the bioreactor making steam stripping and

vapor permeation unfeasible for *in-situ* or slip stream separation. Applying steam stripping as end-of-pipe separation mechanism does not make sense, because the process is very similar to distillation. [64] One would sacrifice the industrial maturity of distillation for comparable costs and process performance. Also, there is no point in replacing distillation with vapor permeation as end-of-pipe separation. The demand of thermal energy is comparable since the reactor outflow needs to be vaporized, but the membrane will be exposed to a high risk of membrane fouling due to the high loading of organics in the reactor outflow. [64,166] Exchanging the membrane more frequent than on a yearly basis will increase the MESP only by less than 0.5 % per additional membrane exchange. [33] However, the plant downtime is not included in the MESP increase and again, the industrial maturity of distillation is sacrificed to overcome the azeotrope in one separation step at comparable costs.

CO<sub>2</sub> stripping seems promising on the first look: Purging bioreactors and thus, an *in-situ* implementation, as well as the condensation of gas stripping streams are well-established processes, the CO<sub>2</sub> gassing ensures anerobic conditions in the bulk phase, CO<sub>2</sub> stripping works properly at the moderate temperature levels in the fermenter, ethanol inhibition of the yeast is avoided, and the CO<sub>2</sub> lost by imperfections of the stripping cycle could be compensated by the CO<sub>2</sub> production of the yeast. [18] However, there are drawbacks, which outweigh these advantages: CO<sub>2</sub> stripping would cause high dissolved CO<sub>2</sub> concentrations in the fermentation broth of an open system. Apart from unfavorable consequences of a pH-drop as consequence of high dissolved CO<sub>2</sub> concentrations, the yeast will be strongly inhibited (ca. 50 % less productivity, Fig. 6.2) by the high dissolved CO<sub>2</sub> concentrations. [17] Furthermore, the above-mentioned equilibrium of 0.04  $\frac{g}{L}$  ethanol concentration in the bioreactor will become an issue again, if *in-situ* stripping with a recovery of 99 % is conducted. However, the maximum stripping recovery is much lower, since a certain bubble residence time is necessary for the ethanol mass transfer to the gas phase, which corresponds to a minimum reactor height ( $h_{\text{reactor, min}} = \tau_{\text{bubble, min}} * v_{\text{bubble}}$ ), and the bubble flow regime is necessary to obtain a sufficient mass transfer rate. To establish a stable bubble flow regime, a minimum diameter of the reactor is required, which allows a maximum reactor height at a given reactor volume ( $h_{\text{reactor, max}} = \frac{V_{\text{reactor}}}{0.25\pi * d_{\text{reactor, min}}^2}$ ). [167] At the given reactor volume, the maximum possible ethanol recovery is 30 %, where the two height requirements match each other (Fig. 6.3). Note, that the influence of the stirring speed is discussed controversially, but the low stirring speed of 50 rpm will not improve the result anyway. [168,169] A maximum ethanol recovery of 3 %, when applying CO<sub>2</sub> stripping *in-situ* obviously is economically not favorable.

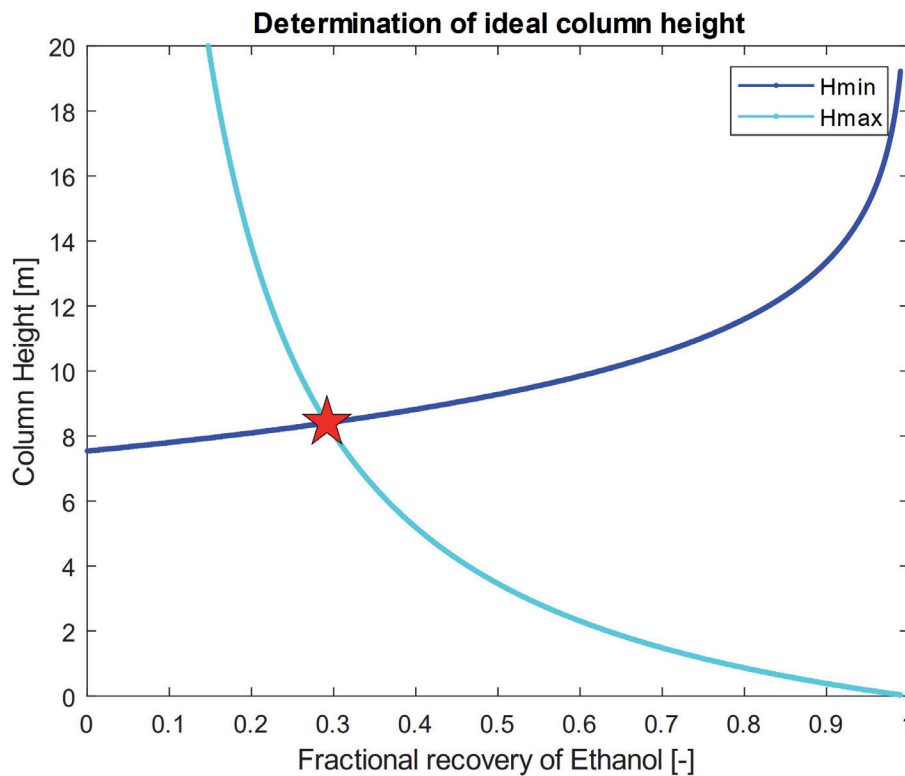


Figure 6.3: Determination of the maximum possible ethanol recovery of 30 % (red asterisks) by applying the reactor height requirements for bubble flow ( $h_{min}$ , blue line) and the bubble residence time ( $h_{max}$ , cyan line)

CO<sub>2</sub> stripping as end-of-pipe separation mechanism is not feasible either considering the amount of CO<sub>2</sub>, which is necessary to achieve the required recovery of 99 % (Fig. 6.4). Even for a poor ethanol recovery of 90 %, almost 5 t CO<sub>2</sub>/s are theoretically needed at industrial scale (chapter 2 according to published, experimentally validated partition coefficients (cf. section C.1). [168] Besides the gas amount, which could be recycled, none of the apparatus (compressor e.g.) could handle these dimensions. A titer of 4 wt.% at such high volume flows makes CO<sub>2</sub> stripping impossible.



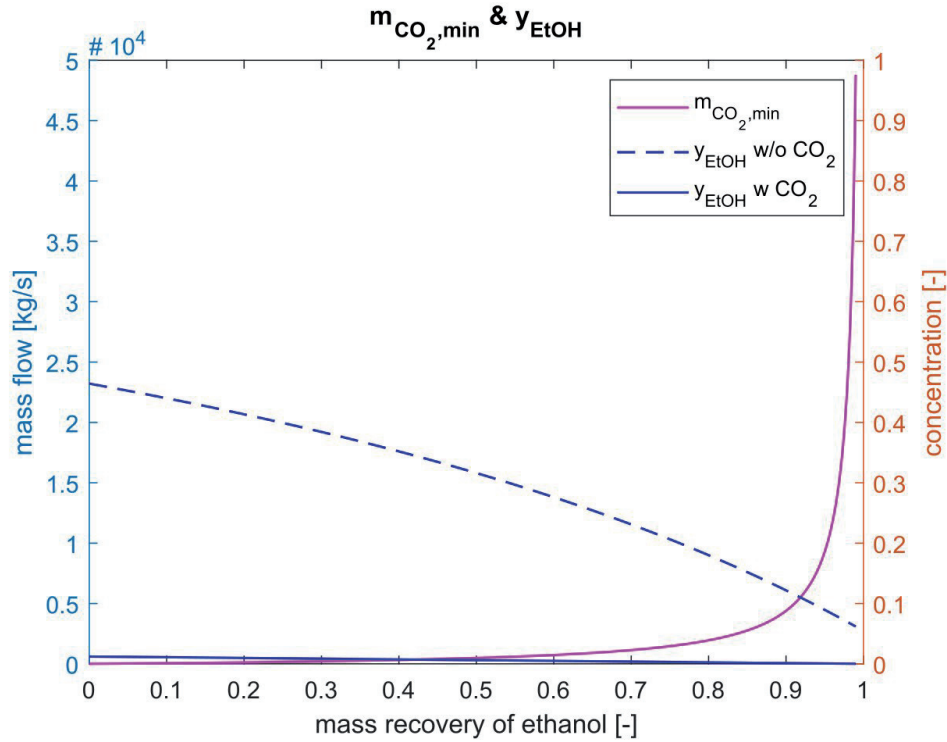


Figure 6.4: Necessary  $CO_2$  mass flow (magenta line) and ethanol concentrations as weight fraction in the gas stream (blue line) and the residual stream (blue dashed line) as function of the ethanol recovery.

Pervaporation is a membrane separation mechanism, where the permeate evaporates due to low pressures on the permeate side (or less common, is withdrawn with a gas purge). [64] The mass transfer rate across the dense membrane may be described with the solution-diffusion model (eq. 6.3). [170,171]

$$J_{EtOH} = Q_{EtOH} (p_{EtOH,sat} x_{EtOH,bulk} - p_p y_{EtOH,p}) \quad (6.3)$$

The rate constant  $Q_{EtOH}$  denotes the permeance  $[\frac{mol}{Pa \cdot s}]$  of ethanol for the given membrane and is a function of the diffusivity of ethanol in the membrane  $D_{EtOH}$ , the membrane thickness  $\delta_m$  and the gas phase sorption coefficient  $K_{EtOH}$ . The ethanol vapor pressure  $p_{EtOH,sat}$  reflects the volatility of ethanol.

$x_{EtOH,bulk}$  and  $y_{EtOH,p}$  represent the ethanol mole fractions in liquid bulk side and the gaseous permeate side, respectively.  $p_p$  denotes the pressure on the permeate side. Given the flux equation, it becomes clear, that pervaporation is the most promising *in-situ* separation concept, because the low mole fraction of ethanol in the liquid phase may be compensated by other design parameters such as the permeate pressure, membrane thickness, a suitable membrane material with high diffusivity for ethanol etc. [64] Furthermore, a PDMS membrane, which was

reported to show good separation characteristics for ethanol [172], is already installed in the bioreactor. However, a second membrane would have to be installed, but this is not an option for two reasons: First, space in the reactor is limited and maintaining a necessary membrane surface during scale-up is very challenging (chapter 5). Thus, a second membrane would put a highly unfavorable design constraint on any scale-up procedure. Second, the additional membrane would be exposed to membrane fouling due to the high concentration of microbial biomass in the bioreactor. [166, 173] The additional mass transfer resistance would accentuate membrane separation problems such as temperature and concentration polarization. [170] Concluding, it can be stated, that an additional membrane decreases the net performance of CBP as valuable space for biofilm formation is sacrificed only for a moderate increase in separation efficiency compared to a design with only one membrane. However, using the already installed membrane for two purposes, oxygen supply for the microbes and *in-situ* product removal, would further integrate the process and thus, perfectly fit the concept of CBP. [4, 52] In order to examine the potential of pervaporation for *in-situ* product removal of CBP, the design constraints for the membrane setup are formulated in the following: Ensuring an optimum fungal biofilm thickness  $\delta_f$ , the partial pressure of oxygen within the membrane must be 0.26 bar (Chapter 5) (mechanical stability of the PDMS membrane is assumed). Operating the membrane with pure oxygen would result in the theoretical minimum possible permeate pressure of 0.26 bar. The aimed ethanol recovery of 9 % results in an ethanol bulk concentration of  $0.04 \frac{g}{L}$  as mentioned above. The required mass flux across the biofilm and the membrane calculates as follows (eq. 6.4):

$$J_{\min, EtOH} = 99 * J_{EtOH, outlet} = 99 * c_{EtOH, bulk} * \dot{V} = 99 * 0.04 \frac{g}{L} * \frac{2.7 L}{5 * 24 h} = 89.1 \frac{mg}{h} \quad (6.4)$$

For this estimation, lab scale parameters were chosen in order to evaluate the pervaporation potential at sufficient membrane area, which corresponds to an ideal case. Considering the mass transfer resistance of the biofilm bulk boundary layer and the biofilm itself as well as ethanol degradation by *T. reesei*, this mass transfer rate is feasible as long as equilibrium is not reached (Chapter 3 & 4). However, equilibrium is reached very fast given the fact, that ethanol has a Henry constant of  $H_{CP}^{EtOH} = 1.9 \frac{mol}{m^3 Pa}$  (eq. 6.5) [174]:

$$p_{EtOH, eq} = \frac{c_{EtOH, bulk}}{H_{CP}^{EtOH}} = 0.457 Pa = 0.046 mbar \quad (6.5)$$

As soon, as the partial pressure of ethanol in the permeate reaches 0.046 mbar, equilibrium is reached, and no further mass transfer occurs. To avoid equilibrium, high volume flow rates within the membrane would be necessary to withdraw and dilute the ethanol concentration.

The ethanol dilution will cause higher costs for separation from the gas phase and the high volume flow rates will cause a large pressure loss over the membrane, which increases the cost of compression for gas recirculation besides threatening the mechanical integrity of the membrane. Concluding, it can be said, that pervaporation is a promising *in-situ* product removal strategy for batch operation of bioprocesses with diluted volatile organics as product as stated elsewhere in literature. [64,170,172] However, at continuous operation, pervaporation is not feasible at any scale.

## 6.4 Conclusion

Popular rate-controlled separation techniques were investigated regarding their potential to outperform distillation as industrial standard, since they offer the potential to reduce yeast inhibition by ethanol, to avoid separation limitations by the azeotrope and they are not bound to the vapor-liquid-equilibrium of highly diluted ethanol-water mixtures. However, except from CO<sub>2</sub> stripping and pervaporation, all mechanism fail to handle the solids of the fermentation broth. CO<sub>2</sub> stripping is limited by a poor ethanol recovery due to the trade-off between bubble residence time and stable bubble flow regime. Pervaporation, being the most promising concept for *in-situ* product removal, would be a cost-saving alternative to distillation for batch operation, but is limited by an unfavorable vapor-liquid equilibrium due to low bulk concentrations during continuous operations.

Distillation as industrial standard for ethanol separation from the fermentation broth remains untouched because there is too little incentive to change the separation design apart from economic savings. At the given titer of 4 wt.% or lower, yeast inhibition by ethanol is almost negligible. *In-situ* product removal strategies exploit their full potential, if the fermentation product is highly toxic, such as butanol, where the productivity increase is significant, when butanol is removed *in-situ*. [64,175]



## CHAPTER 7

---

### Summary and conclusions

---

This work demonstrated that consolidated bioprocessing is a promising concept for conversion of lignocellulose to ethanol at industrial scale. CBP offers a great cost saving potential, is feasible to be operated continuously and may be scaled up due to extensive knowledge of the process from a chemical engineering point of view. The main findings and conclusions of the discussed topics are given in the following.

Cost savings of up to 27.5 % of the total costs compared to conventional bioethanol production from lignocellulose, as stated by a techno-economic assessment, make continuous CBP the strongest lever to reduce processing costs of lignocellulosic ethanol. In the EU, applying CBP offers a sufficient margin for profitable production or the possibility to decrease the plant size to 15 % and thus decentralize the biomass valorization. However, in the US where 56.2 % of the world's ethanol is currently consumed, the market situation is tense (31 % price drop for ethanol since 2007 whereas prices for chemical plants increased by 16 %). A cost sensitivity analysis of several process parameters (scale, titer, yield and residence time) and investment parameters (feedstock price, price level in the country of the plant location and costs of capital) show that scale and yield are the main cost-pushers from a process point of view, whereas the price level of the plant location has the highest impact on the investment conditions. Since outsourcing 2<sup>nd</sup> generation bioethanol production to third world countries with low price levels leaves valuable biomass potential unused and hinders economic growth in rural areas, it should be aimed at meeting the current ethanol market price by taking advantage of the cost levers of multiple process and/or investment parameters if necessary, such as utilizing cheaper waste feedstocks at comparable yields and reducing the costs of capital by accepting lower returns on equity. Alternatively, exploiting the added-value through sustainable production as well as local market disparities such as tariff barriers or tax exemptions may lead to profitable production of lignocellulosic bioethanol. In the short term, retrofitting of depreciated existing

corn ethanol plants to CBP operation, might be an interesting approach to reduce the CAPEX in order to meet the world market price of ethanol with lignocellulosic ethanol.

In order to prove the feasibility of continuous CBP, and therefore the mentioned cost savings of 27.5 %, and to validate a rigorous process model, continuous experiments were successfully conducted. The known obstacles of developing continuous processes could be avoided by adjusting the experimental setup. A maximum titer of  $3.258 \pm 0.007 \frac{\text{g}}{\text{L}}$ , a productivity of  $0.025 \frac{\text{g}}{\text{L} \cdot \text{h}}$  and constant enzyme production over 750 h were achieved. Furthermore, it was proven that the continuous co-cultivation of two competitors, *T. reesei* & *A. phoenicis*, is possible, if the process conditions are adjusted to the identical growth rate. The adding of *A. phoenicis* targeted the better utilization of the inhibiting intermediate cellobiose by balancing the fungal enzyme cocktail in terms of higher  $\beta$ -G concentrations. This goal was achieved, but however did not result in higher yields or productivities. Furthermore, the continuous experiments showed that the oxygen flux per membrane area is a critical parameter for the process. Setups with identical volumetric oxygen transfer rate  $k_L a$ , but different oxygen fluxes per membrane area (large area & low concentration gradient vs. small area and high concentration gradient) showed titer differences of ca. 80 % ( $1.83 \frac{\text{g}}{\text{L}}$  vs  $3.26 \frac{\text{g}}{\text{L}}$ ) in favor of setups with the large membrane surface. The difference was attributed to long diffusion paths in thicker biofilms and thus, shortage in nutrient supply.

A rigorous process model was developed for continuously operated consolidated bioprocessing of cellulose to ethanol to quantitatively describe the phenomena of lower titers at higher  $k_L a$  for optimization purposes. 9 species were considered (oxygen, glucose, *T. reesei*, secondary mycelia of *T. reesei*, enzymes, cellulose, cellobiose, yeast density and ethanol). 8 of these 9 species (all except cellulose) are present in the biofilm and thus, needed to be modelled spatially resolved in order to account properly for mass transfer limitations. The enzyme synthesis rate of the secondary mycelia and the effective diffusivity of  $\beta$ -glucosidase were used as fitting parameter of the model. Compared to literature data of suspended cultures in a batch process [10,124,125], a reduction in enzyme synthesis rate of ca. 40 % ( $0.67 \frac{\text{FPU}}{\text{mL} \cdot \text{d}}$  vs  $1.152 \frac{\text{FPU}}{\text{mL} \cdot \text{d}}$ ) and a ca. 20 % ( $5 \cdot 10^{-11} \frac{\text{m}^2}{\text{s}}$  vs  $4 \cdot 10^{-11} \frac{\text{m}^2}{\text{s}}$ ) reduced effective diffusivity accounting for the affinity of  $\beta$ -G to attach to the cell walls yielded agreement with the continuous experiments within a 15 % confidence interval. The results of the model were able to explain the different productivities observed in the continuous experiments. The fungal biofilm thickness  $\delta_f$  was found to be a critical parameter with an optimum for every membrane configuration. Smaller  $\delta_f$  reduced the fungal biofilm volume and thus, the enzyme production unnecessarily and larger  $\delta_f$  increased the diffusion path length and caused shortage in nutrient supply as well as lower enzyme concentrations in the bulk. The agreement between the model data and the experiments also confirmed the non-proportionality of the fungal growth and enzyme production.

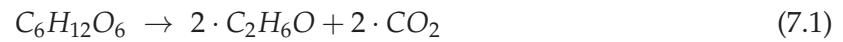
With the process model as centerpiece, a scale-up framework consisting of the model and a set of non-dimensional parameters was developed to scale up consortium-based consolidated bioprocessing of cellulosic substrates from 2.7 L laboratory scale to 130 L pilot scale. The majority of the non-dimensional parameters could be kept constant during scale-up as requested by the similarity paradigm. Necessary changes were simulated with the model. Again, the fungal biofilm thickness  $\delta_f$  served as a relevant parameter for scale-up considerations. In general, the relative loss of biofilm volume should be compensated by longer residence times since the residence time has by far the least impact on the process economics. However, an experimental confirmation of the presented calculations remains still to be done. The expected price increase of ca. 15 % at industrial scale due to the need of pure oxygen could be reduced by exploiting synergies with other bioprocesses in the framework of a biorefinery, where oxygen might be a byproduct of another process.

Finally, popular rate-controlled separation techniques were investigated regarding their potential to outperform distillation as industrial standard, since they offer the potential to reduce yeast inhibition by ethanol, to avoid separation limitations by the azeotrope and they are not bound to the vapor-liquid-equilibrium of highly diluted ethanol-water mixtures. However, except from CO<sub>2</sub> stripping and pervaporation, all mechanism fail to handle the solids of the fermentation broth. CO<sub>2</sub> stripping is limited by a poor ethanol recovery due to the trade-off between bubble residence time and stable bubble flow regime. Pervaporation, being the most promising concept for *in-situ* product removal, would be a cost-saving alternative to distillation for batch operation, but is limited by an unfavorable vapor-liquid equilibrium due to low bulk concentrations during continuous operations. *In-situ* product removal strategies do not exploit their full potential with ethanol, because ethanol is not toxic enough to cause considerable increases in productivity when withdrawn *in-situ*.

Further research should target the conduction of the CBP experiment at pilot scale to prove the scale-invariance rigorous model and thus, the reliability of the scale-up guideline. Other potential obstacles, which need to be overcome for industrial implementation of CBP, might be limited space for the membrane in the reactor and the low productivity. Therefore, investigations regarding other mixing mechanisms such as recirculation by pumping or the development of a stable thermophile consortium to accelerate hydrolysis with higher reactor temperatures might be valuable.

Recalling the urgent need to reduce GHG emissions to keep global warming below 1.5 °C, cost-efficient CBP of non-edible resources is a unique opportunity to secure the supply of chemicals such as ethanol, which must be seized as soon as possible since the technology maturity level is a crucial factor for ubiquitous implementation. When CBP of lignocellulose reaches industrial stage, further improvements should target the efficient conversion of the

substrate's carbon. Given the stoichiometric conversion of glucose to ethanol (7.1), it becomes clear that at least 1/3 of the available carbon is lost as  $CO_2$ .



Recalling the high water content of lignocellulosic biomass and the transport costs, a more efficient use of the carbon is unequivocal. The industrial potential of promising concepts such as the lactate platform could be evaluated in depth at moderate costs by adjusting the presented models to the biological pathways of other microorganisms.



## APPENDIX A

---

### Supplementary material for chapter 2: Techno-economic assessment of consolidated bioprocessing of lignocellulose to ethanol at industrial scale

---

#### A.1 Calculations for redimensioning

##### *Calculation of the CAPEX and OPEX savings by CBP*

In the base case, 2000 dry tons of corn stover per day are converted to ethanol. The costs per dry ton of feedstock are 48.53 \$ (31.75 \$ for the collection, transport and handling; 21.32 \$ for the feedstock itself). The pretreatment is a dilute acid-catalyzed steam explosion pretreatment. The pretreated slurry is conditioned with ammonia. After a residence time of 5 *days* for hydrolysis and fermentation, 271.3 L ethanol per dry ton feedstock are obtained (76 % yield). The final product concentration is 5.4 wt.% ethanol. The enzymes are produced by *T. reesei* and the fermentation is carried out by *Zymomonas mobilis*. The ethanol is recovered by means of a rectification (beer tower and a second distillation column) and adsorption. The beer stillage is separated from the lignin and sent to a wastewater treatment plant (WWT) together with the other waste streams of the process. Lignin and biogas from the anaerobic digestion in the WWT are burned to generate heat and electricity for the process. 0.48 kWh/annual L ethanol of excess electricity is sold to the grid. The calculated annual cost of capital account for 13.1 % of the CAPEX.

Applying the highest degree of process intensification, CBP, by merging enzyme production, hydrolysis and fermentation in one process step as well as the change in pretreatment yield cost savings in capital expenditure (CAPEX) as well as in OPEX. In this work, the saved costs are allocated either to CBP or to steam pretreatment. In general, CAPEX and variable OPEX underlie considerable changes when applying CBP and steam pretreatment whereas

the change of fixed OPEX is almost negligible. The change to CBP mostly affects the areas of enzyme production, hydrolysis and fermentation. CAPEX are saved due to a reduced need of apparatuses as a result of the process integration. Variable OPEX are reduced since no glucose is needed for enzyme production as the fungus metabolizes sugars released from the hydrolyzed feedstock. An experimentally confirmed cellulose-to-ethanol yield of 73 % including the fact that a fraction of the feedstock is consumed for the enzyme production was adapted to 76 % to ensure comparability given the uncertainty of different operation modes (batch vs. continuous), substrates (corn stover vs. pure cellulose), resources for enzyme-production (*in-situ* vs. *ex-situ*) and maturity levels of the technologies. Single yields of the pretreatment (yields of xyloses and glucan) and hydrolysis unit (pentose yield) were taken from the base case. Furthermore, the residence time of 5 *days* for hydrolysis and fermentation was kept constant. Since the enzyme concentration in a steady-state continuous operation stays constant over time (enzyme production equals the wash-out during steady-state), the residence time for enzyme growth in A 400 may be neglected.

The change from dilute acid-catalyzed steam pretreatment to pure steam pretreatment increases the CAPEX of the pretreatment area, because the apparatuses must withstand higher pressures. Variable OPEX are saved due to a strongly reduced use of chemicals, which results in a lower salt concentration in the downstream processing. Thus, the beer stillage is not sent directly to anaerobic digestion like in the base case, but to an evaporator cascade and a subsequent combustion of the obtained solids. Therefore, more electricity can be generated and sold, which reduced variable OPEX as well. An overview of the CAPEX changes presented in Tab. A.1.

The totals correspond to the total installed costs of each unit (next section for further details). The costs of a warehouse, site development and additional piping were determined as percentage of the inside battery limit (ISBL) costs according to the base case. ISBL denotes the total installed costs of the areas, where the actual process happens (A 200, 300, 400 and 500). The sum of the total installed costs and the costs for a warehouse, site development and additional piping give the total direct costs (TDC). Proratable expenses (includes fringe benefits, burdens, and insurance of the construction contractor), field expenses, home office & construction fee (includes engineering plus incidentals, purchasing, and construction), project contingency and other costs for start-up, permits etc. are functions of the TDC and were calculated according to the base case. Their sum plus the TDC yields the fixed capital investment (FCI). The total capital investment (TCI or CAPEX) consists of the FCI and the costs for land and working capital, which were calculated according to the base case as well.

Table A.1: Total Capital Investment (TCI) of the base case and consortium-based CBP derived from the total installed costs of all apparatuses.

	Base Case		Change due to pretreatment		Change due to consortium-based CBP		Sum of changes	
	abs. [MM\$]		abs. [MM\$]	rel. [%]	abs. [MM\$]	rel. [%]	abs. [MM\$]	rel. [%]
Totals (excl. A 100)	232.22		34.50	14.86	-22.07	-9.50	244.65	5.35
ISBL (A 200- A 500)	105.28		19.60	18.62	-22.07	-20.96	102.81	-2.35
Warehouse (4 % ISBL)	4.21		0.78		-0.88		4.11	
Site Development (9 % of ISBL)	9.48		1.76		-1.99		9.25	
Additional Piping (4.5 % of ISBL)	4.74		0.88		-0.99		4.63	
Total Direct Costs (TDC)	250.64		37.93	15.13	-25.93	-10.35	262.64	4.79
Proratable Expenses (10 % TDC)	25.06		3.79		-2.59		26.26	
Field Expenses (10 % TDC)	25.06		3.79		-2.59		26.26	
Home Office & Construction Fee (20 % TDC)	50.13		7.59		-5.19		52.53	
Project Contingency (10 % TDC)	25.06		3.79		-2.59		26.26	
Other Costs (Start-Up, Permits, etc.) (10 % TDC)	25.06		3.79		-2.59		26.26	
Total Indirect Costs (TIC)	150.39		22.76	15.13	-15.56	-10.35	157.58	4.79
Fixed Capital Investment (FCI)	401.03		60.69	15.13	-41.49	-10.35	420.23	4.79
Land	1.85		0.00		0.00		1.85	
Working Capital (5% FCI)	20.05		3.03	15.13	-2.07	-10.35	21.01	4.79
Total Capital Investment (TCI/CAPEX)	422.93		63.72	15.07	-43.57	-10.30	443.09	4.77

*Change in CAPEX for each unit of the base case scenario*

This chapter covers the changes of the process layout for each apparatus in the single process areas. The base case is subdivided into 9 areas (Tab. A.2), which are referred to in the following.

Table A.2: Areas and their functions in the base case

A 100	Feedstock storage & handling
A 200	Pretreatment & conditioning
A 300	Enzymatic hydrolysis & fermentation
A 400	Cellulase enzyme production
A 500	Product, solids & water recovery
A 600	Wastewater treatment
A 700	Product & feed chemical storage
A 800	Combustor, boiler & turbogenerator
A 900	Utilities

**Area A 100: Feedstock storage & handling:** No changes were applied to the feedstock storage and handling since the same amount of feedstock is used and the composition of the corn stover is assumed to be identical. Furthermore, the apparatus of A 100 are not included in the CAPEX calculations identical to the base case. Feedstock purchase, storage and handling are pooled in a price of 48.53 \$/dry *ton*. [2]

**Area A 200: Pretreatment & conditioning:** The change from dilute acid catalyzed steam pretreatment to pure steam pretreatment results in changes of CAPEX and OPEX of A 200: All equipment for the addition of sulfuric acid and the conditioning of the pretreated slurry with ammonia were removed, resulting in cost savings of 1.87 % of the installed costs of A 200. The pH change due to autohydrolysis and its consequences will be discussed in the hydrolysis and fermentation unit (A300). However, to reach a similar pretreatment severity without adding sulfuric acid, the temperature must be increased from 158 °C to 180 °C (10 *bar*) in the first stage and 230 °C (28 *bar*) in the second stage, respectively. [58] To evaluate the cost of a high pressure apparatus based on the costs for low pressure apparatuses, Ulrich et al. proposed the multiplication of the installed costs with a pressure factor  $F_P=1.4$  for pressures up to 11 *bar* and  $F_P= 2.5$  for pressures up to 31 *bar*. [61] Thus, the change from 158 °C to 180 °C can be neglected in terms of installed costs since the vapor pressures of water at 158 °C and 180 °C

are in the same  $F_P$  range. However, the installed costs of the second stage pretreatment need to be increased by a factor of 1.79:

$$\frac{F_{P,CBP}}{F_{P,base\ case}} = \frac{2.5}{1.4} = 1.79 \quad (A.1)$$

Applying this factor to the second stage pretreatment reactor, leads to higher installed costs of 7.9 MM\$. Subtracting the above-mentioned savings yields a net increase in total installed costs for A 200 of 7.26 MM\$ (+22 %), which corresponds to an 3.1 % increase of plant's total installed costs.

**Area A 300: Enzymatic hydrolysis & fermentation:** Since enzymatic hydrolysis and fermentation are conducted in the same reactor, the hydrolysis tank and the transfer pump from the hydrolysis tank to the fermenters are omitted. Furthermore, CBP is carried out continuously in contrast to the batch operation in the base case. Therefore, only 7 fermenters are needed instead of 12, since the batch-inherent downtime is avoided (The volumetric flow after the pretreatment of  $221\ m^3/h$  multiplied with the residence time of 5 days gives a total necessary reactor volume of  $26'500\ m^3$ , which corresponds to 7 fermenters with  $3'785\ m^3$  each). This leads to cost savings of 14.9 MM\$ (47.7 %) of installed costs. The only extra equipment needed is the membrane and its support. The membrane support is modelled with the cost function of stainless-steel internal heating coil as the geometry and the mounting is comparable. [61] Each of the 7 membrane supports has a purchased equipment cost of 10'000 \$ based on the CEPCI from 2004. Applying the CEPCI from 2007 and an installation factor of 1.5 leads to installed costs of 138'000 \$ for the membrane support. Applying the specific membrane surface of  $10\ m^{-1}$ , the total reactor volume of  $26'500\ m^3$  demands  $265'000\ m^2$  of membrane surface. Ulrich et al. propose 30-50 \$/ $m^2$  total installed costs for membranes (based on CEPCI from 2004). [61] Since the membrane is made from PDMS, 30 \$/ $m^2$  are assumed leading to total installed costs of 10.44 MM\$ for the membrane in 2007. The resulting net savings of total installed costs of A 300 are 4.31 MM\$ (13.8 %), which corresponds to 1.9 % savings of the plant's total installed costs.

**Area A 400: Cellulase enzyme production:** The cellulolytic enzyme cocktail is produced in-situ in the membrane reactor. Thus, all apparatus of A 400 can be omitted except the air compressor package and the nutrient pump, because these apparatuses are needed for CBP as well to supply the cellulolytic fungus with oxygen and nutrients. The resulting net savings of total installed costs of A 400 are 17.76 MM\$ (-97 %), which corresponds to 7.6 % savings of the plant's total installed costs.

**Area A 500: Product, solids & water recovery:** No changes were applied to the ethanol distillation and dehydration. However, the beer stillage (bottom of the first distillation column)

is new sent to a cascade of three evaporators, where the top outlet consists of recycling water and the bottom outlet consists of a combustible paste, which is sent to A 800, as it was proposed in the earlier NREL lignocellulosic bioethanol report from 2002. [63] In the base case, the beer stillage needs to be sent to anaerobic digestion of the wastewater treatment due to the high salt concentration resulting from the dilute acid pretreatment and the necessary pH adjustment. Since the salt concentration after the CBP will be much lower due to the pure steam explosion pretreatment, an earlier design case for a cellulosic ethanol plant published by NREL can be adopted. [63] All apparatuses dealing with the beer stillage are removed leading to savings on total installed costs of 6.84 MM\$. They are replaced with the beer stillage processing described in the previous base case leading to total installed costs (CEPCI from 2007) of 18.9 MM\$. The net increase of total installed costs for A 500 is 12 MM\$ (+54 %), which corresponds to 5.2 % savings of the plant's total installed costs.

**Area A 600: Wastewater treatment:** Because of the different processing of the beer stillage in A 500, the wastewater treatment (WWT) inlet flow is reduced to only 13.7 % of the base case. The WWT has a size exponent of 0.6. Thus, 13.7 % of the base case size lead to 30.3 % of the total installed costs, a reduction of 34.4 MM\$ (-69.7 %). This corresponds to 14.8 % savings of the plant's total installed costs.

**Area A 700: Product & feed chemical storage:** No changes were applied to A 700. The tanks for sulfuric acid and ammonia are not used for the pretreatment and conditioning, but for the pH regulation of the reactors. Thus, they might be oversized, but in the light of their negligible fraction of the total CAPEX it was decided to keep them at the current size.

**Area A 800: Combustor, boiler & turbogenerator:** Due to the pure steam explosion pretreatment, the sulfur concentration in the flue gas of the combustor is below the limit demanding flue gas desulfurization (FGD). [63] The costs for the FGD are however included in the combustion package in the base case. Therefore, cost functions from Turton (baghouse filter) [60] and Garrett (spray dryer absorber) [62] were taken to determine these costs without FGD. The equipment costs of the baghouse amount to 290'000 \$ with a CEPCI of 542 (2016). Considering an installation factor of 1.9, the installed costs are 534'000 \$ (CEPCI from 2007). The spray dryer absorber has purchased costs of 290'000 \$ with a CEPCI of 355 and an installation factor of 1.64 leading to installed costs of 703'888 \$ (CEPCI from 2007). Thus, the total installed costs reduction due to removal of the FGD apparatuses is 1.24 MM\$ (CEPCI from 2007). The remaining apparatuses of the combustion unit A 800 (64.72 MM\$) have to be scaled up by a factor of 2.8 since a larger fraction of the beer stillage is sent to combustion (cf. changes in A 500) resulting in an inlet flow, which is 2.8 times higher than in the base case. A size exponent of 0.6 is given for the combustion package in the base case. Scaling the combustion package up by a factor of 2.8 leads to an installed cost increase by a factor of 1.9. Thus, the net increase in

installed costs is 54.42 MM\$ (+82.5 %), which corresponds to a 23.4 % increase of the plant's total installed costs.

**Area A 900: Utilities:** The cooling tower system has a size exponent of 0.6 and needs to be scaled up by the same factor 2.8 as the combustor and boiler system due to the additional heat production. Apart from that, no changes were applied to A 900, since the same utilities are needed. This leads to an increase in total installed costs of 1.88 MM\$ (+27.3 %) for A 900, which corresponds to an 0.8 % increase of the plant's total installed costs.

### *Changes of OPEX*

#### **Fixed OPEX**

The fixed OPEX consist of labor costs, maintenance, property insurance and tax. Maintenance (3 % of the inside battery limits (ISBL; Tab. A.1)) as well as property insurance and tax (0.7 % CAPEX are determined by the CAPEX and account for 6 MM\$, which corresponds to 4.67 ¢/annual L ethanol and an increase of 1 % compared to the base case.

The total labor costs account for 2.04 ¢/annual L ethanol in the base case. However, the base case provides little information about the allocation of workers to areas or apparatuses. Only the workers responsible for enzyme production are explicitly mentioned. Since A 400 could be omitted completely (the only exception is the compressor package and the pump), the costs for the shift operators for the enzyme production were not included in the present design. Despite massive apparatus reductions in A 300 and A 600, no further reductions of labor costs were applied, since it cannot be ensured that the increased number and size of apparatus in A 500 and A 800 do not compensate the reduced need of shift operators in A 300 and A 600. The cost per employed worker was kept constant. Thus, the total labor costs amount to 4.12 MM\$ per year, which corresponds to 1.78 ¢/annual L ethanol and a reduction of 12.5 %.

#### **Variable OPEX**

The variable OPEX consist of the costs for raw materials and disposal of waste streams minus the revenue for selling by-products. Since they are not projected over the lifetime of the plant, they can be directly expressed as costs per liter of ethanol as it is shown in Tab. A.3.

The greatest savings in variable costs come from the integration of the enzyme production in the main fermenter, as this allows the addition of glucose for enzyme production to be omitted. Furthermore, the change from acid-catalyzed steam pretreatment to pure steam explosion pretreatment avoids the use of chemicals during the pretreatment, which contributes substantially to the total raw material cost savings as well. Additional costs result from the need to exchange the membrane on a yearly base. [61] Pure steam pretreatment results in a higher steam demand of 1'460 kg/h (800 kW), which is provided at no additional OPEX, because the



Table A.3: Comparison of the raw material costs between the base case and the case employing consortium-based CBP with steam explosion pretreatment.

Unit	Raw material/ feed chemical	Costs Base case [€/annual L ethanol]	Costs This work [€/annual L ethanol]	Note
A 100	Feedstock	19.57	19.57	21.32 \$/ton feedstock price 31.75 \$/dry ton total costs for collection, processing, storage and transportation
A 200	Sulfuric acid	0.65	0.00	No need for chemicals during steam explosion pretreatment
	Ammonia	1.72	0.00	The reduced amount of ammonia necessary to condition the steam pretreated slurry due to autohydrolysis is negligible (0.00172 €/annual L ethanol)
A 300	CSL	0.24	0.24	The same media consumption for the fermenting microorganism is assumed
	Diammonia phosphate	0.51	0.51	
	Sorbitol	0.18	0.00	Sorbitol is used to accelerate the metabolism of <i>Z. mobilis</i> , it is not necessary for <i>S. cerevisiae</i> [176]
	Membrane	0.00	0.05	The membrane is assumed to be exchanged every year at 30 \$/m <sup>2</sup> [61]
A 400	Glucose	5.11	0.02	Glucose is not needed for enzyme production since the enzyme producer consumes part of the hydrolyzed feedstock during CBP. 0.02 €/annual L ethanol reflect the additional substrate costs for growing the microbial biomass after yearly maintenance
	CSL	0.03	0.03	Other media consumption of the enzyme producer is assumed to be the same as in the base case
	Ammonia	0.19	0.19	
	Host nutrients	0.20	0.20	
	Sulfur dioxide	0.02	0.02	
A 600	NaOH	1.23	0.02	NaOH is used in the base case to flush the fermenters between each batch, which becomes needless for continuous CBP. A little amount of NaOH is necessary for sterilization after yearly maintenance
A800	Boiler chemicals	0.00	0.01	The scale-up by a factor of 2.8 affects linearly the raw material consumption in A 800 (2.8*0.0045)
	Feedstock	0.00	0.00	No feedstock needs to be added for stable combustion
	FGD lime	0.65	0.00	No lime is used since FGD is not needed
A900	Cooling tower chemicals	0.03	0.03	
	Makeup water	0.14	0.14	
<b>Total</b>		<b>30.46</b>	<b>21.02</b>	<b>The reduction of 31.1 % of the total var. OPEX is achieved by the change in pretreatment (10.1 %) and the switch to consortium-based CBP (21 %)</b>



up-scaled combustor and boiler system delivers 2.8 times the heat energy (46'000 kW) of the base case, which is sufficient to supply the additional steam needs.

The only waste stream in the base case, which must be landfilled, is the ash from FGD. As FGD can be omitted, these 0.66 ¢/annual *L* ethanol are saved in this case due to the change in pretreatment.

One-third of the total reduction of variable OPEX of 31.1 % comes from the switch of the pretreatment and two-thirds from the use of consortium-based CBP. The excess electricity generated by the combustion of lignin (8.8 % of the corn stover's LHV) is a by-product, which is sold to the grid. In the base case, 12'814 kW of excess electricity are produced. The scale-up of the combustor will lead to an excess electric power of 36'000 kW, leading to revenues of 7.32 ¢/annual *L* ethanol. The unused heat (44 % of the corn stover's LHV) is released to the atmosphere due to the remote location of the plant analogous to the base case. 6.8 % and 0.9 % of the corn stover's LHV are used for process electricity and process heat, respectively. 39.5 % of the corn stover's LHV are stored in the produced ethanol.

Concluding, the total variable OPEX per annual liter of ethanol for CBP amount to 13.84 ¢/annual *L* ethanol instead of 28.46 ¢/annual *L* ethanol in the base case, which corresponds to a reduction of 51.37 %.

#### **Additional remarks regarding the calculations of the sensitivity analysis:**

- Change of the process layout at small scales:
  1. The size exponent of the hydrolysis and fermentation unit A 300 was changed from 1 to 0.6. Above 10 % of the base case scale, the fermenters are scaled up by parallelizing, which gives a size exponent close to 1. Below 10 %, the remaining reactors become smaller, which can be scaled with a size exponent of 0.6. [60]
  2. Also, below 10 % the costs for combustion and boiler unit reach their minimum size. Further downsizing is not possible with the fuel, i.e. moist lignin, given by the process. [62] Thus, the installed costs of these apparatuses are kept constant for smaller scales.
  3. Below 5 % of the base case scale, the WWT unit cannot be further downscaled [177] and it becomes economically favorable to send the whole beer slurry to the WWT. Thus, the WWT works to capacity and the CAPEX savings of omitting the combustion and boiler unit overcompensate the loss of electricity revenues assuming, that steam and disposal of waste can be purchased at market prices (60 \$/ton steam and 31 ¢/m<sup>3</sup> waste water). [61–63]
- Change of feedstock costs with scale:

Assuming, that the feedstock is collected in a circle around the production site, leads to a linear relationship between the plant size and the areal size of the circle, where the feedstock is collected. But the transport distance (directly proportional to the radius of the circle) scales with a factor of  $1/\sqrt{2}$  to the area. Thus, a half-sized plant would require a half-sized circular area for the collection of feedstock, but the transportation distance would only be reduced to 71 %.

- Correlation of yield and feedstock price:

Neglecting the resizing of apparatus in the units A100-400 due changes in yield for a moment, a yield of 96 % and 56 % instead of 76 % corresponds to 79 % and 136 %, respectively, of the total feedstock costs. Recalling the 30 % MESP share of the feedstock costs explains the strong sensitivity towards the yield.

- Assumptions concerning the MESP sensitivity with the PPP:

It is assumed, that the CAPEX are not affected by the PPP although the possibility of considerable CAPEX differences depending on the plant location is reported in literature. [178] However, the assumption is justified by three reasons:

1. There is little price index data from other countries (only from the Netherlands, Germany, South Africa and Canada)
2. Some of the needed apparatus (i.e. the steam pretreatment unit A 200) are manufactured only by a very limited number of companies worldwide (and thus they are not object to local trading)
3. A conversion of currencies, which is said to be the most important factor of local CAPEX differences, is not necessary in this work due to the dominance of the US\$ as international currency in apparatus pricing. [179,180]

### Calculation of cost changes with varying titer, yield, residence time and capital charge rate

- Ethanol titer 5 (7) wt.% vs. 5.4 wt.%:

The titer influences only the purification unit A 700. Cysewski et al. reported the distillation costs at different weight fractions of sugar in the fermentation feed for a total ethanol production of 90'000 L ethanol/d. [181] Considering a fermentation yield of 95 % of the theoretical limit (0.51 g ethanol/g glucose) leads to 14.5 wt.% glucose concentration for 7 wt.% ethanol titer and 11.1 wt.% glucose concentration for 5.4 wt.% ethanol titer resulting in 0.79 ¢/L ethanol and 0.71 ¢/L ethanol separation costs, respectively. Applying the size exponent of 0.67 for distillation columns [60] and the CEPCI from 2007, a cost difference of 0.8 ¢/L ethanol is found. The difference in distillation costs per liter ethanol

corresponds to a total cost (MESP) difference of 1.39 %. Furthermore, the cascade of the three evaporators for the beer stillage can be smaller for higher titers since less water leaves the beer tower bottom. The difference in titer causes a 1.84 % lower flow inlet. This results in 1.51 % lower total installed costs based on the size exponent of 0.68 for the evaporators. [63] 1.51 % lower total installed costs result in 2.98 % TCI reduction, which corresponds to a 1.26 % MESP reduction. Furthermore, the TCI reduction results in lower fixed OPEX (reduction of maintenance, insurance and tax expenses). The 2.98 % lower TCI lead to a 0.22 % MESP reduction due to lower fixed OPEX.

Concluding, it can be stated, that 1.26 % + 1.39 % + 0.22 % = 2.87 % of additional cost savings can be realized if the titer is increased from 5.4 wt.% to 7 wt.%. Analogue it can be stated that the titer reduction from 5.4 wt.% to 5 wt.% reduces the cost savings by 0.72 %. Thus, the cost savings reported by Lynd et al. exclude 0.72 % of cost savings due to a higher titer in the base case. [3]

- Yield 398.6 L ethanol/dry US ton vs. 299 L ethanol/dry US ton:

A higher yield with constant ethanol titer demands less feedstock. Thus, feedstock costs can be saved and all apparatuses in A 200 and 300 become cheaper because they are smaller since less inlet flow is necessary for the same ethanol titer. Due to better conversion of the feedstock, less revenues are gained with excess electricity since less feedstock is consumed in general and thus, less lignin is available for combustion.

A yield increase by a factor of 1.3291 (=398.6 L ethanol/299 L ethanol) leads to the same ethanol output with 75.24 % of the feedstock. 24.73 % feedstock reduction results in 8.52 % MESP reduction as a consequence of lower feedstock and handling cost. The cost saving due to smaller apparatuses are calculated with weighted size exponents for A 200 and 300. The weighted size exponents were obtained by averaging the size exponents of one unit weighing the with the total installed cost of the corresponding equipment (eq. A.2).

$$\text{weighted size exp. } \bar{n} = \frac{\sum_i n_i * \text{installed costs}_i}{\sum_i \text{installed costs}_i} = \begin{cases} 0.608 \text{ for A200} \\ 0.856 \text{ for A300} \end{cases} \quad (\text{A.2})$$

A flow reduction of 24.73 % of the processing stream due to higher yield leads to an FCI reduction of 2.85 %, which corresponds to a MESP reduction of 1.20 %. Furthermore, changes of the fixed OPEX savings (because the fixed OPEX are coupled with the CAPEX) due to lower maintenance, insurance and tax costs as well as the lost revenue from excess electricity have to be considered. The flow reduction causes an MESP increase of 1.24 % due to less electricity whereas the fixed OPEX savings yield a MESP decrease of 0.23 %. Concluding, it can be stated, that 8.52 % + 1.20 % - 1.24 % + 0.23 % = 8.71 % of the cost savings reported by Lynd et al. are due to the higher yield. [3]

- Residence time 1.5 *d* vs. 5 *d*:

The reduction of the residence time during hydrolysis and fermentation only affect the CAPEX of A 300 as neither the pretreatment nor the post-processing is affected by faster reaction rates. The reduction of the residence time by 70 % yields a size reduction of 70 % for all apparatuses in A 300. Considering the weighted size exponent of 0.856 for A 300, a size reduction of 70 % leads to a reduction of installed costs of 64.3 %, which corresponds to 20.08 MM\$, a TCI reduction of 7.98 % and a MESP reduction of 3.37 %. 0.6 % of fixed OPEX (maintenance, insurance and taxes) are reduced due to the lower CAPEX requirements.

Concluding, it can be stated, that 3.37 % + 0.6 % = 3.97 % of the cost savings reported by Lynd et al. are due to the lower residence time. [3]

- Capital charge rate 16.7 % vs. 13.1 %:

Due to varying equity shares, interests on equity and debts, Lynd et al. calculate with a capital charge rate of 16.7 % whereas the base case assumes 13.1 %. The capital charge rate of Lynd et al. is higher by a factor of 1.2748 ( $= 16.7 \% / 13.1 \%$ ) and affects the capital costs, which account for 42.2 % of the total costs.

Thus, it can be stated that the cost savings reported by Lynd et al. exclude 11.6 % of cost savings due to a lower capital charge rate in the base case [3]

## A.2 Calculations GMO-based CBP

### Adaption of published GMO-based CBP cost data to input parameters of the base case

The published data of GMO-based CBP normalized to the same feedstock and the same process condition as in the base case. The different input parameters are depicted in Tab. A.4.

Table A.4: Differences between the process assumptions of Lynd et al., the base case and this work. Values in brackets denote values of different scenarios published by Lynd et al. [3]

Parameter	Lynd et al. [3]	Base case	This work
Scale [dry <i>ton</i> feedstock/ <i>d</i> ]	4536 (2000)	2000	2000
Ethanol titer [wt.%]	5 (7)	5.4	5.4
Yield [L ethanol/dry <i>ton</i> feedstock]	439.4	329.6	329.6
Residence time [d]	1.5	5	5
Pretreatment	AFEX	Dilute acid catalyzed steam explosion	Steam explosion
Capital charge rate [%]	16.7	13.1	13.1

The single normalization steps are illustrated with a waterfall diagram (Fig. A.1).

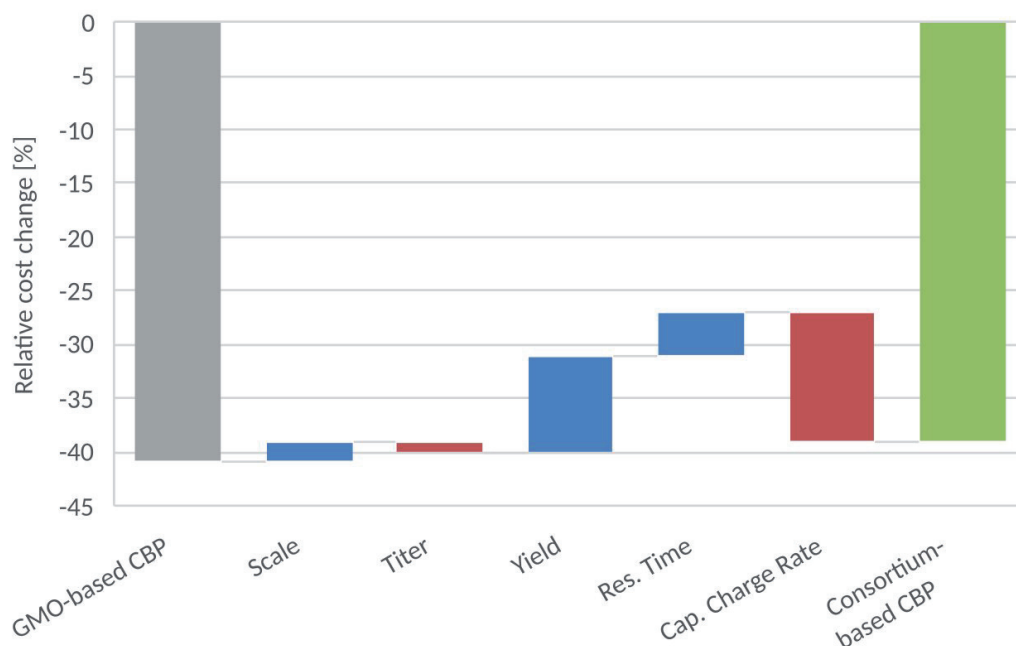


Figure A.1: Waterfall diagram depicting the normalized cost savings through GMO-based CBP published by Lynd et al. [3] The grey bar represents the published cost savings. The red and blue bars represent extra cost savings or reduced cost savings due to adapted titer, yield, residence time and capital charge rate, respectively. The green bar represents the resulting cost saving after applying the adaptations.

Lynd et al. published cost savings of 41 % when GMO-based CBP is applied (grey bar in Fig. A.1). [3] The titer is lower and the capital charge rate is higher than in the base case. Increasing the titer and lowering the capital charge rate to match the base case conditions leads to higher cost savings than published (red bars in Fig. A.1). In contrast, lowering scale as well as yield and increasing the residence time to match base case conditions reduce the published cost savings (blue bars in Fig. A.1). In conclusion, the beneficial and disadvantageous effects almost compensate each other so that the final cost savings of GMO-based CBP (green bar in Fig. A.1) at base case conditions account for 39 % (Supplementary material A.1). The pretreatment was excluded from this calculation, because detailed cost data for the ammonia fiber expansion (AFEX) pretreatment at industrial scale with the conditions assumed by Lynd et al. are not available. However, it seems unlikely, that part of the reported cost savings are realized with the different pretreatment method used given the necessity to use elevated pressures and the use of ammonia. [31]

Furthermore, Lynd et al. report cost savings of 5.5 % when increasing the ethanol titer from 5 wt.% to 7 wt.%. This work obtains cost savings of 3.6 % for the same titer increase

(Supplementary material A.1). 25 % total cost savings are reported by omitting the pretreatment, whereas in the base case 13.4 % of the total costs are allocated to the pretreatment. [3] Thus, levelling the cost savings of 39 % published by Lynd et al. with the ratio 3.6 %/5.5 % or the ratio 13.4 %/25 % in order to have equal impact on the costs by equal technological advance (i.e. applying CBP) yields cost savings of 25.5 % and 21 %, respectively.

### **A.3 Apparatus list of the base and CBP**

Mechanical Equipment List Area										Adjustments due to CBP		Comments regarding adjustments
EQUIPMENT TITLE	NUM REQD	\$	Year of Quote	Scaling Variable	Scaling Exp	Inst Factor	Size Ratio	Scaled Purch Cost	Purch Cost in Proj year	Inst Cost in Proj year	Inst Cost in Proj year (CBP)	
Transfer Conveyor	2	\$5,397,000	2009	Mass flow	0.6	1.7	1.1	\$5,714,628	\$5,752,952	\$9,780,018	\$9,780,018	
High Angle Transfer Conveyor	2	INCLUDED										
Reversing Load-in Conveyor	1	INCLUDED										
Dome Reclaim System	2	\$3,046,000	2009	Mass flow	0.6	1.7	1.1	\$3,225,265	\$3,246,895	\$5,519,721	\$5,519,721	
Reclaim Conveyor	2	INCLUDED										
High Angle Transfer Conveyor	1	INCLUDED										
Elevated Transfer Conveyor	1	INCLUDED										
Process Feed Conveyor	2	\$110,000	2009	Mass flow	0.6	1.7	1.1	\$116,474	\$117,265	\$199,333	\$199,333	
Truck Dumper	2	\$484,000	2009	Mass flow	0.6	1.7	1.1	\$512,465	\$515,922	\$977,067	\$977,067	
Truck Dumper Hopper	2	\$602,000	2009	Mass flow	0.6	1.7	1.1	\$631,544	\$635,109	\$909,685	\$909,685	
Concrete Feedstock Storage Dome	2	\$3,500,000	2009	Mass flow	0.6	1.7	1.1	\$3,705,984	\$3,730,838	\$6,342,424	\$6,342,424	
Belt Scale	2	\$10,790	2009	Mass flow	0.6	1.7	1.1	\$11,425	\$11,502	\$19,553	\$19,553	
Dust Collection System	6	\$279,900	2009	Mass flow	0.6	1.7	1.1	\$296,373	\$298,360	\$507,213	\$507,213	
Area 100 Totals								\$14,114,178	\$14,208,831	\$24,155,013	\$24,155,013	
no changes were applied in A-100												

Mechanical Equipment List Area										Adjustments due to CBP		Comments regarding adjustments
EQUIPMENT TITLE	NUM REQD	\$	Year of Quote	Scaling Variable	Scaling Exp	Inst Factor	Size Ratio	Scaled Purch Cost	Purch Cost in Proj year	Inst Cost in Proj year	Inst Cost in Proj year (CBP)	
In-line Sulfuric Acid Mixer	1	\$6,000	2009	Mass flow	0.5	1	0.28	\$3,202	\$3,223	\$3,223	\$0	
Blowdown Tank Agitator	1	INCLUDED										
Flash Tank Agitator	3	\$90,000	2009	Mass flow	0.5	1.5	1.1	\$94,395	\$95,028	\$142,542	\$142,542	
Oligomer Hold Tank Agitator	3	\$90,000	2009	Mass flow	0.5	1.5	1.1	\$94,641	\$95,276	\$142,914	\$142,914	
Ammonia Addition Tank Agitator	1	\$21,900	2009	Mass flow	0.5	1.5	1.05	\$22,406	\$22,556	\$33,835	\$0	
Ammonia Static Mixer	1	\$5,000	2009	Mass flow	0.5	1	0.96	\$4,902	\$4,935	\$4,935	\$0	
Recalcification Tank Agitator	1	\$0	2009	Mass flow	0.5	1.5	1.05	\$0	\$0	\$0	\$0	
Transfer Conveyor	2	INCLUDED										
Distribution Conveyor	2	INCLUDED										
Overfeed Conveyor	4	INCLUDED										
Pressurized Heating Screw	1	INCLUDED										
Pressurized Pre-heater Discharge	2	INCLUDED										
Pressurized Transport - No. 1	1	INCLUDED										
Pressurized Transport - No. 2	1	INCLUDED										
Pretreatment Water Heater	1	\$92,000	2010	Heat duty	0.7	2.2	1.15	\$101,545	\$97,091	\$213,600	\$213,600	
Waste Vapor Condenser	1	\$34,000	2009	Heat duty	0.7	2.2	3.98	\$89,346	\$89,946	\$197,880	\$197,880	
Doffing Roll Storage Bins	2	INCLUDED										
Pin Drum Feeder	2	INCLUDED										
Plug Screw Feeder	2	INCLUDED										
Prehydrolysis / Vertical Preheater	1	INCLUDED										
Pin Drum Feeder	2	INCLUDED										
Plug Screw Feeder	2	INCLUDED										
Pretreatment Reactor	3	\$19,812,400	2009	Mass flow	0.6	1.5	1	\$19,812,448	\$19,845,315	\$29,917,973	\$37,817,973	
Sulfuric Acid Pump	1	\$8,000	2009	Mass flow	0.8	2.3	0.53	\$4,832	\$4,864	\$11,187	\$0	
Blowdown Tank Discharge Pump	1	\$26,635	2010	Mass flow	0.8	2.3	1.36	\$26,611	\$26,487	\$56,321	\$56,321	
Flash Tank Discharge Pump	1	\$30,000	2009	Mass flow	0.8	2.3	1.36	\$38,391	\$38,649	\$89,892	\$89,892	
Oligomer Hold Tank Discharge	1	\$17,408	2010	Mass flow	0.8	2.3	1	\$17,391	\$16,629	\$38,246	\$38,246	
Hydrolyzate Pump	1	\$22,500	2009	Mass flow	0.8	2.3	1.07	\$23,716	\$23,875	\$54,913	\$0	
Recalcified Hydrolyzate Pump	1	\$0	2009	Mass flow	0.8	2.3	1.07	\$0	\$0	\$0	\$0	
Hydrolyzate Solid-Liquid Separator	1	\$35,000,000	2009	Mass flow	0.7	1.7	0	\$0	\$0	\$0	\$0	
Sulfuric Acid Tank	1	\$5,210	2010	Mass flow	0.7	3	1	\$6,209	\$5,937	\$17,810	\$0	
Blowdown Tank	1	INCLUDED										
Flash Tank	1	\$11,000	2009	Mass flow	0.7	2	1.11	\$549,271	\$551,948	\$1,103,895	\$1,103,895	
Oligomer Conversion Tank	1	\$203,000	2009	Mass flow	0.7	2	1.11	\$219,606	\$219,267	\$438,534	\$438,534	
Ammonia Addition Tank	1	\$238,000	2009	Mass flow	0.7	2	1.05	\$243,670	\$245,304	\$490,609	\$0	
Recalcification Tank	1	\$0	2009	Mass flow	0.7	2	1.05	\$0	\$0	\$0	\$0	
Area 200 Totals								\$21,348,782	\$21,484,330	\$32,957,310	\$40,21731	

Mechanical Equipment List Area										Adjustments due to CBP		Comments regarding adjustments
EQUIPMENT TITLE	NUM REQD	\$	Year of Quote	Scaling Variable	Scaling Exp	Inst Factor	Size Ratio	Scaled Purch Cost	Purch Cost in Proj year	Inst Cost in Proj year	Inst Cost in Proj year (CBP)	
Ethanol Fermentor Agitator	1	\$52,500	2009	Size fermenter	1	1.5	1.2	\$63,400	\$63,425	\$951,337	\$554,947	
Seed Hold Tank Agitator	1	\$31,800	2009	Mass flow	0.5	1.5	1.05	\$32,651	\$32,670	\$49,305	\$49,306	
4th Seed Vessel Agitator	2	\$25,000	2009	Size fermenter	0.5	1.5	1	\$26,000	\$26,174	\$39,262	\$39,263	
5th Seed Vessel Agitator	2	\$43,000	2009	Size fermenter	0.5	1.5	1	\$43,000	\$43,288	\$64,933	\$64,934	
Beer Surge Tank Agitator	2	\$95,300	2009	Mass flow	0.5	1.5	1.06	\$17,265	\$17,027	\$26,105	\$106,105	
Hydrolyzate Mixer	1	\$10,000	2009	Mass flow	0.5	1.7	1.17	\$10,126	\$11,854	\$201,519	\$106,106	
Ethanol Fermentor	12	\$10,126,000	2009	Mass flow/Scale	1	1.5	1	\$10,126,000	\$10,195,921	\$15,293,882	\$9,921,432	
Membrane	7			Size fermenter							\$138,000	
Membrane support construction	7			Size fermenter							\$10,440,000	
1st Seed Fermentor	2	\$75,400	2009	Size fermenter	0.7	1.8	1	\$75,400	\$75,906	\$136,630	\$136,631	
2nd Seed Fermentor	2	\$116,600	2009	Size fermenter	0.7	1.8	1	\$116,600	\$117,382	\$211,288	\$211,289	
3rd Seed Fermentor	2	\$157,600	2009	Size fermenter	0.7	1.8	1	\$157,600	\$158,657	\$285,582	\$285,583	
4th Seed Fermentor	2	\$352,000	2009	Size fermenter	0.7	2	1	\$352,000	\$354,361	\$708,721	\$708,722	
5th Seed Fermentor	2	\$1,180,000	2009	Size fermenter	0.7	2	1	\$1,180,000	\$1,187,913	\$2,375,827	\$2,375,828	

Table A.5: Apparatus list of the base and CBP

Fermentation Cooler	12	\$86,928	2009 Heat duty	1	2.2	1.3	\$87,511	\$102,524	\$192,525
Hydrolyzate Cooler	1	\$85,000	2010 Heat duty	0.7	2.2	1.3	\$97,500	\$214,500	\$214,501
5th Seed Fermentor Coil	1	INCLUDED							
5th Seed Fermentor Cooler	1	INCLUDED							
Fermentation Recirc Transfer Pump	5	\$23,900	2009 Heat duty	0.7	1.8	0	\$0	\$0	\$1
Fermentor Batch Cooler	1	\$47,200	2009 Size fermenter	0.8	2.3	1	\$47,517	\$109,288	\$109,289
Seed Hold Transfer Pump	1	\$9,200	2009 Mass flow	0.8	2.3	0.99	\$8,172	\$18,795	\$18,796
Seed Transfer Pump	2	\$24,300	2009 Mass flow	0.8	2.3	0.99	\$24,095	\$55,698	\$55,699
Beer Transfer Pump	1	\$29,800	2009 Mass flow	0.8	2.3	0.92	\$25,289	\$58,165	\$58,166
Saccharification Transfer Pump	5	\$47,200	2009 Mass flow	0.8	2.3	1.05	\$49,125	\$113,746	\$113,746
Beer Hold Tank	1	\$87,000	2009 Mass flow	0.7	1.8	1.08	\$85,998	\$195,471	\$195,472
Beer Storage Tank	1	\$38,000	2009 Mass flow	0.7	1.8	1.08	\$36,549	\$84,550	\$84,551
Saccharification Tank	8	\$340,000	2009 Mass flow	0.7	2	1.05	\$340,386	\$808,772	\$1,195,772
<b>Area 300 Totals</b>							<b>\$18,484,821</b>	<b>\$31,218,526</b>	<b>\$26,900,520</b>

MECHANICAL EQUIPMENT LIST AREA	NUM REQD	\$	Scaled Installed Year of Quote	Scaling Variable	Scaling Exp	Inst Factor	Size Ratio	Scaled Purch Cost	Purch Cost in Proj year	Inst Cost in Proj year	Adjustments due to CBP Inst Cost in Proj year (CBP)	Comments regarding adjustments
Cellulase Fermentor Agitators	1	\$560,000	2009 Size fermenter	1	1.5	9		\$5,220,000	\$5,255,007	\$7,882,510	\$0	Omitted due to CBP
Cellulase Fermentor Agitators	1	\$3,420	2009 Size fermenter	1	1.5	4		\$13,680	\$13,772	\$20,658	\$0	Omitted due to CBP
Cellulase Fermentor Agitators	1	\$63,000	2009 Size fermenter	1	1.5	4		\$252,000	\$253,690	\$380,535	\$0	Omitted due to CBP
Cellulase Fermentor Agitators	1	\$11,000	2009 Size fermenter	1	1.5	4		\$44,000	\$44,295	\$66,443	\$0	Omitted due to CBP
Media Prep Tank Agitator	1	\$5,500	2009 Mass flow	0.5	1.5	0		\$0	\$0	\$0	\$0	Omitted due to CBP
Cellulase Nutrient Mix Tank Agitator	1	\$29,800	2009 Mass flow	0.5	1.6	1.29		\$5,172	\$5,172	\$8,172	\$0	Omitted due to CBP
Cellulase Fermentor	1	\$405,500	2009 Scale	1	2	1.29		\$3,604,500	\$3,628,673	\$7,257,345	\$0	Omitted due to CBP
1st Cellulase Seed Fermentor	1	\$46,000	2009 Scale	1	1.8	4		\$184,000	\$185,234	\$333,421	\$0	Omitted due to CBP
2nd Cellulase Seed Fermentor	1	\$57,500	2009 Scale	1	1.8	4		\$230,000	\$231,542	\$416,776	\$0	Omitted due to CBP
3rd Cellulase Seed Fermentor	1	\$95,400	2009 Scale	1	1.8	4		\$381,600	\$384,159	\$691,486	\$0	Omitted due to CBP
Cellulase Fermentation Cooler	1	INCLUDED										Omitted due to CBP
Media Prep Tank Cooler	2	\$350,000	2009 Mass flow	0.6	1.6	0.98		\$346,282	\$348,604	\$557,767	\$557,768	Kept for air circulation in A300
Fermentor Air Compressor Package	1	\$7,357	2010 Mass flow	0.8	2.3	1.03		\$7,549	\$7,218	\$16,600	\$0	Omitted due to CBP
Cellulase Transfer Pump	4	\$29,972	2010 Mass flow	0.8	2.3	1.13		\$33,045	\$31,596	\$72,670	\$0	Omitted due to CBP
Cellulase Seed Pump	1	\$7,357	2010 Mass flow	0.8	2.3	0		\$0	\$0	\$0	\$0	Omitted due to CBP
Media Pump	1	\$1,500	2009 Mass flow	0.8	2.3	0.49		\$852	\$858	\$1,974	\$19,741	Kept for nutrient addition in A300
Cellulase Nutrient Transfer Pump	1	\$1,500	2009 Mass flow	0.8	2.3	0.78		\$1,615	\$1,615	\$3,015	\$0	Omitted due to CBP
Cellulase Feed Pump	1	\$1,500	2009 Mass flow	0.8	2.3	1.28		\$1,805	\$1,817	\$4,178	\$0	Omitted due to CBP
SO2 Storage Tank	1	\$0						\$0	\$0	\$0	\$0	Omitted due to CBP
Media Prep Tank	1	\$176,000	2009 Mass flow	0.7	1.8	0		\$0	\$0	\$0	\$0	Omitted due to CBP
Cellulase Nutrient Mix Tank	1	\$9,000	2010 Mass flow	0.7	3	1.27		\$92,000	\$8,605	\$25,815	\$0	Omitted due to CBP
Cellulase Hold Tank	1	\$248,070	2009 Mass flow	0.7	1.8	1.27		\$292,589	\$294,551	\$530,192	\$0	Omitted due to CBP
<b>Area 400 Totals</b>								<b>\$10,861,197</b>	<b>\$10,730,186</b>	<b>\$18,323,460</b>	<b>\$559,741</b>	

MECHANICAL EQUIPMENT LIST AREA	NUM REQD	\$	Scaled Installed Year of Quote	Scaling Variable	Scaling Exp	Inst Factor	Size Ratio	Scaled Purch Cost	Purch Cost in Proj year	Inst Cost in Proj year	Adjustments due to CBP Inst Cost in Proj year (CBP)	Comments regarding adjustments
Filtrate Tank Agitator	1	\$26,000	2009 Mass flow	0.5	1.5	1.05		\$26,869	\$26,848	\$40,272	\$0	Replaced by NREL 2002 water recovery
Lignin Wet Cake Conveyor	1	\$70,000	2009 Mass flow	0.8	1.7	1.28		\$85,062	\$85,053	\$145,910	\$0	Replaced by NREL 2002 water recovery
Lignin Wet Cake Screw	1	\$3,407,000	2009 Mass flow	0.8	2.4	0.98		\$3,327,914	\$3,350,232	\$8,040,557	\$8,040,558	Replaced by NREL 2002 water recovery
Recirculation Column	1	INCLUDED										
Beer Column Reboiler	1	INCLUDED										
Recirculation Column Reboiler	1	INCLUDED										
Beer Column Condenser	1	INCLUDED										
Recirculation Column Condenser	1	INCLUDED										
Beer Column Feed Interchanger	1	\$487,000	2010 Mass flow	0.6	2.8	1		\$486,746	\$465,399	\$1,303,116	\$1,303,117	
Molecular Sieve Package (6 pieces)	1	\$2,601,000	2009 Mass flow	0.6	1.8	0.96		\$2,540,057	\$2,557,091	\$4,602,764	\$4,602,765	
Pressure Filler Pressing Compr	1	\$75,200	2009 Mass flow	0.6	1.6	1		\$75,245	\$75,245	\$121,199	\$121,200	
Pressure Filler Drying Compr	2	\$405,000	2009 Mass flow	0.6	1.6	0.99		\$402,453	\$405,152	\$648,243	\$648,244	
Beer Column Bottoms Recirc Pump	1	INCLUDED										
Beer Column Reflux Pump	1	INCLUDED										
Recirculation Column Reflux Pump	1	INCLUDED										
Recirculation Column Reflux Pump	1	INCLUDED										
Beer Column Stillage Pump	1	INCLUDED										
Scrubber Bottoms Pump	1	\$6,300	2009 Mass flow	0.8	2.3	1.11		\$6,843	\$6,889	\$15,844	\$15,845	
Filtrate Tank Discharge Pump	1	\$13,040	2010 Mass flow	0.8	2.3	1.15		\$14,567	\$13,928	\$32,035	\$32,036	
Feed Pump	1	\$18,173	2010 Mass flow	0.8	2.3	1.15		\$20,301	\$19,411	\$44,845	\$44,845	Replaced by NREL 2002 water recovery
Manifold Flush Pump	1	\$17,057	2010 Mass flow	0.8	2.3	1.15		\$19,054	\$18,219	\$41,903	\$41,904	
Cloth Wash Pump	1	\$29,154	2010 Mass flow	0.8	2.3	1.15		\$32,568	\$31,140	\$71,621	\$71,622	
Filtrate Discharge Pump	1	\$13,040	2010 Mass flow	0.8	2.3	1.15		\$14,567	\$13,928	\$32,035	\$32,036	
Pressure Filler	2	\$3,294,700	2010 Mass flow	0.8	1.7	1.15		\$3,180,519	\$3,519,098	\$5,982,467	\$0	
Beer Column Reflux Drum	1	INCLUDED										
Recirculation Column Reflux Drum	1	INCLUDED										
Wet Scrubber	1	\$15,000	2009 Mass flow	0.6	2.4	0.98		\$919,121	\$211,530	\$607,873	\$607,874	Replaced by NREL 2002 water recovery
Recirculation Column Reflux Tank	1	\$103,000	2010 Mass flow	0.7	2	1.15		\$108,520	\$108,520	\$207,416	\$207,416	
Feed Tank	1	\$174,800	2010 Mass flow	0.7	2	1.15		\$182,595	\$184,139	\$368,278	\$0	Replaced by NREL 2002 water recovery
Recycled Water Tank	1	\$1,520	2010 Mass flow	0.7	3	1.15		\$1,675	\$1,601	\$4,804	\$4,805	

Table A.5: Apparatus list of the base and CBP (continued)



Pressing Air Compressor Receiver	1	\$8,000	2010	Mass flow	0.7	3.1	1.15	\$8,814	\$8,427	\$26,126	\$26,126	\$26,126	
Drying Air Compressor Receiver	2	\$17,000	2010	Mass flow	0.7	3.1	1.15	\$18,730	\$17,908	\$55,516	\$55,516	\$55,517	NREL 2002 water recovery possible due to lower salt concentration
Water recycling system from 2002 NREL report												\$18,900,000	
1st Effect Evaporation	2	INCLUDED	2009	Area	0.68		2.1						
2nd Effect Evaporation	2	INCLUDED	2009	Area	0.68		2.1						
3rd Effect Evaporation	2	INCLUDED	2009	Area	0.68		2.1						
1st Effect Pump	2	INCLUDED	2002	Mass flow	0.79		2.8						
2nd Effect Pump	2	INCLUDED	2002	Mass flow	0.79		2.8						
3rd Effect Pump	2	INCLUDED	2002	Mass flow	0.79		2.8						
Evaporator Condensate Pump	1	INCLUDED	2002	Mass flow	0.79		2.8						
Evaporator Condenser	1	INCLUDED	2002	Mass flow	0.79		2.8						
Evaporator Condensate Drum	1	INCLUDED	2002	Heat Duty	0.68		2.1						
Recycled Water Tank	1	INCLUDED	2002	Mass flow	0.93		2.1						
Pneumagress Filler	4	INCLUDED	2002	Mass flow	0.745		1.4						
Lignin Wet Cake Screw	1	INCLUDED	2002	Mass flow	0.6		1.04						
Area 500 Totals							1.4	\$11,302,300	\$11,145,318	\$22,343,314		\$34,343,314	
Mechanical Equipment List Area													
EQUIPMENT TITLE	NUM REQD	\$	Scaled Installed Year of Quote	Scaling Variable	Scaling Exp	Inst Factor	Size Ratio	Scaled Purch Cost	Purch Cost in Proj year	Inst Cost in Proj year	Adjustments due to CBP Inst Cost in Proj year (CBP)	Comments regarding adjustments	
Bioass Blower	4	INCLUDED	2010	Mass flow	0.6	1	1.05	\$1,986,627	\$1,899,498	\$1,899,498			
Anaerobic Digester Blower	8	\$1,933,750	2010	Mass flow	0.6	1	1.05	\$25,684	\$24,557	\$24,557			
Anaerobic Sludge Screw	1	\$25,000	2010	Mass flow	0.6	1	1.05	\$86,156	\$82,378	\$82,378			
Anaerobic Digester Feed Cooler	1	\$83,843	2010	Mass flow	0.6	1	1.05	\$33,856	\$32,371	\$32,371			
Bioass Emergency Flare	4	\$32,955	2010	Mass flow	0.6	1	1.05	\$9,135	\$9,135	\$9,135			
Polymer Addition System	1	\$9,300	2010	Mass flow	0.6	1	1.05	\$22,396	\$22,396	\$22,396			
Caulic Feed System	3	\$22,800	2010	Mass flow	0.6	1	1.05	\$3,905,034	\$3,733,767	\$3,733,767			
Evaporator System	4	\$3,801,095	2010	Mass flow	0.6	1	1.05	\$237,818	\$227,388	\$227,388			
Anaerobic Reactor Feed Pump	4	\$231,488	2010	Mass flow	0.6	1	1.05	\$95,851	\$91,647	\$91,647			
Anaerobic Reactor Recirc Pump	4	\$231,488	2010	Mass flow	0.6	1	1.05	\$95,851	\$91,647	\$91,647			
Anaerobic Reactor Feed Pump	4	\$231,488	2010	Mass flow	0.6	1	1.05	\$95,851	\$91,647	\$91,647			
Anaerobic Reactor Recirc Pump	4	\$231,488	2010	Mass flow	0.6	1	1.05	\$95,851	\$91,647	\$91,647			
Return Activated Sludge Pump	6	\$84,000	2010	Mass flow	0.6	1	1.05	\$86,207	\$82,512	\$82,512			
Reverse Osmosis Feed Pump	1	INCLUDED	2010	Mass flow	0.6	1	1.05	\$182,148	\$174,160	\$174,160			
Centrifuge Feed Pump	2	\$61,200	2010	Mass flow	0.6	1	1.05	\$62,873	\$60,116	\$60,116			
Centrifuge Pump	2	\$70,800	2010	Mass flow	0.6	1	1.05	\$72,736	\$69,546	\$69,546			
Treated Water Pump	1	INCLUDED	2010	Mass flow	0.6	1	1.05	\$5,392,274	\$5,155,780	\$5,155,780			
Membrane Bioreactor	3	\$5,248,750	2010	Mass flow	0.6	1	1.05	\$2,271,437	\$2,171,816	\$2,171,816			
Reverse Osmosis System	1	\$2,210,979	2010	Mass flow	0.6	1	1.05	\$6,671,062	\$6,378,482	\$6,378,482			
Centrifuge	4	\$6,495,500	2010	Mass flow	0.6	1	1.05	\$27,738,302	\$26,521,754	\$26,521,754			
Anaerobic Basin	4	\$27,000,000	2010	Mass flow	0.6	1	1.05	\$2,652,175	\$2,652,175	\$2,652,175			
Aeration Digester	3	\$2,700,000	2010	Mass flow	0.6	1	1.05	\$51,654,984	\$49,389,478	\$49,389,478			
Sludge Holding Tank	1	INCLUDED	2010	Mass flow	0.6	1	1.05	\$2,652,175	\$2,652,175	\$2,652,175			
Area 600 Totals								\$51,654,984	\$49,389,478	\$49,389,478		\$14,389,478	Only 13.7% of the original size due to adapted water recycling
Mechanical Equipment List Area													
EQUIPMENT TITLE	NUM REQD	\$	Scaled Installed Year of Quote	Scaling Variable	Scaling Exp	Inst Factor	Size Ratio	Scaled Purch Cost	Purch Cost in Proj year	Inst Cost in Proj year	Adjustments due to CBP Inst Cost in Proj year (CBP)	Comments regarding adjustments	
Denatrant In-line Mixer	1	\$3,850	2009	Mass flow	0.5	1	0.96	\$3,776	\$3,801	\$3,801			
CSL Storage Tank Agitator	1	\$21,200	2009	Mass flow	0.5	1.5	0.95	\$20,660	\$20,798	\$20,798			
DAP Make-up Tank Agitator	1	\$9,800	2009	Mass flow	0.5	1.5	0.97	\$9,152	\$9,214	\$9,214			
DAP Bulk Bag Unloader	1	\$30,000	2009	Mass flow	0.6	1.7	0.87	\$27,636	\$27,622	\$27,622			
Ethanol Product Pump	2	\$9,200	2009	Mass flow	0.8	3.1	0.96	\$8,916	\$8,975	\$8,975			
Sulfuric Acid Pump	1	\$15,000	2009	Mass flow	0.8	3.1	0.96	\$14,633	\$14,633	\$14,633			
Flare Gas Pump	1	\$3,000	2009	Mass flow	0.8	3.1	0.96	\$2,936	\$2,979	\$2,979			
Gasoline Pump	1	\$3,000	2009	Mass flow	0.8	3.1	0.95	\$2,879	\$2,888	\$2,888			
CSL Pump	1	\$3,000	2009	Mass flow	0.8	3.1	0.95	\$2,879	\$2,888	\$2,888			
DAP Pump	1	\$3,000	2009	Mass flow	0.8	3.1	0.97	\$2,699	\$2,707	\$2,707			
Ethanol Product Storage Tank	2	\$1,340,000	2009	Mass flow	0.7	1.7	0.96	\$1,303,683	\$1,312,426	\$1,312,426			
Sulfuric Acid Storage Tank	1	\$96,000	2010	Mass flow	0.7	1.5	0.96	\$95,987	\$91,777	\$91,777			
Firewater Storage Tank	1	\$803,000	2009	Mass flow	0.7	1.7	0.96	\$781,201	\$786,440	\$1,336,948			
Ammonia Storage Tank	2	\$196,000	2010	Mass flow	0.7	2	0.96	\$195,389	\$186,820	\$373,639			
Gasoline Storage Tank	1	\$200,000	2009	Mass flow	0.7	1.7	0.98	\$197,602	\$196,927	\$338,176			
CSL Storage Tank	1	\$70,000	2009	Mass flow	0.7	2.6	0.95	\$67,516	\$67,969	\$176,720			
DAP Bulk Bag Holder	1	INCLUDED	2009	Mass flow	0.7	1.8	0.72	\$81,192	\$81,737	\$147,126			
DAP Make-up Tank	1	\$102,000	2009	Mass flow	0.7	1.8	0.72	\$81,192	\$81,737	\$147,126			
Area 700 Totals								\$2,825,265	\$2,827,686	\$4,955,787		\$4,955,787	
Mechanical Equipment List Area													
EQUIPMENT TITLE	NUM REQD	\$	Scaled Installed Year of Quote	Scaling Variable	Scaling Exp	Inst Factor	Size Ratio	Scaled Purch Cost	Purch Cost in Proj year	Inst Cost in Proj year	Adjustments due to CBP Inst Cost in Proj year (CBP)	Comments regarding adjustments	
Burner Combustion Air Preheater	1	INCLUDED	2009	Heat duty	0.7	2.2	0.93	\$38,856	\$39,117	\$86,057			
BFW Preheater	1	\$41,000	2009	Heat duty	0.7	2.2	0.93	\$38,856	\$39,117	\$86,057			
Pretreatment/BFW heat recovery	1	INCLUDED	2010	Mass flow	0.6	1.8	0.98	\$28,269,041	\$27,029,216	\$48,652,599			
Air Intake Fan	1	\$28,550,000	2010	Mass flow	0.6	1.8	0.98	\$28,269,041	\$27,029,216	\$48,652,599			
Boiler	1												

Table A.5: Apparatus list of the base and CBP (continued)

Omitted since no FGD is needed											
Combustion Gas Baghouse		INCLUDED									
Turbine/Generator	1	\$9,500,000	2010 Heat duty	0.6	1.8	0.98	\$9,381,215	\$8,969,773		\$16,145,591	
Hot Process Water Softener System	1	\$78,000	2010 Mass flow	0.6	1.8	1	\$77,798	\$74,386		\$133,894	
Amine Addition Pkg	1	\$40,000	2010 Mass flow	0	1.8	1	\$40,000	\$38,246		\$68,842	
Ammonia Addition Pkg	1	INCLUDED									
Phosphate Addition Pkg	1	INCLUDED									
Condensate Pump	2	INCLUDED									
Turbine Condensate Pump	2	INCLUDED									
Deaerator Feed Pump	2	INCLUDED									
BFW Pump	5	INCLUDED									
Blowdown Pump	2	INCLUDED									
Aniline Transfer Pump	1	INCLUDED									
Condensate Collection Tank	1	INCLUDED									
Condensate Surge Drum	1	INCLUDED									
Deaerator	1	\$395,000	2010 Mass flow	0.6	3	1	\$394,209	\$290,867		\$872,600	
Blowdown Flash Drum	1	INCLUDED									
Aniline Drum	1	INCLUDED									
Area 700 Totals									\$38,111,118	\$36,441,604	\$120,379,573
Base case: \$1,240,000 because the FGD is not necessary anymore due to lower salt concentrations, but all remaining apparatus need to be scaled up by a factor of 2.8 since more solids are sent to combustion											

Mechanical Equipment List Area	NUM REQD	\$	Scaled Installed Year of Onset	Scaling Variable	Scaling Exp	Inst Factor	Size Ratio	Scaled Purch Cost	Purch Cost in Proj year	Inst Cost in Proj year	Adjustments due to CBP	Comments regarding adjustments
Cooling Tower System	1	\$1,375,000	2010 Mass flow	0.6	1.5	1.19	1.19	\$1,524,650	\$1,457,782	\$2,186,673	\$1,066,673	Cooling duty increases with larger combustor unit
Plant Air Compressor	1	\$26,000	2010 Mass flow	0.6	1.6	1.6	0.95	\$1,234,354	\$6,772	\$42,835	\$42,835	
Chilled Water Package	1	\$1,275,750	2010 Heat duty	0.6	1.8	1.8	2.3	\$694,222	\$698,878	\$1,888,348	\$1,888,348	
CIP System	1	\$421,000	2009 Mass flow	0.6	1.8	1.8	2.3	\$302,961	\$289,678	\$1,257,980	\$1,257,980	
Cooling Water Pump	3	\$283,671	2010 Mass flow	0.8	3.1	1.09	1.09	\$6,565	\$6,277	\$897,989	\$897,989	
Make-up Water Pump	1	\$6,864	2010 Mass flow	0.8	3.1	1.01	1.01	\$15,399	\$14,724	\$19,459	\$19,459	
Process Water Circulating Pump	1	\$15,292	2010 Mass flow	0.8	3.1	1.01	1.01	\$15,399	\$14,724	\$45,643	\$45,643	
Instrument Air Dryer	1	\$15,000	2009 Mass flow	0.6	1.8	1.8	1.8	\$15,000	\$15,101	\$27,181	\$27,181	
Plant Air Receiver	1	\$16,000	2009 Mass flow	0.6	3.1	1.19	1.19	\$277,245	\$16,107	\$49,933	\$49,933	
Process Water Tank No. 1	1	\$250,000	2009 Mass flow	0.7	1.7	1.7	1.16	\$277,245	\$279,104	\$74,476	\$74,476	
Area 900 Totals									\$3,984,635	6,890,517	\$8,770,517	

Table A.5: Apparatus list of the base and CBP (continued)

## APPENDIX B

### Supplementary material for chapter 4: Set-up and validation of a rigorous, spatially resolved model of the kinetics and mass transfer limitations of consortium-based consolidated bioprocessing for ethanol production

#### B.1 Overview of the validation of the model

Table B.1: Overview of the experimentally obtained validation parameters and the model results

Substance	Run	Reactor	Experiment	Model
Ethanol	1	1	1.45 g/L	1.49 g/L
	1	2	3.26 g/L	3.30 g/L
	2	1	0.70 g/L	0.68 g/L
	2	2	1.82 g/L	1.79 g/L
	3	1	0.69 g/L	0.71 g/L
	3	2	2.63 g/L	2.75 g/L
Cellobiose	1	1	0 g/L	0.12 g/L
	1	2	0.18 g/L	0.20 g/L
	2	1	0.37 g/L	0.33 g/L
	2	2	0.51 g/L	0.55 g/L
	3	1	0.11 g/L	0.13 g/L
	3	2	0.24 g/L	0.19 g/L
Glucose	1	1	0 g/L	0.15 g/L
	1	2	0 g/L	0.23 g/L
	2	1	0 g/L	0.09 g/L
	2	2	0 g/L	0.14 g/L
	3	1	0 g/L	0.16 g/L
	3	2	0 g/L	0.19 g/L
Endoglucanase	1	1	5.01 IU/mL	5.76 IU/mL
	1	2	9.47 IU/mL	9.06 IU/mL
	2	1	8.33 IU/mL	7.65 IU/mL
	2	2	11.09 IU/mL	10.65 IU/mL
	3	1	4.50 IU/mL	4.59 IU/mL
	3	2	8.98 IU/mL	9.32 IU/mL
Cellobiohydrolase	1	1	0.08 IU/mL	0.10 IU/mL
	1	2	0.14 IU/mL	0.14 IU/mL
	2	1	0.12 IU/mL	0.10 IU/mL
	2	2	0.18 IU/mL	0.20 IU/mL
	3	1	0.06 IU/mL	0.07 IU/mL
	3	2	0.11 IU/mL	0.11 IU/mL
$\beta$ -Glucosidase	1	1	0.01 IU/mL	0.01 IU/mL
	1	2	0.02 IU/mL	0.02 IU/mL
	2	1	0.02 IU/mL	0.02 IU/mL
	2	2	0.02 IU/mL	0.02 IU/mL
	3	1	0.00 IU/mL	0.02 IU/mL
	3	2	0.02 IU/mL	0.02 IU/mL

## B.2 Matlab programming files

```

1 %% Design and set parameters
2 % Enter all design and set parameters in the corresponding blocks below
3 %%
4 % *Temperature for temperature dependence of the following parameters*
5 param.T_m_C=28; % temperature within membrane [ C ]
6 % needs to be between 0 C and 70 C !
7 param.T_m_K = param.T_m_C+273.15; % Temperature within membrane [K]
8 param.T_v_C = 28; % bulk temperature [ C ]
9 param.T_v=param.T_v_C+273.15; % bulk temperature [K]
10 param.titer_EtOH = 0.003; % starting value for ethanol titer [kg/m^3]
11 %%
12 % *Reactor geometry*
13 geo.d_t_i = 1.58e-03; % tube membrane inner diameter [m]
14 geo.r_t_i = 0.5*geo.d_t_i; % tube membrane inner radius [m]
15 geo.d_t_o = 3.18e-03; % tube membrane outer diameter [m]
16 geo.r_t_o = 0.5*geo.d_t_o; % tube membrane outer radius [m]
17 geo.A_m = geo.r_t_o-geo.r_t_i;
18 geo.l_t = 5.6; % tube membrane length [m]
19 geo.A_m_cross = pi*(geo.r_t_i^2); % Cross-sectional area [m^2]
20 % of the tube membrane
21 geo.A_t_i = pi*geo.d_t_i*geo.l_t; % tube membrane inner wall area [m^2]
22 geo.A_t_o = pi*geo.d_t_o*geo.l_t; % tube membrane outer wall area [m^2]
23 geo.h_wind = geo.d_t_o; % height of membrane winding [m]
24 geo.d_wind = 0.07; % diameter of membrane winding [m]
25 geo.d_curv = geo.d_wind*(1+((geo.h_wind/(pi*geo.d_wind))^2));
26 % curvature diameter according to VDI heat atlas chapter G3
27 geo.d_v = 0.2; % vessel diameter [m]
28 geo.d_stirrer = 0.15; % stirrer diameter [m]
29 geo.V_v = 0.0027; % reactor working volume [m^3]
30 geo.h_fill = geo.V_v/(0.25*pi*(geo.d_v^2)); % reactor filling height [m]
31 %%
32 % *Chemicals*
33 chem.R_gas = 8.31446261815324; % Universal gas constant [J/(mol*K)]
34 chem.M_ox = 0.031998; % Molar mass oxygen [kg/mol]
35 chem.M_air = 0.02896; % Molar mass air [kg/mol]
36 chem.M_m_n = 0.0280134; % Molar mass nitrogen [kg/mol]
37 chem.M_EtOH = 0.04607; % Molar mass ethanol [kg/mol]
38 chem.M_G = 0.180156; % Molar mass glucose [kg/mol]
39 chem.M_CO2 = 0.04401; %Molar mass CO2 [kg/mol]
40 chem.D_m_ox = 3.4*(10^(-9));
41 % Diffusivity of oxygen in PDMS [m^2/s] (@35 C) Merkel et al. 2000
42 chem.D_m_n = 3.4*(10^(-9));
43 % Diffusivity of nitrogen in PDMS [m^2/s] (@35 C) Merkel et al. 2000

```

```

44 chem.D_m_CO2 = 2.2*(10^(-9));
45 % Diffusivity of CO2 in PDMS [m^2/s] (@35 C) Merkel et al. 2000
46 chem.D_m_EtOH = 1.338*(10^(-6))*exp((-27760)/(chem.R_gas*param.T_m_K));
47 % Diffusivity of ethanol in PDMS membrane [m^2/s] Xia et al. 2015
48 chem.sol_m_ox = ((10^(-5))/1.013)*0.18*((chem.M_ox*(10^5))/...
49     (chem.R_gas*273.15)); % Solubility oxygen in PDMS membrane
50 %[kg/(m^3*Pa)] (@35 C) Merkel et al. 2000
51 chem.sol_m_n = ((10^(-5))/1.013)*0.09*((chem.M_m_n*(10^5))/...
52     (chem.R_gas*273.15)); % Solubility nitrogen in PDMS membrane
53 %[kg/(m^3*Pa)] (@35 C) Merkel et al. 2000
54 chem.sol_m_CO2 = ((10^(-5))/1.013)*1.29*((chem.M_CO2*(10^5))/...
55     (chem.R_gas*273.15)); % Solubility CO2 in PDMS membrane
56 %[kg/(m^3*Pa)] (@35 C) Merkel et al. 2000
57 chem.sol_m_EtOH = chem.M_EtOH*2.67*(10^(-11))/chem.D_m_EtOH;
58 % Solubility ethanol in PDMS membrane [kg/(m^3*Pa)] Lue et al. 2015
59 chem.H_EtOH = 1.9*chem.M_EtOH; %Henry coefficient for ethanol in water
60 %[kg/(m^3*Pa)] Sander et al. 2015
61 chem.D_w_ox = 2e-9;
62 % Oxygen diffusivity in water [m^2/s] (Stewart et al. 2003)
63 chem.D_w_n = 1.88e-9;
64 chem.D_w_CO2 = 1.92e-9;
65 chem.D_w_G = 0.698e-9;
66 % glucose diffusivity in water [m^2/s] (Suhaimi et al. 2015)
67 chem.D_w_Cb = 0.59e-9;
68 % Cellobiose diffusivity in water [m^2/s]
69 % (Traving et al. 2015; Hardy et al. 1993)
70 chem.D_w_E = 0.05e-9;
71 % Enzyme diffusivity in water [m^2/s] (Traving et al. 2015)
72 % 0.14e-9 (Kim et al. 1996)
73 chem.D_w_EtOH = (1e-9)*(1/((5-0)*(30-25)))*...
74     [5-param.titer_EtOH param.titer_EtOH-0]*[1.24 1.41;0.91 1.13]*...
75     [30-param.T_v_C;param.T_v_C-25];
76 % 2D interpolation for EtOH diffusivity [m^2/s]
77 % (data from Pratt et al. 1974)
78 chem.P_ox = 0.12; %Partition coefficient for oxygen between PDMS and H2O
79 %PhD thesis Michael Hanspeter Studer ETHZ
80 %%
81 % *Membrane*
82 param.n_ox_m=0.21; % oxygen fraction in gas within membrane [-]
83 param.dVdt_m_Lmin = 0.368; % volumetric flow within membrane [L/min]
84 param.dVdt_m = param.dVdt_m_Lmin/(1000*60); %
85 % volumetric flow within membrane [m^3/s]
86 param.visc_m = 1e-7*((0.0010714286)*(param.T_m_C^2))+...
87     (0.8895238095*param.T_m_C)+134.9916666667);
88 % Kinematic viscosity [m^2/s] of the fluid within the membrane
89 % approximated with fitted air data from VDI heat atlas (chapter D2.2)
90 param.visc_ox = (0.0011170100*(param.T_m_C^2))+...

```

```

91      (0.9077425018*param.T_m_C)+135.7002517027;
92 % Kinematic viscosity [m^2/s] of oxygen
93 % (fitted data from VDI heat atlas (chapter D2.5)
94 param.Re_m = (geo.d_t_i*param.dVdt_m/geo.A_m_cross)/param.visc_m;
95 % Reynolds number [-] within membrane
96 param.Re_m_crit=2300*(1+(8.6*((geo.d_t_i/geo.d_curv)^0.45)));
97 % critical Reynolds number
98 % in a helical coil according to VDI heat atlas chapter G3
99 param.Pr_m = ((5e-7)*param.T_m_C^2)-(param.T_m_C*0.000155)+0.711;
100 % Prandtl number [-] of the fluid within the membrane
101 % approximated with fitted air data from VDI heat atlas (chapter D2.2)
102 param.Sc_ox = param.visc_ox/chem.D_w_ox;
103 % Schmidt number of oxygen in the inner membrane phase
104 %%
105 % _The following parameters are calculated based on the entries_
106
107
108 rho_m=1.149; % starting value for density of air
109 %at given tmeperature [m^2/s] (VDI heat atlas D 2.2)
110
111 H_cp_ox=1.2e-5; % Henry constant for oxygen [mol/(m^3/Pa)] R. Sander 2015
112 %%
113 % *Biofilm*
114 param.mu_max_tr = 2.3/(24*3600); % max. growth rate T. reesei [1/s]
115 param.K_ox_tr = 0.001; % half-saturation constant
116 % of T. reesei for oxygen [kg/m^3]
117 param.K_G_tr = 4.0/(24*3600); % half-saturation constant
118 % of T. reesei for glucose [kg/m^3]
119 param.K_tr_ps = 2.2/(24*3600); % rate constant [1/s] for T. reesei
120 % conversion of primary mycelia to secondary mycelia
121 param.K_tr_dec = 0.09/(24*3600); % rate constant [1/s] of T. reesei
122 % secondary mycelia decay
123 param.K_tr_synth = (1/32)*19.8*0.45/(24*3600);
124 % enzyme synthesis rate constant
125 % [g enzymes/(g secondary mycelium * s) ]
126 param.K_E_dec = 0.0092/(24*3600); % enzyme decay rate [1/s]
127 %all above mentioned data is from Velkovska et al. 1997
128 param.Y_ox_tr = 0.0323/chem.M_ox; % kg biomass/kg O2
129 param.Y_G_tr = 0.44; % kg biomass/kg glucose
130 param.M_ox_tr = chem.M_ox*(1000/3600)*0.85e-3; % kg O2/(kg biomass*s)
131 param.M_G_tr = chem.M_G*(1000/3600)*0.14e-3; % kg glucose/(kg biomass*s)
132 param.mean_rho_tr = 50.1; % mean fungal biofilm density [kg/m^3]
133 % Ercan et al. 2015 & Lecauly et al. 2009
134 param.mean_rho_Y = 0.15*1100; % mean yeast density [kg/m^3]
135 % Ercan et al. 2015; Baldwin et al. 1984; Bryan et al. 2010
136 param.K_y_dec = 6.48e-5*5*24/3600; %decay rate S. cerevisiae
137 % Fan et al. 2015

```

```

138 param.K_DEGR_EtOH = 0.0306/(5*3600); %ethanol degradation constant of
139 %T. reesei if no substrate is present (own experiments)
140 param.K_degr_EtOH = 0.01183/(5*3600); %ethanol degradation constant of
141 %T. reesei if another substrate is present (own experiments)
142
143 %
144 %%
145 % *Reactor bulk & hydrolysis*
146 param.T_v_C = 28; % bulk temperature [ C ]
147 param.T_v=param.T_v_C+273.15; % bulk temperature [K]
148 param.tau = 5*24*3600; %Residence time [s]
149 param.sol_load_feed = 17.5; % solid loading of the feed stream [kg/m^3]
150 param.feed_frac_s = 1; % cellulose fraction of feed solid content [-]
151 param.c_C_in = param.sol_load_feed*param.feed_frac_s;
152 %cellulose feed stream
153 param.sol_load = 17.5; % solid loading of the bulk [kg/m^3]
154 param.c_EtOH_max = param.sol_load_feed*param.feed_frac_s*...
155     (360/324)*(2*chem.M_EtOH/chem.M_G);
156 % stoichiometric conversion of cellulose to glucose to ethanol
157 param.N_stirrer = 50/60; % Rotational speed stirrer [1/s]
158 param.visc_v = 0.03539435*exp(27.0464373*0.001*param.sol_load);
159 %fitted curve for data from Pimenova et al. 2003
160 param.Re_v = param.N_stirrer*(geo.d_stirrer^2)/param.visc_v;%(0.8335e-6);
161 % Reynolds number for stirred vessels
162 param.Sc_v_E=chem.D_w_E/param.visc_v;
163 param.c_ox_b = 1e-6; %oxygen concentration in the bulk [kg/m^3]
164
165 param.frac_E_endo_Tr = 0.9899; % fraction of endoglucanase activity
166 %of total enzyme activity [-] (Xiros et al, 2017)
167 param.frac_E_exo_Tr = 0.0085; % fraction of exoglucanase (=CBH) activity
168 %of total enzyme activity [-] (Xiros et al, 2017)
169 param.frac_E_betaG_Tr = 0.0016; % fraction of beta-glucosidase activity
170 %of total enzyme activity [-] (Xiros et al, 2017)
171 param.frac_exo_sites_C_in = 0.0033; %fraction of active sites for
172 %exoglucanase of Avicel [-] (Zhang et al. 2004)
173 param.k_endo = 0.110/3600;%hydrolysis rate constant of endoglucanase [1/s]
174 % van Zyl et al. 2010
175 param.k_exo = 0.07/3600; %hydrolysis rate constant of exoglucanase [1/s]
176 % van Zyl et al. 2010
177 param.K_C_Cb = 5.85; % Inhibition constant of cellobiose on
178 %cellulose conversion [kg/m^3]
179 % van Zyl et al. 2010
180 param.K_C_EtOH = 50.35; % Inhibition constant of ethanol on
181 %cellulose conversion [kg/m^3]
182 % van Zyl et al. 2010
183 param.sigma_endo = 0.084; % endoglucanase capacity on Avicel [-]
184 % van Zyl et al. 2010

```

```

185 param.sigma_exo = 0.084; % exoglucanase capacity on Avicel [-]
186 % van Zyl et al. 2010
187 param.k_fc = 1.8366/3600; % enzyme adsorption constant
188 % on Avicel [m^3/(kg*s)]
189 % van Zyl et al. 2010
190 param.K_endo = 1.84; % equilibrium constant for endoglucanase [m^3/kg]
191 % van Zyl et al. 2010
192 param.K_exo = 55; % equilibrium constant for exoglucanase [m^3/kg]
193 % van Zyl et al. 2010
194 param.K_Cb = 0.02/3600; % rate constant of cellobiose hydrolysis [1/s]
195 % van Zyl et al. 2010
196 param.K_m = 10.56; %Michael constant of beta-G for cellobiose [kg/m^3]
197 % van Zyl et al. 2010
198 param.K_Cb_G = 0.62; %inhibition constant of glucose on cellobiose
199 %conversion [kg/m^3]
200 % van Zyl et al. 2010
201 param.Y_X_Y_G = 0.12; %yield coefficient of yeast biomass from glucose [-]
202 % van Zyl et al. 2010
203 param.mu_max_Y = 0.4/3600; %maximum anaerobic growth rate S. cerevisiae
204 % [1/s]
205 % van Zyl et al. 2010
206 param.K_G = 0.476; % Half-saturation glucose [kg/m^3]
207 % van Zyl et al. 2010
208 param.K_X_EtOH = 87; %inhibition constant of ethanol on yeast growth
209 % [kg/m^3]
210 % van Zyl et al. 2010
211 param.Y_EtOH_G = 0.419; %yield coefficient of ethanol from glucose [-]
212 % van Zyl et al. 2010
213
214 %
215 %%
216 % _The following parameters are calculated based on the entries_
217 % rho_w_v=((T_v_C^3)*0.000033603)+((T_v_C^2)*(- 0.0349738131))+...
218 % (T_v_C*11.6350223258)-253.6172523896;
219 % % density of pure liquid water in vessel between 0 C and 50 C [kg/m^3]
220 % visc_w_v=(10^-6)*(((T_v_C^3)*(-0.0000079042))+...
221 % ((T_v_C^2)*(0.0075055404))+(T_v_C*(-2.3873231021))+254.9613281728);
222 % %kinematic viscosity of liquid water between 0 C and 50 C [m^2/s]
223
224 %%
225 % % *Discretization grid*
226 geo.n=25; % grid resolution for each layer
227 % (membrane, fungal biofilm and yeast biofilm)
228 %including inner membrane and bulk boundary condition
229 geo.M=50; %grid resolution in Z-direction
230 geo.N=3*geo.n+4; % total grid resolution in R-direction including inner
231 % membrane and bulk boundary condition as well as the bulk itself

```



```

232 geo.dz=geo.l_t/geo.M; %axial length of discretized element [m]
233 geo.dr=(geo.r_t_o-geo.r_t_i)/geo.n;
234 % radial length of discretized element [m]
235 geo.r = zeros (1,geo.M*geo.N); %radius at position i in the grid [m]
236 for i = 1 : geo.M
237     geo.r(i)=0;
238 end
239 for i = geo.M+1 : geo.N*geo.M
240     geo.r(i)=geo.r_t_i+(geo.dr*floor((i-(geo.M+1))/geo.M));
241 end
242 geo.dV = zeros (1,geo.M*geo.N); %volume at position i in the grid [m^3]
243 for i = 1 : geo.M
244     geo.dV(i)= pi*(geo.r_t_i^2)*geo.dz;
245 end
246 for i = geo.M+1 : (geo.N-1)*geo.M
247     geo.dV(i)= pi*geo.dz*((geo.r(i+geo.M)^2)-(geo.r(i)^2));
248 end
249 for i = (geo.M*(geo.N-1))+1 : geo.N*geo.M
250     geo.dV(i) = (geo.V_v-sum(geo.dV(1:geo.N*(geo.M-1)))/geo.M;
251 end
252 %%
253 % % *Temporary values*
254 geo.r_f = geo.r_t_o+(geo.n*geo.dr);
255 %starting value for fungal biofilm thickness

```

```

1 errvec = zeros(geo.M*geo.N,1);
2 maxerrvec = zeros(geo.M*geo.N,1);
3 error = zeros(8*geo.N*geo.M,1);
4 param.last_iter = zeros(geo.M*geo.N,1);
5 solvec=solvec_0;
6 hydrosolvec_0=[0.99*param.c_C_in , 0 , 10 , -1.4e-5 ,
7     6 , 6 , 6 , 6, 0 , 6 , 0 , 6, 0.5 , 7 , 1e-5 , 3 , 3];
8 param.max_rel_error_EtOH=1;
9 itercount=0;
10 param.max_rel_error_ox=1;
11 %maximum relative error oxygen concentration [%]
12 while itercount<1500 || param.max_rel_error_EtOH>0.5 ||
13     param.max_rel_error_ox>0.5%
14 %% Concentration profiles oxygen, fungal biomass & enzymes
15     % oxygen inner membrane phase
16 for i= 1: geo.M
17     solvec(i) = (chem.M_ox*param.n_ox_m*
18         (1/(chem.R_gas*param.T_m_K))*param.p_m(i));
19     %(chem.sol_m_ox*param.p_m(i)*param.n_ox_m);
20 end
21 %oxygen at membrane wall (neglecting convective boundary layer)

```

```

22 for i = geo.M+1
23     solvec(i) = (chem.sol_m_ox*param.p_m(i-geo.M)*param.n_ox_m);
24 end
25 for i = geo.M+2 : 2*geo.M
26     solvec(i) = solvec(i-1)+(2*pi*chem.D_m_ox*geo.dz*(solvec(i-1)-
27     solvec(i+geo.M-1))/(param.dVdt_m*log(geo.r_t_i/(geo.r_t_i+geo.dr))));
28 end
29 %oxygen in membrane
30 for i = (2*geo.M)+1 : (1+geo.n)*geo.M
31     n = floor((i-1)/geo.M)-1;
32     solvec(i) = sqrt(((solvec(i-(n*geo.M))*log(geo.r_t_o/geo.r(i)))+
33     (solvec(i+((geo.n-n)*geo.M))*log(geo.r(i)/geo.r_t_i)))/
34     log(geo.r_t_i/geo.r_t_o))^2);
35 end
36 for i = ((1+geo.n)*geo.M)+1 : (2+geo.n)*geo.M
37     solvec(i) = (1/((chem.D_w_ox*chem.P_ox/log(geo.r_t_o/geo.r_f))+
38     (chem.D_m_ox/log(geo.r_t_i/geo.r_t_o))))*((solvec(i-(geo.n*geo.M))*
39     chem.D_m_ox/log(geo.r_t_i/geo.r_t_o)+(solvec(i+(geo.n*geo.M))*
40     chem.D_w_ox/log(geo.r_t_o/geo.r_f)));
41 end
42 %oxygen in fungal biofilm
43 for i = ((2+geo.n)*geo.M)+1 : ((3+geo.n)*geo.M)
44     solvec(i) = 0.12*solvec(i-geo.M);
45 end
46 for i = ((3+geo.n)*geo.M)+1 : ((2+(2*geo.n))*geo.M)
47     if (i-1)/(geo.M)~=floor((i-1)/(geo.M)) && i/(geo.M)~=floor(i/(geo.M))
48     solvec(i) = sqrt(((1/((-4*pi*chem.D_w_ox/(geo.dr^2))+
49     (-4*pi*chem.D_w_ox/(geo.dz^2))+(0)))*((solvec(i+1)*
50     (2*pi*chem.D_w_ox/(geo.dz^2)))+(solvec(i-1)*(2*pi*chem.D_w_ox/
51     (geo.dz^2)))+(solvec(i+geo.M)*((2*pi*chem.D_w_ox/(geo.dr^2))+
52     (2*pi*chem.D_w_ox/(2*geo.dr*geo.r(i)))))+(solvec(i-geo.M)*
53     ((2*pi*chem.D_w_ox/(geo.dr^2))-(2*pi*chem.D_w_ox/
54     (2*geo.dr*geo.r(i)))))+((-param.mu_max_tr/param.Y_ox_tr)*
55     min((solvec(i+(5*geo.N*geo.M))/(param.K_G+solvec(i+(5*geo.N*geo.M)))),
56     (solvec(i)/(param.K_ox_tr+solvec(i)))*(param.K_tr_dec/
57     ((param.mu_max_tr*min((solvec(i+(5*geo.N*geo.M))/(param.K_G+
58     solvec(i+(5*geo.N*geo.M))), (solvec(i)/(param.K_ox_tr+solvec(i)))))+
59     param.K_tr_dec))*solvec(i+(geo.N*geo.M)))+(-param.M_ox_tr*
60     solvec(i+(geo.M*geo.N))))))^2);
61     elseif (i-1)/(geo.M)==floor((i-1)/(geo.M))
62     solvec(i) = sqrt(((1/((-4*pi*chem.D_w_ox/(geo.dr^2))+
63     (2*pi*chem.D_w_ox/(geo.dz^2))+(0)))*((solvec(i+1)*(-4*pi*chem.D_w_ox/
64     (geo.dz^2)))+(solvec(i+2)*(2*pi*chem.D_w_ox/(geo.dz^2)))+
65     (solvec(i+geo.M)*((2*pi*chem.D_w_ox/(geo.dr^2))+(2*pi*chem.D_w_ox/
66     (2*geo.dr*geo.r(i)))))+(solvec(i-geo.M)*((2*pi*chem.D_w_ox/(geo.dr^2))
67     -(2*pi*chem.D_w_ox/(2*geo.dr*geo.r(i)))))+((-param.mu_max_tr/
68     param.Y_ox_tr)*min((solvec(i+(5*geo.N*geo.M))/(param.K_G+

```

```

69     solvec(i+(5*geo.N*geo.M))), (solvec(i)/(param.K_ox_tr+solvec(i)))) *
70     (param.K_tr_dec/((param.mu_max_tr*min((solvec(i+(5*geo.N*geo.M)) /
71     (param.K_G+solvec(i+(5*geo.N*geo.M))), (solvec(i)/(param.K_ox_tr+
72     solvec(i))))+param.K_tr_dec))*solvec(i+(geo.N*geo.M)))+
73     (-param.M_ox_tr*solvec(i+(geo.M*geo.N))))^2);
74     elseif i/(geo.M)==floor(i/(geo.M))
75     solvec(i) = sqrt(((1/((-4*pi*chem.D_w_ox/(geo.dr^2))+
76     (2*pi*chem.D_w_ox/(geo.dz^2))+0)))*((solvec(i-1)*(-4*pi*chem.D_w_ox/
77     (geo.dz^2)))+(solvec(i-2)*(2*pi*chem.D_w_ox/(geo.dz^2)))+
78     (solvec(i+geo.M)*(2*pi*chem.D_w_ox/(geo.dr^2)))+(2*pi*chem.D_w_ox/
79     (2*geo.dr*geo.r(i)))))+(solvec(i-geo.M)*((2*pi*chem.D_w_ox/(geo.dr^2))
80     -(2*pi*chem.D_w_ox/(2*geo.dr*geo.r(i))))))+((-param.mu_max_tr/
81     param.Y_ox_tr)*min((solvec(i+(5*geo.N*geo.M))/(param.K_G+
82     solvec(i+(5*geo.N*geo.M))), (solvec(i)/(param.K_ox_tr+solvec(i))))*
83     (param.K_tr_dec/((param.mu_max_tr*min((solvec(i+(5*geo.N*geo.M)) /
84     (param.K_G+solvec(i+(5*geo.N*geo.M))), (solvec(i)/(param.K_ox_tr+
85     solvec(i))))+param.K_tr_dec))*solvec(i+(geo.N*geo.M)))+
86     (-param.M_ox_tr*solvec(i+(geo.M*geo.N))))^2);
87     end
88 end
89 %oxygen in yeast biofilm
90 for i = ((2+(2*geo.n))*geo.M)+1 : ((2+(3*geo.n))*geo.M)
91     solvec(i) = param.c_ox_b;
92 end
93 %oxygen at biofilm boundary layer
94 for i = ((2+(3*geo.n))*geo.M)+1 : ((3+(3*geo.n))*geo.M)
95     solvec(i) = param.c_ox_b;
96 end
97 %oxygen within bulk
98 for i = ((3+(3*geo.n))*geo.M)+1
99     solvec(i) = param.c_ox_b;
100 end
101 for i = ((3+(3*geo.n))*geo.M)+2 : geo.N*geo.M
102     solvec(i)=solvec(i-1);
103 end
104
105
106 %Fungal biomass
107 %average growth rate
108 ox_lim=zeros(geo.n*geo.M,1);
109 for i = ((2+geo.n)*geo.M)+1 : ((2+(2*geo.n))*geo.M)
110     ox_lim(i-((2+geo.n)*geo.M)) = solvec(i)/(param.K_ox_tr+solvec(i));
111 end
112 param.avg_ox_lim=mean(ox_lim);
113 %fungal biomass inner membrane phase, membrane boundary layer & membrane
114 for i = (geo.N*geo.M)+1 : ((geo.N*geo.M)+(2+geo.n)*geo.M)
115     solvec(i)=0;

```

```

116 end
117 %fungal biomass in fungal/yeast biofilm
118 for i = ((geo.N*geo.M)+(2+geo.n)*geo.M)+1 :
119     ((geo.N*geo.M)+((2+(2*geo.n))*geo.M))
120     if solvec(i-(geo.M*geo.N)) ≤ param.c_ox_b
121         solvec(i)=0;
122     else
123         solvec(i)= ((param.mean_rho_tr*min((1), (solvec(i-(geo.M*geo.N)) /
124             (param.K_ox_tr+solvec(i-(geo.M*geo.N)))))) / param.avg_ox_lim);
125 %         (min((1), (mean(solvec(((2+geo.n)*geo.M)+1) : ((2+(2*geo.n))*geo.M)))
126 %         / (param.K_ox_tr+mean(solvec(((2+geo.n)*geo.M)+1) :
127 %         ((2+(2*geo.n))*geo.M))))));
128     end
129 end
130 %fungal biomass in fungal/yeast biofilm, biofilm boundary layer and bulk
131 for i = ((geo.N*geo.M)+((2+(2*geo.n))*geo.M))+1 : (2*geo.N*geo.M)
132     if solvec(i-(geo.M*geo.N)) ≤ param.c_ox_b
133         solvec(i)=0;
134     else
135         solvec(i)= ((param.mean_rho_tr*min((1), (solvec(i-(geo.M*geo.N)) /
136             (param.K_ox_tr+solvec(i-(geo.M*geo.N)))))) / param.avg_ox_lim);
137 %         (min((1), (mean(solvec(((2+geo.n)*geo.M)+1) : ((2+(2*geo.n))*geo.M)))
138 %         / (param.K_ox_tr+mean(solvec(((2+geo.n)*geo.M)+1) :
139 %         ((2+(2*geo.n))*geo.M))))));
140     end
141 end
142 %secondary mycelia in the system
143 for i = (2*geo.N*geo.M)+1 : (3*geo.N*geo.M)
144     solvec(i) = solvec(i-(geo.M*geo.N))*param.mu_max_tr*
145         (solvec(i-(2*geo.M*geo.N)) / (param.K_ox_tr+solvec(i-(2*geo.M*geo.N)))) /
146         ((param.mu_max_tr*(solvec(i-(2*geo.M*geo.N)) / (param.K_ox_tr+
147             solvec(i-(2*geo.M*geo.N)))))+param.K_tr_dec);
148 end
149 %enzyme concentration in the inner membrane phase & membrane
150 for i = (3*geo.N*geo.M)+1 : (3*geo.N*geo.M)+((2+geo.n)*geo.M)
151     solvec(i)=0;
152 end
153 %enzyme concentration in the fungal/yeast biofilm
154 for i = (3*geo.N*geo.M)+((2+geo.n)*geo.M)+1
155     solvec(i) = (1/((chem.D_w_E/(geo.dz^2))+(2*pi*chem.D_w_E*geo.dz/
156         log(geo.r(i-(3*geo.N*geo.M))/geo.r(geo.M+i-(3*geo.N*geo.M)))+
157         param.K_E_dec)))*((chem.D_w_E*solvec(i+1)/(geo.dz^2))+
158         (2*pi*chem.D_w_E*geo.dz*solvec(i+geo.M)/log(geo.r(i-(3*geo.N*geo.M))/
159         geo.r(geo.M+i-(3*geo.N*geo.M)))+(param.K_tr_synth*
160         solvec(i-(geo.N*geo.M))));
161 end
162 for i = (3*geo.N*geo.M)+((2+geo.n)*geo.M)+2 :

```

```

163     ((3*geo.N*geo.M)+(3+geo.n)*geo.M))-1
164     solvec(i) = (1/((2*chem.D_w_E/(geo.dz^2))+
165     (2*pi*chem.D_w_E*geo.dz/log(geo.r(i-(3*geo.N*geo.M)))/
166     geo.r(geo.M+i-(3*geo.N*geo.M)))+param.K_E_dec)))*(chem.D_w_E*
167     (solvec(i-1)+solvec(i+1))/(geo.dz^2))+(2*pi*chem.D_w_E*geo.dz*
168     solvec(i+geo.M)/log(geo.r(i-(3*geo.N*geo.M)))/
169     geo.r(geo.M+i-(3*geo.N*geo.M)))+(param.K_tr_synth*
170     solvec(i-(geo.N*geo.M))));
171 end
172 for i = ((3*geo.N*geo.M)+(3+geo.n)*geo.M)
173     solvec(i) = (1/((chem.D_w_E/(geo.dz^2))+(2*pi*chem.D_w_E*geo.dz/
174     log(geo.r(i-(3*geo.N*geo.M)))/geo.r(geo.M+i-(3*geo.N*geo.M)))+
175     param.K_E_dec)))*(chem.D_w_E*solvec(i-1)/(geo.dz^2))+
176     (2*pi*chem.D_w_E*geo.dz*solvec(i+geo.M)/log(geo.r(i-(3*geo.N*geo.M)))/
177     geo.r(geo.M+i-(3*geo.N*geo.M)))+(param.K_tr_synth*
178     solvec(i-(geo.N*geo.M))));
179 end
180 for i = (3*geo.N*geo.M)+(3+geo.n)*geo.M+1 :
181     ((3*geo.N*geo.M)+(2+(3*geo.n))*geo.M)
182     if solvec(i-(3*geo.M*geo.N))>param.c_ox_b
183         if (i-1)/(geo.M)~=floor((i-1)/(geo.M)) &&
184             i/(geo.M)~=floor(i/(geo.M))
185             solvec(i) = sqrt(((1/((-4*pi*chem.D_w_E/(geo.dr^2))+
186             (-4*pi*chem.D_w_E/(geo.dz^2))+(-param.K_E_dec)))*((solvec(i+1)*
187             (2*pi*chem.D_w_E/(geo.dz^2)))+(solvec(i-1)*(2*pi*chem.D_w_E/
188             (geo.dz^2)))+(solvec(i+geo.M)*((2*pi*chem.D_w_E/(geo.dr^2))+
189             (2*pi*chem.D_w_E/(2*geo.dr*geo.r(i-(3*geo.N*geo.M))))))+
190             (solvec(i-geo.M)*((2*pi*chem.D_w_E/(geo.dr^2))-(2*pi*chem.D_w_E/
191             (2*geo.dr*geo.r(i-(3*geo.N*geo.M)))))))+(param.K_tr_synth*
192             solvec(i-(geo.N*geo.M))))))^2);
193         elseif (i-1)/(geo.M)==floor((i-1)/(geo.M))
194             solvec(i) = sqrt(((1/((-4*pi*chem.D_w_E/(geo.dr^2))+
195             (2*pi*chem.D_w_E/(geo.dz^2))+(-param.K_E_dec)))*((solvec(i+1)*
196             (-4*pi*chem.D_w_E/(geo.dz^2)))+(solvec(i+2)*(2*pi*chem.D_w_E/
197             (geo.dz^2)))+(solvec(i+geo.M)*((2*pi*chem.D_w_E/(geo.dr^2))+
198             (2*pi*chem.D_w_E/(2*geo.dr*geo.r(i-(3*geo.N*geo.M))))))+
199             (solvec(i-geo.M)*((2*pi*chem.D_w_E/(geo.dr^2))-(2*pi*chem.D_w_E/
200             (2*geo.dr*geo.r(i-(3*geo.N*geo.M)))))))+(param.K_tr_synth*
201             solvec(i-(geo.N*geo.M))))))^2);
202         elseif i/(geo.M)==floor(i/(geo.M))
203             solvec(i) = sqrt(((1/((-4*pi*chem.D_w_E/(geo.dr^2))+
204             (2*pi*chem.D_w_E/(geo.dz^2))+(-param.K_E_dec)))*((solvec(i-1)*
205             (-4*pi*chem.D_w_E/(geo.dz^2)))+(solvec(i-2)*(2*pi*chem.D_w_E/
206             (geo.dz^2)))+(solvec(i+geo.M)*((2*pi*chem.D_w_E/(geo.dr^2))+
207             (2*pi*chem.D_w_E/(2*geo.dr*geo.r(i-(3*geo.M*geo.N))))))+
208             (solvec(i-geo.M)*((2*pi*chem.D_w_E/(geo.dr^2))-(2*pi*chem.D_w_E/
209             (2*geo.dr*geo.r(i-(3*geo.N*geo.M)))))))+(param.K_tr_synth*

```

```

210         solvec(i-(geo.N*geo.M)))))) ^2);
211     end
212 elseif solvec(i-(3*geo.M*geo.N)) ≤ param.c_ox_b
213     if (i-1)/(geo.M) ≠ floor((i-1)/(geo.M)) &&
214         i/(geo.M) ≠ floor(i/(geo.M))
215         solvec(i) = sqrt(((1/((-4*pi*chem.D_w_E/(geo.dr^2)) +
216             (-4*pi*chem.D_w_E/(geo.dz^2)) + (-param.K_E_dec)) * (((solvec(i+1)*
217             (2*pi*chem.D_w_E/(geo.dz^2)) + (solvec(i-1)*(2*pi*chem.D_w_E/
218             (geo.dz^2)) + (solvec(i+geo.M)*(2*pi*chem.D_w_E/(geo.dr^2)) +
219             (2*pi*chem.D_w_E/(2*geo.dr*geo.r(i-(3*geo.N*geo.M)))))) +
220             (solvec(i-geo.M)*(2*pi*chem.D_w_E/(geo.dr^2)) - (2*pi*chem.D_w_E/
221             (2*geo.dr*geo.r(i-(3*geo.N*geo.M))))))))) ^2);
222     elseif (i-1)/(geo.M) == floor((i-1)/(geo.M))
223         solvec(i) = sqrt(((1/((-4*pi*chem.D_w_E/(geo.dr^2)) +
224             (2*pi*chem.D_w_E/(geo.dz^2)) + (-param.K_E_dec)) * (((solvec(i+1)*
225             (-4*pi*chem.D_w_E/(geo.dz^2)) + (solvec(i+2)*(2*pi*chem.D_w_E/
226             (geo.dz^2)) + (solvec(i+geo.M)*(2*pi*chem.D_w_E/(geo.dr^2)) +
227             (2*pi*chem.D_w_E/(2*geo.dr*geo.r(i-(3*geo.N*geo.M)))))) +
228             (solvec(i-geo.M)*(2*pi*chem.D_w_E/(geo.dr^2)) - (2*pi*chem.D_w_E/
229             (2*geo.dr*geo.r(i-(3*geo.N*geo.M))))))))) ^2);
230     elseif i/(geo.M) == floor(i/(geo.M))
231         solvec(i) = sqrt(((1/((-4*pi*chem.D_w_E/(geo.dr^2)) +
232             (2*pi*chem.D_w_E/(geo.dz^2)) + (-param.K_E_dec)) * (((solvec(i-1)*
233             (-4*pi*chem.D_w_E/(geo.dz^2)) + (solvec(i-2)*(2*pi*chem.D_w_E/
234             (geo.dz^2)) + (solvec(i+geo.M)*(2*pi*chem.D_w_E/(geo.dr^2)) +
235             (2*pi*chem.D_w_E/(2*geo.dr*geo.r(i-(3*geo.M*geo.N)))))) +
236             (solvec(i-geo.M)*(2*pi*chem.D_w_E/(geo.dr^2)) - (2*pi*chem.D_w_E/
237             (2*geo.dr*geo.r(i-(3*geo.N*geo.M))))))))) ^2);
238     end
239 end
240 end
241 %enzyme concentration in biofilm boundary layer
242 for i = ((3*geo.N*geo.M) + ((2+(3*geo.n))*geo.M)) + 1 :
243     ((3*geo.N*geo.M) + ((3+(3*geo.n))*geo.M))
244     %no mass transfer limiting convective boundary layer is assumed
245     % solvec(i) = ((chem.D_w_E*solvec(i-geo.M)/log(geo.r(i-(3*geo.N*geo.M))
246     %/(geo.r(i-(3*geo.N*geo.M))-geo.dr)) - (param.k_conv_E_v*geo.r(i-(3*geo.N*geo.M))*
247     %solvec(i+geo.M)))/(chem.D_w_E/log(geo.r(i-(3*geo.N*geo.M))/(geo.r
248     % (i-(3*geo.N*geo.M))-geo.dr)) - (param.k_conv_E_v*geo.r(i-(3*geo.N*geo.M))));
249
250 end
251 %enzyme concentration in the bulk
252 for i = ((3*geo.N*geo.M) + ((3+(3*geo.n))*geo.M)) + 1
253     solvec(i) = sqrt(((1/((param.K_E_dec + (1/param.tau))*geo.M*
254     geo.dV(i-(3*geo.N*geo.M)))) * ((param.K_tr_synth*
255     sum(solvec((2*geo.N*geo.M)+1):(3*geo.N*geo.M)).*(geo.dV.'))) -
256     (param.K_E_dec*sum(solvec((3*geo.N*geo.M)+1):(3*geo.N*geo.M) +

```

```

257     ((2+(3*geo.n))*geo.M)).*((geo.dV(1:((2+(3*geo.n))*geo.M)).'))))^2);
258 %     solvec(i) = (param.k_conv_E_v*2*pi*geo.dz*geo.r(i-(3*geo.N*geo.M))*
259 % solvec(i-geo.M))/((geo.V_v/geo.M)*(param.K_E_dec+(1/param.tau)))+
260 % (param.k_conv_E_v*2*pi*geo.dz*geo.r(i-(3*geo.N*geo.M))));
261 end
262 for i = ((3*geo.N*geo.M)+((3+(3*geo.n))*geo.M))+2 : (4*geo.N*geo.M)
263     solvec(i) = solvec(i-1);
264 end
265
266 %% Hydrolysis network
267 param.c_E_b = solvec(4*geo.N*geo.M);
268 param.c_E_b_endo = param.frac_E_endo_Tr*param.c_E_b;
269 param.c_E_b_exo = param.frac_E_exo_Tr*param.c_E_b;
270 param.c_E_b_BG = param.frac_E_betaG_Tr*param.c_E_b;
271 if itercount==0
272     hydrosolvec_0(9) = 0.5*param.c_E_b_endo;
273     hydrosolvec_0(11) = 0.5*param.c_E_b_exo;
274 end
275
276 % call fsolve to solve the hydrolysis reaction network
277 opt = optimset('LargeScale','off','Jacobian','off','TolX',1.0e-15,
278 'TolFun',1.0e-15);%'TolX',1.0e-15,'TolFun',1.0e-15);
279 [hydrosolvec, fval, exitflag] =
280 fsolve(@fsolve_bulk_reactions,hydrosolvec_0,opt,param);
281 hydrosolvec_0=hydrosolvec;
282
283 param.c_C_in_endo = abs(hydrosolvec(1));
284 param.c_C_b = abs(hydrosolvec(3));
285 param.r_C = hydrosolvec(4);
286 param.c_EC_endo = abs(hydrosolvec(5));
287 param.c_EC_exo = abs(hydrosolvec(6));
288 param.c_C_endo = abs(hydrosolvec(7));
289 param.c_C_exo = abs(hydrosolvec(8));
290 param.c_E_f_endo = abs(hydrosolvec(9));
291 param.c_C_f_endo = abs(hydrosolvec(10));
292 param.c_E_f_exo = abs(hydrosolvec(11));
293 param.c_C_f_exo = abs(hydrosolvec(12));
294 param.c_Cb_b = abs(hydrosolvec(13));
295 param.c_G_b = abs(hydrosolvec(14));
296 param.r_y_b = hydrosolvec(15);
297 param.c_X_y_b = abs(hydrosolvec(16));
298 param.c_EtOH_b = abs(hydrosolvec(17));
299
300 %% Concentration profiles cellobiose, glucose, yeast & ethanol
301
302 %cellobiose concentration in the inner membrane phase & membrane
303 for i = (4*geo.N*geo.M)+1 : (4*geo.N*geo.M)+((2+geo.n)*geo.M)

```

```

304     solvec(i)=0;
305 end
306 %cellobiose concentration in the fungal/yeast biofilm
307 for i = (4*geo.N*geo.M)+((2+geo.n)*geo.M)+1
308     solvec(i) = (1/((chem.D_w_Cb/(geo.dz^2)))+(2*pi*chem.D_w_Cb*geo.dz/
309     log(geo.r(i-(4*geo.N*geo.M)))/geo.r(geo.M+i-(4*geo.N*geo.M)))+
310     (param.K_Cb*param.frac_E_betaG_Tr*solvec(i-(geo.N*geo.M)))/
311     ((param.K_m*(1+(solvec(i+(geo.N*geo.M))))+(solvec(i)))))))*
312     ((chem.D_w_Cb*solvec(i+1)/(geo.dz^2)))+(2*pi*chem.D_w_Cb*geo.dz*
313     solvec(i+geo.M)/log(geo.r(i-(4*geo.N*geo.M)))/
314     geo.r(geo.M+i-(4*geo.N*geo.M)))));
315 end
316 for i = (4*geo.N*geo.M)+((2+geo.n)*geo.M)+2 :
317     ((4*geo.N*geo.M)+((3+geo.n)*geo.M))-1
318     solvec(i) = (1/((2*chem.D_w_Cb/(geo.dz^2))+
319     (2*pi*chem.D_w_Cb*geo.dz/log(geo.r(i-(4*geo.N*geo.M)))/
320     geo.r(geo.M+i-(4*geo.N*geo.M)))+(param.K_Cb*param.frac_E_betaG_Tr*
321     solvec(i-(geo.N*geo.M)))/((param.K_m*(1+(solvec(i+(geo.N*geo.M))))+
322     (solvec(i)))))))*((chem.D_w_Cb*(solvec(i-1)+solvec(i+1))/(geo.dz^2))+
323     (2*pi*chem.D_w_Cb*geo.dz*solvec(i+geo.M)/log(geo.r(i-(4*geo.N*geo.M)))/
324     geo.r(geo.M+i-(4*geo.N*geo.M)))));
325 end
326 for i = ((4*geo.N*geo.M)+((3+geo.n)*geo.M))
327     solvec(i) = (1/((chem.D_w_Cb/(geo.dz^2)))+(2*pi*chem.D_w_Cb*geo.dz/
328     log(geo.r(i-(4*geo.N*geo.M)))/geo.r(geo.M+i-(4*geo.N*geo.M)))+
329     (param.K_Cb*param.frac_E_betaG_Tr*solvec(i-(geo.N*geo.M)))/((param.K_m*
330     (1+(solvec(i+(geo.N*geo.M))))+(solvec(i)))))))*((chem.D_w_Cb*
331     solvec(i-1)/(geo.dz^2)))+(2*pi*chem.D_w_Cb*geo.dz*solvec(i+geo.M)/
332     log(geo.r(i-(4*geo.N*geo.M)))/geo.r(geo.M+i-(4*geo.N*geo.M)))));
333 end
334 for i = (4*geo.N*geo.M)+((3+geo.n)*geo.M)+1 :
335     ((4*geo.N*geo.M)+((2+(3*geo.n))*geo.M))
336         if (i-1)/(geo.M)~=floor((i-1)/(geo.M)) &&
337             i/(geo.M)~=floor(i/(geo.M))
338             solvec(i) = sqrt(((1/((-4*pi*chem.D_w_Cb/(geo.dr^2))+
339             (-4*pi*chem.D_w_Cb/(geo.dz^2))+(-(param.K_Cb*
340             param.frac_E_betaG_Tr*solvec(i-(geo.N*geo.M)))/
341             ((param.K_m*(1+(solvec(i+(geo.N*geo.M))))+(solvec(i)))))))*
342             (((solvec(i+1)*(2*pi*chem.D_w_Cb/(geo.dz^2)))+(solvec(i-1)*
343             (2*pi*chem.D_w_Cb/(geo.dz^2)))+(solvec(i+geo.M)*((2*pi*chem.D_w_Cb/
344             (geo.dr^2)))+(2*pi*chem.D_w_E/(2*geo.dr*geo.r(i-(4*geo.N*geo.M))))))
345             +(solvec(i-geo.M)*((2*pi*chem.D_w_Cb/(geo.dr^2))-(2*pi*chem.D_w_E/
346             (2*geo.dr*geo.r(i-(4*geo.N*geo.M))))))))^2);
347             elseif (i-1)/(geo.M)==floor((i-1)/(geo.M))
348             solvec(i) = sqrt(((1/((-4*pi*chem.D_w_Cb/(geo.dr^2))+
349             (2*pi*chem.D_w_Cb/(geo.dz^2))+(-(param.K_Cb*param.frac_E_betaG_Tr*
350             solvec(i-(geo.N*geo.M)))/((param.K_m*(1+(solvec(i+(geo.N*geo.M))))+

```



```

351         (solvec(i)))))))*(((solvec(i+1)*(-4*pi*chem.D_w_Cb/(geo.dz^2)))+
352         (solvec(i+2)*(2*pi*chem.D_w_Cb/(geo.dz^2)))+(solvec(i+geo.M)*
353         ((2*pi*chem.D_w_Cb/(geo.dr^2))+(2*pi*chem.D_w_E/(2*geo.dr*
354         geo.r(i-(4*geo.N*geo.M)))))+(solvec(i-geo.M)*((2*pi*chem.D_w_Cb/
355         (geo.dr^2))-(2*pi*chem.D_w_E/(2*geo.dr*
356         geo.r(i-(4*geo.N*geo.M))))))))^2);
357     elseif i/(geo.M)==floor(i/(geo.M))
358         solvec(i) = sqrt(((1/((-4*pi*chem.D_w_Cb/(geo.dr^2)))+
359         (2*pi*chem.D_w_Cb/(geo.dz^2)))+(-(param.K_Cb*param.frac_E_betaG_Tr*
360         solvec(i-(geo.N*geo.M))/(param.K_m*(1+(solvec(i+(geo.N*geo.M)))))+
361         (solvec(i))))))*(((solvec(i-1)*(-4*pi*chem.D_w_Cb/(geo.dz^2)))+
362         (solvec(i-2)*(2*pi*chem.D_w_Cb/(geo.dz^2)))+(solvec(i+geo.M)*
363         ((2*pi*chem.D_w_Cb/(geo.dr^2))+(2*pi*chem.D_w_E/(2*geo.dr*
364         geo.r(i-(4*geo.M*geo.N)))))+(solvec(i-geo.M)*((2*pi*chem.D_w_Cb/
365         (geo.dr^2))-(2*pi*chem.D_w_E/(2*geo.dr*
366         geo.r(i-(4*geo.N*geo.M))))))))^2);
367     end
368 end
369 %cellobiose concentration in biofilm boundary layer
370 for i = ((4*geo.N*geo.M)+((2+(3*geo.n))*geo.M))+1 :
371     ((4*geo.N*geo.M)+((3+(3*geo.n))*geo.M))
372     solvec(i)=solvec(i+geo.M);
373     %no mass transfer limiting convective boundary layer is assumed
374
375 end
376 %cellobiose concentration in the bulk
377 for i = ((4*geo.N*geo.M)+((3+(3*geo.n))*geo.M))+1 : (5*geo.N*geo.M)
378     solvec(i)= param.c_Cb_b;
379 end
380
381 %glucose concentration in the inner membrane phase & membrane
382 for i = (5*geo.N*geo.M)+1 : (5*geo.N*geo.M)+((2+geo.n)*geo.M)
383     solvec(i)=0;
384 end
385 %glucose concentration in the fungal/yeast biofilm
386 for i = (5*geo.N*geo.M)+((2+geo.n)*geo.M)+1
387     solvec(i) = (1/((chem.D_w_E/(geo.dz^2))+(2*pi*chem.D_w_G*geo.dz/
388     log(geo.r(i-(5*geo.N*geo.M))/geo.r(geo.M+i-(5*geo.N*geo.M)))+(
389     param.K_E_dec)))*((chem.D_w_G*solvec(i+1)/(geo.dz^2))+(2*pi*chem.D_w_G*
390     geo.dz*solvec(i+geo.M)/log(geo.r(i-(5*geo.N*geo.M))/
391     ,geo.r(geo.M+i-(5*geo.N*geo.M)))+(param.K_tr_synth*
392     solvec(i-(geo.N*geo.M)))));
393 end
394 for i = (5*geo.N*geo.M)+((2+geo.n)*geo.M)+2 :
395     ((5*geo.N*geo.M)+((3+geo.n)*geo.M))-1
396     solvec(i) = (1/((2*chem.D_w_E/(geo.dz^2))+(2*pi*chem.D_w_G*geo.dz/
397     log(geo.r(i-(5*geo.N*geo.M))/geo.r(geo.M+i-(5*geo.N*geo.M)))+(

```

```

398     param.K_E_dec)) * ((chem.D_w_G*(solvec(i-1)+solvec(i+1))/(geo.dz^2)) +
399     (2*pi*chem.D_w_G*geo.dz*solvec(i+geo.M))/log(geo.r(i-(5*geo.N*geo.M)))/
400     geo.r(geo.M+i-(5*geo.N*geo.M)))) + (param.K_tr_synth*
401     solvec(i-(geo.N*geo.M))));
402 end
403 for i = ((5*geo.N*geo.M)+((3+geo.n)*geo.M))
404     solvec(i) = (1/((chem.D_w_E/(geo.dz^2))+(2*pi*chem.D_w_G*geo.dz/
405     log(geo.r(i-(5*geo.N*geo.M)))/geo.r(geo.M+i-(5*geo.N*geo.M)))+
406     param.K_E_dec)) * ((chem.D_w_G*solvec(i-1)/(geo.dz^2))+(2*pi*chem.D_w_G*
407     geo.dz*solvec(i+geo.M))/log(geo.r(i-(5*geo.N*geo.M)))/
408     geo.r(geo.M+i-(5*geo.N*geo.M)))) + (param.K_tr_synth*
409     solvec(i-(geo.N*geo.M))));
410 end
411 for i = (5*geo.N*geo.M)+((3+geo.n)*geo.M)+1 :
412     ((5*geo.N*geo.M)+((2+(3*geo.n))*geo.M))
413     if solvec(i-(5*geo.M*geo.N))>param.c_ox_b
414         if (i-1)/(geo.M)~=floor((i-1)/(geo.M)) &&
415             i/(geo.M)~=floor(i/(geo.M))
416             solvec(i) = sqrt(((1/((-4*pi*chem.D_w_G/(geo.dr^2)) +
417             (-4*pi*chem.D_w_G/(geo.dz^2)) + ((360/342)*param.K_Cb*
418             solvec(i-(geo.N*geo.M))*param.frac_E_betaG_Tr*
419             solvec(i-(2*geo.N*geo.M))/(param.K_m*(1+(solvec(i)))) +
420             (solvec(i-(geo.N*geo.M)))))) * ((solvec(i+1)*(2*pi*chem.D_w_G/
421             (geo.dz^2)) + (solvec(i-1)*(2*pi*chem.D_w_G/(geo.dz^2)) +
422             (solvec(i+geo.M)*((2*pi*chem.D_w_G/(geo.dr^2)) + (2*pi*chem.D_w_G/
423             (2*geo.dr*geo.r(i-(5*geo.N*geo.M)))))) + (solvec(i-geo.M)*
424             ((2*pi*chem.D_w_G/(geo.dr^2)) - (2*pi*chem.D_w_G/(2*geo.dr*
425             geo.r(i-(5*geo.N*geo.M)))))) + (((-param.mu_max_tr/param.Y_G_tr)*
426             min((solvec(i)/(param.K_G+solvec(i))), (solvec(i-(5*geo.M*geo.N)))/
427             (param.K_ox_tr+solvec(i-(5*geo.N*geo.M)))) * (param.K_tr_dec/
428             ((param.mu_max_tr*min((solvec(i)/(param.K_G+solvec(i))),
429             (solvec(i-(5*geo.M*geo.N)))/(param.K_ox_tr+
430             solvec(i-(5*geo.N*geo.M)))))) + param.K_tr_dec)) *
431             solvec(i-(4*geo.N*geo.M)) + (-param.M_G_tr*
432             solvec(i-(4*geo.M*geo.N))))))^2);
433         elseif (i-1)/(geo.M)==floor((i-1)/(geo.M))
434             solvec(i) = sqrt(((1/((-4*pi*chem.D_w_G/(geo.dr^2)) +
435             (2*pi*chem.D_w_G/(geo.dz^2)) + ((360/342)*param.K_Cb*
436             solvec(i-(geo.N*geo.M))*param.frac_E_betaG_Tr*
437             solvec(i-(2*geo.N*geo.M))/(param.K_m*(1+(solvec(i)))) +
438             (solvec(i-(geo.N*geo.M)))))) * ((solvec(i+1)*(-4*pi*chem.D_w_G/
439             (geo.dz^2)) + (solvec(i+2)*(2*pi*chem.D_w_G/(geo.dz^2)) +
440             (solvec(i+geo.M)*((2*pi*chem.D_w_G/(geo.dr^2)) + (2*pi*chem.D_w_G/
441             (2*geo.dr*geo.r(i-(5*geo.N*geo.M)))))) + (solvec(i-geo.M)*
442             ((2*pi*chem.D_w_G/(geo.dr^2)) - (2*pi*chem.D_w_G/(2*geo.dr*
443             geo.r(i-(5*geo.N*geo.M)))))) + (((-param.mu_max_tr/param.Y_G_tr)*
444             min((solvec(i)/(param.K_G+solvec(i))), (solvec(i-(5*geo.M*geo.N)))/

```

```

445     (param.K_ox_tr+solvec(i-(5*geo.N*geo.M)))))*(param.K_tr_dec/
446     ((param.mu_max_tr*min((solvec(i)/(param.K_G+solvec(i))),
447     (solvec(i-(5*geo.M*geo.N))/(param.K_ox_tr+
448     solvec(i-(5*geo.N*geo.M)))))+param.K_tr_dec))*
449     solvec(i-(4*geo.N*geo.M))+(-param.M_G_tr*
450     solvec(i-(4*geo.M*geo.N))))))^2);
451     elseif i/(geo.M)==floor(i/(geo.M))
452     solvec(i) = sqrt(((1/((-4*pi*chem.D_w_G/(geo.dr^2)))+(
453     (2*pi*chem.D_w_G/(geo.dz^2)))+(360/342)*param.K_Cb*
454     solvec(i-(geo.N*geo.M))*param.frac_E_betaG_Tr*
455     solvec(i-(2*geo.N*geo.M))/(param.K_m*(1+(solvec(i))))+
456     (solvec(i-(geo.N*geo.M))))))*((solvec(i-1)*
457     (-4*pi*chem.D_w_G/(geo.dz^2)))+(solvec(i-2)*(2*pi*chem.D_w_G/
458     (geo.dz^2)))+(solvec(i+geo.M)*((2*pi*chem.D_w_G/(geo.dr^2))+(
459     (2*pi*chem.D_w_G/(2*geo.dr*geo.r(i-(5*geo.M*geo.N))))))+
460     (solvec(i-geo.M)*((2*pi*chem.D_w_G/(geo.dr^2))-(2*pi*chem.D_w_G/
461     (2*geo.dr*geo.r(i-(5*geo.N*geo.M)))))))+
462     ((-param.mu_max_tr/param.Y_G_tr)*min((solvec(i)/
463     (param.K_G+solvec(i))), (solvec(i-(5*geo.M*geo.N))/(
464     (param.K_ox_tr+solvec(i-(5*geo.N*geo.M)))))*(param.K_tr_dec/
465     ((param.mu_max_tr*min((solvec(i)/(param.K_G+solvec(i))),
466     (solvec(i-(5*geo.M*geo.N))/(param.K_ox_tr+
467     solvec(i-(5*geo.N*geo.M)))))+param.K_tr_dec))*
468     solvec(i-(4*geo.N*geo.M))+(-param.M_G_tr*
469     solvec(i-(4*geo.M*geo.N))))))^2);
470     end
471     elseif solvec(i-(5*geo.M*geo.N)) <= param.c_ox_b
472         if (i-1)/(geo.M)~=floor((i-1)/(geo.M)) &&
473             i/(geo.M)~=floor(i/(geo.M))
474             solvec(i) = sqrt(((1/((-4*pi*chem.D_w_G/(geo.dr^2)))+(4*pi*
475             chem.D_w_G/(geo.dz^2)))+(360/342)*param.K_Cb*
476             solvec(i-(geo.N*geo.M))*param.frac_E_betaG_Tr*
477             solvec(i-(2*geo.N*geo.M))/(param.K_m*(1+(solvec(i))))+
478             (solvec(i-(geo.N*geo.M))))-(1/param.Y_X_Y_G)*
479             (param.mu_max_Y*solvec(i+(geo.N*geo.M))/(solvec(i)+param.K_G))*
480             (1-(solvec(i+(2*geo.M*geo.N))))))*((solvec(i+1)*(2*pi*chem.D_w_G/
481             (geo.dz^2)))+(solvec(i-1)*(2*pi*chem.D_w_G/(geo.dz^2)))+(
482             (solvec(i+geo.M)*((2*pi*chem.D_w_G/(geo.dr^2))+(2*pi*chem.D_w_G/
483             (2*geo.dr*geo.r(i-(5*geo.N*geo.M)))))+(solvec(i-geo.M)*
484             ((2*pi*chem.D_w_G/(geo.dr^2))-(2*pi*chem.D_w_G/(2*geo.dr*
485             geo.r(i-(5*geo.N*geo.M)))))))))^2);
486             elseif (i-1)/(geo.M)==floor((i-1)/(geo.M))
487             solvec(i) = sqrt(((1/((-4*pi*chem.D_w_G/(geo.dr^2)))+(
488             (2*pi*chem.D_w_G/(geo.dz^2)))+(360/342)*param.K_Cb*
489             solvec(i-(geo.N*geo.M))*param.frac_E_betaG_Tr*
490             solvec(i-(2*geo.N*geo.M))/(param.K_m*(1+(solvec(i))))+
491             (solvec(i-(geo.N*geo.M))))-(1/param.Y_X_Y_G)*

```

```

492     (param.mu_max_Y*solvec(i+(geo.N*geo.M))/(solvec(i)+param.K_G))*
493     (1-(solvec(i+(2*geo.M*geo.N))))))*((solvec(i+1)*
494     (-4*pi*chem.D_w_G/(geo.dz^2)))+(solvec(i+2)*(2*pi*chem.D_w_G/
495     (geo.dz^2)))+(solvec(i+geo.M)*((2*pi*chem.D_w_G/(geo.dr^2))+
496     (2*pi*chem.D_w_G/(2*geo.dr*geo.r(i-(5*geo.N*geo.M))))))+
497     (solvec(i-geo.M)*((2*pi*chem.D_w_G/(geo.dr^2))-(2*pi*chem.D_w_G/
498     (2*geo.dr*geo.r(i-(5*geo.N*geo.M))))))))^2);
499     elseif i/(geo.M)==floor(i/(geo.M))
500     solvec(i) = sqrt(((1/((-4*pi*chem.D_w_G/(geo.dr^2)))+
501     (2*pi*chem.D_w_G/(geo.dz^2)))+(360/342)*param.K_Cb*
502     solvec(i-(geo.N*geo.M))*param.frac_E_betaG_Tr*
503     solvec(i-(2*geo.N*geo.M))/(param.K_m*(1+(solvec(i))))+
504     (solvec(i-(geo.N*geo.M))))-(1/param.Y_X_Y_G)*
505     (param.mu_max_Y*solvec(i+(geo.N*geo.M))/(solvec(i)+param.K_G))*
506     (1-(solvec(i+(2*geo.M*geo.N))))))*((solvec(i-1)*(-4*pi*
507     chem.D_w_G/(geo.dz^2)))+(solvec(i-2)*(2*pi*chem.D_w_G/(geo.dz^2)))+
508     (solvec(i+geo.M)*((2*pi*chem.D_w_G/(geo.dr^2))+(2*pi*chem.D_w_G/
509     (2*geo.dr*geo.r(i-(5*geo.M*geo.N)))))+(solvec(i-geo.M)*
510     ((2*pi*chem.D_w_G/(geo.dr^2))-(2*pi*chem.D_w_G/(2*geo.dr*
511     geo.r(i-(5*geo.N*geo.M))))))))^2);
512     end
513     end
514 end
515 %glucose concentration in biofilm boundary layer
516 for i = ((5*geo.N*geo.M)+((2+(3*geo.n))*geo.M))+1 :
517     ((5*geo.N*geo.M)+((3+(3*geo.n))*geo.M))
518     solvec(i) = solvec(i+geo.M);
519     %no mass transfer limiting convective boundary layer is assumed
520 end
521 %glucose concentration in the bulk
522 for i = ((5*geo.N*geo.M)+((3+(3*geo.n))*geo.M))+1 : (6*geo.N*geo.M)
523     solvec(i)= param.c_G_b;
524 end
525
526 %yeast concentration in the inner membrane phase & membrane
527 for i = (6*geo.N*geo.M)+1 : (6*geo.N*geo.M)+((2+geo.n)*geo.M)
528     solvec(i)=0;
529 end
530 %yeast concentration in the fungal/yeast biofilm
531 for i = (6*geo.N*geo.M)+((2+geo.n)*geo.M)+1 :
532     ((6*geo.N*geo.M)+((2+(3*geo.n))*geo.M))
533     if solvec(i-(6*geo.M*geo.N))>param.c_ox_b
534         solvec(i) = 0;
535     elseif solvec(i-(6*geo.M*geo.N))≤ param.c_ox_b
536         solvec(i) = param.mean_rho_Y*solvec(i-(geo.N*geo.M))/
537         (sum(solvec(((5*geo.N*geo.M)+((2+geo.n)*geo.M)+1):((5*geo.N*geo.M)+
538         ((2+(3*geo.n))*geo.M)))))/nnz(solvec(((5*geo.N*geo.M)+

```

```

539         ((2+geo.n)*geo.M)+1):(5*geo.N*geo.M)+((2+(3*geo.n))*geo.M)))));
540     end
541 end
542 %yeast concentration in biofilm boundary layer
543 for i = ((6*geo.N*geo.M)+((2+(3*geo.n))*geo.M))+1 :
544     ((6*geo.N*geo.M)+((3+(3*geo.n))*geo.M))
545     solvec(i) = solvec(i+geo.M);
546     %no mass transfer limiting convective boundary layer is assumed
547 end
548 %yeast concentration in the bulk
549 for i = ((6*geo.N*geo.M)+((3+(3*geo.n))*geo.M))+1 : (7*geo.N*geo.M)
550     solvec(i)= param.c_X_y_b;
551 end
552
553 param.last_iter =solvec(((7*geo.N*geo.M)+1):(8*geo.N*geo.M));
554 %ethanol concentration in the inner membrane phase & inner membrane wall
555 for i = (7*geo.N*geo.M)+1 : (7*geo.N*geo.M)+(2*geo.M)
556     solvec(i)=(param.c_EtOH_b/chem.H_EtOH)*chem.M_EtOH/
557     (chem.R_gas*param.T_m_K);
558     %no mass transfer limiting convective boundary layer is assumed
559 end
560 %ethanol concentration within the membrane
561 for i = (7*geo.N*geo.M)+(2*geo.M)+1 : (7*geo.N*geo.M)+((2+geo.n)*geo.M)
562     solvec(i)=(param.c_EtOH_b/chem.H_EtOH)*chem.sol_m_EtOH;
563 end
564 %ethanol concentration in the fungal/yeast biofilm
565 for i = (7*geo.N*geo.M)+((2+geo.n)*geo.M)+1
566     if solvec(i-(2*geo.N*geo.M))≤0.05
567         solvec(i) = (1/((chem.D_w_EtOH/(geo.dz^2)))+(2*pi*chem.D_w_EtOH*geo.dz/
568         log(geo.r(i-(7*geo.N*geo.M))/geo.r(geo.M+i-(7*geo.N*geo.M)))+
569         param.K_DEGR_EtOH)))*((chem.D_w_EtOH*solvec(i+1)/(geo.dz^2))+
570         (2*pi*chem.D_w_EtOH*geo.dz*solvec(i+geo.M)/
571         log(geo.r(i-(7*geo.N*geo.M))/geo.r(geo.M+i-(7*geo.N*geo.M)))));
572     end
573     if solvec(i-(2*geo.N*geo.M))≥0.05
574         solvec(i) = (1/((chem.D_w_EtOH/(geo.dz^2)))+(2*pi*chem.D_w_EtOH*
575         geo.dz/log(geo.r(i-(7*geo.N*geo.M))/geo.r(geo.M+i-(7*geo.N*geo.M)))+
576         param.K_degr_EtOH)))*((chem.D_w_EtOH*solvec(i+1)/(geo.dz^2))+
577         (2*pi*chem.D_w_EtOH*geo.dz*solvec(i+geo.M)/
578         log(geo.r(i-(7*geo.N*geo.M))/geo.r(geo.M+i-(7*geo.N*geo.M)))));
579     end
580 end
581 for i = (7*geo.N*geo.M)+((2+geo.n)*geo.M)+2 :
582     ((5*geo.N*geo.M)+((3+geo.n)*geo.M))-1
583     if solvec(i-(2*geo.N*geo.M))≤0.05
584         solvec(i) = (1/((2*chem.D_w_EtOH/(geo.dz^2)))+(2*pi*chem.D_w_EtOH*
585         geo.dz/log(geo.r(i-(7*geo.N*geo.M))/geo.r(geo.M+i-(7*geo.N*geo.M)))+

```

```

586     param.K_DEGR_EtOH))) * ((chem.D_w_EtOH*(solvec(i-1)+solvec(i+1)) /
587     (geo.dz^2)) + (2*pi*chem.D_w_EtOH*geo.dz*solvec(i+geo.M) /
588     log(geo.r(i-(7*geo.N*geo.M))/geo.r(geo.M+i-(7*geo.N*geo.M)))));
589     end
590     if solvec(i-(2*geo.N*geo.M)) >= 0.05
591     solvec(i) = (1/((2*chem.D_w_EtOH/(geo.dz^2)) + (2*pi*chem.D_w_EtOH*
592     geo.dz/log(geo.r(i-(7*geo.N*geo.M))/geo.r(geo.M+i-(7*geo.N*geo.M))) +
593     param.K_degr_EtOH))) * ((chem.D_w_EtOH*(solvec(i-1)+solvec(i+1)) /
594     (geo.dz^2)) + (2*pi*chem.D_w_EtOH*geo.dz*solvec(i+geo.M) /
595     log(geo.r(i-(7*geo.N*geo.M))/geo.r(geo.M+i-(7*geo.N*geo.M)))));
596     end
597 end
598 for i = ((7*geo.N*geo.M) + ((3+geo.n)*geo.M))
599     if solvec(i-(2*geo.N*geo.M)) <= 0.05
600     solvec(i) = (1/((chem.D_w_EtOH/(geo.dz^2)) + (2*pi*chem.D_w_EtOH*
601     geo.dz/log(geo.r(i-(7*geo.N*geo.M))/geo.r(geo.M+i-(7*geo.N*geo.M))) +
602     param.K_DEGR_EtOH))) * ((chem.D_w_EtOH*solvec(i-1)/(geo.dz^2)) +
603     (2*pi*chem.D_w_EtOH*geo.dz*solvec(i+geo.M) /
604     log(geo.r(i-(7*geo.N*geo.M))/geo.r(geo.M+i-(7*geo.N*geo.M)))));
605     end
606     if solvec(i-(2*geo.N*geo.M)) >= 0.05
607     solvec(i) = (1/((chem.D_w_EtOH/(geo.dz^2)) + (2*pi*chem.D_w_EtOH*
608     geo.dz/log(geo.r(i-(7*geo.N*geo.M))/geo.r(geo.M+i-(7*geo.N*geo.M))) +
609     param.K_degr_EtOH))) * ((chem.D_w_EtOH*solvec(i-1)/(geo.dz^2)) +
610     (2*pi*chem.D_w_EtOH*geo.dz*solvec(i+geo.M) /
611     log(geo.r(i-(7*geo.N*geo.M))/geo.r(geo.M+i-(7*geo.N*geo.M)))));
612     end
613 end
614 for i = (7*geo.N*geo.M) + ((3+geo.n)*geo.M) + 1 :
615     ((7*geo.N*geo.M) + ((2+(3*geo.n))*geo.M))
616     if solvec(i-(7*geo.M*geo.N)) > param.c_ox_b
617         if solvec(i-(2*geo.N*geo.M)) <= 0.05
618             if (i-1)/(geo.M) ~= floor((i-1)/(geo.M)) &&
619                 i/(geo.M) ~= floor(i/(geo.M))
620                 solvec(i) = sqrt((((1/((-4*pi*chem.D_w_EtOH/(geo.dr^2)) +
621                 (-4*pi*chem.D_w_EtOH/(geo.dz^2)) - param.K_DEGR_EtOH))) *
622                 (((solvec(i+1)*(2*pi*chem.D_w_EtOH/(geo.dz^2)) + (solvec(i-1)*
623                 (2*pi*chem.D_w_EtOH/(geo.dz^2)) + (solvec(i+geo.M)*
624                 (2*pi*chem.D_w_EtOH/(geo.dr^2)) + (2*pi*chem.D_w_EtOH/
625                 (2*geo.dr*geo.r(i-(7*geo.N*geo.M)))))) + (solvec(i-geo.M)*
626                 (2*pi*chem.D_w_EtOH/(geo.dr^2)) - (2*pi*chem.D_w_EtOH/
627                 (2*geo.dr*geo.r(i-(7*geo.N*geo.M)))))))))^2);
628             elseif (i-1)/(geo.M) == floor((i-1)/(geo.M))
629                 solvec(i) = sqrt((((1/((-4*pi*chem.D_w_EtOH/(geo.dr^2)) +
630                 (2*pi*chem.D_w_EtOH/(geo.dz^2)) - param.K_DEGR_EtOH))) *
631                 (((solvec(i+1)*(-4*pi*chem.D_w_EtOH/(geo.dz^2)) + (solvec(i+2)*
632                 (2*pi*chem.D_w_EtOH/(geo.dz^2)) + (solvec(i+geo.M)*

```

```

633     ((2*pi*chem.D_w_EtOH/(geo.dr^2))+(2*pi*chem.D_w_EtOH/
634     (2*geo.dr*geo.r(i-(7*geo.N*geo.M)))))+(solvec(i-geo.M)*
635     ((2*pi*chem.D_w_EtOH/(geo.dr^2))-(2*pi*chem.D_w_EtOH/
636     (2*geo.dr*geo.r(i-(7*geo.N*geo.M))))))^(2);
637     elseif i/(geo.M)==floor(i/(geo.M))
638     solvec(i) = sqrt(((1/((-4*pi*chem.D_w_EtOH/(geo.dr^2))+
639     (2*pi*chem.D_w_EtOH/(geo.dz^2))-param.K_DEGR_EtOH)))*
640     (((solvec(i-1)*(-4*pi*chem.D_w_EtOH/(geo.dz^2)))+(solvec(i-2)*
641     (2*pi*chem.D_w_EtOH/(geo.dz^2)))+(solvec(i+geo.M)*
642     ((2*pi*chem.D_w_EtOH/(geo.dr^2))+(2*pi*chem.D_w_EtOH/
643     (2*geo.dr*geo.r(i-(7*geo.N*geo.M)))))))+(solvec(i-geo.M)*
644     ((2*pi*chem.D_w_EtOH/(geo.dr^2))-(2*pi*chem.D_w_EtOH/
645     (2*geo.dr*geo.r(i-(7*geo.N*geo.M))))))^(2);
646     end
647     end
648     if solvec(i-(2*geo.N*geo.M))≥0.05
649     if (i-1)/(geo.M)≠floor((i-1)/(geo.M)) &&
650         i/(geo.M)≠floor(i/(geo.M))
651     solvec(i) = sqrt(((1/((-4*pi*chem.D_w_EtOH/(geo.dr^2))+
652     (-4*pi*chem.D_w_EtOH/(geo.dz^2))-param.K_degr_EtOH)))*
653     (((solvec(i+1)*(2*pi*chem.D_w_EtOH/(geo.dz^2)))+(solvec(i-1)*
654     (2*pi*chem.D_w_EtOH/(geo.dz^2)))+(solvec(i+geo.M)*
655     ((2*pi*chem.D_w_EtOH/(geo.dr^2))+(2*pi*chem.D_w_EtOH/
656     (2*geo.dr*geo.r(i-(7*geo.N*geo.M)))))))+(solvec(i-geo.M)*
657     ((2*pi*chem.D_w_EtOH/(geo.dr^2))-(2*pi*chem.D_w_EtOH/
658     (2*geo.dr*geo.r(i-(7*geo.N*geo.M))))))^(2);
659     elseif (i-1)/(geo.M)==floor((i-1)/(geo.M))
660     solvec(i) = sqrt(((1/((-4*pi*chem.D_w_EtOH/(geo.dr^2))+
661     (2*pi*chem.D_w_EtOH/(geo.dz^2))-param.K_degr_EtOH)))*
662     (((solvec(i+1)*(-4*pi*chem.D_w_EtOH/(geo.dz^2)))+(solvec(i+2)*
663     (2*pi*chem.D_w_EtOH/(geo.dz^2)))+(solvec(i+geo.M)*
664     ((2*pi*chem.D_w_EtOH/(geo.dr^2))+(2*pi*chem.D_w_EtOH/
665     (2*geo.dr*geo.r(i-(7*geo.N*geo.M)))))))+(solvec(i-geo.M)*
666     ((2*pi*chem.D_w_EtOH/(geo.dr^2))-(2*pi*chem.D_w_EtOH/
667     (2*geo.dr*geo.r(i-(7*geo.N*geo.M))))))^(2);
668     elseif i/(geo.M)==floor(i/(geo.M))
669     solvec(i) = sqrt(((1/((-4*pi*chem.D_w_EtOH/(geo.dr^2))+
670     (2*pi*chem.D_w_EtOH/(geo.dz^2))-param.K_degr_EtOH)))*
671     (((solvec(i-1)*(-4*pi*chem.D_w_EtOH/(geo.dz^2)))+(solvec(i-2)*
672     (2*pi*chem.D_w_EtOH/(geo.dz^2)))+(solvec(i+geo.M)*
673     ((2*pi*chem.D_w_EtOH/(geo.dr^2))+(2*pi*chem.D_w_EtOH/
674     (2*geo.dr*geo.r(i-(7*geo.N*geo.M)))))))+(solvec(i-geo.M)*
675     ((2*pi*chem.D_w_EtOH/(geo.dr^2))-(2*pi*chem.D_w_EtOH/
676     (2*geo.dr*geo.r(i-(7*geo.N*geo.M))))))^(2);
677     end
678     end
679     elseif solvec(i-(7*geo.M*geo.N))≤ param.c_ox_b

```

```

680     if (i-1)/(geo.M)~=floor((i-1)/(geo.M)) &&
681         i/(geo.M)~=floor(i/(geo.M))
682     solvec(i) = sqrt((((1/((-4*pi*chem.D_w_EtOH/(geo.dr^2))+
683         (-4*pi*chem.D_w_EtOH/(geo.dz^2))-param.K_degr_EtOH)))*
684         (((solvec(i+1)*(2*pi*chem.D_w_EtOH/(geo.dz^2)))+(solvec(i-1)*
685         (2*pi*chem.D_w_EtOH/(geo.dz^2)))+(solvec(i+geo.M)*
686         ((2*pi*chem.D_w_EtOH/(geo.dr^2))+(2*pi*chem.D_w_EtOH/
687         (2*geo.dr*geo.r(i-(7*geo.N*geo.M)))))+(solvec(i-geo.M)*
688         ((2*pi*chem.D_w_EtOH/(geo.dr^2))-(2*pi*chem.D_w_EtOH/
689         (2*geo.dr*geo.r(i-(7*geo.N*geo.M)))))))))+
690         ((param.Y_EtOH_G/param.Y_X_Y_G)*(solvec(i-(2*geo.M*geo.N)))/
691         (param.K_G+solvec(i-(2*geo.M*geo.N)))))*
692         (1-(solvec(i)/param.K_X_EtOH)))^2);
693     elseif (i-1)/(geo.M)==floor((i-1)/(geo.M))
694     solvec(i) = sqrt((((1/((-4*pi*chem.D_w_EtOH/(geo.dr^2))+
695         (2*pi*chem.D_w_EtOH/(geo.dz^2))-param.K_degr_EtOH)))*
696         (((solvec(i+1)*(-4*pi*chem.D_w_EtOH/(geo.dz^2)))+(solvec(i+2)*
697         (2*pi*chem.D_w_EtOH/(geo.dz^2)))+(solvec(i+geo.M)*
698         ((2*pi*chem.D_w_EtOH/(geo.dr^2))+(2*pi*chem.D_w_EtOH/
699         (2*geo.dr*geo.r(i-(7*geo.N*geo.M)))))+(solvec(i-geo.M)*
700         ((2*pi*chem.D_w_EtOH/(geo.dr^2))-(2*pi*chem.D_w_EtOH/
701         (2*geo.dr*geo.r(i-(7*geo.N*geo.M)))))))))+
702         ((param.Y_EtOH_G/param.Y_X_Y_G)*(solvec(i-(2*geo.M*geo.N)))/
703         (param.K_G+solvec(i-(2*geo.M*geo.N)))))*
704         (1-(solvec(i)/param.K_X_EtOH)))^2);
705     elseif i/(geo.M)==floor(i/(geo.M))
706     solvec(i) = sqrt((((1/((-4*pi*chem.D_w_EtOH/(geo.dr^2))+
707         (2*pi*chem.D_w_EtOH/(geo.dz^2))-param.K_degr_EtOH)))*
708         (((solvec(i-1)*(-4*pi*chem.D_w_EtOH/(geo.dz^2)))+
709         (solvec(i-2)*(2*pi*chem.D_w_EtOH/(geo.dz^2)))+(solvec(i+geo.M)*
710         ((2*pi*chem.D_w_EtOH/(geo.dr^2))+(2*pi*chem.D_w_EtOH/
711         (2*geo.dr*geo.r(i-(7*geo.M*geo.N)))))+(solvec(i-geo.M)*
712         ((2*pi*chem.D_w_EtOH/(geo.dr^2))-(2*pi*chem.D_w_EtOH/
713         (2*geo.dr*geo.r(i-(7*geo.N*geo.M)))))))))+
714         ((param.Y_EtOH_G/param.Y_X_Y_G)*(solvec(i-(2*geo.M*geo.N)))/
715         (param.K_G+solvec(i-(2*geo.M*geo.N)))))*
716         (1-(solvec(i)/param.K_X_EtOH)))^2);
717     end
718 end
719 end
720 %ethanol concentration in biofilm boundary layer
721 for i = ((7*geo.N*geo.M)+((2+(3*geo.n))*geo.M))+1 :
722     ((7*geo.N*geo.M)+((3+(3*geo.n))*geo.M))
723     solvec(i) = solvec(i+geo.M);
724     %no mass transfer limiting convective boundary layer is assumed
725 end
726 %ethanol concentration in the bulk

```



```

727 for i = ((7*geo.N*geo.M)+(3+(3*geo.n))*geo.M)+1 : (8*geo.N*geo.M)
728     solvec(i)= param.c_EtOH_b;
729 end
730
731 %% error calculation oxygen
732 % oxygen inner membrane phase
733 for i= 1: geo.M
734     errvec(i) = (chem.sol_m_ox*param.p_m(i)*param.n_ox_m);
735 end
736 %oxygen at membrane wall (neglecting convective boundary layer)
737 for i = geo.M+1 : 2*geo.M
738     errvec(i) = (chem.sol_m_ox*param.p_m(i-geo.M)*param.n_ox_m);
739 end
740 %oxygen in membrane
741 for i = (2*geo.M)+1 : (2+geo.n)*geo.M
742     if (i-1)/(geo.M)~=floor((i-1)/(geo.M)) && i/(geo.M)~=floor(i/(geo.M))
743         errvec(i) = (1/((-4*pi*chem.D_m_ox/(geo.dr^2))+(-4*pi*chem.D_m_ox/
744             (geo.dz^2))+(0)))*((solvec(i+1)*(2*pi*chem.D_m_ox/(geo.dz^2)))+(
745             solvec(i-1)*(2*pi*chem.D_m_ox/(geo.dz^2)))+(solvec(i+geo.M)*
746             ((2*pi*chem.D_m_ox/(geo.dr^2))+(2*pi*chem.D_m_ox/(2*geo.dr*geo.r(i))))))
747             +(solvec(i-geo.M)*((2*pi*chem.D_m_ox/(geo.dr^2))-(2*pi*chem.D_m_ox/
748             (2*geo.dr*geo.r(i))))));
749     elseif (i-1)/(geo.M)==floor((i-1)/(geo.M))
750         errvec(i) = (1/((-4*pi*chem.D_m_ox/(geo.dr^2))+(-4*pi*chem.D_m_ox/
751             (geo.dz^2))+(0)))*((solvec(i+1)*(-4*pi*chem.D_m_ox/(geo.dz^2)))+(
752             solvec(i+2)*(2*pi*chem.D_m_ox/(geo.dz^2)))+(solvec(i+geo.M)*
753             ((2*pi*chem.D_m_ox/(geo.dr^2))+(2*pi*chem.D_m_ox/(2*geo.dr*geo.r(i))))))
754             +(solvec(i-geo.M)*((2*pi*chem.D_m_ox/(geo.dr^2))-(2*pi*chem.D_m_ox/
755             (2*geo.dr*geo.r(i))))));
756     elseif i/(geo.M)==floor(i/(geo.M))
757         errvec(i) = (1/((-4*pi*chem.D_m_ox/(geo.dr^2))+(-4*pi*chem.D_m_ox/
758             (geo.dz^2))+(0)))*((solvec(i-1)*(-4*pi*chem.D_m_ox/(geo.dz^2)))+(
759             solvec(i-2)*(2*pi*chem.D_m_ox/(geo.dz^2)))+(solvec(i+geo.M)*
760             ((2*pi*chem.D_m_ox/(geo.dr^2))+(2*pi*chem.D_m_ox/(2*geo.dr*geo.r(i))))))
761             +(solvec(i-geo.M)*((2*pi*chem.D_m_ox/(geo.dr^2))-(2*pi*chem.D_m_ox/
762             (2*geo.dr*geo.r(i))))));
763     end
764 end
765 %oxygen in fungal biofilm
766 for i = ((2+geo.n)*geo.M)+1 : ((2+(2*geo.n))*geo.M)
767     if (i-1)/(geo.M)~=floor((i-1)/(geo.M)) && i/(geo.M)~=floor(i/(geo.M))
768         errvec(i) = (1/((-4*pi*chem.D_w_ox/(geo.dr^2))+(-4*pi*chem.D_w_ox/
769             (geo.dz^2))+(0)))*((solvec(i+1)*(2*pi*chem.D_w_ox/(geo.dz^2)))+(
770             solvec(i-1)*(2*pi*chem.D_w_ox/(geo.dz^2)))+(solvec(i+geo.M)*
771             ((2*pi*chem.D_w_ox/(geo.dr^2))+(2*pi*chem.D_w_ox/(2*geo.dr*geo.r(i))))))
772             +(solvec(i-geo.M)*((2*pi*chem.D_w_ox/(geo.dr^2))-(2*pi*chem.D_w_ox/
773             (2*geo.dr*geo.r(i))))))+((-param.mu_max_tr/param.Y_ox_tr)*

```

```

774     min((1), (solvec(i)/(param.K_ox_tr+solvec(i))))*(param.K_tr_dec/
775     ((param.mu_max_tr*min((1), (solvec(i)/(param.K_ox_tr+solvec(i)))))+
776     param.K_tr_dec))*solvec(i+(geo.N*geo.M)))+(-param.M_ox_tr*
777     solvec(i+(geo.M*geo.N))));
778     elseif (i-1)/(geo.M)==floor((i-1)/(geo.M))
779     errvec (i) = (1/((-4*pi*chem.D_w_ox/(geo.dr^2))+
780     (2*pi*chem.D_w_ox/(geo.dz^2))+(0)))*((solvec(i+1)*
781     (-4*pi*chem.D_w_ox/(geo.dz^2)))+(solvec(i+2)*
782     (2*pi*chem.D_w_ox/(geo.dz^2)))+(solvec(i+geo.M)*
783     ((2*pi*chem.D_w_ox/(geo.dr^2))+(2*pi*chem.D_w_ox/(2*geo.dr*geo.r(i))))))
784     +(solvec(i-geo.M)*((2*pi*chem.D_w_ox/(geo.dr^2))-(2*pi*chem.D_w_ox/
785     (2*geo.dr*geo.r(i))))))+((-param.mu_max_tr/param.Y_ox_tr)*
786     min((1), (solvec(i)/(param.K_ox_tr+solvec(i))))*(param.K_tr_dec/
787     ((param.mu_max_tr*min((1), (solvec(i)/(param.K_ox_tr+solvec(i)))))+
788     param.K_tr_dec))*solvec(i+(geo.N*geo.M)))+(-param.M_ox_tr*
789     solvec(i+(geo.M*geo.N))));
790     elseif i/(geo.M)==floor(i/(geo.M))
791     errvec (i) = (1/((-4*pi*chem.D_w_ox/(geo.dr^2))+
792     (2*pi*chem.D_w_ox/(geo.dz^2))+(0)))*((solvec(i-1)*
793     (-4*pi*chem.D_w_ox/(geo.dz^2)))+(solvec(i-2)*(2*pi*chem.D_w_ox/
794     (geo.dz^2)))+(solvec(i+geo.M)*((2*pi*chem.D_w_ox/(geo.dr^2))+
795     (2*pi*chem.D_w_ox/(2*geo.dr*geo.r(i)))))+(solvec(i-geo.M)*
796     ((2*pi*chem.D_w_ox/(geo.dr^2))-(2*pi*chem.D_w_ox/
797     (2*geo.dr*geo.r(i))))))+((-param.mu_max_tr/param.Y_ox_tr)*
798     min((1), (solvec(i)/(param.K_ox_tr+solvec(i))))*(param.K_tr_dec/
799     ((param.mu_max_tr*min((1), (solvec(i)/(param.K_ox_tr+solvec(i))))))
800     +param.K_tr_dec))*solvec(i+(geo.N*geo.M)))+(-param.M_ox_tr*
801     solvec(i+(geo.M*geo.N))));
802     end
803 end
804 %oxygen in yeast biofilm
805 for i = ((2+(2*geo.n))*geo.M)+1 : ((2+(3*geo.n))*geo.M)
806     errvec(i) = param.c_ox_b;
807 end
808 %oxygen at biofilm boundary layer
809 for i = ((2+(3*geo.n))*geo.M)+1 : ((3+(3*geo.n))*geo.M)
810     errvec(i) = param.c_ox_b;
811 end
812 %oxygen within bulk
813 for i = ((3+(3*geo.n))*geo.M)+1 : geo.N*geo.M
814     errvec(i) = param.c_ox_b;
815 end
816 for i = 1 : geo.N*geo.M
817     maxerrvec(i)=(errvec(i)-solvec(i))/solvec(i);
818 end
819
820 %ethanol concentration in the inner membrane phase & inner membrane wall

```

```

821 for i = (7*geo.N*geo.M)+1 : (7*geo.N*geo.M)+(2*geo.M)
822     error(i)=solvec(i)-((param.c_EtOH_b/chem.H_EtOH)*chem.M_EtOH/
823         (chem.R_gas*param.T_m_K));
824     %no mass transfer limiting convective boundary layer is assumed
825 end
826 %ethanol concentration within the membrane
827 for i = (7*geo.N*geo.M)+(2*geo.M)+1 : (7*geo.N*geo.M)+((2+geo.n)*geo.M)
828     error(i)=solvec(i)-((param.c_EtOH_b/chem.H_EtOH)*chem.sol_m_EtOH);
829 end
830 %ethanol concentration in the fungal/yeast biofilm
831 for i = (7*geo.N*geo.M)+((2+geo.n)*geo.M)+1
832     if solvec(i-(2*geo.N*geo.M)) ≤ 0.05
833         error(i) = solvec(i)-((1/((chem.D_w_EtOH/(geo.dz^2))+
834             (2*pi*chem.D_w_EtOH*geo.dz/log(geo.r(i-(7*geo.N*geo.M)))/
835             geo.r(geo.M+i-(7*geo.N*geo.M)))+param.K_DEGR_EtOH)))*
836             ((chem.D_w_EtOH*solvec(i+1)/(geo.dz^2))+(2*pi*chem.D_w_EtOH*
837             geo.dz*solvec(i+geo.M)/log(geo.r(i-(7*geo.N*geo.M)))/
838             geo.r(geo.M+i-(7*geo.N*geo.M)))));
839     end
840     if solvec(i-(2*geo.N*geo.M)) ≥ 0.05
841         error(i) = solvec(i)-((1/((chem.D_w_EtOH/(geo.dz^2))+
842             (2*pi*chem.D_w_EtOH*geo.dz/log(geo.r(i-(7*geo.N*geo.M)))/
843             geo.r(geo.M+i-(7*geo.N*geo.M)))+param.K_degr_EtOH)))*
844             ((chem.D_w_EtOH*solvec(i+1)/(geo.dz^2))+(2*pi*chem.D_w_EtOH*geo.dz*
845             solvec(i+geo.M)/log(geo.r(i-(7*geo.N*geo.M)))/
846             geo.r(geo.M+i-(7*geo.N*geo.M)))));
847     end
848 end
849 for i = (7*geo.N*geo.M)+((2+geo.n)*geo.M)+2 :
850     ((5*geo.N*geo.M)+((3+geo.n)*geo.M))-1
851     if solvec(i-(2*geo.N*geo.M)) ≤ 0.05
852         error(i) = solvec(i)-((1/((2*chem.D_w_EtOH/(geo.dz^2))+
853             (2*pi*chem.D_w_EtOH*geo.dz/log(geo.r(i-(7*geo.N*geo.M)))/
854             geo.r(geo.M+i-(7*geo.N*geo.M)))+param.K_DEGR_EtOH)))*
855             ((chem.D_w_EtOH*(solvec(i-1)+solvec(i+1))/(geo.dz^2))+
856             (2*pi*chem.D_w_EtOH*geo.dz*solvec(i+geo.M)/
857             log(geo.r(i-(7*geo.N*geo.M))/geo.r(geo.M+i-(7*geo.N*geo.M)))));
858     end
859     if solvec(i-(2*geo.N*geo.M)) ≥ 0.05
860         error(i) = solvec(i)-((1/((2*chem.D_w_EtOH/(geo.dz^2))+
861             (2*pi*chem.D_w_EtOH*geo.dz/log(geo.r(i-(7*geo.N*geo.M)))/
862             geo.r(geo.M+i-(7*geo.N*geo.M)))+param.K_degr_EtOH)))*
863             ((chem.D_w_EtOH*(solvec(i-1)+solvec(i+1))/(geo.dz^2))+
864             (2*pi*chem.D_w_EtOH*geo.dz*solvec(i+geo.M)/
865             log(geo.r(i-(7*geo.N*geo.M))/geo.r(geo.M+i-(7*geo.N*geo.M)))));
866     end
867 end

```

```

868 for i = ((7*geo.N*geo.M)+(3+geo.n)*geo.M)
869     if solvec(i-(2*geo.N*geo.M)) ≤ 0.05
870         error(i) = solvec(i)-((1/((chem.D_w_EtOH/(geo.dz^2))+
871         (2*pi*chem.D_w_EtOH*geo.dz/log(geo.r(i-(7*geo.N*geo.M)) /
872         geo.r(geo.M+i-(7*geo.N*geo.M)))+param.K_DEGR_EtOH))) *
873         ((chem.D_w_EtOH*solvec(i-1)/(geo.dz^2))+
874         (2*pi*chem.D_w_EtOH*geo.dz*solvec(i+geo.M) /
875         log(geo.r(i-(7*geo.N*geo.M))/geo.r(geo.M+i-(7*geo.N*geo.M))))));
876     end
877     if solvec(i-(2*geo.N*geo.M)) ≥ 0.05
878         error(i) = solvec(i)-((1/((chem.D_w_EtOH/(geo.dz^2))+
879         (2*pi*chem.D_w_EtOH*geo.dz/log(geo.r(i-(7*geo.N*geo.M)) /
880         geo.r(geo.M+i-(7*geo.N*geo.M)))+param.K_degr_EtOH))) *
881         ((chem.D_w_EtOH*solvec(i-1)/(geo.dz^2))+
882         (2*pi*chem.D_w_EtOH*geo.dz*solvec(i+geo.M) /
883         log(geo.r(i-(7*geo.N*geo.M))/geo.r(geo.M+i-(7*geo.N*geo.M))))));
884     end
885 end
886 for i = (7*geo.N*geo.M)+((3+geo.n)*geo.M)+1 :
887     ((7*geo.N*geo.M)+(2+(3*geo.n))*geo.M)
888     if solvec(i-(7*geo.M*geo.N)) > param.c_ox_b
889         if solvec(i-(2*geo.N*geo.M)) ≤ 0.05
890             if (i-1)/(geo.M) ≠ floor((i-1)/(geo.M)) &&
891                 i/(geo.M) ≠ floor(i/(geo.M))
892                 error(i) = solvec(i)-(sqrt(((1/((-4*pi*chem.D_w_EtOH/(geo.dr^2))
893                 +(-4*pi*chem.D_w_EtOH/(geo.dz^2))-param.K_DEGR_EtOH))) *
894                 (((solvec(i+1)*(2*pi*chem.D_w_EtOH/(geo.dz^2)))+(solvec(i-1)*
895                 (2*pi*chem.D_w_EtOH/(geo.dz^2)))+(solvec(i+geo.M)*
896                 ((2*pi*chem.D_w_EtOH/(geo.dr^2))+(2*pi*chem.D_w_EtOH/
897                 (2*geo.dr*geo.r(i-(7*geo.N*geo.M)))))+(solvec(i-geo.M)*
898                 ((2*pi*chem.D_w_EtOH/(geo.dr^2))-(2*pi*chem.D_w_EtOH/
899                 (2*geo.dr*geo.r(i-(7*geo.N*geo.M))))))))^2));
900             elseif (i-1)/(geo.M) == floor((i-1)/(geo.M))
901                 error(i) = solvec(i)-(sqrt(((1/((-4*pi*chem.D_w_EtOH/(geo.dr^2))
902                 + (2*pi*chem.D_w_EtOH/(geo.dz^2))-param.K_DEGR_EtOH))) *
903                 (((solvec(i+1)*(-4*pi*chem.D_w_EtOH/(geo.dz^2)))+(solvec(i+2)*
904                 (2*pi*chem.D_w_EtOH/(geo.dz^2)))+(solvec(i+geo.M)*
905                 ((2*pi*chem.D_w_EtOH/(geo.dr^2))+(2*pi*chem.D_w_EtOH/
906                 (2*geo.dr*geo.r(i-(7*geo.N*geo.M)))))+(solvec(i-geo.M)*
907                 ((2*pi*chem.D_w_EtOH/(geo.dr^2))-(2*pi*chem.D_w_EtOH/
908                 (2*geo.dr*geo.r(i-(7*geo.N*geo.M))))))))^2));
909             elseif i/(geo.M) == floor(i/(geo.M))
910                 error(i) = solvec(i)-(sqrt(((1/((-4*pi*chem.D_w_EtOH/(geo.dr^2))
911                 + (2*pi*chem.D_w_EtOH/(geo.dz^2))-param.K_DEGR_EtOH))) *
912                 (((solvec(i-1)*(-4*pi*chem.D_w_EtOH/(geo.dz^2)))+(solvec(i-2)*
913                 (2*pi*chem.D_w_EtOH/(geo.dz^2)))+(solvec(i+geo.M)*
914                 ((2*pi*chem.D_w_EtOH/(geo.dr^2))+(2*pi*chem.D_w_EtOH/(2*geo.dr*

```

```

915     geo.r(i-(7*geo.N*geo.M)))))+(solvec(i-geo.M)*((2*pi*chem.D_w_EtOH/
916     (geo.dr^2))-(2*pi*chem.D_w_EtOH/(2*geo.dr*
917     geo.r(i-(7*geo.N*geo.M))))))^2));
918     end
919     end
920     if solvec(i-(2*geo.N*geo.M)) ≥ 0.05
921     if (i-1)/(geo.M) ≠ floor((i-1)/(geo.M)) &&
922         i/(geo.M) ≠ floor(i/(geo.M))
923     error(i) = solvec(i)-(sqrt(((1/((-4*pi*chem.D_w_EtOH/(geo.dr^2))+
924     (-4*pi*chem.D_w_EtOH/(geo.dz^2))-param.K_degr_EtOH)))*
925     (((solvec(i+1)*(2*pi*chem.D_w_EtOH/(geo.dz^2)))+(solvec(i-1)*
926     (2*pi*chem.D_w_EtOH/(geo.dz^2)))+(solvec(i+geo.M)*
927     ((2*pi*chem.D_w_EtOH/(geo.dr^2))+(2*pi*chem.D_w_EtOH/
928     (2*geo.dr*geo.r(i-(7*geo.N*geo.M)))))+(solvec(i-geo.M)*
929     ((2*pi*chem.D_w_EtOH/(geo.dr^2))-(2*pi*chem.D_w_EtOH/
930     (2*geo.dr*geo.r(i-(7*geo.N*geo.M))))))^2));
931     elseif (i-1)/(geo.M) == floor((i-1)/(geo.M))
932     error(i) = solvec(i)-(sqrt(((1/((-4*pi*chem.D_w_EtOH/(geo.dr^2))+
933     (2*pi*chem.D_w_EtOH/(geo.dz^2))-param.K_degr_EtOH)))*
934     (((solvec(i+1)*(-4*pi*chem.D_w_EtOH/(geo.dz^2)))+
935     (solvec(i+2)*(2*pi*chem.D_w_EtOH/(geo.dz^2)))+(solvec(i+geo.M)*
936     ((2*pi*chem.D_w_EtOH/(geo.dr^2))+(2*pi*chem.D_w_EtOH/
937     (2*geo.dr*geo.r(i-(7*geo.N*geo.M)))))+(solvec(i-geo.M)*
938     ((2*pi*chem.D_w_EtOH/(geo.dr^2))-(2*pi*chem.D_w_EtOH/
939     (2*geo.dr*geo.r(i-(7*geo.N*geo.M))))))^2));
940     elseif i/(geo.M) == floor(i/(geo.M))
941     error(i) = solvec(i)-(sqrt(((1/((-4*pi*chem.D_w_EtOH/(geo.dr^2))+
942     (2*pi*chem.D_w_EtOH/(geo.dz^2))-param.K_degr_EtOH)))*
943     (((solvec(i-1)*(-4*pi*chem.D_w_EtOH/(geo.dz^2)))+(solvec(i-2)*
944     (2*pi*chem.D_w_EtOH/(geo.dz^2)))+(solvec(i+geo.M)*
945     ((2*pi*chem.D_w_EtOH/(geo.dr^2))+(2*pi*chem.D_w_EtOH/
946     (2*geo.dr*geo.r(i-(7*geo.N*geo.M)))))+(solvec(i-geo.M)*
947     ((2*pi*chem.D_w_EtOH/(geo.dr^2))-(2*pi*chem.D_w_EtOH/
948     (2*geo.dr*geo.r(i-(7*geo.N*geo.M))))))^2));
949     end
950     end
951     elseif solvec(i-(7*geo.M*geo.N)) ≤ param.c_ox_b
952     if (i-1)/(geo.M) ≠ floor((i-1)/(geo.M)) &&
953         i/(geo.M) ≠ floor(i/(geo.M))
954     error(i) = solvec(i)-(sqrt(((1/((-4*pi*chem.D_w_EtOH/
955     (geo.dr^2))+(-4*pi*chem.D_w_EtOH/(geo.dz^2))-param.K_degr_EtOH)))*
956     (((solvec(i+1)*(2*pi*chem.D_w_EtOH/(geo.dz^2)))+(solvec(i-1)*
957     (2*pi*chem.D_w_EtOH/(geo.dz^2)))+(solvec(i+geo.M)*
958     ((2*pi*chem.D_w_EtOH/(geo.dr^2))+(2*pi*chem.D_w_EtOH/
959     (2*geo.dr*geo.r(i-(7*geo.N*geo.M)))))+(solvec(i-geo.M)*
960     ((2*pi*chem.D_w_EtOH/(geo.dr^2))-(2*pi*chem.D_w_EtOH/
961     (2*geo.dr*geo.r(i-(7*geo.N*geo.M))))))^2));

```

```

962     ((param.Y_EtOH_G/param.Y_X_Y_G)*(solvec(i-(2*geo.M*geo.N)))/
963     (param.K_G+solvec(i-(2*geo.M*geo.N))))*
964     (1-(solvec(i)/param.K_X_EtOH)))^2));
965     elseif (i-1)/(geo.M)==floor((i-1)/(geo.M))
966     error(i) = solvec(i)-(sqrt((((1/((-4*pi*chem.D_w_EtOH/
967     (geo.dr^2))+(2*pi*chem.D_w_EtOH/(geo.dz^2))-param.K_degr_EtOH)))*
968     (((solvec(i+1)*(-4*pi*chem.D_w_EtOH/(geo.dz^2)))+(solvec(i+2)*
969     (2*pi*chem.D_w_EtOH/(geo.dz^2)))+(solvec(i+geo.M)*
970     ((2*pi*chem.D_w_EtOH/(geo.dr^2))+(2*pi*chem.D_w_EtOH/
971     (2*geo.dr*geo.r(i-(7*geo.N*geo.M)))))+(solvec(i-geo.M)*
972     ((2*pi*chem.D_w_EtOH/(geo.dr^2))-(2*pi*chem.D_w_EtOH/
973     (2*geo.dr*geo.r(i-(7*geo.N*geo.M)))))))))+
974     ((param.Y_EtOH_G/param.Y_X_Y_G)*(solvec(i-(2*geo.M*geo.N)))/
975     (param.K_G+solvec(i-(2*geo.M*geo.N))))*
976     (1-(solvec(i)/param.K_X_EtOH)))^2));
977     elseif i/(geo.M)==floor(i/(geo.M))
978     error(i) = solvec(i)-(sqrt((((1/((-4*pi*chem.D_w_EtOH/(geo.dr^2))
979     +(2*pi*chem.D_w_EtOH/(geo.dz^2))-param.K_degr_EtOH)))*
980     (((solvec(i-1)*(-4*pi*chem.D_w_EtOH/(geo.dz^2)))+
981     (solvec(i-2)*(2*pi*chem.D_w_EtOH/(geo.dz^2)))+(solvec(i+geo.M)*
982     ((2*pi*chem.D_w_EtOH/(geo.dr^2))+(2*pi*chem.D_w_EtOH/
983     (2*geo.dr*geo.r(i-(7*geo.M*geo.N)))))+(solvec(i-geo.M)*
984     ((2*pi*chem.D_w_EtOH/(geo.dr^2))-(2*pi*chem.D_w_EtOH/
985     (2*geo.dr*geo.r(i-(7*geo.N*geo.M)))))))))+
986     ((param.Y_EtOH_G/param.Y_X_Y_G)*(solvec(i-(2*geo.M*geo.N)))/
987     (param.K_G+solvec(i-(2*geo.M*geo.N))))*
988     (1-(solvec(i)/param.K_X_EtOH)))^2));
989     end
990     end
991 end
992 %ethanol concentration in biofilm boundary layer
993 for i = ((7*geo.N*geo.M)+((2+(3*geo.n))*geo.M))+1 :
994     ((7*geo.N*geo.M)+((3+(3*geo.n))*geo.M))
995     error(i) = solvec(i)-solvec(i+geo.M);
996     %no mass transfer limiting convective boundary layer is assumed
997 end
998 %ethanol concentration in the bulk
999 for i = ((7*geo.N*geo.M)+((3+(3*geo.n))*geo.M))+1 : (8*geo.N*geo.M)
1000     error(i) = solvec(i)-param.c_EtOH_b;
1001 end
1002
1003 param.max_rel_error_ox = 100*max(maxerrvec);
1004 param.max_rel_error_EtOH = 100*max(error(((7*geo.N*geo.M)+1):
1005     (8*geo.N*geo.M))./solvec(((7*geo.N*geo.M)+1):(8*geo.N*geo.M)));
1006 itercount=itercount+1;
1007 end

```

```

1 function sol = fsolve_bulk_reactions(hydrosolvec,param)
2
3 sol = zeros(12,1);
4 % 12 unknowns:
5 % hydrosolvec(1) = c_C_in_endo
6 % hydrosolvec(2) = c_C_in_exo = param.frac_exo_sites_C_in*param.c_C_in
7 % not included in the equation solving
8 % hydrosolvec(3) = c_C
9 % hydrosolvec(4) = r_C
10 % hydrosolvec(5) = c_EC_endo
11 % hydrosolvec(6) = c_EC_exo
12 % hydrosolvec(7) = c_C_endo
13 % hydrosolvec(8) = c_C_exo
14 % hydrosolvec(9) = c_E_f_endo
15 % hydrosolvec(10) = c_C_f_endo
16 % hydrosolvec(11) = c_E_f_exo
17 % hydrosolvec(12) = c_C_f_exo
18 % hydrosolvec(13) = c_Cb_b
19 % hydrosolvec(14) = c_G_b
20 % hydrosolvec(15) = r_y_b
21 % hydrosolvec(16) = c_X_y_b
22 % hydrosolvec(17) = c_EtOH_b
23
24 % 12 equations:
25 sol(1) = sqrt((hydrosolvec(1))^2+(param.frac_exo_sites_C_in*
26 param.c_C_in)-param.c_C_in);
27 sol(2) = param.c_C_in+(hydrosolvec(4)*param.tau)+
28 sqrt((hydrosolvec(3))^2);
29 sol(3) = ((-1)*param.k_endo*(sqrt((hydrosolvec(5))^2)/
30 (1+param.sigma_endo))*(param.K_C_Cb/(sqrt((hydrosolvec(13))^2)+
31 param.K_C_Cb))*(param.K_C_EtOH/(sqrt((hydrosolvec(17))^2)+param.K_C_EtOH)))
32 +(1/param.tau)*(sqrt((hydrosolvec(1))^2)-sqrt((hydrosolvec(7))^2)));
33 sol(4) = ((-1)*param.k_exo*(sqrt((hydrosolvec(6))^2)/(1+param.sigma_exo))*
34 (param.K_C_Cb/(sqrt((hydrosolvec(13))^2)+param.K_C_Cb))*(param.K_C_EtOH/
35 (sqrt((hydrosolvec(13))^2)+param.K_C_EtOH)))+(1/param.tau)*
36 ((param.frac_exo_sites_C_in*param.c_C_in)-sqrt((hydrosolvec(8))^2)));
37 sol(5) = sqrt((hydrosolvec(7))^2+sqrt((hydrosolvec(8))^2)-
38 sqrt((hydrosolvec(3))^2);
39 sol(6) = (param.k_fc*sqrt((hydrosolvec(9))^2)*sqrt((hydrosolvec(10))^2)*
40 (1+param.sigma_endo))-(sqrt((hydrosolvec(5))^2)*((param.k_fc/param.K_endo)+
41 (1/param.tau)));
42 sol(7) = (param.k_fc*sqrt((hydrosolvec(11))^2)*sqrt((hydrosolvec(12))^2)*
43 (1+param.sigma_exo))-(sqrt((hydrosolvec(6))^2)*((param.k_fc/param.K_exo)+
44 (1/param.tau)));
45 sol(8) = param.c_E_b_endo-((sqrt((hydrosolvec(5))^2)*
46 param.sigma_endo/(1+param.sigma_endo))+sqrt((hydrosolvec(9))^2));

```

```

47 sol(9) = param.c_E_b_exo-((sqrt((hydrosolvec(6))^2)*
48 param.sigma_exo/(1+param.sigma_exo))+sqrt((hydrosolvec(11))^2));
49 sol(10) = sqrt((hydrosolvec(7))^2)-((sqrt((hydrosolvec(5))^2)/
50 (1+param.sigma_endo))+sqrt((hydrosolvec(10))^2));
51 sol(11) = sqrt((hydrosolvec(8))^2)-((sqrt((hydrosolvec(6))^2)/
52 (1+param.sigma_endo))+sqrt((hydrosolvec(12))^2));
53 sol(12) = ((342/324)*sqrt((hydrosolvec(4))^2))+((param.K_Cb*
54 sqrt((hydrosolvec(13))^2)*param.c_E_b_BG/((param.K_m*
55 (1+(sqrt((hydrosolvec(14))^2)/param.K_Cb_G)))+(sqrt((hydrosolvec(13))^2))))
56 -(sqrt((hydrosolvec(13))^2)/param.tau));
57 sol(13) = ((360/342)*(param.K_Cb*sqrt((hydrosolvec(13))^2)*
58 param.c_E_b_BG/((param.K_m*(1+(sqrt((hydrosolvec(14))^2)/param.K_Cb_G)))+(
59 sqrt((hydrosolvec(13))^2))))-((sqrt((hydrosolvec(15))^2)/param.Y_X_Y_G)+
60 (sqrt((hydrosolvec(14))^2)/param.tau));
61 sol(14) = ((param.mu_max_Y*sqrt((hydrosolvec(14))^2)/(param.K_G+
62 sqrt((hydrosolvec(14))^2)))*sqrt((hydrosolvec(16))^2)*
63 (1-(sqrt((hydrosolvec(17))^2)/param.K_X_EtOH)))-sqrt((hydrosolvec(15))^2);
64 sol(15) = sqrt((hydrosolvec(15))^2)-(sqrt((hydrosolvec(16))^2)/param.tau);
65 sol(16) = ((param.Y_EtOH_G/param.Y_X_Y_G)*sqrt((hydrosolvec(15))^2))-
66 (sqrt((hydrosolvec(17))^2)/param.tau);
67
68 end

```

```

1 %% Plot commands
2 figure()
3 surf(z_axis,r_axis,O2);
4 colorbar;
5 axis ij;
6 % set(gca,'zscale','log')
7 title('Oxygen concentration profile across the membrane reactor');
8 xlabel('Membrane length [m]');
9 ylabel('Radius [m]');
10 zlabel('Oxygen concentration [g/L]');
11
12 figure()
13 surf(z_axis,r_axis,X_tr);
14 colorbar;
15 axis ij;
16 %set(gca,'zscale','log')
17 title...
18 ('Fungal biomass concentration profile across the membrane reactor');
19 xlabel('Membrane length [m]');
20 ylabel('Radius [m]');
21 zlabel('Fungal biomass concentration [g/L]');
22
23 figure()

```



```
24 surf(z_axis,r_axis,X_tr_sec);
25 colorbar;
26 axis ij;
27 %set(gca,'zscale','log')
28 title...
29 ('Secondary mycelia concentration profile across the membrane reactor');
30 xlabel('Membrane length [m]');
31 ylabel('Radius [m]');
32 zlabel('Secondary mycelia concentration [g/L]');
33
34 figure()
35 surf(z_axis,r_axis,E);
36 colorbar;
37 axis ij;
38 %set(gca,'zscale','log')
39 title('Enzyme concentration profile across the membrane reactor');
40 xlabel('Membrane length [m]');
41 ylabel('Radius [m]');
42 zlabel('Enzyme concentration [g/L]');
43
44 figure()
45 surf(z_axis,r_axis,Cb);
46 colorbar;
47 axis ij;
48 %set(gca,'zscale','log')
49 title('Cellobiose concentration profile across the membrane reactor');
50 xlabel('Membrane length [m]');
51 ylabel('Radius [m]');
52 zlabel('Cellobiose concentration [g/L]');
53
54 figure()
55 surf(z_axis,r_axis,G);
56 colorbar;
57 axis ij;
58 %set(gca,'zscale','log')
59 title('Glucose concentration profile across the membrane reactor');
60 xlabel('Membrane length [m]');
61 ylabel('Radius [m]');
62 zlabel('Glucose concentration [g/L]');
63
64 figure()
65 surf(z_axis,r_axis,X_y);
66 colorbar;
67 axis ij;
68 %set(gca,'zscale','log')
69 title('Yeast concentration profile across the membrane reactor');
70 xlabel('Membrane length [m]');
```

```

71 ylabel('Radius [m]');
72 zlabel('Yeast concentration [g/L]');
73
74 figure()
75 surf(z_axis,r_axis,EtOH);
76 colorbar;
77 axis ij;
78 %set(gca,'zscale','log')
79 title('Ethanol concentration profile across the membrane reactor');
80 xlabel('Membrane length [m]');
81 ylabel('Radius [m]');
82 zlabel('Ethanol concentration [g/L]');
83
84 % figure()
85 % plot(r_axis,mu_tr,'o')
86 % % plot(r_axis,c_O2_z_L,'-')
87 x1=zeros(geo.M,1);
88 for i=1:geo.M
89 x1(i)=(i-1)*geo.dz;
90 end
91 y1=100*O2(2,:)./(1/param.n_ox_m)*O2(2,1));
92 figure()
93 plot(x1,y1,'-')
94 title('Oxygen saturation in PDMS over membrane length');
95 xlabel('Membrane length [m]');
96 ylabel('Oxygen saturation [%]');

```

```

1  if param.Re_m>param.Re_crit
2      disp('Fully developed turbulent flow!')
3      disp('Corresponding Nusselt/Sherwood correlations are applied')
4  end
5  if param.Re_m<2300
6      disp('Fully developed laminar flow! Corresponding Nusselt/')
7      disp('Sherwood correlations are applied')
8  end
9  if param.Re_m>2300 && param.Re_m<param.Re_crit
10     disp('Transient flow! All quantities are calculated by')
11     disp('interpolation between laminar flow at Re_m=2300')
12     disp('and turbulent flow at Re_m=Re_crit')
13 end
14 if param.Re_m>10^5 || param.Re_m<1
15     disp('Expression for pressure loss not valid!')
16     disp('Nusselt/Sherwood correlations for turbulent flow are valid')
17 end
18
19 if param.Re_m>param.Re_crit

```

```

20     zeta=(0.3164/(param.Re_m^0.25))*...
21         (1+(0.095*sqrt(geo.d_t_i/geo.d_curv)*(param.Re_m^0.25)));
22     %friction factor for helical coils
23 end
24 if param.Re_m<=2300
25     zeta=(64/param.Re_m)*(1+(0.033*...
26         (((log10(param.Re_m*sqrt(geo.d_t_i/geo.d_curv)))^4)))));
27     %friction factor for helical coils [-]
28 end
29 if Re_m>2300 && Re_m<Re_crit
30     p_loss=((Re_m-2300)/(Re_crit-2300))*((((0.3164/(Re_crit^0.25))*...
31         (1+(0.095*sqrt(di_m/d_curv)*(Re_crit^0.25))))*(L_m/di_m)*...
32         (0.5*rho_w_m*(u_m^2)))))-...
33         (((64/2300)*(1+(0.033*(((log10(2300*sqrt(di_m/d_curv)))^4)))))...
34         *(L/di_m)*(0.5*rho_m*(u_m^2)))))+(((64/2300)*(1+(0.033*...
35         (((log10(2300*sqrt...
36         (di_m/d_curv)))^4)))))*(L/di_m)*(0.5*rho_m*(u_m^2)));
37 %interpolated pressure loss [Pa]
38 end
39
40
41
42 % Nusselt correlations according to VDI heat atlas chapter G1
43
44 if param.Re_m>=param.Re_crit
45     Xi=((1.8*log10(param.Re_m))-1.5)^(-2);
46     %factor for Nusselt correlation [-]
47     Nu_m=((0.125*Xi*param.Re_m*param.Pr_m)/(1+(12.7*sqrt(0.125*Xi)*...
48         ((param.Pr_m^(2/3))-1))))*(1+((geo.d_t_i/geo.l_t)^(2/3)));
49     %Nusselt number for inner membrane flow & medium [-]
50     Sh_m=((0.125*Xi*param.Re_m*param.Sc_m)/(1+(12.7*sqrt(0.125*Xi)*...
51         ((param.Sc_m^(2/3))-1))))*(1+((geo.d_t_i/geo.l_t)^(2/3)));
52     %Sherwood number for inner membrane flow & medium [-]
53 end
54
55 if param.Re_m<=2300
56     Nu_m=((3.66^3)+0.343+(((1.615*((param.Re_m*param.Pr_m*...
57         (geo.d_t_i/geo.l_t))^(1/3))-0.7)^3))^(1/3);
58     %Nusselt number for inner membrane flow & medium [-]
59     %(under assumption of a long pipe)
60     Sh_m=((3.66^3)+0.343+(((1.615*((param.Re_m*param.Sc_m*...
61         (geo.d_t_i/geo.l_t))^(1/3))-0.7)^3))^(1/3);
62     %Sherwood number for inner membrane flow & medium [-]
63     %(under assumption of a long pipe)
64 end
65
66 if param.Re_m>2300 && param.Re_m<param.Re_crit

```

```

67     Nu_m=((param.Re_m-2300)/(param.Re_crit-2300))*...
68         (((0.125*((1.8*log10(param.Re_crit))-1.5)^(-2))*...
69         param.Re_crit*param.Pr_m)/(1+(12.7*sqrt(0.125*((1.8*...
70         log10(param.Re_crit))-1.5)^(-2)))*((param.Pr_m^(2/3))-1))))*...
71         (1+((geo.d_t_i/geo.l_t)^(2/3)))-4.364))+4.364;
72     %Nusselt number for inner membrane flow & medium [-]
73     Sh_m=((param.Re_m-2300)/(param.Re_crit-2300))*...
74         (((0.125*((1.8*log10(param.Re_crit))-1.5)^(-2))*...
75         param.Re_crit*param.Sc_m)/(1+(12.7*sqrt(0.125*((1.8*...
76         log10(param.Re_crit))-1.5)^(-2)))*((param.Sc_m^(2/3))-1))))*...
77         (1+((geo.d_t_i/geo.l_t)^(2/3)))-4.364))+4.364;
78     %Sherwood number for inner membrane flow & medium [-]
79 end
80
81 % Chilton-Colburn mass transfer analogy
82 %Sh_m=Nu_m*((Sc_m/Pr_m)^(1/3));
83 k_conv_ox_m=Sh_m*param.D_O2_m/geo.d_t_i;
84 k_conv_E=6e-6;
85
86
87 %Sherwood correlation for enzymes biofilm bulk boundary layer
88 Sh_v_lam_E=0.664*sqrt(param.Re_v)*(param.Sc_v_E^(1/3));
89 Sh_v_turb_E=0.037*(param.Re_v^0.8)*param.Sc_v_E/(1+(2.443*...
90     (param.Re_v^(-0.1))*((param.Sc_v_E^(2/3))-1)));
91 Sh_v_E=0.3+sqrt((Sh_v_lam_E^2)+(Sh_v_turb_E^2));
92 char_L_v=geo.h_wind*geo.l_t/(pi*geo.d_wind);
93 k_conv_E_v=Sh_v_E*chem.D_w_E/char_L_v;

```

## APPENDIX C

---

### Supplementary material for chapter 6: Evaluation of *in-situ* product removal strategies to improve the productivity and economics of consolidated bioprocessing

---

#### C.1 Calculations for CO<sub>2</sub> stripping

```
1  %%%%%%%%%%%%%%%%%%%%%%%%%%%%%%%%%%%%%%%%%%%%%%%%%%%%%%%%%%%%%%%%%%%%%%%%%%
2  % Name:      CO2stripping.m
3  % Author:    Philipp Stampfli
4  % E-Mail:    stamphil@student.ethz.ch
5  % Date:      11. July 2018
6  % Update:    06.08.18
7  %
8  % Purpose:   Calculating the needed CO2-gas flow for stripping out the EtOH
9  %            from the fermentation broth. In a 2nd step the design criteria
10 %            for the bioreactor to reach the desired stripping effect
11 %            (residence time of bubbles in the liquid)
12 % Notes:     -...
13 % References: -...
14 %%%%%%%%%%%%%%%%%%%%%%%%%%%%%%%%%%%%%%%%%%%%%%%%%%%%%%%%%%%%%%%%%%%%%%%%%%
15
16 clear all
17 clc
18
19 %% Properties incoming stream and reactor volume
20
21 m_EtOH=21941/3600;%31.907/3600; % [kg/s], mass stream of EtOH generated
22 m_H2O=378525/3600;%234.594/3600; %[kg/s], mass stream of H2O total leaving
23 m_CO2=20955/3600;%33.833/3600; %[kg/s], mass stream of CO2 generated
```

```

24 m_in=450740/3600;%368.506/3600; %[kg/s], mass stream in reactor
25
26 p_reac=1.013; %[bar], pressure in reactor
27 T_reac=28+273;%50+273; %[K], temperature in reactor
28 V_reac=7*3785.411;%44.221; %[m3], total volume of reactors
29 V_ves=V_reac/7;%V_reac/5; %[m3], volume of each reactor vessel
30
31 %% specifications
32
33 FRg_EtOH=0.0001:0.0001:0.99; % mass recovery of EtOH in gas stream
34 lFR=length(FRg_EtOH);
35 %% conversion in moleflows and fractions
36 n_EtOH=m_EtOH/0.046; %[mol/s], mole flow of EtOH generated
37 n_CO2=m_CO2/0.044; %[mol/s], mole flow of CO2 generated
38 n_H2O=m_H2O/0.018; %[mol/s], mole flow of H2O total leaving
39
40 L=m_EtOH+m_H2O;
41 Ln=n_EtOH+n_H2O;
42
43 z_EtOH=m_EtOH/L;
44 z_H2O=m_H2O/L;
45
46 zn_EtOH=n_EtOH/Ln;
47 zn_H2O=n_H2O/Ln;
48
49 %% physiochemical constants
50 H_EtOH=4.7*exp(13/(1.9872*10^(-3))*(1/T_reac-1/298))*1000;
51 %Henry constant of Ethanol in water according to Snider et Dawson, 1985
52 KH_CO2=HenryCO2(zn_EtOH,T_reac);
53
54 %density of fluid: assumption all density same as the one for water
55 %density of vanillin (assumption for lignin from NREL) is 1060 kg/m3
56 %so all can be assumed as same density as water
57 rho_l=1000; %[kg/m3]
58
59 % density CO2
60 rho_g=0.044*p_reac*10^5/(8314*T_reac);
61 %surface tension of EtOH/water mixture (Khattab et al., 2012)
62 sigma_l=48.37+(zn_EtOH-0.033)*(38.77-48.37)/(0.072-0.033);
63
64 % shear rate according to NV Pimenove et al., 2004
65 % shear=K*N, where N [rps] of mixer
66 shear(1)=10.8*300/60;
67 shear(2)=10.8*500/60;
68 shear(3)=10.8*1100/60;
69 % viscosity of slurry (non-newtonian) from NV Pimenova et al., 2004
70 % mu_l= Tau/shear=K2*shear^(n-1)

```

```
71 mu_l(1)=1.87*shear(1)^(0.91-1);
72 mu_l(2)=1.87*shear(2)^(0.91-1);
73 mu_l(3)=1.87*shear(3)^(0.91-1);
74
75 % gravity constant
76 g=9.81; %[m/s]
77 %% CO2 absorbed in liquid phase
78 xn_CO2=p_reac/KH_CO2;
79 absn_CO2=xn_CO2*Ln;
80 absm_CO2=absn_CO2*0.044;
81 x_CO2=absm_CO2/L;
82 %% Partition Coefficient K_pLG acc. to Loser et al. 2005
83
84 % Loser et al. are calculating in their paper the partition coefficient as
85 % follows:
86 %
87 %  $K_{pLG} = (p_0 \cdot T_G \cdot \rho_{wL} \cdot v_0) / (p_{vapEtOH} \cdot T_0 \cdot \gamma_{EtOH} \cdot M_w)$ ;
88 %
89 % unit of partition coefficient is: [-]
90 % where:
91 %  $T_G = T_{reac}$ 
92
93 p0=1.01325; %[bar], used same as for Loser et al.
94 T0=273; %[K], acc. to Loser et al.
95 v0=22.41; %[L/mole], acc. to Loser et al.
96 Mw=18; %[g/mole], MW of water
97 rho_wL=1000; %[g/l], density of water, same as used by Loser et al.
98 pvapEtOH=pvapEtOH(T_reac); %[bar], saturation pressure @T_reac
99 [gamEtOH,gamH2O]=unifac(zn_EtOH,T_reac); %activity coefficients
100
101 K_pLG=p0*T_reac*rho_wL*v0/(pvapEtOH*T0*gamEtOH*Mw);
102
103 %% gas stream needed Fg needed to remove the ETOH
104 Fg=zeros(3,1FR);
105 ng_CO2=zeros(3,1FR);
106 mg_CO2=zeros(3,1FR);
107
108 Fg_avg=zeros(1,1FR);
109 ngavg_CO2=zeros(1,1FR);
110 mgavg_CO2=zeros(1,1FR);
111
112 % massbalance acc. Ponce et al. 2016:
113 %
114 %  $dP/dt = r_p - r_{ps}$  (1), where it is for a batch process
115 % P=concentration of EtOH inside vessel, [kg/m3]
116 %  $r_p$ : produced EtOH
117 %  $r_{ps}$ : removed EtOH by stripping with CO2
```

```

118 %
119 % since a continuous process is at steady state and the concentration
120 % inside the vessel is always equal the final concentration (assumption of
121 % perfect mixing), the production rate times the volume
122 % ( $r_p \cdot V_{\text{reac}}/t$ ) is equal to the total produced ethanol
123 %
124 %  $dP/dt = 0 = r_p - r_{ps} - r_{pL}$  (2)
125 %  $r_{pL}$  = rate of EtOH leaving with the liquid stream
126 %
127 % Loser et al. formulated the eqn (2) in dependendcy of stripping rate and
128 % dilution rate:
129 %
130 %  $dP/dt = -[r_{ps}/(P+D)] \cdot P + r_p$  (3)
131 % where D is the dilution rate:  $D = F_l/V_{\text{reac}}$ 
132 % and  $F_l$  is the incoming liquid stream ( $F_l = L/\rho_{\text{in}}$ )
133  $F_l = L/\rho_{\text{in}}$ ;
134  $D = F_l/V_{\text{reac}}$ ;
135 %
136 % Loser et al. brought the definitions for the stripping rate:
137 %
138 %  $r_{ps} = [(F_g \cdot k_{\text{pla}}) / (F_g + V_{\text{reac}} \cdot k_{\text{pla}} \cdot K_{\text{pLG}})] \cdot P$  (4)
139 %
140 % we can now combine eq (3) and (4) resulting in:
141 %
142 %  $dP/dt = -[(F_g \cdot k_{\text{pla}}) / (F_g + V_{\text{reac}} \cdot k_{\text{pla}} \cdot K_{\text{pLG}}) + D] \cdot P + r_p$ 
143 %
144 % the fractional recovery is defined as:
145 %
146 %  $FR = m_{\text{eg}} / (m_{\text{eg}} + m_{\text{el}}) = m_{\text{eg}} / m_{\text{EtOH}}$ 
147 %
148 % with  $m = F \cdot C$  and  $C_{\text{eg}} = r_{ps}$  we get:
149 %
150 %  $FR = 1 / (1 + D \cdot [1/k_{\text{pla}} + V_{\text{reac}} \cdot K_{\text{pLG}}/F_g])$  (5)
151 %
152 % For checking, if a desired recovery is feasible, one need so to take the
153 % limit for infinit gasstream. We then get:
154 %
155 %  $FR = 1 / (1 + D/k_{\text{Pla}})$ , the dilution rate is give, so we can calculate the
156 % minimum masstransfer coefficient:
157 for i=1:lFR
158  $k_{\text{plamin}} = D \cdot FR_{\text{EtOH}}(i) / (1 - FR_{\text{EtOH}}(i));$ 
159 %
160 % the only unknown in this eq. is the variable of  $k_{\text{pla}}$ . This can be
161 % calculated by the empirical correlation of Truong et Blackburn (1984)
162 % for volatile organic components:
163 %
164 %  $k_{\text{pla}} \cdot V_{\text{reac}}/F_g = b \cdot (H_c)^m$ , with  $b = 0.0093$  and  $m = 0.872$ 

```



```

165 % k_pla=(Fg/V_reac)*0.0093*(H_c)^0.872=(Fg/V_reac)*H_tild (9)
166 % H_tild=0.0093*(H_c)^0.872;
167 H_tild=0.0093*(H_EtOH)^0.872;
168 %
169 % H_c is the dimensionless solubility of the
170 % organic compound (EtOH) in water and can be
171 % calculated by the approach of Snider et al (cf. calculation of H_EtOH)
172 % We can plug eq (9) in eq(8) and then by rearranging we get a dependency
173 % of the variable Fg:
174 %
175 % Fg=V_reac*(1/H_tild+K_pLG)/((1-FRg_EtOH)*1/(FRg_EtOH*D));
176 Fg(1,i)=V_reac*(1/H_tild+K_pLG)/((1-FRg_EtOH(i))*1/(FRg_EtOH(i)*D));
177
178 % Alternatively, the mass transfer coefficient (MTC)
179 % can be calculated according
180 % to the calculations of Loser et al. They determined the mass transfer
181 % coefficient for O2 for different stirring rates and stated that the
182 % MTC is only dependent on the
183 % diffusion coefficient of the component.
184 %
185 % k_elA=k_O2a*D_EtOH/D_O2
186 %
187 % The diffusion coefficient for ethanol can be calculated for another
188 % temperature according to the Einstein law:
189 % D_iT2=D_iT1*(T2/T1)
190 D_O2=2.6*10^(-9); %[m2/s]
191 D_EtOH=1.3*10^(-9)*T_reac/303; %[m2/s]
192 k_elA500=130/3600*D_EtOH/D_O2; %[1/s]
193 k_elA1100=350/3600*D_EtOH/D_O2; %[1/s]
194
195 if k_elA500<k_plamin
196     warning('mass transfer coefficient k_elA500 lower than the minimum')
197     warning('mass transfer coefficient! The specifications cannot be met,')
198     warning('please adjust specs or conditions')
199 end
200 if k_elA1100<k_plamin
201     warning('mass transfer coefficient k_elA1100 lower than the minimum')
202     warning('mass transfer coefficient! The specifications cannot be met,')
203     warning('please adjust specs or conditions')
204 end
205 % Using these MTCs, we can rearrange eqn (5):
206 % Fg2=V_reac*K_pLG/((1-FR)*1/(FR*D)-1/k_pla)
207 Fg(2,i)=V_reac*K_pLG/((1-FRg_EtOH(i))*1/(FRg_EtOH(i)*D)-1/k_elA500);
208 Fg(3,i)=V_reac*K_pLG/((1-FRg_EtOH(i))*1/(FRg_EtOH(i)*D)-1/k_elA1100);
209 % calculation of required mass stream by applying the ideal gas law with
210 % V=Fg
211 ng_CO2(1,i)=p_reac*10^5*Fg(1,i)/(8.312*T_reac)-n_CO2; %[mole/s],

```

```

212 % mole stream required of CO2
213 mg_CO2(1,i)=ng_CO2(1,i)*0.044; %[kg/s], mass stream required of CO2
214
215 ng_CO2(2,i)=p_reac*10^5*Fg(2,i)/(8.312*T_reac)-n_CO2; %[mole/s],
216 % mole stream required of CO2
217 mg_CO2(2,i)=ng_CO2(2,i)*0.044; %[kg/s], mass stream required of CO2
218
219 ng_CO2(3,i)=p_reac*10^5*Fg(3,i)/(8.312*T_reac)-n_CO2; %[mole/s],
220 % mole stream required of CO2
221 mg_CO2(3,i)=ng_CO2(3,i)*0.044; %[kg/s], mass stream required of CO2
222
223 %averaged
224 Fg_avg(i)=(Fg(1,i)+Fg(2,i)+Fg(3,i))/3;
225 ngavg_CO2(i)=p_reac*10^5*Fg_avg(i)/(8.312*T_reac);%-n_CO2; %[mole/s],
226 % mole stream required of CO2
227 mgavg_CO2(i)=ngavg_CO2(i)*0.044; %[kg/s], mass stream required of CO2
228 end
229 %% amount of water stripped off
230 % applying same steps as for EtOH, we result in same eqns.
231
232 pvapH2O=pvapH2O(T_reac);
233 % partition coefficient for water
234 K_HLG=p0*T_reac*rho_wL*v0/(pvapH2O*T0*gamH2O*Mw);
235
236 % mass transfer coefficient
237 DH2O=3.89310^(-9); %[m2/s]
238 k_hla500=130/3600*DH2O/D_O2; %[1/s]
239 k_hla1100=350/3600*DH2O/D_O2; %[1/s]
240
241 %fractional recoveries
242 FRgH2O=zeros(2,1FR);
243 % mass recovered
244 mg_H2O=zeros(2,1FR);
245 mgavg_H2O=zeros(1,1FR);
246
247 for i=1:1FR
248     FRgH2O(1,i)=1/(1+D*(1/k_hla500+V_reac*K_HLG/Fg(2,i)));
249     mg_H2O(1,i)=m_H2O*FRgH2O(1,i);
250
251     FRgH2O(2,i)=1/(1+D*(1/k_hla1100+V_reac*K_HLG/Fg(3,i)));
252     mg_H2O(2,i)=m_H2O*FRgH2O(2,i);
253
254     mgavg_H2O(i)=(mg_H2O(1,i)+mg_H2O(2,i))/2;
255 end
256
257 %% plot the results for the gasstream
258 figure

```

```
259 yyaxis left
260 plot(FRg_EtOH,mgavg_CO2,'m-','LineWidth',1)
261 xlabel('mass recovery of ethanol [-]')
262 ylabel('CO2 mass flow required [kg/s]')
263 axis([0 1 0 16])
264
265 yyaxis right
266 plot(FRg_EtOH,mgavg_H2O,'c--','LineWidth',1)
267 ylabel('recovered water mass flow [kg/s]')
268
269 title('required gasstream and recovered water in gas phase')
270 legend('CO2', 'water in gas recovered')
271
272 %% concentration of EtOH in gas stream w & w/o CO2
273 y_EtOH=zeros(3,lFR); %mass(1&2,:) and mole fraction (3,:)
274 % fraction of water in gasstream
275 y_H2O=zeros(3,lFR); %mass (1&2,:) and mole (3,:)
276 % fraction of EtOH on gasstream
277 for i=1:lFR
278     y_EtOH(1,i)=FRg_EtOH(i)*m_EtOH/(FRg_EtOH(i)*m_EtOH+mgavg_H2O(i));
279     y_EtOH(2,i)=FRg_EtOH(i)*m_EtOH/(FRg_EtOH(i)*m_EtOH+mgavg_H2O(i)...
280         +mgavg_CO2(i));
281     y_EtOH(3,i)=FRg_EtOH(i)*m_EtOH*0.046/(FRg_EtOH(i)*m_EtOH*0.046+...
282         mgavg_H2O(i)*0.018+mgavg_CO2(i)*0.044);
283     y_H2O(1,i)=mgavg_H2O(i)/(FRg_EtOH(i)*m_EtOH+mgavg_H2O(i));
284     y_H2O(2,i)=mgavg_H2O(i)/(FRg_EtOH(i)*m_EtOH+mgavg_H2O(i)+mgavg_CO2(i));
285     y_H2O(3,i)=mgavg_H2O(i)*0.018/(FRg_EtOH(i)*m_EtOH*0.046+...
286         mgavg_H2O(i)*0.018+mgavg_CO2(i)*0.044);
287 end
288
289 %% plot of concentration vs. fractional recovery
290 figure
291 yyaxis left
292 plot(FRg_EtOH,mgavg_CO2,'m-','LineWidth',1)
293 ylabel('mass flow [kg/s]')
294 yyaxis right
295 plot(FRg_EtOH,y_EtOH(1,:), 'b--','LineWidth',1)
296 hold on
297 plot(FRg_EtOH,y_EtOH(2,:), 'b-','LineWidth',1)
298 hold off
299 xlabel('mass recovery of ethanol [-]')
300 ylabel('concentration [-]')
301 axis([0 1 0 1])
302 title('m_{CO_{2},min} & y_{EtOH}')
303 legend('m_{CO_{2},min}', 'y_{EtOH} w/o CO_2', 'y_{EtOH} w CO_2')
304
305 figure
```

```

306 yyaxis left
307 plot(FRg_EtOH,mgavg_CO2,'m-','LineWidth',1)
308 ylabel('mass flow [kg/s]')
309 yyaxis right
310 plot(FRg_EtOH,y_EtOH(1,:), 'b--','LineWidth',1.5)
311
312 xlabel('mass recovery of ethanol [-]')
313 ylabel('concentration [-]')
314
315 title('m_{CO_{2},min} & y_{EtOH}')
316 legend('m_{CO_{2},min}','y_{EtOH}')
317 %% max. mole fraction in gasphase
318 y_H2Osat=pvapH2O/p_reac;
319 y_EtOHsat=pvapEtOH/p_reac;
320 y_CO2sat=1-y_H2Osat-y_EtOHsat;
321 y_CO2=zeros(1,lFR);
322 for i=1:lFR
323     if y_EtOH(3,i)≥y_EtOHsat %check if calculated concentrations
324         % are lower than saturated
325         warning('mole fraction of EtOH above saturated mole fraction!')
326         disp('this element is above:')
327         i
328         y_EtOH(3,i)
329         disp('For the desired fractional recovery:')
330         FRg_EtOH(i)
331     end
332
333     if y_H2O(3,i)≥y_H2Osat %check if calculated concentrations
334         % are lower than saturated
335         warning('mole fraction of H2O above saturated mole fraction!')
336         disp('this element is above:')
337         i
338         y_H2O(3,i)
339         disp('For the desired fractional recovery:')
340         FRg_EtOH(i)
341     end
342     y_CO2(i)=1-y_EtOH(3,i)-y_H2O(3,i);
343 end
344
345 %% gas and bubble characteristics
346 wg_max=0.05; %[m/s], max superficial gas velocity for
347 % bubbly flow regime (Kantarci et al, 2005)
348 epsg=zeros(1,3); %[], gas hold up
349 w0g=zeros(1,3); %[m/s], interstitial gas velocity
350 wb=zeros(1,3); %[m/s], bubble rise velocity
351 Db=zeros(1,3); %[m], bubble diameter
352

```

```

353 for n=1:3
354     epsg(n)=(2.25+0.379/wg_max*(rho_l/72)^0.31*mu_l(n)^.016)^(-1);
355     %gas holdup correlation acc. to smith et al.
356 %     for aqn alcohol with solids
357     w0g(n)=epsg(n)*wg_max;
358     wb(n)=wg_max*(1-epsg(n))^1.75;
359     %bubble velocity according to Ishii and Zuber (1979) where  $\mu_l > \mu_g$ 
360
361     %iteration for bubble diameter calculation via direct
362     %substitution method and function call
363     Db(n)=bubDia2(wb(n),rho_g,rho_l,mu_l(n),sigma_l);
364 %     DbH(1)=10^(-3); %help variable for diameter [m]
365 %     Re=wb(n)*rho_l*DbH(1)/mu_l(n); %Reynolds number for bubble
366 %
367 %     %calculation of drag coefficient according to lecture
368 %     %multiphase flow
369 %     if Re<2.2 % rigid sphere (stokes)
370 %         cD=24/Re;
371 %     end
372 %     if Re>2.2 && Re<4.02*(rho_l*sigma_l^3/(g*mu_l(n)^4))^0.214
373 %internal circulation
374 %         cD=18.7/Re^0.68;
375 %     end
376 %     if Re>4.02*(rho_l*sigma_l^3/(g*mu_l(n)^4))^0.214 && Re<3.1*...
377 % (rho_l*sigma_l^3/(g*mu_l(n+1)^4))^0.25 %flattening
378 %         cD=0.366*g*rho_l*DbH(1)^2/(sigma_l);
379 %     end
380 %     if Re>3.1*(rho_l*sigma_l^3/(g*mu_l(n)^4))^0.25 %cap shaped bubbles
381 %         cD=2.61;
382 %     end
383 %
384 %     DbH(2)=3*rho_l*wb(n)^2*cD/(4*(rho_l-rho_g)*g);
385 %help variable no2 for bubble diameter [m]
386 %     diffD=abs(DbH(1)-DbH(2));
387 %
388 %     while abs(diffD)>10^(-6)
389 %         DbH(1)=DbH(2);
390 %         Re=wb(n)*rho_l*DbH(1)/mu_l(n); %Reynolds number for bubble
391 %
392 %         %calculation of drag coefficient according to lecture
393 %         %multiphase flow
394 %         if Re<2.2 % rigid sphere (stokes)
395 %             cD=24/Re;
396 %         end
397 %         if Re>2.2 && Re<4.02*(rho_l*sigma_l^3/(g*mu_l(n)^4))^0.214
398 %internal circulation
399 %             cD=18.7/Re^0.68;

```

```

400 %           end
401 %           if Re>4.02*(rho_l*sigma_l^3/(g*mu_l(n)^4))^0.214 && ...
402 % Re<3.1*(rho_l*sigma_l^3/(g*mu_l(n)^4))^0.25 %flattening
403 %           cD=0.366*g*rho_l*DbH(1)^2/(sigma_l);
404 %           end
405 %           if Re>3.1*(rho_l*sigma_l^3/(g*mu_l(n)^4))^0.25 %cap shaped bubbles
406 %           cD=2.61;
407 %           end
408 %
409 %           DbH(2)=3*rho_l*wb(n)^2*cD/(4*(rho_l-rho_g)*g);
410 %           diffD=abs(DbH(2)-DbH(1));
411 %       end % while diffD>10^-6
412 %       Db(n)=DbH(2);
413
414 %Volume of the bubble [m3]
415 Vb(n)=4/3*pi*(Db(n)/2)^3;
416 end %for n=0:2
417
418 %% Masstransfer
419
420 for n=1:3
421     ng_CO2(n)=p_reac*Vb(n)/(8.314*T_reac);
422     %total amount of CO2 moles in bubble
423     n_sat(n)=ng_CO2(n)/y_CO2sat; %total amount of moles at saturation
424     ng_EtOHsat(n)=y_EtOHsat*n_sat(n);
425     %total amount of EtOH moles at saturation
426     Vbsat(n)=Vb(n)/(1-y_EtOHsat-y_H2Osat); %volume of bubble at saturation
427     Csat(n)=ng_EtOHsat/Vbsat; %[mole/m3], EtOH concentration at saturation
428 end
429
430 t=zeros(3,lFR); %[s], time required to reach desired concentration
431 ng_EtOH=zeros(3,lFR); %moles of EtOH at end of column
432 n_reac=zeros(3,lFR); %final amount of moles
433 Vb_reac=zeros(3,lFR); %final volume of bubble
434 C=zeros(3,lFR); %[mole/m3], final concentration of EtOH
435 for i=1:lFR
436     for n=1:3
437         n_reac(n,i)=ng_CO2(n)/y_CO2(i);
438         ng_EtOH(n,i)=y_EtOH(3,i)*n_reac(n,i);
439         Vb_reac(n,i)=Vb(n)/(1-y_EtOH(3,i)-y_H2O(3,i));
440         C(n,i)=ng_EtOH(n,i)/Vb_reac(n,i);
441         if n==1
442             kla=Fg_avg(i)/V_reac*H_tild;
443         end
444         if n==2
445             kla=k_ela500;
446         end

```

```

447         if n==3
448             kla=k_ela1100;
449         end
450         t(n,i)=1/kla*(1-log(C(n,i)/Csat(n)));
451     end
452 end
453
454 %% column sizing
455 Hmin=zeros(3,lFR);
456 %[m], minimum height of column according to mass transfer
457 Hmax=zeros(3,lFR);
458 %[m], maximum height of column according towards volume specifications
459 Amin=zeros(3,lFR);
460 %[m2], minimum crosssectional area according to flow regime limitations
461 Dmin=zeros(3,lFR); %[m], minimum diameter
462
463 max=zeros(1,3);
464 maxH=zeros(1,3);
465 for i=1:lFR
466     for n=1:3
467         Amin(n,i)=Fg_avg(i)/(5*wg_max);
468         Dmin(n,i)=2*sqrt(Amin(n,i)/pi);
469         Hmax(n,i)=V_ves/Amin(n,i);
470         % Hmin1(n,i)=t(n,i)*wOg(n);
471         Hmin(n,i)=t(n,i)*wb(n);
472         delthH=abs(Hmax(n,i)-Hmin(n,i));
473         if delthH<10^(-3)
474             max(n)=FRg_EtOH(i);
475             maxH(n)=Hmax(n,i);
476         end
477     end
478 end
479
480 %% plotting sizing results
481
482 figure
483 subplot(3,1,1)
484 yyaxis left
485 plot(FRg_EtOH,Dmin(1,:), '--g', 'LineWidth',1)
486 title('column sizes for 300 rpm')
487 xlabel('Fractional recovery of Ethanol')
488 ylabel('Column Diameter [m]')
489 axis([0 1 0 20])
490 yyaxis right
491 plot(FRg_EtOH,Hmin(1,:), ':b', 'LineWidth',1.5)
492 hold on
493 plot(FRg_EtOH, Hmax(1,:), ':c', 'LineWidth',1.5)

```

```

494 plot(max(1),maxH(1),'-rh','LineWidth',1)
495 ylabel('Column Height [m]')
496 legend('Diameter','Min. Height','Max Height','Max possible')
497 axis([0 1 0 20])
498 hold off
499
500 subplot(3,1,2)
501 yyaxis left
502 plot(FRg_EtOH,Dmin(2,:),'--g','LineWidth',1)
503 title('column sizes for 500 rpm')
504 xlabel('Fractional recovery of Ethanol')
505 ylabel('Column Diameter [m]')
506 axis([0 1 0 20])
507 yyaxis right
508 plot(FRg_EtOH,Hmin(2,:),'b','LineWidth',1.5)
509 hold on
510 plot(FRg_EtOH,Hmax(2,:),'c','LineWidth',1.5)
511 plot(max(2),maxH(2),'-rh','LineWidth',1)
512 ylabel('Column Height [m]')
513 legend('Diameter','Min. Height','Max Height','Max possible')
514 axis([0 1 0 20])
515 hold off
516
517 subplot(3,1,3)
518 yyaxis left
519 plot(FRg_EtOH,Dmin(3,:),'--g','LineWidth',1)
520 title('column sizes for 1100 rpm')
521 xlabel('Fractional recovery of Ethanol')
522 ylabel('Column Diameter [m]')
523 axis([0 1 0 20])
524 yyaxis right
525 plot(FRg_EtOH,Hmin(3,:),'b','LineWidth',1.5)
526 hold on
527 plot(FRg_EtOH,Hmax(3,:),'c','LineWidth',1.5)
528 plot(max(3),maxH(3),'-rh','LineWidth',1)
529 ylabel('Column Height [m]')
530 legend('Diameter','Min. Height','Max Height','Max possible')
531 axis([0 1 0 20])
532 hold off
533
534 figure
535 plot(FRg_EtOH,Hmin(3,:),'--r','LineWidth',1)
536 hold on
537 plot(FRg_EtOH,Hmax(3,:),'--m','LineWidth',1)
538 plot(max(3),maxH(3),'-ro','LineWidth',1)
539 plot(FRg_EtOH,Hmin(2,:),'.-b','LineWidth',1)
540 plot(FRg_EtOH,Hmax(2,:),'.-c','LineWidth',1)

```



```
541 plot(max(2),maxH(2),'-rp','LineWidth',1)
542 plot(FRg_EtOH,Hmin(1,:),'g','LineWidth',2)
543 plot(FRg_EtOH, Hmax(1,:),'k','LineWidth',1.5)
544 plot(max(1),maxH(1),'-rh','LineWidth',1)
545 title('influence of mixer speed on column size')
546 xlabel('Fractional recovery of Ethanol')
547 ylabel('Column Height [m]')
548 legend('Hmin 1100rpm','Hmax 1100rpm', 'Max Possible 1100rpm',...
549        'Hmin 500rpm','Hmax 500rpm', 'Max Possible 500rpm','Hmin 300rpm',...
550        'Hmax 300rpm', 'Max Possible 300rpm')
551 axis([0 1 0 20])
552 hold off
553
554 % figure
555 % plot(FRg_EtOH,Hmin(2,:),'.-b','LineWidth',1)
556 % hold on
557 % plot(FRg_EtOH, Hmax(2,:),'.-c','LineWidth',1)
558 % plot(max(2),maxH(2),'-rp','LineWidth',1)
559 %
560 % title('influence of mixer speed on column size')
561 % xlabel('Fractional recovery of Ethanol')
562 % ylabel('Column Height [m]')
563 % legend('Hmin 500rpm','Hmax 500rpm', 'Max Possible 500rpm')
564 % axis([0 1 0 20])
565 % hold off
566 figure
567 plot(FRg_EtOH,Hmin(2,:),'.-b','LineWidth',1)
568 hold on
569 plot(FRg_EtOH, Hmax(2,:),'.-c','LineWidth',1)
570 % plot(max(2),maxH(2),'-rp','LineWidth',1)
571
572 title('Determination of ideal column height')
573 xlabel('Fractional recovery of Ethanol')
574 ylabel('Column Height [m]')
575 legend('Hmin','Hmax', 'Max Possible 500rpm')
576 axis([0 1 0 20])
577 hold off
```



## APPENDIX D

---

### References

---

- [1] Masson-Delmotte, V., P. Zhai, H.-O. Pörtner, D. Roberts, J. Skea, P.R. Shukla, A. Pirani, W. Moufouma-Okia, C. Péan, R. Pidcock, S. Connors, J.B.R. Matthews, Y. Chen, X. Zhou, M.I. Gomis, E. Lonnoy, T. Maycock, M. Tignor, and T. Waterfield, editor. *Mitigation Pathways Compatible with 1.5°C in the Context of Sustainable Development*. In: *Global Warming of 1.5°C*. An IPCC Special Report on the impacts of global warming of 1.5°C above pre-industrial levels and related global greenhouse gas emission pathways, in the context of strengthening the global response to the threat of climate change, sustainable development, and efforts to eradicate poverty [2018].
- [2] D. Humbird, R. Davis, L. Tao *et al.* *Process design and economics for biochemical conversion of lignocellulosic biomass to ethanol: Dilute-acid pretreatment and enzymatic hydrolysis of corn stover* [2011]. doi: 10.2172/1013269.
- [3] L. R. Lynd, M. S. Laser, D. Bransby *et al.* *How biotech can transform biofuels*. *Nature biotechnology*, 26(2):169–172 [2008]. doi: 10.1038/nbt0208-169.
- [4] S. Brethauer and M. H. Studer. *Consolidated bioprocessing of lignocellulose by a microbial consortium*. *Energy & Environmental Science*, 7(4):1446 [2014]. doi: 10.1039/c3ee41753k.
- [5] *Ethanol futures historical prices - investing.com*. <https://www.investing.com/commodities/ethanol-futures-historical-data>. [14.08.2019].
- [6] *Biofuelscan | s&p global platts*. <https://www.spglobal.com/platts/en/products-services/agriculture/biofuelscan>. [11.11.2020].
- [7] S. Brethauer, M. H. Studer and C. E. Wyman. *Application of a slurry feeder to 1 and 3 stage continuous simultaneous saccharification and fermentation of dilute acid pretreated corn stover*. *Bioresource technology*, 170:470–476 [2014]. doi: 10.1016/j.biortech.2014.07.049.

- 
- [8] G. Wang, C. Haringa, H. Noorman *et al.* *Developing a computational framework to advance bioprocess scale-up.* Trends in biotechnology, 38(8):846–856 [2020]. doi: 10.1016/j.tibtech.2020.01.009.
- [9] R. L. Shahab, S. Brethauer, M. P. Davey *et al.* *A heterogeneous microbial consortium producing short-chain fatty acids from lignocellulose.* Science, 369(6507):eabb1214 [2020]. doi: 10.1126/science.abb1214.
- [10] S. Velkovska, M. R. Marten and D. F. Ollis. *Kinetic model for batch cellulase production by trichoderma reesei rut c30.* Journal of Biotechnology, 54(2):83–94 [1997]. doi: 10.1016/S0168-1656(97)01669-6.
- [11] S. M. Zarook, A. A. Shaikh, Z. Ansar *et al.* *Biofiltration of volatile organic compound (voc) mixtures under transient conditions.* Chemical Engineering Science, 52(21-22):4135–4142 [1997]. doi: 10.1016/S0009-2509(97)00256-X.
- [12] T. A. Shaler and G. M. Klecka. *Effects of dissolved oxygen concentration on biodegradation of 2,4-dichlorophenoxyacetic acid.* Applied and environmental microbiology, 51(5):950–955 [1986]. doi: 10.1128/aem.51.5.950-955.1986.
- [13] G. Alagappan and R. M. Cowan. *Effect of temperature and dissolved oxygen on the growth kinetics of pseudomonas putida f1 growing on benzene and toluene.* Chemosphere, 54(8):1255–1265 [2004]. doi: 10.1016/j.chemosphere.2003.09.013.
- [14] S. Mazumder. *Numerical methods for partial differential equations: Finite difference and finite volume methods.* Academic Press, Amsterdam [2015]. ISBN 9780128498941.
- [15] N. V. Pimenova and T. R. Hanley. *Effect of corn stover concentration on rheological characteristics.* Applied Biochemistry and Biotechnology, 114(1-3):347–360 [2004]. doi: 10.1385/ABAB:114:1-3:347.
- [16] T. K. Ghose and R. D. Tyagi. *Rapid ethanol fermentation of cellulose hydrolysate. ii. product and substrate inhibition and optimization of fermentor design.* Biotechnology and Bioengineering, 21(8):1401–1420 [1979]. doi: 10.1002/bit.260210808.
- [17] S. L. Chen and F. Gutmains. *Carbon dioxide inhibition of yeast growth in biomass production.* Biotechnology and bioengineering, 18(10):1455–1462 [1976]. doi: 10.1002/bit.260181012.
- [18] J. L. S. Sonogo, D. A. Lemos, G. Y. Rodriguez *et al.* *Extractive batch fermentation with co 2 stripping for ethanol production in a bubble column bioreactor: Experimental and modeling.* Energy & Fuels, 28(12):7552–7559 [2014]. doi: 10.1021/ef5018797.

- [19] D. Ryu, R. Andereotti, M. Mandels *et al.* *Studies on quantitative physiology of trichoderma reesei with two-stage continuous culture for cellulose production*. *Biotechnology and Bioengineering*, 21(11):1887–1903 [1979]. doi: 10.1002/bit.260211102.
- [20] W. Steffen, J. Rockström, K. Richardson *et al.* *Trajectories of the earth system in the anthropocene*. *Proceedings of the National Academy of Sciences*, 115(33):8252–8259 [2018]. doi: 10.1073/pnas.1810141115.
- [21] H. Zabed, J. Sahu, A. Sueyly *et al.* *Bioethanol production from renewable sources: Current perspectives and technological progress*. *Renewable and Sustainable Energy Reviews*, 71:475–501 [2017]. doi: <https://doi.org/10.1016/j.rser.2016.12.076>.
- [22] A. Wanitschke and S. Hoffmann. *Are battery electric vehicles the future? an uncertainty comparison with hydrogen and combustion engines*. *Environmental Innovation and Societal Transitions*, 35:509–523 [2020]. doi: 10.1016/j.eist.2019.03.003.
- [23] S. Brethauer and M. H.-P. Studer. *Towards net zero greenhouse gas emissions in the energy and chemical sectors in switzerland and beyond - a review*. *Chimia*, 75(9):788–799 [2021]. doi: 10.2533/chimia.2021.788.
- [24] V. Codina Gironès, S. Moret, E. Peduzzi *et al.* *Optimal use of biomass in large-scale energy systems: Insights for energy policy*. *Energy*, 137:789–797 [2017]. doi: 10.1016/j.energy.2017.05.027.
- [25] V. Burg, G. Bowman, M. Erni *et al.* *Analyzing the potential of domestic biomass resources for the energy transition in switzerland*. *Biomass and Bioenergy*, 111:60–69 [2018]. doi: 10.1016/j.biombioe.2018.02.007.
- [26] B. Strohm. *Ethanol*. In *Encyclopedia of Toxicology*, pp. 488–491. Elsevier [2014]. ISBN 9780123864550. doi: 10.1016/B978-0-12-386454-3.00379-1.
- [27] A. D. Celebi, A. V. Ensinas, S. Sharma *et al.* *Early-stage decision making approach for the selection of optimally integrated biorefinery processes*. *Energy*, 137:908–916 [2017]. doi: 10.1016/j.energy.2017.03.080.
- [28] OECD-FAO *Agricultural Outlook 2019-2028*. OECD [2019]. ISBN 9789264312456. doi: 10.1787/agr\_outlook-2019-en.
- [29] J. Fargione, J. Hill, D. Tilman *et al.* *Land clearing and the biofuel carbon debt*. *Science (New York, N.Y.)*, 319(5867):1235–1238 [2008]. doi: 10.1126/science.1152747.
- [30] S. Brethauer and M. H. Studer. *Biochemical conversion processes of lignocellulosic biomass to fuels and chemicals - a review*. *Chimia*, 69(10):572–581 [2015]. doi: 10.2533/chimia.2015.572.

- 
- [31] C. Ricardo Soccol, V. Faraco, S. Karp *et al.* *Lignocellulosic bioethanol*. In *Biofuels*, pp. 101–122. Elsevier [2011]. ISBN 9780123850997. doi: 10.1016/B978-0-12-385099-7.00005-X.
- [32] A. Arevalo-Gallegos, Z. Ahmad, M. Asgher *et al.* *Lignocellulose: A sustainable material to produce value-added products with a zero waste approach-a review*. *International journal of biological macromolecules*, 99:308–318 [2017]. doi: 10.1016/j.ijbiomac.2017.02.097.
- [33] D. Dempfle, O. Kröcher and M. H.-P. Studer. *Techno-economic assessment of bioethanol production from lignocellulose by consortium-based consolidated bioprocessing at industrial scale*. *New biotechnology*, 65:53–60 [2021]. doi: 10.1016/j.nbt.2021.07.005.
- [34] J. J. Minty, M. E. Singer, S. A. Scholz *et al.* *Design and characterization of synthetic fungal-bacterial consortia for direct production of isobutanol from cellulosic biomass*. *Proceedings of the National Academy of Sciences of the United States of America*, 110(36):14592–14597 [2013]. doi: 10.1073/pnas.1218447110.
- [35] S. Brethauer, R. L. Shahab and M. H. Studer. *Impacts of biofilms on the conversion of cellulose*. *Applied microbiology and biotechnology*, 104(12):5201–5212 [2020]. doi: 10.1007/s00253-020-10595-y.
- [36] B. E. Della-Bianca, T. O. Basso, B. U. Stambuk *et al.* *What do we know about the yeast strains from the brazilian fuel ethanol industry?* *Applied microbiology and biotechnology*, 97(3):979–991 [2013]. doi: 10.1007/s00253-012-4631-x.
- [37] H. van Acker, P. van Dijck and T. Coenye. *Molecular mechanisms of antimicrobial tolerance and resistance in bacterial and fungal biofilms*. *Trends in microbiology*, 22(6):326–333 [2014]. doi: 10.1016/j.tim.2014.02.001.
- [38] Federal Department of the Environment, Transport Energy and Communications DE-TEC. *Energy strategy 2050*. <https://www.uvek.admin.ch/uvek/en/home/energy/energy-strategy-2050.html>. [22.09.2021].
- [39] *Portrait sccer biosweet*. <https://www.sccer-biosweet.ch/de/portrait/>. [22.09.2021].
- [40] U.S. Energy Information Administration. *International energy outlook 2020 (ieo2020)*. <https://www.eia.gov/outlooks/ieo/pdf/ieo2020.pdf>. [19.07.2021].
- [41] J. Conti, P. Holtberg, J. Diefenderfer *et al.* *International Energy Outlook 2016 With Projections to 2040* [2016]. doi: 10.2172/1296780.
- [42] L. M. Fulton, L. R. Lynd, A. Körner *et al.* *The need for biofuels as part of a low carbon energy future*. *Biofuels, Bioproducts and Biorefining*, 9(5):476–483 [2015]. doi: 10.1002/bbb.1559.

- [43] U.S. Energy Information Administration. *International energy outlook 2019: with projections to 2050*. <https://www.eia.gov/outlooks/ieo/pdf/ieo2019.pdf>. [04.03.2021].
- [44] O. for Economic Co-operation and Development. *Energy technology perspectives 2016: Towards sustainable urban energy systems* [2016].
- [45] P. IEA. *Energy technology perspectives 2012: Pathways to a clean energy system* [2012].
- [46] J. van Haveren, E. Scott and J. Sanders. *Bulk chemicals from biomass*. *Biofuels Bioproducts and Biorefining*, 2(1):41–57 [2008]. doi: 10.1002/bbb.43.
- [47] *Alternative fuels data center: Second generation biofuel producer tax credit*. <https://afdc.energy.gov/laws/10515>. [19.07.2021].
- [48] Y. Pu, D. Zhang, P. M. Singh *et al.* *The new forestry biofuels sector*. *Biofuels, Bioproducts and Biorefining*, 2(1):58–73 [2008]. doi: 10.1002/bbb.48.
- [49] L. da Costa Sousa, S. P. Chundawat, V. Balan *et al.* 'Cradle-to-grave' assessment of existing lignocellulose pretreatment technologies. *Current Opinion in Biotechnology*, 20(3):339–347 [2009]. doi: 10.1016/j.copbio.2009.05.003.
- [50] R. L. Shahab, J. S. Luterbacher, S. Brethauer *et al.* *Consolidated bioprocessing of lignocellulosic biomass to lactic acid by a synthetic fungal-bacterial consortium*. *Biotechnology and bioengineering*, 115(5):1207–1215 [2018]. doi: 10.1002/bit.26541.
- [51] L. R. Lynd, X. Liang, M. J. Bidy *et al.* *Cellulosic ethanol: status and innovation*. *Current opinion in biotechnology*, 45:202–211 [2017]. doi: 10.1016/j.copbio.2017.03.008.
- [52] A. I. Stankiewicz and J. A. Moulijn. *Process intensification: transforming chemical engineering*. *Chemical Engineering Progress*, 96(1):22–34 [2000].
- [53] R. L. Shahab, S. Brethauer, J. S. Luterbacher *et al.* *Engineering of ecological niches to create stable artificial consortia for complex biotransformations*. *Current opinion in biotechnology*, 62:129–136 [2020]. doi: 10.1016/j.copbio.2019.09.008.
- [54] S. Brethauer, R. Shahab and M. Studer. *Impacts of biofilms on the conversion of cellulose*. *Applied Microbiology and Biotechnology*, 104 [2020]. doi: 10.1007/s00253-020-10595-y.
- [55] G. W. Roell, J. Zha, R. R. Carr *et al.* *Engineering microbial consortia by division of labor*. *Microbial cell factories*, 18(1):35 [2019]. doi: 10.1186/s12934-019-1083-3.
- [56] X. N. Peng, S. P. Gilmore and M. A. O'Malley. *Microbial communities for bioprocessing: lessons learned from nature*. *Current Opinion in Chemical Engineering*, 14:103–109 [2016]. doi: 10.1016/j.coche.2016.09.003.



- 
- [57] R. L. Shahab. *Labor division in engineered cross-kingdom consortia: Consolidated bioprocessing of lignocellulosic biomass to carboxylic acids*. Ph.D. thesis, EPFL, Lausanne. doi: 10.5075/epfl-thesis-9420.
- [58] S. Brethauer, A. Antczak, R. Balan *et al.* *Steam explosion pretreatment of beechwood. part 2: Quantification of cellulase inhibitors and their effect on avicel hydrolysis*. *Energies*, 13(14) [2020]. doi: 10.3390/en13143638.
- [59] K. L. Kadam, E. C. Rydholm and J. D. McMillan. *Development and validation of a kinetic model for enzymatic saccharification of lignocellulosic biomass*. *Biotechnology progress*, 20(3):698–705 [2004]. doi: 10.1021/bp034316x.
- [60] R. Turton. *Analysis, synthesis, and design of chemical processes*. Prentice Hall international series in the physical and chemical engineering sciences. Prentice Hall, Boston, 5th edition edn. [2018]. ISBN 0134177401.
- [61] G. D. Ulrich and P. T. Vasudevan. *Chemical engineering process design and economics: A practical guide*. Process Pub, Durham N.H., 2nd ed. edn. [2004]. ISBN 0970876823.
- [62] D. E. Garrett. *Chemical engineering economics*. Springer Science & Business Media [2012]. doi: 10.1007/978-94-011-6544-0.
- [63] A. Aden, M. Ruth, K. Ibsen *et al.* *Lignocellulosic biomass to ethanol process design and economics utilizing co-current dilute acid prehydrolysis and enzymatic hydrolysis for corn stover*. doi: 10.2172/15001119.
- [64] L. M. Vane. *Separation technologies for the recovery and dehydration of alcohols from fermentation broths*. *Biofuels, Bioproducts and Biorefining*, 2(6):553–588 [2008]. doi: 10.1002/bbb.108.
- [65] J. B. Haelssig, A. Y. Tremblay and J. Thibault. *Technical and economic considerations for various recovery schemes in ethanol production by fermentation*. *Industrial & Engineering Chemistry Research*, 47(16):6185–6191 [2008]. doi: 10.1021/ie0715005.
- [66] *Design, Control and Economics of Distillation*, chap. 2, pp. 37–65. John Wiley Sons, Ltd [2013]. ISBN 9781118543702. doi: <https://doi.org/10.1002/9781118543702.ch2>.
- [67] *Conversion rates - purchasing power parities (ppp) - oecd data*. <https://data.oecd.org/conversion/purchasing-power-parities-ppp.htm>. [16.08.2019].
- [68] O. Ezekoye, A. Milutinovic and T. J. Simons. *Chemicals and capital markets: Back at the top*. McKinsey & Company [1052018].
- [69] *Faostat*. <http://www.fao.org/faostat/en/data/QC>. [16.08.2019].



- [70] M. Tsagkari, J.-L. Couturier, A. Kokossis *et al.* *Early-stage capital cost estimation of biorefinery processes: A comparative study of heuristic techniques*. *ChemSusChem*, 9(17):2284–2297 [2016]. doi: 10.1002/cssc.201600309.
- [71] *Abengoa sells hugoton cellulosic ethanol plant for synata bio | the wichita eagle*. <https://www.kansas.com/news/business/article119902263.html>. [15.08.2019].
- [72] *Assets of former ineos bio plant to be sold piecemeal via auction | biomass-magazine.com*. <http://biomassmagazine.com/articles/15871/assets-of-former-ineos-bio-plant-to-be-sold-piecemeal-via-auction>. [15.08.2019].
- [73] *Dupont seeks to sell cellulosic ethanol plant | chemical & engineering news*. <https://cen.acs.org/articles/95/web/2017/11/DuPont-seeks-sell-cellulosic-ethanol.html>. [15.08.2019].
- [74] *Ethanol producer magazine – the latest news and data about ethanol production*. <http://www.ethanolproducer.com/articles/15344/zero-to-10-million-in-5-years>. [15.08.2019].
- [75] K. Plumb. *Continuous processing in the pharmaceutical industry*. *Chemical Engineering Research and Design*, 83(6):730–738 [2005]. doi: 10.1205/cherd.04359.
- [76] C. Windmark, J.-E. Ståhl, P. Gabrielson *et al.*, editors. *A production performance analysis regarding downtime and downtime pattern* [2012].
- [77] S. Brethauer and C. E. Wyman. *Review: Continuous hydrolysis and fermentation for cellulosic ethanol production*. *Bioresource technology*, 101(13):4862–4874 [2010]. doi: 10.1016/j.biortech.2009.11.009.
- [78] J. Hong. *Optimal substrate feeding policy for a fed batch fermentation with substrate and product inhibition kinetics*. *Biotechnology and bioengineering*, 28(9):1421–1431 [1986]. doi: 10.1002/bit.260280916.
- [79] T. Li, X.-b. Chen, J.-c. Chen *et al.* *Open and continuous fermentation: products, conditions and bioprocess economy*. *Biotechnology journal*, 9(12):1503–1511 [2014]. doi: 10.1002/biot.201400084.
- [80] M. Schofield. *Current state of the art in continuous bioprocessing*. *Biotechnology Letters*, 40(9-10):1303–1309 [2018]. doi: 10.1007/s10529-018-2593-5.
- [81] E. Rivera and P. Lopolito. *Cleaning validation in continuous manufacturing*. *Pharmaceutical Technology*, 40(11):34–42 [2016].

- 
- [82] G.-Q. Chen. *New challenges and opportunities for industrial biotechnology*. Microbial Cell Factories, 11(1):111 [2012]. doi: 10.1186/1475-2859-11-111.
- [83] D. S. Christen. *Praxiswissen der chemischen Verfahrenstechnik: Handbuch für Chemiker und Verfahreningenieure*. VDI-Buch. Springer-Verlag Berlin Heidelberg, Berlin, Heidelberg, 2., bearb. und erg. aufl. edn. [2010]. ISBN 9783540889748.
- [84] M. Butler and M. Moo-Young. *Comprehensive biotechnology*. Elsevier, Saint Louis, Mo., 2nd ed. edn. [2011]. ISBN 978-0-08-088504-9.
- [85] N. N. Gamarra, G. K. Villena and M. Gutiérrez-Correa. *Cellulase production by aspergillus niger in biofilm, solid-state, and submerged fermentations*. Applied Microbiology and Biotechnology, 87(2):545–551 [2010]. doi: 10.1007/s00253-010-2540-4.
- [86] R. Luedeking and E. L. Piret. *A kinetic study of the lactic acid fermentation. batch process at controlled ph*. Journal of Biochemical and Microbiological Technology and Engineering, 1(4):393–412 [1959]. doi: 10.1002/jbmte.390010406.
- [87] C. Xiros and M. H. Studer. *A multispecies fungal biofilm approach to enhance the cellulolytic efficiency of membrane reactors for consolidated bioprocessing of plant biomass*. Frontiers in microbiology, 8:1930 [2017]. doi: 10.3389/fmicb.2017.01930.
- [88] Dowe N. and J. D. McMillan. *SSF experimental protocols: lignocellulosic biomass hydrolysis and fermentation*. National Renewable Energy Laboratory [2001].
- [89] R. L. Shahab. *Labor division in engineered cross-kingdom consortia: Consolidated bioprocessing of lignocellulosic biomass to carboxylic acids*. Phd thesis, EPFL, Lausanne [2019]. doi: 10.5075/epfl-thesis-9420.
- [90] C. Moukamnerd, M. Kino-oka, M. Sugiyama et al. *Ethanol production from biomass by repetitive solid-state fed-batch fermentation with continuous recovery of ethanol*. Applied Microbiology and Biotechnology, 88(1):87–94 [2010]. doi: 10.1007/s00253-010-2716-y.
- [91] L. Liu, F. Wang, G. Pei et al. *Repeated fed-batch strategy and metabolomic analysis to achieve high docosahexaenoic acid productivity in cryptothecodinium cohnii*. Microbial Cell Factories, 19(1):91 [2020]. doi: 10.1186/s12934-020-01349-6.
- [92] S. Bridges and L. Robinson. *Centrifuges*. In *A Practical Handbook for Drilling Fluids Processing*, pp. 475–488. Elsevier [2020]. ISBN 9780128213414. doi: 10.1016/B978-0-12-821341-4.00021-X.
- [93] L. Guzzella. *Analysis and Synthesis of Single-input Single-output Control Systems*. vdf Hochschulverlag AG [2011]. ISBN 9783728133861.

- [94] E. Pereira, A. Santos, F. Reis *et al.* *A new effective assay to detect antimicrobial activity of filamentous fungi.* Microbiological research, 168(1):1–5 [2013]. doi: 10.1016/j.micres.2012.06.008.
- [95] J.-J. Jeong, K.-A. Kim, S.-E. Jang *et al.* *Orally administrated lactobacillus pentosus var. plantarum c29 ameliorates age-dependent colitis by inhibiting the nuclear factor-kappa b signaling pathway via the regulation of lipopolysaccharide production by gut microbiota.* PloS one, 10(2):e0116533 [2015]. doi: 10.1371/journal.pone.0116533.
- [96] H. G. Crabtree. *Observations on the carbohydrate metabolism of tumours.* The Biochemical journal, 23(3):536–545 [1929]. doi: 10.1042/bj0230536.
- [97] M. M. Bisschops, T. Vos, R. Martínez-Moreno *et al.* *Oxygen availability strongly affects chronological lifespan and thermotolerance in batch cultures of saccharomyces cerevisiae.* Microbial cell (Graz, Austria), 2(11):429–444 [2015]. doi: 10.15698/mic2015.11.238.
- [98] L. Paulova, P. Patakova, B. Branska *et al.* *Lignocellulosic ethanol: Technology design and its impact on process efficiency.* Biotechnology advances, 33(6 Pt 2):1091–1107 [2015]. doi: 10.1016/j.biotechadv.2014.12.002.
- [99] P. Våljamäe, G. Pettersson and G. Johansson. *Mechanism of substrate inhibition in cellulose synergistic degradation.* European journal of biochemistry, 268(16):4520–4526 [2001]. doi: 10.1046/j.1432-1327.2001.02377.x.
- [100] D. Quintanilla, T. Hagemann, K. Hansen *et al.* *Fungal morphology in industrial enzyme production—modelling and monitoring.* In R. Krull and T. Bley, editors, *Filaments in Bioprocesses*, pp. 29–54. Springer International Publishing, Cham [2015]. ISBN 978-3-319-20511-3. doi: 10.1007/10{\textunderscore}2015{\textunderscore}309.
- [101] E. L. Gaden. *Fermentation process kinetics.* Journal of Biochemical and Microbiological Technology and Engineering, 1(4):413–429 [1959]. doi: 10.1002/jbmte.390010407.
- [102] J. M. van Zyl, E. van Rensburg, W. H. van Zyl *et al.* *A kinetic model for simultaneous saccharification and fermentation of avicel with saccharomyces cerevisiae.* Biotechnology and bioengineering, 108(4):924–933 [2011]. doi: 10.1002/bit.23000.
- [103] T. Palmer and P. L. Bonner. *Kinetics of single-substrate enzyme-catalysed reactions.* In *Enzymes*, pp. 105–125. Elsevier [2011]. ISBN 9781904275275. doi: 10.1533/9780857099921.2.105.
- [104] G. P. Philippidis, D. D. Spindler and C. E. Wyman. *Mathematical modeling of cellulose conversion to ethanol by the simultaneous saccharification and fermentation process.* Applied Biochemistry and Biotechnology, 34-35(1):543–556 [1992]. doi: 10.1007/BF02920577.

- [105] J. Blomqvist, T. Eberhard, J. Schnürer *et al.* *Fermentation characteristics of dekkera bruxellensis strains*. Applied Microbiology and Biotechnology, 87(4):1487–1497 [2010]. doi: 10.1007/s00253-010-2619-y.
- [106] W. Z. Lidicker. *A clarification of interactions in ecological systems*. BioScience, 29(8):475–477 [1979]. doi: 10.2307/1307540.
- [107] L. Pacciani-Mori, A. Giometto, S. Suweis *et al.* *Dynamic metabolic adaptation can promote species coexistence in competitive microbial communities*. PLoS computational biology, 16(5):e1007896 [2020]. doi: 10.1371/journal.pcbi.1007896.
- [108] D. Machado, O. M. Maistrenko, S. Andrejev *et al.* *Polarization of microbial communities between competitive and cooperative metabolism*. Nature ecology & evolution, 5(2):195–203 [2021]. doi: 10.1038/s41559-020-01353-4.
- [109] R. J. van Tatenhove-Pel, T. Rijavec, A. Lapanje *et al.* *Microbial competition reduces metabolic interaction distances to the low  $\mu\text{m}$ -range*. The ISME journal, 15(3):688–701 [2021]. doi: 10.1038/s41396-020-00806-9.
- [110] C. Xiros, R. L. Shahab and M. H.-P. Studer. *A cellulolytic fungal biofilm enhances the consolidated bioconversion of cellulose to short chain fatty acids by the rumen microbiome*. Applied microbiology and biotechnology, 103(8):3355–3365 [2019]. doi: 10.1007/s00253-019-09706-1.
- [111] N. J. Essila, M. J. Semmens and V. R. Voller. *Modeling biofilms on gas-permeable supports: Concentration and activity profiles*. Journal of Environmental Engineering, 126(3):250–257 [2000]. doi: 10.1061/(ASCE)0733-9372(2000)126:3(250).
- [112] E. Nagy. *Survey on biocatalytic membrane reactor and membrane aerated biofilm reactor*. Current Organic Chemistry, 21(17) [2017]. doi: 10.2174/1385272821666170317155828.
- [113] F. P. Incropera, F. P. F. o. h. Incropera and mass transfer. *Fundamentals of heat and mass transfer*. Wiley and Chichester : John Wiley [distributor], Hoboken, N.J., 6th ed. / frank p. incropera ... [et al.] edn. [2007]. ISBN 0471457280.
- [114] *VDI Heat Atlas: with 539 tables*. Springer reference. Springer, Heidelberg, 2. ed. edn. [2010]. ISBN 9783540778769. doi: 10.1007/978-3-540-77877-6.
- [115] J. Crank. *The mathematics of diffusion*. Clarendon Press, Oxford, 2nd ed. edn. [1975]. ISBN 0198533446.
- [116] J. G. H. Wijmans and R. W. Baker. *The solution-diffusion model: A unified approach to membrane permeation*. In Y. Yampolskii, I. Pinnau and B. Freeman, editors, *Materials Science of Membranes for Gas and Vapor Separation*, pp. 159–189. John Wiley & Sons, Ltd, Chichester, UK [2006]. ISBN 9780470029039. doi: 10.1002/047002903X.ch5.

- [117] K. Nipp and D. Stoffer. *Lineare Algebra: Eine Einführung für Ingenieure unter besonderer Berücksichtigung numerischer Aspekte*. vdf Hochsch.-Verl. an der ETH Zürich, Zürich, 5., durchges. Aufl. edn. [2002]. ISBN 372812818X.
- [118] V. Lecault, N. Patel and J. Thibault. *An image analysis technique to estimate the cell density and biomass concentration of trichoderma reesei*. Letters in applied microbiology, 48(4):402–407 [2009]. doi: 10.1111/j.1472-765X.2008.02544.x.
- [119] D. Ercan and A. Demirci. *Current and future trends for biofilm reactors for fermentation processes*. Critical reviews in biotechnology, 35(1):1–14 [2015]. doi: 10.3109/07388551.2013.793170.
- [120] W. W. Baldwin and H. E. Kubitschek. *Buoyant density variation during the cell cycle of saccharomyces cerevisiae*. Journal of bacteriology, 158(2):701–704 [1984]. doi: 10.1128/jb.158.2.701-704.1984.
- [121] A. K. Bryan, A. Goranov, A. Amon *et al.* *Measurement of mass, density, and volume during the cell cycle of yeast*. Proceedings of the National Academy of Sciences, 107(3):999–1004 [2010]. doi: 10.1073/pnas.0901851107.
- [122] D. Lloyd and C. J. James. *The pasteur effect in yeasts: Mass spectrometric monitoring of oxygen uptake, and carbon dioxide and ethanol production*. FEMS Microbiology Letters, 42(1):27–31 [1987].
- [123] M. Necati Özişik, Helcio R.B. Orlande, Marcelo José Colaço, Renato Machado Cotta. *Finite Difference Methods in Heat Transfer, Second Edition*. CRC Press [2017]. ISBN 9781315121475. doi: 10.1201/9781315121475.
- [124] Y.-C. Kim and A. S. Myerson. *Diffusivity of protein in aqueous solutions*. Korean Journal of Chemical Engineering, 13(3):288–293 [1996]. doi: 10.1007/BF02705952.
- [125] S. J. Traving, U. H. Thygesen, L. Riemann *et al.* *A model of extracellular enzymes in free-living microbes: which strategy pays off?* Applied and environmental microbiology, 81(21):7385–7393 [2015]. doi: 10.1128/AEM.02070-15.
- [126] T. W. House. *National bioeconomy blueprint, april 2012*. Industrial Biotechnology, 8(3):97–102 [2012]. doi: 10.1089/ind.2012.1524.
- [127] A. R. Lara, E. Galindo, O. T. Ramírez *et al.* *Living with heterogeneities in bioreactors: Understanding the effects of environmental gradients on cells*. Molecular Biotechnology, 34(3):355–382 [2006]. doi: 10.1385/MB:34:3:355.
- [128] G. Festel. *Industrial biotechnology: Market size, company types, business models, and growth strategies*. Industrial Biotechnology, 6(2):88–94 [2010]. doi: 10.1089/ind.2010.0006.



- 
- [129] M. Chen, P. Smith and M. Wolcott. *U.s. biofuels industry: A critical review of opportunities and challenges*. BioProducts Business, 1:42–59 [2016].
- [130] Beta Analytic - ASTM D6866 Lab, Nitrates in Water Testing. *Unterscheiden zwischen bioethanol und erdöl-ethanol* [2016].
- [131] R. Ahmad Dar, E. Ahmad Dar, A. Kaur *et al.* *Sweet sorghum-a promising alternative feedstock for biofuel production*. Renewable and Sustainable Energy Reviews, 82:4070–4090 [2018]. doi: 10.1016/j.rser.2017.10.066.
- [132] A. Anstruther, I. Russell and G. G. Stewart, editors. *Handbook of brewing*. Food science and technology. CRC Press, Boca Raton, Florida, 3rd ed. edn. [2017]. ISBN 1-351-23081-6.
- [133] L.-K. Ju and G. G. Chase. *Improved scale-up strategies of bioreactors*. Bioprocess Engineering, 8(1-2):49–53 [1992]. doi: 10.1007/BF00369263.
- [134] D. J. M. Hayes. *Second-generation biofuels: why they are taking so long*. Wiley Interdisciplinary Reviews: Energy and Environment, 2(3):304–334 [2013]. doi: 10.1002/wene.59.
- [135] J. M. Melillo, J. M. Reilly, D. W. Kicklighter *et al.* *Indirect emissions from biofuels: how important?* Science (New York, N.Y.), 326(5958):1397–1399 [2009]. doi: 10.1126/science.1180251.
- [136] M. Zlokarnik. *Scale-up: Modellübertragung in der Verfahrenstechnik*. Wiley-VCH-Verl., Weinheim, 2., vollst. überarb. und erw. Aufl. edn. [2005]. ISBN 9783527314225. doi: 10.1002/352760765X.
- [137] J. H. Evans. *Dimensional analysis and the buckingham pi theorem*. American Journal of Physics, 40(12):1815–1822 [1972]. doi: 10.1119/1.1987069.
- [138] G. Donati and R. Paludetto. *Scale up of chemical reactors*. Catalysis Today, 34(3-4):483–533 [1997]. doi: 10.1016/S0920-5861(96)00069-7.
- [139] J. Xia, G. Wang, J. Lin *et al.* *Advances and practices of bioprocess scale-up*. In J. Bao, Q. Ye and J.-J. Zhong, editors, *Bioreactor Engineering Research and Industrial Applications II*, pp. 137–151. Springer Berlin Heidelberg, Berlin, Heidelberg [2016]. ISBN 978-3-662-48347-3. doi: 10.1007/10\_2014\_293.
- [140] Y. C. Ho and D. L. Pepyne. *Simple explanation of the no-free-lunch theorem and its implications*. Journal of Optimization Theory and Applications, 115(3):549–570 [2002]. doi: 10.1023/A:1021251113462.
- [141] V. V. Mozhaev, K. Heremans, J. Frank *et al.* *Exploiting the effects of high hydrostatic pressure in biotechnological applications*. Trends in biotechnology, 12(12):493–501 [1994]. doi: 10.1016/0167-7799(94)90057-4.

- [142] J. Thibault, A. Leduy and F. Côté. *Production of ethanol by saccharomyces cerevisiae under high-pressure conditions*. Biotechnology and Bioengineering, 30(1):74–80 [1987]. doi: 10.1002/bit.260300111.
- [143] V. Carniello, B. W. Peterson, H. C. van der Mei *et al.* *Physico-chemistry from initial bacterial adhesion to surface-programmed biofilm growth*. Advances in Colloid and Interface Science, 261:1–14 [2018]. doi: 10.1016/j.cis.2018.10.005.
- [144] P. Kaali, D. Momcilovic, A. Markström *et al.* *Degradation of biomedical polydimethylsiloxanes during exposure to in vivo biofilm environment monitored by fe-sem, atr-ftir, and maldi-tof ms*. Journal of Applied Polymer Science, 115(2):802–810 [2010]. doi: 10.1002/app.31119.
- [145] D. Ludwig, B. Michael, T. Hirth *et al.* *High solids enzymatic hydrolysis of pretreated lignocellulosic materials with a powerful stirrer concept*. Applied Biochemistry and Biotechnology, 172(3):1699–1713 [2014]. doi: 10.1007/s12010-013-0607-2.
- [146] Y.-Y. Tsui and Y.-C. Hu. *Flow characteristics in mixers agitated by helical ribbon blade impeller*. Engineering Applications of Computational Fluid Mechanics, 5(3):416–429 [2011]. doi: 10.1080/19942060.2011.11015383.
- [147] C. Kuncewicz, K. Szulc and T. Kurasinski. *Hydrodynamics of the tank with a screw impeller*. Chemical Engineering and Processing: Process Intensification, 44(7):766–774 [2005]. doi: 10.1016/j.cep.2004.08.006.
- [148] A. P. Weber. *Continuous-flow reactor for high viscosity materials: worldwide*. <https://patents.google.com/patent/US4007016A/en>. [13.09.2021].
- [149] J. L. Awange and B. Paláncz. *Solutions of Overdetermined Systems*, pp. 89–112. Springer International Publishing, Cham [2016]. ISBN 978-3-319-25465-4. doi: 10.1007/978-3-319-25465-4\_7.
- [150] E. Syron and E. Casey. *Membrane-aerated biofilms for high rate biotreatment: performance appraisal, engineering principles, scale-up, and development requirements*. Environmental Science & Technology, 42(6):1833–1844 [2008]. doi: 10.1021/es0719428.
- [151] *Producer price index by industry: Industrial gas manufacturing*. <https://fred.stlouisfed.org/series/PCU325120325120> [2021]. [09.09.2021].
- [152] S. K. Maity. *Opportunities, recent trends and challenges of integrated biorefinery: Part i*. Renewable and Sustainable Energy Reviews, 43:1427–1445 [2015]. doi: 10.1016/j.rser.2014.11.092.

- 
- [153] R. L. Chapman. *Algae: the world's most important "plants"—an introduction*. Mitigation and Adaptation Strategies for Global Change, 18(1):5–12 [2013]. doi: 10.1007/s11027-010-9255-9.
- [154] P. C. Wankat. *Separation process engineering : includes mass transfer analysis*. Prentice Hall, Place of publication not identified, 3rd ed. edn. [2012]. ISBN 0-13-138227-6.
- [155] J. Crank. *The mathematics of diffusion*. Clarendon Press, Oxford, second ed., [reprinted] edn. [1983]. ISBN 0198534116.
- [156] N. van Uden. *Ethanol toxicity and ethanol tolerance in yeasts*. vol. 8 of *Annual Reports on Fermentation Processes*, pp. 11–58. Elsevier [1985]. ISBN 9780120403080. doi: 10.1016/B978-0-12-040308-0.50006-9.
- [157] W. van Hecke, G. Kaur and H. de Wever. *Advances in in-situ product recovery (ispr) in whole cell biotechnology during the last decade*. Biotechnology advances, 32(7):1245–1255 [2014]. doi: 10.1016/j.biotechadv.2014.07.003.
- [158] T. Yamamoto, Y. H. Kim, B. C. Kim et al. *Adsorption characteristics of zeolites for dehydration of ethanol: Evaluation of diffusivity of water in porous structure*. Chemical Engineering Journal, 181-182:443–448 [2012]. doi: 10.1016/j.cej.2011.11.110.
- [159] I. I. El-Sharkawy, K. Uddin, T. Miyazaki et al. *Adsorption of ethanol onto parent and surface treated activated carbon powders*. International Journal of Heat and Mass Transfer, 73:445–455 [2014]. doi: 10.1016/j.ijheatmasstransfer.2014.02.046.
- [160] I. I. El-Sharkawy, K. Uddin, T. Miyazaki et al. *Adsorption of ethanol onto phenol resin based adsorbents for developing next generation cooling systems*. International Journal of Heat and Mass Transfer, 81:171–178 [2015]. doi: 10.1016/j.ijheatmasstransfer.2014.10.012.
- [161] J. Cilliers and S. Harrison. *Yeast flocculation aids the performance of yeast dewatering using mini-hydrocyclones*. Separation and Purification Technology, 209:159–163 [2019]. doi: <https://doi.org/10.1016/j.seppur.2018.06.019>.
- [162] M. Gyamerah and J. Glover. *Production of ethanol by continuous fermentation and liquid-liquid extraction*. Journal of Chemical Technology & Biotechnology, 66(2):145–152 [1996]. doi: 10.1002/(SICI)1097-4660(199606)66:2<145::AID-JCTB484>3.0.CO;2-2.
- [163] N. Bizmark and M. A. Ioannidis. *Ethyl cellulose nanoparticles at the alkane-water interface and the making of pickering emulsions*. Langmuir, 33(40):10568–10576 [2017]. doi: 10.1021/acs.langmuir.7b02051.



- [164] N. Ghavidel and P. Fatehi. *Interfacial and emulsion characteristics of oil-water systems in the presence of polymeric lignin surfactant*. *Langmuir*, 37(11):3346–3358 [2021]. doi: 10.1021/acs.langmuir.0c03458.
- [165] Haihang Industry. *dodecane cas 112-40-3 - haihang industry* [21052021].
- [166] W. Guo, H.-H. Ngo and J. Li. *A mini-review on membrane fouling*. *Bioresource technology*, 122:27–34 [2012]. doi: 10.1016/j.biortech.2012.04.089.
- [167] C. R. Silva, M. N. Esperança, A. Cruz *et al.* *Stripping of ethanol with co<sub>2</sub> in bubble columns: Effects of operating conditions and modeling*. *Chemical Engineering Research and Design*, 102:150–160 [2015]. doi: 10.1016/j.cherd.2015.06.022.
- [168] C. Löser, A. Schröder, S. Deponete *et al.* *Balancing the ethanol formation in continuous bioreactors with ethanol stripping*. *Engineering in Life Sciences*, 5(4):325–332 [2005]. doi: 10.1002/elsc.200520084.
- [169] A. Bakker and H.E.A. Van den Akker. *A computational model for the gas-liquid flow in stirred reactor*. *Chemical Engineering Research and Design*, 72(A4):594–606 [1994].
- [170] H. Thiess, A. Schmidt and J. Strube. *Development of a scale-up tool for pervaporation processes*. *Membranes*, 8(1) [2018]. doi: 10.3390/membranes8010004.
- [171] J. G. Wijmans and R. W. Baker. *The solution-diffusion model: a review*. *Journal of Membrane Science*, 107(1-2):1–21 [1995]. doi: 10.1016/0376-7388(95)00102-I.
- [172] T. Mohammadi, A. Aroujalian and A. Bakhshi. *Pervaporation of dilute alcoholic mixtures using pdms membrane*. *Chemical Engineering Science*, 60(7):1875–1880 [2005]. doi: 10.1016/j.ces.2004.11.039.
- [173] F. Meng, S.-R. Chae, A. Drews *et al.* *Recent advances in membrane bioreactors (mbrs): membrane fouling and membrane material*. *Water research*, 43(6):1489–1512 [2009]. doi: 10.1016/j.watres.2008.12.044.
- [174] R. Sander. *Compilation of henry's law constants (version 4.0) for water as solvent*. *Atmospheric Chemistry and Physics*, 15(8):4399–4981 [2015]. doi: 10.5194/acp-15-4399-2015.
- [175] V. Outram, C.-A. Lalander, J. G. M. Lee *et al.* *Applied in situ product recovery in abe fermentation*. *Biotechnology progress*, 33(3):563–579 [2017]. doi: 10.1002/btpr.2446.
- [176] K. Sootsuwan, P. Thanonkeo, N. Keeratirakha *et al.* *Sorbitol required for cell growth and ethanol production by zymomonas mobilis under heat, ethanol, and osmotic stresses*. *Biotechnology for Biofuels*, 6(1):180 [2013]. doi: 10.1186/1754-6834-6-180.

- [177] S. Sipala, G. Mancini and F. Vagliasindi. *Development of a web-based tool for the calculation of costs of different wastewater treatment and reuse scenarios*. Water Science and Technology: Water Supply, 3(4):89–96 [2003]. doi: 10.2166/ws.2003.0049.
- [178] D. W. Green and M. Z. Southard. *Perry's chemical engineers' handbook / editor-in-chief, Don W. Green, associate editor, Marylee Z. Southard*. McGraw-Hill Education, New York, NY, ninth edition, 85th anniversary edition edn. [2019]. ISBN 0071834087.
- [179] M. Gerrad. Rugby: Institution of Chemical Engineers, New York, NY, 4th ed. edn. [1998]. ISBN 0852953992 9780852953990.
- [180] D. Mignard. *Correlating the chemical engineering plant cost index with macro-economic indicators*. Chemical Engineering Research and Design, 92:285–294 [2014]. doi: 10.1016/j.cherd.2013.07.022.
- [181] G. R. Cysewski and C. R. Wilke. *Utilization of cellulosic materials through enzymatic hydrolysis. i. fermentation of hydrolysate to ethanol and single-cell protein*. Biotechnology and bioengineering, 18(9):1297–1313 [1976]. doi: 10.1002/bit.260180908.

## APPENDIX E

---

### List of publications

---

#### Publications

- to be submitted**     *Scale-up of consolidated bioprocessing from 2.7 L laboratory scale to 130 L pilot scale based on a rigorous model*  
D. Dempfle, P. Bühler, S. Bowald, D. Blaser, O. Kröcher, M. H. Studer
- to be submitted**     *Continuous consolidated bioprocessing of cellulosic ethanol based on a microbial consortium in a membrane aerated biofilm reactor to validate a rigorous spatially resolved model*  
D. Dempfle, C. Wagner, O. Kröcher, M. H. Studer
- 2021**     *Techno-economic assessment of bioethanol production from lignocellulose by consortium-based consolidated bioprocessing at industrial scale*  
D. Dempfle, O. Kröcher, M. H. Studer  
New Biotechnology. 65 (2021) 53–60, doi: 10.1016/j.nbt.2021.07.005
- 2018**     *External mass transfer in a laser sintered structured reactor for continuous hydrogenation of alkynes*  
S. Vernuccio, D. Dempfle, Roman Goy, J. Medlock, P. Rudolf von Rohr  
Chemical Engineering and Processing. doi: 10.1016/j.cep.2018.02.005.

**Conference contributions**

**04/2020**                    **42nd Symposium on Biomaterials, Fuels and Chemicals**, New Orleans,  
United States of America  
*Techno-economic assessment of bioethanol production from lignocellulose by  
consortium-based consolidated bioprocessing at industrial scale*  
D. Dempfle, O. Kröcher, M. H. Studer

## APPENDIX F

---

### Curriculum vitae

---

**Name** David Beat Dempfle  
**Date of birth** 22<sup>th</sup> June 1992  
**Nationality** German

#### Education

**09/2017 - 11/2021** **Doctoral student**

École Polytechnique Fédérale de Lausanne, Group of Catalysis for Biofuels and Bern University of Applied Sciences, Laboratory of Biofuels and Biochemicals

**PhD thesis** *Model-based scale-up of a continuously operated consolidated bioprocess based on a microbial consortium to produce ethanol from lignocellulose*  
Prof. Dr. Oliver Kröcher & Dr. Michael Studer

**09/2011 - 05/2017** **Master of Science ETH in Process Engineering**

Swiss Federal Institute of Technology Zurich

**Specialization** *Process Engineering*

**Master thesis** *Continuous hydrogenation of 2-methyl-3-butyn-2-ol in a structured reactor*  
Swiss Federal Institute of Technology Zurich, Institute for Process Engineering  
Prof. Dr. Philipp Rudolf von Rohr  
**Semester thesis** *Scale-up of microfluidic devices and effect of water evaporation on droplet volume distribution and shape*

Swiss Federal Institute of Technology Zurich  
Prof. Dr. Marco Mazotti & Prof. Dr. Philipp Rudolf von Rohr  
Bachelor thesis *Improvement of flowability of graphite powder by means of plasma-enhanced chemical vapor deposition*  
Swiss Federal Institute of Technology Zurich  
Prof. Dr. Philipp Rudolf von Rohr

**08/2005 - 07/2011 High school student (Abitur)**  
Gymnasium Aloisiuskolleg, Bonn

### **Professional experience**

**04/2017 - 07/2017 Research assistant**  
Swiss Federal Institute of Technology Zurich  
Research topic *Reactive multiphase flows in porous structures & Development of a business case for ethanol production in Switzerland*  
Prof. Dr. Philipp Rudolf von Rohr

**04/2015 - 07/2015 Intern**  
ThyssenKrupp Industrial Solutions  
Department *Process Engineering*

**06/2011 - 07/2011 Intern**  
Bayer Technology Services  
Scope *Basic knowledge of machining, joining and forming production processes*